

**THE MEASUREMENT OF WEB STRESSES
DURING ROLL WINDING**

By

DAVID R. ROISUM

**Bachelor of Science
University of Wisconsin
Madison, Wisconsin
1979**

**Master of Science
University of Wisconsin
Madison, Wisconsin
1984**

**Submitted to the Faculty of the
Graduate College of the
Oklahoma State University
in partial fulfillment of
the requirements for
the Degree of
DOCTOR OF PHILOSOPHY
May, 1990**

COPYRIGHT

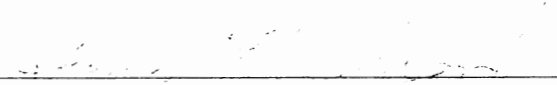
by

DAVID ROBERT ROISUM

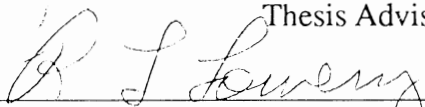
MAY 1990

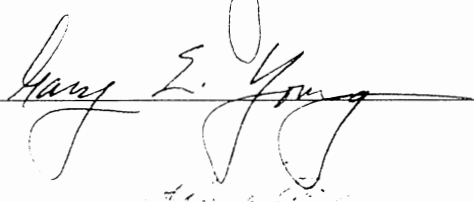
**THE MEASUREMENT OF WEB STRESSES
DURING ROLL WINDING**

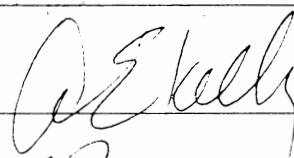
Thesis Approved:

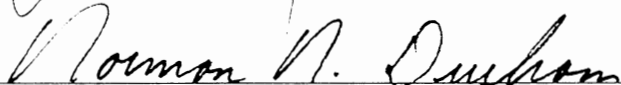


Thesis Advisor









Dean of the Graduate College

PREFACE

This work actually began in 1985 while in the position of Manager of Winding Development at Beloit R&D where I recognized the need to develop a means of accurately measuring the fundamental roll structure variables of stress and strain during winding for production quality control, as well as the possible closed-loop control of the entire winding process. The need for such a measurement became even more apparent when I developed a consistent means of evaluating the resolution of roll structure measurements that were based on different quantities such as hardness, tension and density. The resolution evaluation was based on the number of measurements required to discern a known change in roll structure to a specified statistical confidence. The outcome of an extensive series of tests showed that all current methods were unreliable, but the density analyzer fared better than most and had the additional advantage that it was inherently capable of automated on-line measurements.

Assisted by my staff computer programmer who wrote the background data acquisition task, we sought to improve the density hardware and software. Simultaneously, I began an extensive review of winding models with the hopes of tying these stress models to experimental measurement. In particular, I hoped that a simple conversion formula could be constructed which changed density measurements into wound-in-stress. The pursuit of this formula proved as elusive as the alchemy of changing lead to gold.

In 1987 I left full-time employment at Beloit to work in the newly formed Web Handling Research Center, and simultaneously pursue a Ph.D. in Mechanical Engineering. Though I had many accomplishments in the nearly three years at Beloit R&D, I was frustrated not to find the alchemy of the density to stress transformation. Still convinced that the successful measurement of web stresses during winding could revolutionize the field, I proposed the topic as both a Web Handling project and thesis topic.

In the summer of 1988, the project was restarted with careful emphasis on a building block approach. The inspiration that seeded this final successful effort was a recognition that all winding models to date were determined systems so that perhaps by reformulating the constitutive equations we could determine wound-in-stress from some other measurement of the winding roll. All winding models to date were boundary valued problems defined by a 2nd order differential equation with core stiffness and wound-in-tension boundary conditions. The problem with the wound-in-stress boundary condition was that it is extremely difficult to determine. Indeed, that is the parameter we most want to know about winding. The breakthrough came when I rewrote the boundary condition for the outer radius as the sum of the deformed thicknesses of all layers of the web plus the inner core radius. This radius boundary condition could be measured with equipment similar to the density analyzer, but in addition required web thickness measurements.

Now the problem is formulated in terms of quantities that could be measured during winding! However, preliminary work indicated that the resolution of the density analyzer type diameter measurements needed to be improved several orders of magnitude to be suitable to this new approach. Additionally, a means of accurately measuring web thickness had to be developed. Once again, I began the redesign of the density type measurement, however this time without staff assistance. In December of 1988, the new data acquisition system composed of high count encoders, caliper measurement, data acquisition boards and computer were used to measure the winding of about 40 rolls of paper at Beloit's winding lab in Rockton Illinois.

Analysis of the data back at Oklahoma State University showed an order of magnitude improvement in the resolution of the new measurements. Also, a superior alternative to the density quantity was defined as radial compression which also served as the boundary condition which drives the stress calculation routines. Though I now realize that a direct conversion formula from density to stress is not the correct approach, density-like measurements are the input to stress calculation routines.

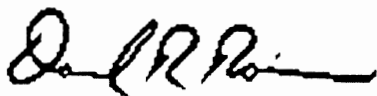
The primary outcomes of this research are vastly improved roll structure measurements that can be made during winding or unwinding based on the fundamental parameters of stresses and strains. Additional contributions are the measurement of caliper and an improved understanding of winding and winding models. I sincerely hope that this work will be extended by others to include alternative methods of caliper and radii measurement, new winding models and most importantly, application to the closed-loop control of the winding process.

ACKNOWLEDGEMENTS

I wish to express my gratitude to all the people who assisted me in this work including my thesis advisor and committee chairman Dr. J. Keith Good and my other committee members, Dr. Richard Lowery, Dr. Gary Young, Dr. John Shelton and Dr. Allen Kelly. Additional thanks to Dr. Karl Reid, for his vision in establishing the Web Handling Research Center, for my employment, and giving me the freedom to perform.

Additionally, I would like to thank Richard Adams and Phil Smith of the Beloit Corporation for giving assistance and access to the Winding Lab for a major portion of the experimental work. Let me also recognize my former staff who helped me with much of the work to re-establish the science of winding. I also give special appreciation to Bill Whitford and Scott Baum who were excellent sounding boards for new ideas, and who had the conviction to tell me when I was wrong.

However, my deepest gratitude is as always given to my wife Jane. She tolerated my excesses so that I could follow my vision, while managing our home, son, and her own career much as a single parent. Finally, I hope my son Zach who asked me why I had to work on weekends will also find his own vision and commitment.



February 5, 1989

TABLE OF CONTENTS

Chapter	Page
1. INTRODUCTION	1
Winding	1
The TNT's of Winding	5
Web Properties	9
Winding Models	9
Roll Structure Measurement	10
The Measurement of Web Stresses During Winding	11
Basic Contributions of this Research	12
Thesis Overview	14
2. PHYSICS OF THE WOUND ROLL	15
Roll Physics and Boundary Conditions	15
The Roll	16
The Core	23
The Roll Outside	30
The Accretion Nature of Winding	32
3. WOUND ROLL MODELS	33
Overview of Wound Roll Models	33
A Simple Linear Isotropic Model	34
Linear Anisotropic Models	39
Altmann Model	40
Yagoda Model	50
Nonlinear Moduli	55
Hakiel Model	61
Willett and Poesch Model	71

Chapter	Page
Pfeiffer Model	72
Lekhnitskii Model	73
A Tangential Stress Formulation	74
Summary of Winding Models	77
4 . COMPLEX WOUND ROLL BEHAVIOR	79
Overview of Complex Behavior	79
The Effect of a Nip on Wound-In-Tension	81
The Effect of Torque Differential on Wound-In-Stress	85
The Effect of Speed Changes on Torque and Nip	85
Centrifugally Induced Stresses	86
Air Entrainment	89
The Cross Direction	91
Hygrothermal Response	92
Anelastic Response	98
Interlayer Slippage	99
Gravity and External Loading	111
Roll Defect Theory	113
5 . ROLL STRUCTURE MEASUREMENT	116
Background	116
Rhometer	118
Schmidt Hammer	119
Backtender's Friend	120
Smith Needle	122
Core Torque Test	122
Pull Tab Test	124
Axial Press Test	126
Thin Pressure Transducers	126
Acoustic Interlayer Pressure Measurement	127
Caliper Method	127
Cameron Gap	128
Slit Roll Face	128
Radially Drilled Holes	129
Strain Gages	129

Chapter	Page
J-Line	129
WIT-WOT Rewinder	130
X-Ray Tomography	130
Roll Shape Profiling	132
Nip Width and Pressure	133
Summary	134
6. THE DENSITY ANALYZER	135
Density	135
Density as a Roll Structure Analysis Tool	137
Theory of Operation	138
The Density Calculation	140
Caliper Sensitivity and Correction	142
Raw Density Data	146
Density as a Derivative	146
Density Noise Reduction	149
Sizing Density Data Acquisition	151
Density and Stress	156
Summary	157
7. A NEW WINDING MODEL FORMULATION	158
Why a New Approach is Needed	158
Overview of the New Model	159
A New Outer Boundary Condition	163
Caliper Cautions	167
Radial Compression	169
The Displacement Formulation	171
Finite Difference Approximations to Differential Equations	175
Simulating Displacement Data for Model Evaluation	185
Extended Hakiel Formulation	190
Accelerating the Solution	192
Additional Experimental Validation	198
Conclusion	202

Chapter	Page
8. DATA ACQUISITION HARDWARE	204
Introduction	204
The Winder	206
Incremental Encoders	208
Quadrature Conversion	212
Counter Data Acquisition	215
Off-Line Caliper Measurement	219
On-Line Caliper Measurement	221
The Schaevitz Non-Contacting Gage	222
Calibrating the Caliper Gage	226
Schaevitz Caliper Readings and Paper Test Lab Standards	227
Conclusion	229
9. DATA ACQUISITION SOFTWARE	230
Introduction	230
Polling and Interrupts	232
Data Acquisition Program Structure	235
Program Profiling	238
Data Preprocessing	241
Conclusion	243
10. SENSITIVITY ANALYSIS	244
Introduction	244
Accuracy and Resolution Overview	245
Roll Structure Resolution	247
Radial Compression Resolution	253
Wound Roll Model Accuracy	261
Data Acquisition Sensitivity Analysis	262
Model Sensitivity Base Case	266
Model Numerical Stability	269
Sensitivity to Material Parameters	270
Conclusion	276

Chapter	Page
11. CONCLUSIONS AND RECOMMENDATIONS	277
Project Summary	277
Contributions	279
Complications	282
BIBLIOGRAPHY	285
Selected	285
Cores	286
Density	287
Web Handling	289
Web Property Measurement	290
Winding	293
Winding Models	296
Wound Roll Structure Measurement	298
Late Additions	300
APPENDIX A - WINDING MODEL COMPUTER PROGRAMS	302
Linear Anisotropic Model	302
Altmann Model	306
Yagoda Model	309
Hakiel Model	312
APPENDIX B - WINDING MODEL COMPUTER OUTPUT	316
Standard Sets of Input Parameters	316
Linear Anisotropic Model	317
Altmann Model	318
Yagoda Model	320
The Hakiel Model	322
APPENDIX C - STRESS MEASUREMENT PROGRAMS	325
Data Acquisition	325
Density & Radial Compression	337
Stress Calculation	343

Chapter	Page
APPENDIX D - EXPERIMENTAL RUN DETAILS	350
Web Material Properties	350
Winder and Data Acquisition Setup	351

LIST OF TABLES

Table	Page
1. The Stiffness of Commonly Used Cores	28
2. Winding Integral Evaluation Errors	49
3. Stress Differences Between Yagoda and Altmann Models	52
4. Radial Moduli	60
5. WIT Coefficients for Three Paper Grades	83
6. J-Line Shape Measurements	105
7. Derivative Finite Difference Approximations	176
8. Matrix Coefficients	181
9. Beloit Two-Drum Lab Winder Specifications	206
10. Encoder Specifications	209
11. Effective Pulse Rates	210
12. Metrabyte CTM-05 Counter Board Specifications	215
13. Schaevitz Non-Contacting Gage Specifications	223
14. Resolution of Roll Structure Measurements	260
15. Sensitivity Analysis Parameters	268
16. Minimal Inputs for the Displacement-to-Stress Measurement System	283

LIST OF FIGURES

Figure	Page
1. INTRODUCTION	
1. Winder Configurations	2
2. Chucks and Shafts	3
3. Winder Components	5
4. Black Box Model of Winding	6
5. The TNT's of Winding	7
6. Typical Setpoint Functions for the TNT's	8
7. Optimum Roll Structure	11
8. Basic Contributions of this Research	14
2. PHYSICS OF THE WOUND ROLL	
9. Spiral Winding and Ring Approximation	17
10. Forces Acting on a Wrap Segment	18
11. Displacements of a Wrap Segment	18
12. Stresses Acting on a Wrap Segment	22
13. Core Stiffness and Tangential Stress	29
3. WOUND ROLL MODELS	
14. Stress Distribution for the Isotropic Model	38
15. The Winding Integral vs Radial Position	44
16. Stress Distribution for Altmann Model	45
17. Nonlinear Stack Stress-Strain Curves	56
18. Effect of Grid Size	68
19. Effect of Grid Size	69
20. Effect of Grid Size on Radial Stress Error	70

4. COMPLEX WOUND ROLL BEHAVIOR

21. Contact Pressures in a Winding Nip	82
22. Effect of Nip and Tension on WIT	84
23. Effect of Deceleration on Torque and Nip	86
24. Centrifugal Stresses - Isotropic Model	88
25. Air Entrainment into a Roll or Roller	90
26. Paper Roll Moisture/Temperature Distribution	96
27. Viscoelastic Models	99
28. J-Line Geometry	101
29. Slippage Function Schematic	101
30. Slippage Function and J-Line	103
31. Slippage Function Plots	105
32. J-Line Deformation	106
33. Progression of the J-Line During Winding	108
34. J-Line Slippage on a Core-Supported Unwind	108
35. Typical External Loads	112

5. ROLL STRUCTURE MEASUREMENT

36. The Rhometer Roll Hardness Tester	121
37. The Schmidt Roll Hardness Tester	121
38. The Smith Roll Tightness Tester	123
39. The Core Torque Test	123
40. The Pull Tab Test	125
41. The Axial Press Test	125
42. The J-Line Test for Interlayer Slippage	131
43. The WIT-WOT Rewinder	131

6. THE DENSITY ANALYZER

44. The Density Analyzer	139
45. Effect of Caliper on Density	144
46. Effect of Caliper Correction on Density	144
47. Effect of Caliper Correction on Density	145
48. Effect of Caliper Correction on Density	145
49. Raw Density Data	147

Figure	Page
50. Density Derivative	147
51. Effect of Sample Size on Density	149
52. Histogram of Pulse Differences	150
53. Fourier Transform of Pulse Differences	150
54. Rewound Roll Surface and Rotational Speed	154

7. A NEW WINDING MODEL FORMULATION

55. Solution Map of Winding Models	161
56. Incremental Layer Compaction	164
57. Radial Displacements	164
58. A Radial Compression Profile	171
59. Wound Roll Equation System	179
60. Displacement Data Simulation to Check Stress Model	187
61. WIS Error - Displacement Formulation	189
62. WIS for Tension Drop - Calculated vs Measured	193
63. Incremental Radial Stress vs Depth and E_T/E_R	195
64. Incremental Radial Stress vs Depth and Radius	195
65. WIS - Conventional and Accelerated Solutions	197
66. Predicted Roll Stresses Run #38	198
67. WIS for Nip Drop - Calculated vs Pfeiffer Equation	199
68. WIS for Nip Drop - Calculated vs Measured	201

8. DATA ACQUISITION HARDWARE

69. Two-Drum Winder at Beloit R&D	207
70. Winder Benchboard	207
71. Encoder With External Multiplier	209
72. Encoder Pulse Trains	213
73. Quadrature Conversion and Isolation Circuit	214
74. Metrabyte CTM-05 Block Diagram Schematic	216
75. Peak-Peak and Effective Caliper	220
76. Schaevitz Non-Contacting LVDT Gage	223
77. Caliper Gage Location	225
78. Caliper Repeatability - LWC	228
79. Caliper Repeatability - NC	228
80. Caliper Measurement Comparison	229

9. DATA ACQUISITION SOFTWARE

81. Encoder and Counter Schematic	233
82. Data Acquisition Program Execution Time	240

10. SENSITIVITY ANALYSIS

83. TNT Step Change to Evaluate Resolution	249
84. Rhometer Hardness vs Diameter	254
85. Schmidt Hardness vs Diameter	254
86. Smith Hardness vs Diameter	255
87. Cameron Gap vs Diameter	255
88. Density vs Diameter	257
89. Density vs Diameter	257
90. Radial Compression vs Diameter	258
91. Radial Compression vs Diameter	258
92. Wound-Off-Tension vs Diameter	259
93. Effect of Averaging on Input Data	264
94. Effect of Low-Pass Filter on Input Data	265
95. Deflection Input and WIS Output - Base Case	267
96. Radial and Tangential Stress - Base Case	267
97. Sensitivity to Calculation Grid Size	270
98. Sensitivity to Calculation Depth	271
99. Sensitivity to Calculation Replication	271
100. Sensitivity to Radial Modulus	272
101. Sensitivity to Tangential Modulus	272
102. Sensitivity to Core Modulus	273
103. Sensitivity to Radial Poisson Ratio	275
104. Sensitivity to Tangential Poisson Ratio	275
105. Sensitivity to Caliper Gain	276

NOMENCLATURE

b	basis weight (lb/in ²)
c	caliper (in)
CD	cross machine direction
CPU	(computer) central processing unit
d	diameter (in)
E _C	core modulus (lb/in ²)
E _R	radial modulus (lb/in ²)
E _T	tangential modulus (lb/in ²)
f	frequency (hz)
h	thickness (in)
IO	(computer) input / output
k ₁	constant for radial modulus
k ₂	constant for radial modulus
l	length (in)
LVDT	linear variable differential transformer
MD	machine direction
mil	0.001 inches
n/a	not applicable
p	pulses
P	pressure (lb/in ²)
pli	pounds per linear inch of width
ppr	pulses per revolution of encoder
psi	pounds per square inch
r	radius (in)
s	speed (in/sec)
SD	standard error of the estimate
t	time (sec)
TNT's	torque, nip, tension and speed
v	tangential displacement (in)
w	radial displacement (in)
WIS	wound-in-stress (lb/in ²)
WIT	wound-in-tension (lb/in)

Z	statistic
ZD	Z direction
ϵ_R	radial strain (in/in)
ϵ_T	tangential strain (in/in)
m	mean or average
μ_R	radial poisson ratio (contraction in length due to radial load)
μ_T	tangential poisson ratio (contraction in thickness due to tang. load)
ρ	density (lb/in ³)
σ	standard deviation
σ_R	radial stress (lb/in ²)
σ_T	tangential stress (lb/in ²)
σ_W	wound-in tangential stress (lb/in ²)

Subscripts

0	subscript for sample at core
i	subscript for sample i
j	subscript for sample j
k	subscript for sample k
n	subscript for outer sample
d	drum roller
r	rewound roll
-	bar indicates nondimensionalized

CHAPTER I

INTRODUCTION

Winding

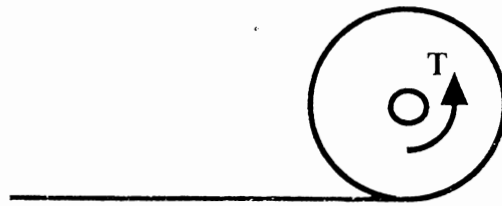
Winding is a process whereby a thin, flat and flexible material is wound in a spiral fashion into a roll. Materials such as film, foil, paper and textiles are wound into rolls that range from just a fraction of an ounce, such as capacitors, to reels of paper more than ten feet in diameter and 30 feet long weighing more than 60 tons, to coils of metal that are even heavier. A common motivation for winding is that a wound roll provides a convenient geometry to produce, ship and use. Also, roll-to-roll winding is used to edit the web, add an intermediate process such as coating or finishing, or to salvage unacceptable rolls. Finally, rolls may be used to provide a buffer between two stages of web processing so that the upstream process can run more consistently despite changes in throughput of the downstream process.

Winding machines are composed of multiple *rollers* made of aluminum, steel or synthetics upon which are processed one or more winding or unwinding *rolls* of web. Though winding machines have been running well before the turn of the century and vary considerably in appearance, the basic configurations remain unchanged. As seen in Figure 1, the roll may be center wound without a lay-on roller, surface wound with a roller, or a combination of center and surfacing winding. A lay-on roller, sometimes also called a rider roller, is nipped against the winding roll and partially wrapped by the incoming web. Configurations can be further subdivided by noting there may be more than one roller, such as the two-drum winder, have multiple axially staggered rolls such as the duplex winder, or have multiple sequentially processed rolls such as the turret winder.

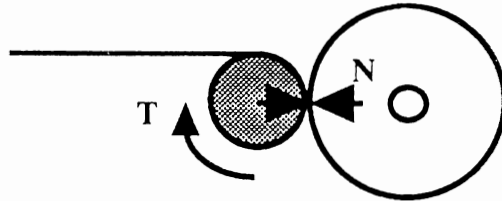
Rolls may be wound upon cores made of fiber, plastic or steel, or upon shafts which may be solid or expandable, or without any support at the roll's interior [1-13, 124]. As seen in Figure 2, rolls are often restrained from axial or CD (cross direction) movement during winding by chuck or shaft holders. Without this restraint, it would be difficult to wind a roll with straight planar edges.

Figure 1
WINDER CONFIGURATIONS

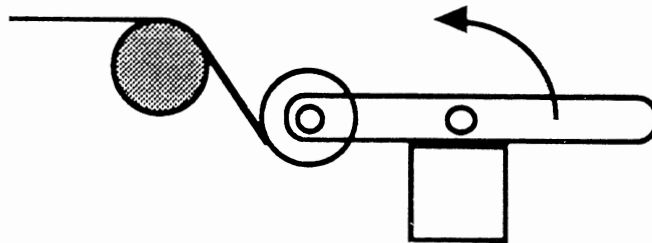
a. Centerwind



b. Surfacewind



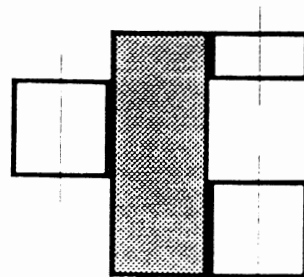
c. Turret



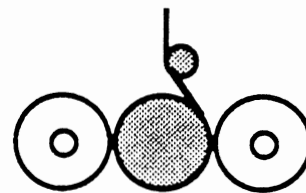
d. Two Drum



e. Duplex



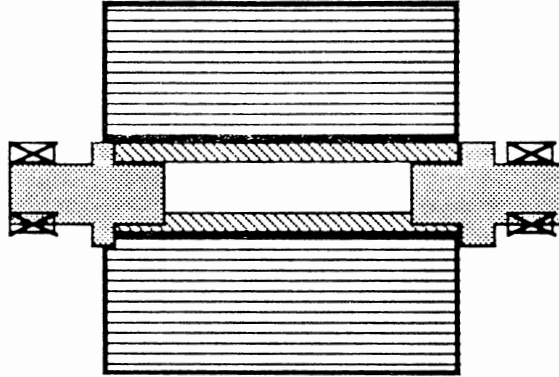
Top View



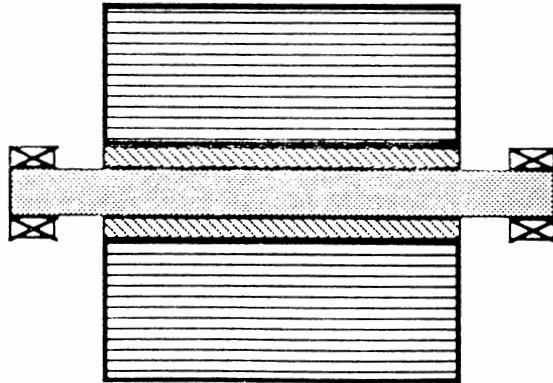
End View

Figure 2
CHUCKS AND SHAFTS

a. Roll Held by Core Chucks



b. Roll Held by Core Shaft

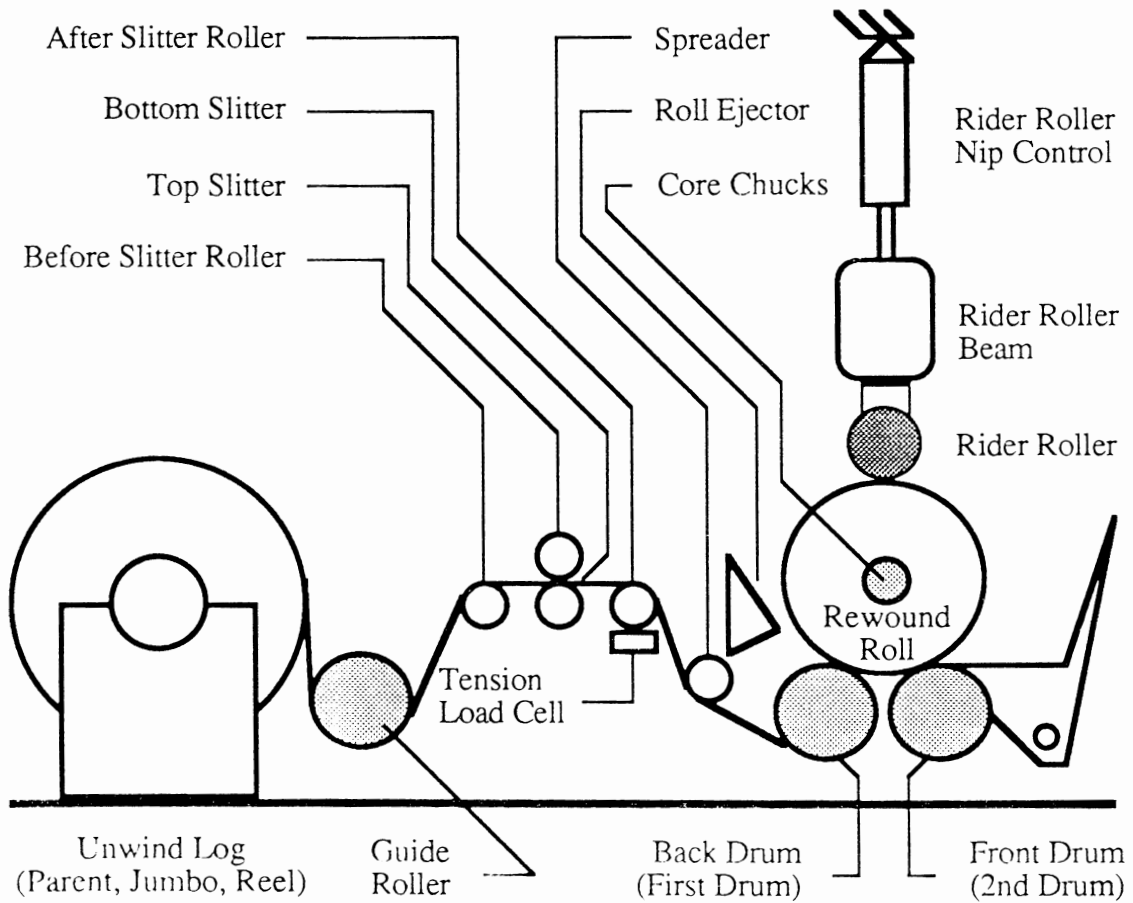


Though there are numerous winder designs for the myriad of applications, the components in a winder are typified by those of the two-drum winder, shown in Figure 3, which is commonly used in the paper industry. The unwind stand holds the parent roll securely but may move sideways to 'chase' the winding roll to cause a straight buildup of the roll edges [51]. The guide roller is used to preserve web geometry on downstream components and even out tension from front to back of the web by pivoting on one end. Spreader rollers may be used to lay the web flat as well as to spread individually cut webs on winders equipped with slitters [107]. The windup section may include one or more rollers or drums to provide additional web tension and to squeeze out entrained air [103]. Fully automated winders also include additional equipment to insert cores, fasten the web to cores, and to eject the finished rolls [92]. Finally, winders have many sensors such as load cells for web tension [69, 71], actuators such as electric drives and pneumatic brakes [101] to set speed and tension, and controllers such as PLC's, drives and computers [90, 100, 104, 105].

The two essential issues in the economics of winding are productivity and quality. Productivity is the ability of the winder and crew to match or exceed the output of the upstream process. If the winder should fall sufficiently behind, the upstream process may have to be temporarily shut down until the winder can catch up, causing a loss of output. Productivity parameters include the acceleration and top speed of the winder, roll change time and reliability [91-93, 126]. Though productivity is an important consideration, it is not the subject of this thesis and will not be considered further.

Roll quality is also vitally important to the profitability of web processes because rolls which do not meet customer requirements must be salvaged or scrapped. Roll quality is defined as the absence of defects that make the roll unsalable, and may be either present prior to winding or induced during the winding process [95-97, 125]. Those defects present prior to winding such as nonuniform thickness, nonplanarity or uneven coating are seldom improved by the winding process. However, there are many roll quality defects that the winder itself can introduce such as tears, starring and telescoping [99, 108, 109, 123]. These winder induced defects are commonly attributed to improper roll structuring which are best quantified as radial and tangential stress distributions inside a wound roll though historically roll structure was also described using hardness, tension and density [116, 117, 119].

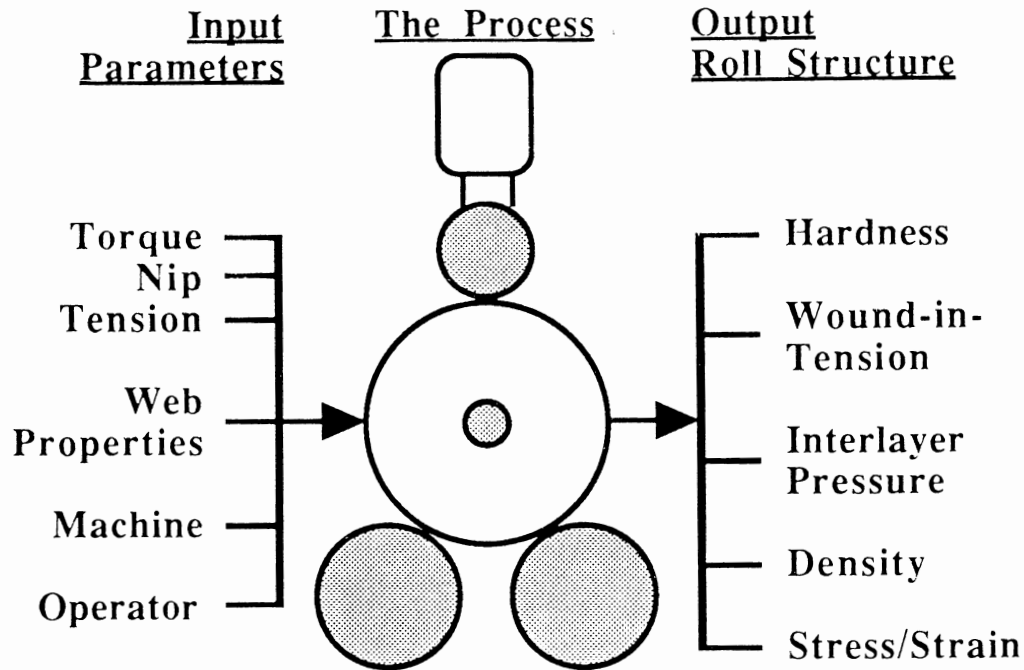
Figure 3
WINDER COMPONENTS



The TNT's of Winding

The complex details of the winding process can be avoided for a time by using a black-box approach as seen in Figure 4. Knowledge of the system then falls into three categories: input parameters, the process laws, and output results. Input parameters are variables which may be controlled to optimize the output results which can be loosely described as roll quality. The process laws are the constant and inviolate behavior of physical systems which are described by engineering mechanics, material behavior, and other basic sciences. Ultimately, the goal of winding research is to determine values for the controllable input parameters such that roll quality is maximized. This involves winding models, parameter measurement required by the models, and optimization theory.

Figure 4
BLACK BOX MODEL OF WINDING

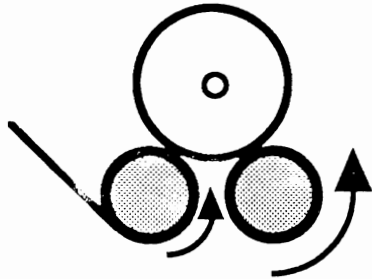


The input parameters which are the easiest to control are the TNT's of winding: Torque, Nip, Tension, and speed [102]. Machine builders will usually give the operator the ability to adjust the TNT's via benchboard controls [90]. As seen in Figure 5, torque may be applied as a differential between the front and back drum on two-drum winders, or through a center-shaft on duplex winders. Nip is the pressure in PLI (lbs per lineal inch of width) between the winding roll and a roller or drum. Tension is the lineal load (PLI) applied on the web draw immediately upstream of the winding roll.

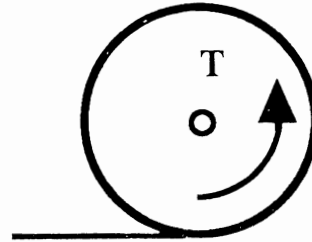
The TNT's (Torque, Nip, Tension and speed) of winding are setpoint functions of rewound roll diameter, as seen in Figure 6. The TNT's of winding are often linearly decreasing from start to finish to give the roll a structure which is hard near the core and decreasing smoothly to a softer finish at the outside. Rider roll nip on a two drum winder is perhaps the most complicated of the controls because the total back drum nip is the sum of rider roll nip, roll weight and winding angle geometry [102, 103].

Figure 5
THE TNT'S OF WINDING

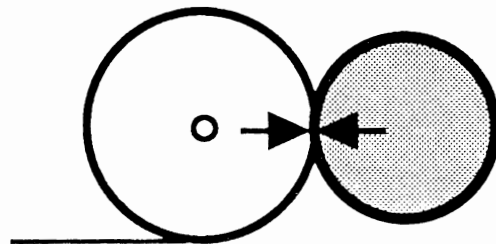
Torque Differential



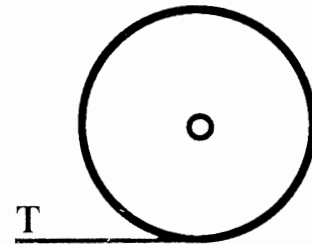
Centerwind Torque



Nip

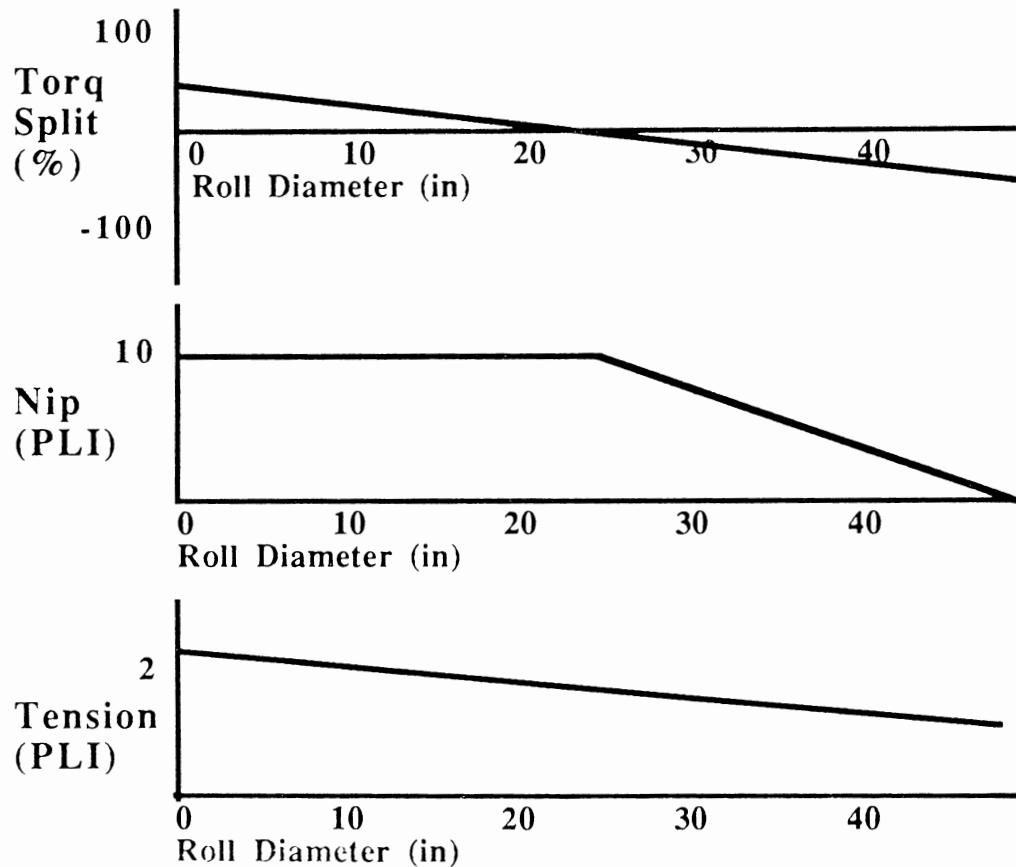


Tension



Increasing any of the TNT's will usually make the roll harder at that point and vice versa. However, the TNT's can't be arbitrarily specified on an unlimited range. Torque is limited to the available friction which depends on the coefficient of friction between drum and web and the normal force determined by roll weight, geometry and (rider roll) nip loading. Exceeding the friction limit will simply cause slipping and possible instability and sheet marking. Nip can't be negative, nor can it be so much as to knead the rewind roll to increased interlayer slippage to the point of creping or shear bursts on paper. Nip also must not be too low on nonporous materials such as film, or air entrainment will increase. Tension can't be too low else the propensity to wrinkling will be increased and the sheet run may flutter. Additionally, web tension can't be increased too much because paper web breaks are an exponential function of web tension. High web tension on film may cause undesirable plastic creep which may not be even across the width, if the properties of the film are not uniform across the width.

Figure 6
TYPICAL SETPOINT FUNCTIONS FOR THE TNT'S



The point to remember is that though the TNT's are the most easily controlled inputs, they often have narrow ranges of useful adjustment. The operator must find a delicate balance between all of these parameters to wind acceptable rolls [94]. Additionally, the task is made even more difficult because the material properties change intentionally with grade changes and unintentionally due to manufacturing process instabilities. These material property changes cause the optimum winding profiles to vary with time.

Though some quantitative knowledge exists of the relationship between the TNT's and roll defects, this is usually empirical in nature so that the relationships are application dependent. In practice, the determination of TNT setpoints is usually done by the operator based on prior subjective experience. Additionally, different operators may chose different setpoints for the same product and machine.

Web Properties

Some web properties have a strong influence on roll structure. These include caliper [73, 74, 89], density, yield and tensile strengths, coefficient of friction [66], coefficients of expansion, porosity, as well as the elastic moduli in the z-direction (ZD) [79, 88] and machine-direction (MD) [54-64, 70, 75, 82-87, 89]. However, there are many web properties that are routinely tested which have essentially no effect on the quality of roll structuring including optical properties such as brightness, color and opacity. If one was to choose an optimum (fictitious) web for winding, it would probably have high: caliper, strength, friction, porosity; and low: anisotropy (MD/ZD modulus), and coefficients of expansion.

Two points must be made about web properties as inputs to the winding process. First, though some properties have a profound influence on winding, they can't usually be considered an input variable for the purpose of optimizing winding because they are generally specified by end use. Therefore, average web properties are not an input variable that can be used to optimize winding. Neither are paper properties a modifiable output from the winding system because web properties are seldom measurably changed by the winding process [111].

Secondly, the mechanical properties vary with MD position (or time) and cross-direction (CD) position. These variations or deviations from target have as much influence on the winding behavior as the averages or means. One example of this behavior is paper web breaks which occur at rare local weaknesses in the web. It can be shown that the web break problem is more influenced by the variations of strength than by the average strength [178, 191, 192]. Another example is ropes and corrugations that are almost entirely related to variations of caliper across the web. Reducing web property variations to optimize winding though desirable, is difficult in practice because the production and winding of webs may be on widely separated machines under different supervision.

Winding Models

The winding process is the connection between input variables and output results. The process is a system of inviolate physical laws that describe the paper stresses in a roll resulting from various input parameters. The importance of these physical laws are that they can quantitatively describe some aspects of roll quality, allowing roll structure predictions for any set of input parameters. These laws, which are usually solid mechanics formulations, can be coded into a computer to run 'what if' scenarios to optimize winding on a computer much like businesses use spreadsheets to model products.

The advantage of computer modeling is that many combinations of inputs can be run in a short time at no risk to the product, while searching for optimum combinations of inputs. The difficulties of modeling are that some web properties required by the models such as radial modulus and caliper are difficult to measure, model verification is difficult because stresses are difficult to measure, and defect models are just emerging.

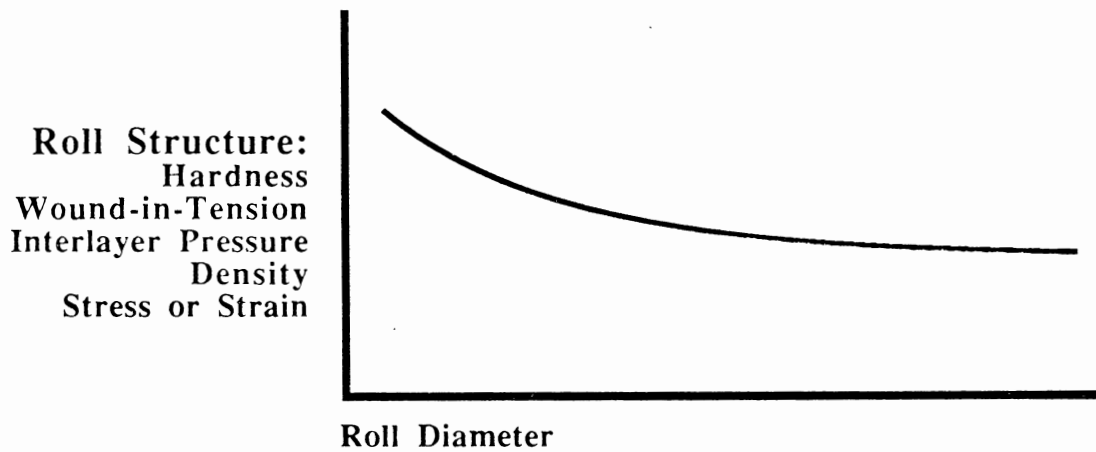
The analytical modeling of roll winding using mechanics equations began in the late 50's using linear isotropic hoop stress formulas in an accretion model [115, 129, 131]. The model superimposed the stresses due to the addition of a single wrap upon the existing stress distribution as wraps are added from the core to the finish diameter. Subsequent works removed model restrictions by allowing for anisotropy [127, 137, 149-153], and later nonlinear anisotropy [132, 133, 140, 141, 186]. The current state of art of winding models gives a close description of centerwinding. However, the effects of the nip, air entrainment, interlayer slippage and CD variations remain to be incorporated into a single description of winding.

Roll Structure Measurement

Returning to Figure 4, it can be seen the output results from winding are loosely described as roll structure, which is some measure related to winding stress as a function of roll diameter. For most roll structure measurements and for most materials, the ideal roll structure will be a *profile shape* similar to Figure 7, which shows a hard (tight) start, with a smooth transition to a softer (looser) finish. Differences in ideal roll structuring for a particular grade are represented by different *values* of the starting and finish hardness. This often used figure is the result of the cumulative experiences of many winding experts, but is not presently quantifiable. This means that roll structure quality control efforts are limited to measuring roll structure profiles to compare with the ideal profile shape, and using other techniques such as judgment or statistics to set initial and final magnitudes. As a consequence, roll structuring has been and still is primarily an art rather than a science.

The earliest device used to measure roll-structure quality was the backtender's stick or "billy club", which is a short wooden stick that the operator struck against the roll to sound its tightness or hardness. Quantification of hardness became possible with the invention of the Rhometer and Schmidt Hammer in the 1960's [155, 156, 159]. Techniques for the measurement of tension, stress and strain were developed and include the Cameron Gap [174], J-line [106, 108, 121], strain gages [160, 161, 168, 172], and the Beloit WIT-WOT rewinder [166, 167]. Interlayer pressure or radial stress have been quantified by using the Smith needle, Core Torque [161], thin pressure gages [128, 163] and acoustic techniques [165]

Figure 7
OPTIMUM ROLL STRUCTURE



The most recent innovation in roll structure measurement is the density analyzer which enables online measurement of roll structure [14-38]. The density analyzer is a computerized data acquisition system which calculates the bulk compression of wound rolls based on rewound roll diameter measurements. The density analyzer is the first truly automated roll structure measurement method with high resolution [169, 171]. Since the density analyzer hardware serves as a platform for this new stress measurement technique, it will be described in more detail in Chapter 6.

The Measurement of Web Stresses During Winding

Though there are numerous methods of measuring roll structure, none is currently able to measure the fundamental parameters of wound-in-stress during winding or unwinding. The primary objective of this work is to develop a successful WIS (wound-in-stress) measurement technique that could be used for laboratory studies, production quality control and perhaps for later application by others to the closed-loop control of winding to a target stress level. This measurement technique is a merging and extension of the density analyzer, which has demonstrated a relatively high sensitivity, with the fundamental and first principle winding models.

The difficulty with current winding models is that they all assume an outer boundary condition of a known WIS, which is extremely difficult to measure or determine except for the limited case of pure centerwinding on machines equipped with tension and caliper sensors. To avoid this difficulty, a new boundary condition was defined which uniquely determines the state of a roll and allows displacements, strains, and stresses to be calculated. This new boundary condition is a displacement of the outer surface of the roll caused by winding stresses. This new boundary condition simply states that the change in roll diameter over some sample interval is equal to the sum of the thicknesses of web added, plus the sum of the incremental deformations of each layer and the core caused by winding stresses.

Since web caliper and changes in roll diameter can be measured, the sum of the deflections can be calculated as a resultant deformation of the outer surface. The equipment to prototype this new stress measurement system are encoders for measuring diameter, a caliper gage, and a computer data acquisition system. Thus, the hardware is similar to the density analyzer except that in addition to diameters, web caliper must also be measured. However, the stress measurement algorithm, which is essentially a reformulation of traditional winding models, bears no resemblance to the density analyzer.

Current winding models are second order differential equations written in terms of radial stresses with a core stiffness inner boundary condition, and a radial pressure boundary condition just under the outer layer. However, the same constitutive equations of winding can be also be assembled into a differential equation formulated in terms of displacements instead of radial stresses. In this case, the outer boundary condition is a displacement of the outer surface of the roll which can be measured using equipment described above. Once the displacement field is calculated, strains and then stresses can be calculated. Thus, by reformulating the winding differential equation using displacements, and measuring the displacement outer boundary condition, all web stresses and strains can be calculated at any location in the roll, and at any time during winding. Thus, the new measurement technique calculates the condition of the roll based on web material properties, caliper, and diameter.

Basic Contributions of this Research

The primary contribution of this work is a new boundary condition for all winding models which allows the solution of displacements, strains, stresses, and most importantly, wound-in-stresses from easily measured quantities of roll diameter and web caliper. This results in not only a new winding model, but a new way to solve all existing winding models. Thus for the first time, winding stresses can be easily measured.

Another major contribution resulting from this project is an improvement in the hardware and software of the existing density analyzer that yields an order of magnitude improvement in resolution over existing methods. Also a new roll structure parameter, radial compression, was defined which removes the floating zero and caliper dependence problems of density calculations.

Additional work includes a very complete review of current winding models such as those of Altmann [127], Yagoda [149-154], Pfeiffer [140, 141], and Hakiel [132, 133] and others. This review includes a check of their derivations, determining the numerical accuracy of stress computations based on a standardized set of input parameters, and a review of the scope of application and limitations. As a consequence of this careful check, errors and limitations in winding models were revealed that were not previously documented. Computer codes written for these models, which are included in the appendices, are some of the few ever published.

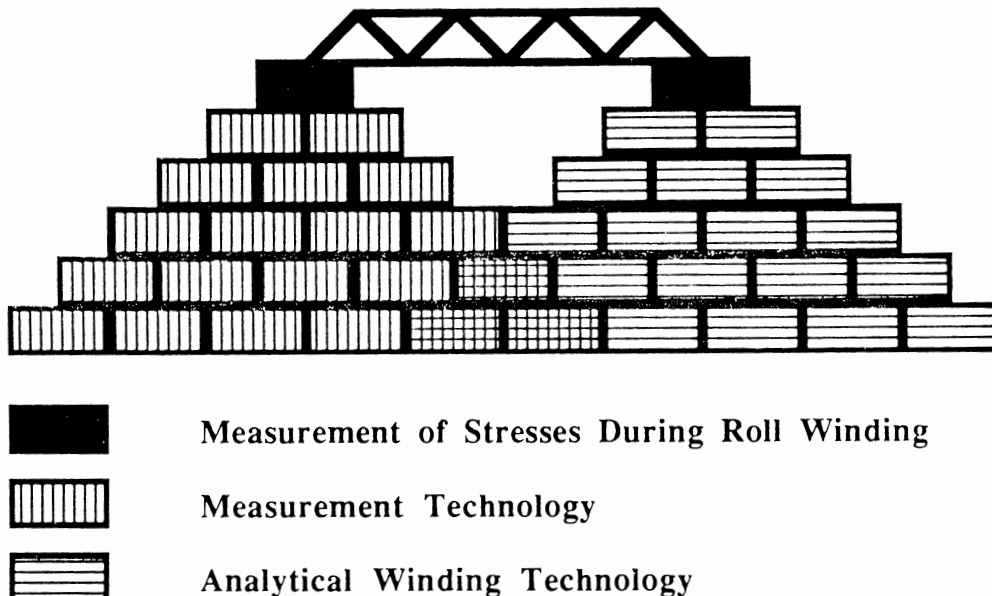
Similarly, all roll structure measurement methods are reviewed, and the most common are evaluated for accuracy, resolution and other criteria. A method of comparing the resolution of unlike measurements is fully developed. Similarly, data acquisition design for density and stress analysis is also fully documented so that a system can be optimized for a particular application.

All careful research work such as this begins by laying a solid foundation, which represents previous work in the area, upon which is placed new contributions. This can be represented by a pyramid made of technology blocks. These blocks of technology should ideally mate closely with their neighbors such that a solid structure is obtained. As seen in Figure 8, the pyramids of analytical and experimental technologies will have only a partial overlap because some analytical work has not been experimentally verified and some experimental work has yet no identified underlying analytical expression.

What makes this work unique in the winding area is that a bridge has been made between analytical and experimental technologies at the highest level. The analytical portion of this new measurement system not only can accommodate all present fundamental winding models, it is extensible because it is a methodology rather than a distinct model in itself. Similarly, the experimental measurement techniques used are the most sensitive yet developed for winding, yet are easily applied in a lab or production environment.

Ultimately, perhaps the greatest contribution of this work is to embody the greater part of roll structure analytical and experimental knowledge in a single source. Thus, this work can serve as both a comprehensive tutorial and reference where none other exists.

Figure 8
BASIC CONTRIBUTIONS OF THIS RESEARCH



Thesis Overview

In addition to detailing the prototype measurement of stresses during winding, this thesis is also a rather complete treatment of roll structure. Chapter 2 develops the constitutive equations which describe the physics of the wound roll, and how they are assembled into models. Chapter 3 is a review of existing winding models, their application, and their limitations. Chapter 4 describes more complex roll behavior for which some analytical work exists such as air entrainment, centrifugal stresses, anelastic behavior and nips. Chapter 5 describes roll structure measurements based on impact, friction, strain, pressure and other parameters.

Chapter 6 derives the equations for the density analyzer, as well as documenting system design and sizing criteria. Chapter 7 derives the mathematics of a new winding model formulation which is the basis of this new work. Chapter 8 describes the particular hardware and Chapter 9 outlines the software used for this prototype. Chapter 10 develops a method for evaluating the accuracy and resolution of any roll structure measurement in general, and stresses in particular. Finally, Chapter 11 gives recommendations for improvement and future work. An extensive set of appendices is included which contains a complete bibliography, computer programs and output listings for the various winding models.

CHAPTER 2

PHYSICS OF THE WOUND ROLL

Roll Physics and Boundary Conditions

This chapter develops the constitutive equations which model elements of the behavior of a wound roll. These constitutive equations can then be assembled into a larger equation which describe the stresses resulting from the addition of a single wrap onto an existing roll. To model the winding of an entire roll, the effects of each wrap from the core to the finish diameter are added or superposed onto the previous stresses of all underlying layers. The principal results of this wound roll modeling are a prediction of material stresses at any diametral location, and at any time during the course of the winding of a roll.

The constitutive equations serve as the foundation of wound roll modeling. These equations include equilibrium which means the material is in a stable balance, strain-displacement which means no gaps or overlaps in the material are allowed, and stress-strain relations which describe the stiffness of a material. Though nearly all winding models use the same set of constitutive equations, they are approximations of real behavior. For example, the static equilibrium equation assumes the wound roll is not accelerating, yet the wound roll is in a very dynamic state during winding. The strain-displacement relations state there are no gaps formed, yet adjacent layers in a roll may not be in contact due to air entrainment, wrinkling and other causes. Finally, stress-strain relationships assume a single equation time invariant dependency, yet stress-strain curves vary with loading and unloading as well as with time due to creep and stress relaxation.

Despite the inevitable differences between modeling and real system behavior however, the constitutive equations are a close description of many winding situations. However, the assumptions and approximations of modeling must be clearly understood as they apply to any particular application. To validate wound roll analytical modeling, internal consistency can be checked as given in Chapter 3, and experimental measurements can be made such as outlined in Chapter 5. For this project, internal consistency is checked in Chapter 7, and experimental measurements are reported in Chapter 10.

The constitutive equations are then assembled into a larger second order differential equation which must be solved for the incremental stresses caused by the addition of a single wrap. This equation is described in the section on the roll. Additionally, a second order differential equation requires two boundary conditions. These boundary conditions are at the core and the outside of the roll, and are also described in the following sections. One of the major contributions of this research is an alternative description of the outer boundary condition. Finally, the differential equation must be solved for each wrap added from the core to the finish diameter of the roll. Though the winding equation will not be solved until Chapter 3, the accretion nature of the winding solution is described here.

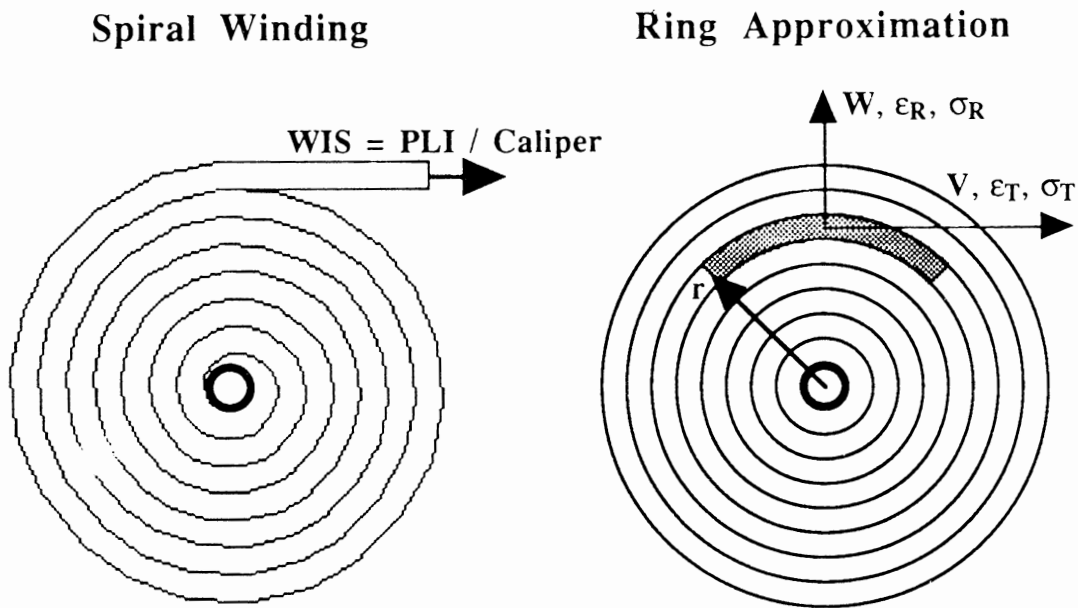
The Roll

The roll is wound under tension from the core outward to the finish diameter as a continuous spiral of a thin, flat and relatively flexible material. The number of layers comprising the finished roll can be as few as a couple dozen wraps for materials such as fiberglass batts or carpet, to more than 10,000 wraps for a large reel of paper. The objective of wound roll modeling is to calculate the incremental stresses within each layer of the roll due to the addition of each wrap of material, and ultimately to sum or integrate the effects of all wraps on the final stress distribution of the roll. Though the effect of each wrap is similar to the previous, the wound-in-tension (WIT), the roll outside diameter, radial modulus and other parameters will vary slightly.

The addition of wraps makes the wound roll model different from more typical structural analysis of cylinders whose geometry does not change significantly. Due to this geometry change, winding is an accretion problem which is difficult to analyze using more traditional approaches such as Finite Element Modeling, which would require changing the mesh and rerunning the analysis for each wrap added from the core to the finish diameter. Thus, the computational demand and complexity suggests an alternative approach may be more appropriate.

Most of the winding models begin by constructing a set of constitutive equations which define the behavior of the material in a cylindrical coordinate system as will be outlined below. Though winding is a spiral geometry, winding models make the approximation that each wrap is a separate concentric ring in non-sliding contact with the ring above and beneath as seen in Figure 9. Further assumptions typically state that the winding roll always remains cylindrical with no circumferential or axial variations.

Figure 9
SPIRAL WINDING AND RING APPROXIMATION



The next step is to derive the static equilibrium equations which state that the forces on any segment of a ring must balance in both the radial and tangential directions as seen in Figure 10. Though Yagoda [150, 151] and Chang [130] considered dynamic forces, most authors will simplify the math greatly by assuming dynamics are negligible. Since the model has cylindrical symmetry, the tangential direction equilibrium is automatically satisfied which leaves only the radial equilibrium to consider.

Summing the forces (stress times area) in the radial direction gives,

$$(1) \quad \sigma_R r d\theta - \left(\sigma_R + \frac{d\sigma_R}{dr} dr \right) (r + dr) d\theta + 2 (\sigma_T dr) \sin \frac{d\theta}{2} = 0$$

which can be simplified for small $d\theta$ to the equilibrium equation for plane stress as

$$(2) \quad r \frac{d\sigma_R}{dr} + \sigma_R - \sigma_T = 0$$

Figure 10
FORCES ACTING ON A WRAP SEGMENT

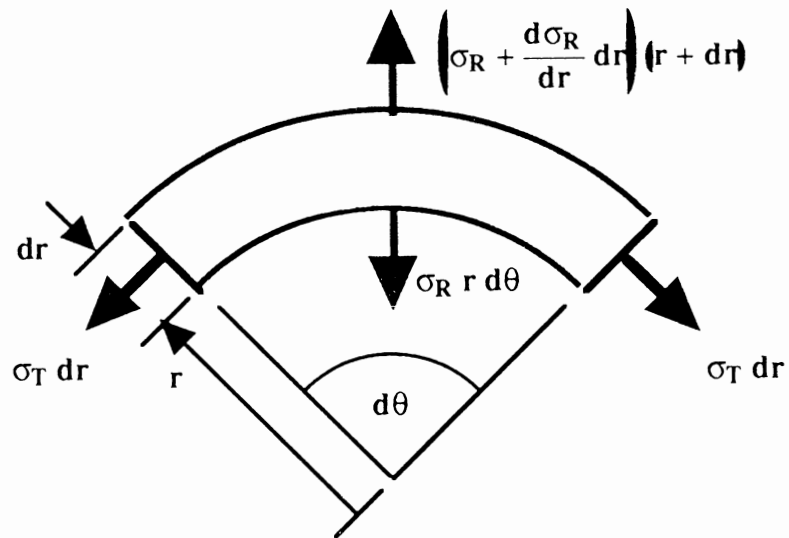
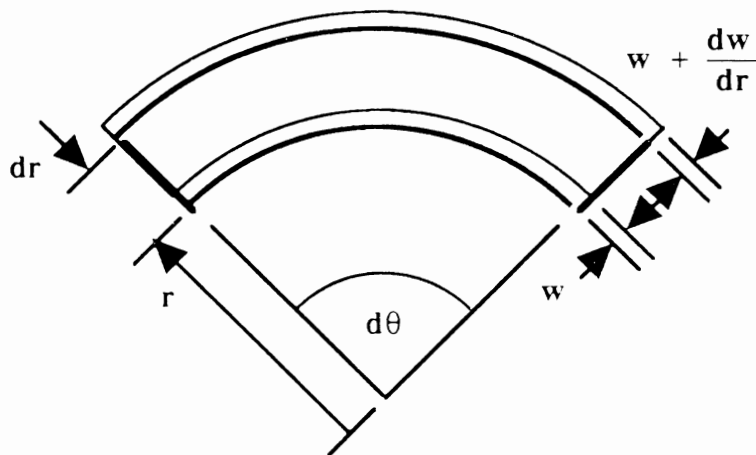


Figure 11
DISPLACEMENTS OF A WRAP SEGMENT



The strain-displacement relations are derived from the assumed displacements of the wrap segment as seen in Figure 11. Defining displacement w to be positive outward, the net radial deformation is

$$(3) \quad \left(w + \frac{dw}{dr} dr \right) - w = \frac{dw}{dr}$$

and the radial strain is the differential displacement divided by initial thickness or

$$(4) \quad \epsilon_R = \left(\frac{dw}{dr} dr / dr \right) = \frac{dw}{dr}$$

Similarly, the net circumferential deformation is

$$(5) \quad r d\theta - (r + w) d\theta$$

Hence, the circumferential strain is change in length divided by initial length or

$$(6) \quad \epsilon_T = \frac{w d\theta}{r d\theta} = \frac{w}{r}$$

Finally, the anisotropic material stress-strain relations are given by

$$(7) \quad \epsilon_R = \frac{\sigma_R}{E_R} - \mu_T \frac{\sigma_T}{E_T}$$

$$(8) \quad \epsilon_T = \frac{\sigma_T}{E_T} - \mu_R \frac{\sigma_R}{E_R}$$

Simultaneously solving equations (4), (6), (7) and (8) for the displacement w gives the second order differential equation for winding of linear anisotropic materials as

$$(9) \quad r^2 \frac{d^2 w}{dr^2} + \left(1 + \mu_T - \frac{E_T}{E_R} \mu_R \right) r \frac{dw}{dr} + \frac{-E_T}{E_R} w = 0$$

which has a solution of the form

$$(10) \quad w = C_1 r^\alpha + C_2 r^{-\beta}$$

At this time, it is appropriate to note that the winding differential equation can just as easily be expressed in terms of stresses and strains in addition to the displacement formulation shown above. Indeed, the equation will always be of the form

$$(11) \quad r^2 \frac{d^2x}{dr^2} + A r \frac{dx}{dr} + B x = 0$$

where the variable x could be either displacement w , stresses σ_R or σ_T , or strains ϵ_R or ϵ_T . Though the constants A and B as well as the two boundary conditions will depend on which variable the equation is expressed in, the solution techniques are the same and the results will be equivalent. As an example, the equation could be formulated in terms of σ_R as

$$(12) \quad r^2 \frac{d^2\sigma_R}{dr^2} + A r \frac{d\sigma_R}{dr} + B \sigma_R = 0$$

in which case the coefficients A and B are given as

$$(13a) \quad A = 3$$

$$(13b) \quad B = 1 - \frac{E_T}{E_R}$$

where equations (13) were simplified using a strain energy constraint [132, 133]

$$(14) \quad \frac{\mu_R}{E_R} = \frac{\mu_T}{E_T}$$

A *single ply* of many materials has a near linear stress-strain response for z -direction loading, which results in a constant out-of-plane modulus. However, a *stack* of even linear materials is often significantly non-linear for out-of-plane loading. Consequently, the radial modulus, E_R , is non-constant and is typically a function primarily of the radial loading, σ_R [79, 132, 133]. Thus in general,

$$(15a) \quad E_R = f(\sigma_R)$$

$$(15b) \quad E_T = f(\sigma_T)$$

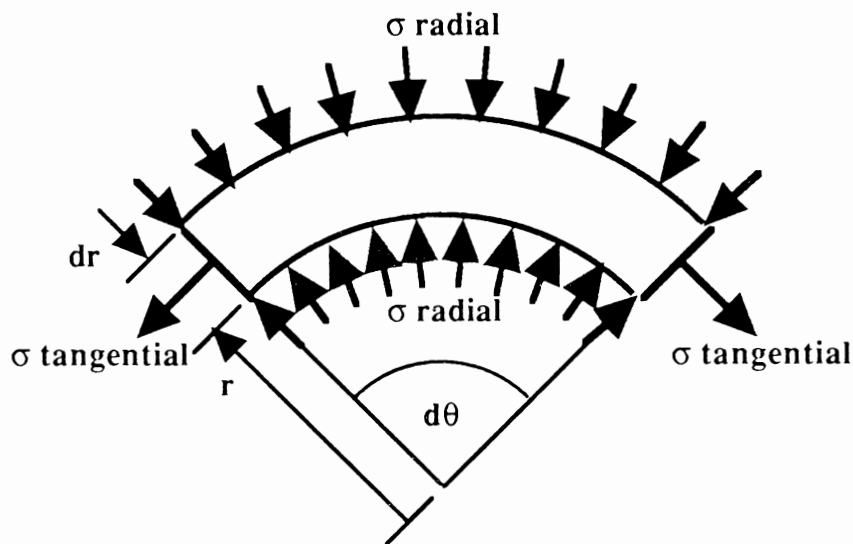
This non-constant modulus complication has numerous implications that will be treated more thoroughly in the next chapter on wound roll models. However, at this time it is appropriate to note that the assembly of the constitutive equations requires taking a derivative of an expression containing E_R and/or E_T with respect to radius. Since both moduli are varying with respect to radius because stresses vary with radius, high order terms will then appear in the A and B constants. These additional terms have not been noted in any of the previous winding models, which can be a significant oversight for some formulations.

In any case, the wound roll is described by a linear second order differential equation with non-constant coefficients. However, before a complete solution can be found, two boundary conditions associated with this second order equation must be specified. The first boundary condition is determined by the amount of support or stiffness provided by the core while the second is determined by the amount of tension on the outer wrap as it is wound into the roll. These essential boundary conditions will be described shortly.

It is timely to again restate the objective in wound roll modeling which is to calculate the material stresses inside the roll, at any radial location (wrap) and at any time during the winding process. As seen in Figure 12, the state of stress on any wrap is described by both radial stresses and tangential stresses which are interdependent through the equilibrium equation. The radial stresses are always compressive for non-adhering materials and represent the pressure between the layers of material. However, the tangential stresses may be tensile or compressive and represent the inplane loading of the material. As will be shown shortly, the value of these stresses are different for each layer of material.

Web stresses inside the roll are important as they have a profound influence on many defects. For example, if the compressive radial stresses are too low, the friction force between layers might be insufficient to lock the layers together to form a stable structure. Undesirable axial slippage, known as telescoping, and circumferential slippage, known as J-lining or gearing, result from external loading on rolls with low interlayer pressures [106, 108]. Additionally, a core supported roll may open up on the underside of the core if the interlayer pressure is less than the stresses due to gravity and core support loading [96, 102]. Conversely if the compressive radial stresses are too high, soft materials such as tissue may lose bulk permanently due to creep, while coated webs could smudge, and some films may 'wring' together. Tangential stresses also have similar restrictions. If tangential stresses are excessively high, materials can tear, burst or rupture. Conversely, if tangential stresses are too compressive on a thin flexible material, creping and starring could occur [109].

Figure 12
STRESSES ACTING ON A WRAP SEGMENT



Though analytical roll defect theories are yet to be developed, one can envision optimizing the structural design of a roll by specifying values for controllable variables which minimize defects associated with undesirable stress distributions. Blaedel outlined such an approach in his thesis 'A Design Approach to Winding a Roll of Paper' [128]. In his work, he described how penalty functions could be assembled and a minimum found which in theory would also minimize defects. As described earlier, the controllable parameters also have constraints, not necessarily related to roll structure, which also must be specified if the optimizing model is to well represent real winding.

Finally, it must be noted that the radial and tangential stresses can't be optimized independently because they are intimately coupled through the equilibrium equation. Generally this means that an optimum radial stress profile for example, could well result in an undesirable tangential stress profile and vice versa. For example, the typical near constant radial stress profile as a function of diameter provides pressure and friction required for roll structural stability. However, the coupled tangential stresses are then compressive and could lead to creping and buckling.

The Core

Core stiffness is one of the two boundary conditions used in all winding models. Though core stiffness is not as important as the wound-in-tension at the roll's current outer surface because it affects a much smaller volume of web, it is still important enough that it be treated thoroughly. Unfortunately, core stiffness has been inadequately covered in winding articles to date. Typically, core stiffness is defined without derivation or explanation of application. As a consequence, there has been confusion over the distinction between core stiffness and core material modulus. In this section, core stiffness is derived and discussed in detail, and will be shown to depend primarily by the modulus of the material it is made from (paper, steel or plastic), as well as its inside and outside diameters.

A derivation of core stiffness (E_c) begins by defining stiffness as a radial stress divided by a radial strain (nondimensional displacement w/r) at the core outer radius:

$$(16) \quad E_c = \left. \frac{\sigma_R}{w/r} \right|_{r=r_0}$$

where

E_c = core stiffness input to winding models

σ_R = radial pressure

w = radial displacement (positive outward)

r_0 = core outer radius = roll inner radius

Inserting the tangential strain-displacement relation (6), $\epsilon_T = \frac{w}{r}$, and pressure as a negative radial stress, into (16) gives

$$(17) \quad E_c = \left. \frac{\sigma_R}{\epsilon_T} \right|_{r=r_0} = \frac{-P_0}{\epsilon_T @ r=r_0}$$

where

P_0 = radial pressure between roll and core

ϵ_T = tangential strain

If we rewrite this equation in a more familiar form, we see that this definition of core stiffness appears similar to Hooke's Law except that the coupling is between radial stress and tangential strain.

$$(18) \quad \sigma_R = E_c \epsilon_T$$

The radial strain-stress relation for an isotropic material in cylindrical coordinates is

$$(19) \quad \epsilon_T = \frac{\sigma_T - \mu_c \sigma_R}{E_{cm}}$$

where E_{cm} is the Young's modulus for the core material which is different from the core modulus which we seek to define which is dependent on geometry as well as material.

The stresses on a pressurized isotropic cylinder are given by Roark and Young's "Formulas for Stress and Strain" [176] as

$$(20a) \quad \sigma_R = \frac{a^2 b^2 (P_o - P_i)}{b^2 - a^2} \frac{1}{r^2} + \frac{P_i a^2 - P_o b^2}{b^2 - a^2}$$

$$(20b) \quad \sigma_T = -\frac{a^2 b^2 (P_o - P_i)}{b^2 - a^2} \frac{1}{r^2} + \frac{P_i a^2 - P_o b^2}{b^2 - a^2}$$

where

- a = inner radius
- b = outer radius
- P_i = inner pressure
- P_o = outer pressure

Setting $r = b$, $P_i = 0$ and relabeling; P_o as P_0 , a as r_c , b as r_0 to be consistent with wound roll terminology, the radial and tangential stresses at the roll/core interface are given from equations (20) as:

$$(21a) \quad \sigma_R = -P_0$$

$$(21b) \quad \sigma_T = -P_0 \frac{r_0^2 + r_c^2}{r_0^2 - r_c^2}$$

Inserting (21a), (21b), and (19) into (17) and simplifying we get an equation for isotropic core stiffness as

$$(22) \quad E_c = E_{cm} \frac{r_0^2 - r_c^2}{r_0^2 + r_c^2 - \mu_c (r_0^2 - r_c^2)}$$

where

E_c = core modulus used in winding models

E_{cm} = core material modulus

μ_c = core Poisson ratio

r_0 = roll inner (core outer) radius

r_c = core inner radius

This equation can be nondimensionalized, as will be done shortly, or can be manipulated into a form more suitable for engineering calculation. Noting that core, pipes and tubes are commonly specified by an inner diameter ($d_c = 2 r_c$) and a wall thickness ($t_c = r_0 - r_c$) instead of radii, we can rewrite equation (22) as

$$(23) \quad E_c = 2 E_{cm} t_c \frac{d_c + t_c}{d_c^2 + 2(1 - \mu_c)[d_c t_c + t_c^2]}$$

At this time, it is appropriate to again clearly delineate the difference between E_c and E_{cm} . E_c is used in all winding models and is a core system stiffness which depends on material and geometry. E_{cm} is a material property which is the Young's modulus of the core material.

While equations (22) and (23) are descriptive of cores constructed of isotropic materials, fiber cores are slightly anisotropic so that this case must also be developed. The anisotropic case can be derived from previous definitions along with the tangential stress distribution of an anisotropic cylinder with external pressure which can be derived from Altmann's [127] equation (44)

$$(24) \quad dT = \left(\frac{\alpha - a \beta r^{-2\gamma}}{r^b} \right) \left(\frac{s^b}{1 + a s^{-2\gamma}} \right) \frac{T_w}{s} ds$$

where dT is the contribution of tangential stress at nondimensionalized radius r by a pressure T_w / s on the outside of an anisotropic cylinder of nondimensionalized outer radius s and

$$\begin{aligned}\Xi_R &= \frac{E_T}{E_R} \\ \Xi_C &= \frac{E_T}{E_C} \\ \mu &= \frac{1}{2}(\mu_T + \Xi_R \mu_R) \\ \delta &= \frac{1}{2}(\mu_T - \Xi_R \mu_R) \\ \gamma &= \left| \sqrt{\delta^2 + \Xi_R} \right| \\ \alpha &= \gamma - \delta \\ \beta &= \gamma + \delta \\ a &= \frac{\gamma - \mu - \Xi_C}{\gamma + \mu + \Xi_C} \\ b &= 1 - a\end{aligned}$$

Noting that for this application, $r = s$ and $dT = \sigma_T$, and $T_w/s = \sigma_R$, we can rewrite (24) as

$$(25) \quad \sigma_T = \sigma_R \left(\frac{\alpha - a \beta s^{-2\gamma}}{1 + a s^{-2\gamma}} \right) @ r = s$$

where s is the ratio r_0 / r_c . Inserting (25) into the core stiffness definition (17) and using the stress-strain relation (6), a solution of the anisotropic core stiffness is given as

$$(26) \quad E_c = \frac{E_{cR} E_{cT}}{E_{cR} \left(\frac{\alpha - a \beta s^{-2\gamma}}{1 + a s^{-2\gamma}} \right) - \mu_{cR} E_{cT}}$$

where $\Xi_C = 0$ for the intermediate parameters given in (24). The radial and tangential moduli can be measured by cutting a small rectangular specimen and measuring strains as it is loaded uniaxially in two directions.

The anisotropic core equation (26) can be checked against the isotropic core equation (22) by setting $E_{cm} = E_{cR} = E_{cT}$ and $\mu = \mu_{cR} = \mu_{cT}$ giving intermediate parameters

$$\Xi_R = 1, \Xi_C = \infty, \mu = \mu, \delta = 0, \gamma = 1, \alpha = 1, \beta = 1, a = -1, \text{ and } b = 0$$

and equation (26) then becomes for the isotropic case

$$(27) \quad E_c = \frac{E_{cm}}{\frac{\left(\frac{r_0}{r_c}\right)^2 + 1}{\left(\frac{r_0}{r_c}\right)^2 - 1} - \mu}$$

which is entirely equivalent to (22).

With equations (22), (23) or (27), core stiffnesses can be calculated for commonly used cores and compared against values used in the literature. Table 1 was generated using $E_{cm} = 500,000$ PSI and $\mu_c = 0.3$ which are typical values for the fibre and plastic material used to manufacture cores.

From this table, it can be seen that E_c increases with increasing E_{cm} and increasing nondimensional wall thickness (t_c / r_c). Additionally, with the exception of Schedule 40 steel pipe, the core modulus varies only slightly for the wide range of applications shown. These results are similar to the historically assumed values of core stiffness; Yagoda [149-153] with a modulus of 20,000-100,000; Altmann [127] with a modulus of 100,000; and Hakiel [132, 133] with 100,000 and 200,000 psi.

If we use Yagoda's model [152, 153] and a standard set of input parameters, to be detailed later, we can observe the effect of core stiffness on the stresses near the core. Figure 13 shows that the tangential stresses on the first few wraps near the core vary from a 2600 psi compressive stress for a zero stiffness core to a 500 psi tensile stress for an infinitely stiff core. Unfortunately, the largest sensitivity to core stiffness corresponds to values similar to real cores so that greater care should be used to select appropriate values. If the core is too soft, the tangential stresses near the core will be large and compressive which increases the potential for buckling and creping.

Radial stresses near the core are not plotted here because there is much less sensitivity to core stiffness. The radial stresses vary from only 0 to 61 psi for core stiffnesses of zero and infinity respectively. Additionally, the depth of effect is also somewhat smaller. As the anisotropy of the web material is increased however, the effect of core stiffness is somewhat greater in magnitude and influences a much larger depth and volume of web material. For the case presented here however, the effect of core stiffness extends to only about 10% of the radius range which comprises only about 1% of the volume of material in that roll.

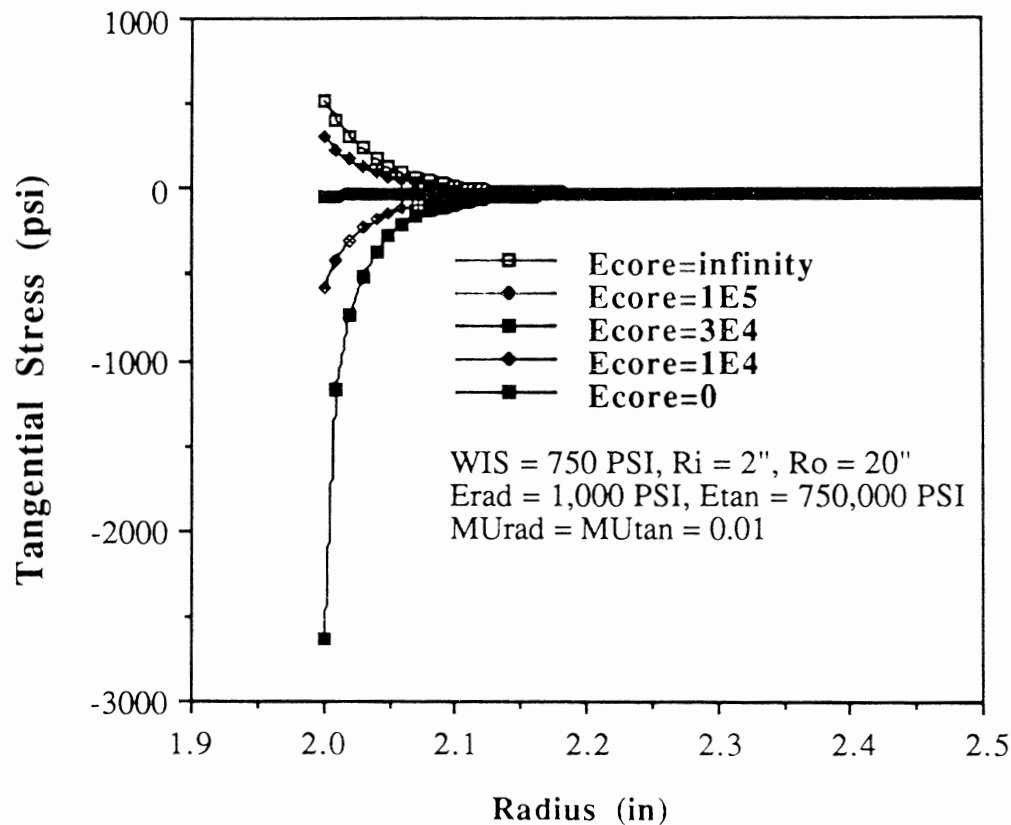
Table I
THE STIFFNESS OF COMMONLY USED CORES

<u>Material</u>	<u>Inner Diam.</u>	<u>Wall Thick.</u>	<u>E_c</u>	<u>Notes</u>
Fibre/Plastic	1.5	0.1	64,672	consumer rolls
"	3.0	0.25	80,147	film, paper
"	"	0.50	152,838	"
"	4.0	0.50	117,493	"
"	"	1.0	217,391	"
"	6.0	1.0	152,838	board grades of paper
Steel	3.068	0.216	4,090,124	lightweight coated paper

Despite the seemingly well behaved core boundary condition as presented previously in this section, there are several complications that need to be considered for accurate wound roll modeling. These complications include hygroscopic behavior of fiber cores, deflections and geometry. However, this project will only briefly review the major mechanics implications of complex core behavior on roll winding. For further information, the reader can turn to the bibliography which contains a separate section for publications on cores.

Spiral fiber cores are continuously wound from multiple narrow strips of kraft paper which have passed through a (sodium silicate) adhesive bath [2, 3, 5, 9, 13]. The number of strips and their thickness determines the nominal wall thickness of the core. These strips are continuously wound on a helix under tension from a crossed winding belt on a mandrel [136]. After the cores are cut to length, they are then air or oven dried [1]. However, a problem results if fiber cores are not dried to hygroscopic equilibrium prior to winding. A wet core inside a roll will give up moisture to its environment and shrink radially in the process. As a consequence, some or all of the radial pressure at the core can be lost as the core dries which increases the propensity to telescoping.

Figure 13
CORE STIFFNESS AND TANGENTIAL STRESS



Other core modeling problems result from deflection. An example is the extremely nonuniform nip across the width of an end loaded core which is nipped against a drum or roller [11]. Not only does the deflection result in deviations from cylindricity, the wound-in-tension (WIT) is also nonuniform across the width because of nip non-uniformity. Another example is cores that are bowed due to residual stresses of manufacturing or creep during storage [11]. These bowed cores cause winding tensions and nips to be nonuniform across the width, and as a function of rotational position. Additionally, cores will tend to buckle under excessive axial chuck load which causes nonuniform nips and tensions.

Finally, cores are not necessarily uniform in geometry. Diametrical differences between cores of a single set will cause large differences in wound-in-tension on a two drum winder. The small cores will see a much smaller torque, nip and tension than the larger cores in that set. Similarly, diametrical differences within a single core are even found on recycled iron cores which are belled on the ends from unwind chucks [10]. Also, many cores are notched on the ends which gives a nonuniform radial support and can cause high roll reject rates due to crepe wrinkling on lightweight grades [11, 191, 192].

The Roll Outside

The second boundary condition required to solve the second order differential boundary valued winding equation comes from the outer surface of the roll. The ingoing wrap of material is under some tension which varies with diameter, and as a function of the TNT's (torque, nip, and tension), as well as other physical properties such as drum roller surface, drum capstan wrap angle, and the coefficient of friction between the web and the drum roller. Traditionally the wound roll models have assumed a wound-in-tension (WIT) as a function of rewind roll diameter. From WIT, one can calculate the outer boundary condition either as

$$(28a) \quad \sigma_R = \frac{-WIT}{r_n} @ r = r_n \quad \text{or}$$

$$(28b) \quad \sigma_T = WIS = \frac{WIT}{h} @ r = r_n$$

where

WIS = wound-in-stress (lb/in²)

WIT = wound-in-tension (lb/in)

h = web sample thickness or caliper (in)

r_n = radius to the roll outside at the current sample (in)

If the winding differential equation is posed in terms of radial stress as most authors have done, then the boundary condition (28a) is used. However as mentioned earlier, the differential equation can be formulated in terms of radial stress, tangential stress, radial strain, tangential strain, or radial displacements. If the equation is posed in terms of tangential stresses, then (28b) could be used. However, there is a subtle difference because (28b) is a tangential boundary condition for the middle of the outer wrap, while (28a) is for the pressure between the underside of the outer wrap and the top side of second wrap.

Similarly, the differential equation could also be posed in terms of strains. However, the boundary conditions would then require known strains which are presently unmeasurable. Though another valid boundary condition is that the radial stress is zero at the outer surface, this would yield a zero stress solution because the outer boundary condition needs to be nonzero to 'force' a non-trivial solution.

To reiterate, the winding differential equation can be formulated in a number of equivalent ways. However to apply the winding models, the outer boundary condition must be measurable. For the traditional radial stress formulations, WIT has been extremely difficult to measure in practice except for the rather limiting case of pure centerwinding. Thus, wound roll modeling with the traditional formulation has been more of an academic exercise than an applicable tool. This is exacerbated by a dearth of roll defect theories which could help determine optimum stress profiles.

Another approach, which is the basis of this work, is to use an alternative boundary condition that could be more easily measured. This is done by noting that web caliper and roll radii can be measured during winding, and that the deformation of the outer roll surface uniquely determines a boundary condition. More specifically, the stress induced displacement of the outer surface of the roll is the difference in radii between consecutive samples minus the summation of the caliper of the N individual layers comprising that sample, or written as an expression,

$$(28c) \quad w_k = (r_k - r_j) - \sum_{n=1}^N c_{k,n}$$

This new boundary condition, more completely described in Chapter 7, is one of the major contributions of this research and allows a new and useful way to reformulate all present winding models.

The radii at consecutive samples can be accurately measured in a manner similar to the density analyzer using encoders as described in Chapter 6, and the caliper can be measured using a variety of contacting or non-contacting gages. Hence, the outer roll displacement can be determined which allows a unique solution of the WIS during that sample. Since this allows an indirect measure of WIS as a function of roll diameter, radial and tangential stresses at any point in the roll and at any current diameter can be calculated using one of many wound roll models. Thus, instead of assuming a WIS profile, it can be inferred from measurements of radius and caliper using wound roll equations.

The Accretion Nature of Winding

With a solution to the boundary valued winding differential equation, to be derived later, one can calculate the incremental stresses inside the roll due to the addition of only one 'wrap'. However, a complete solution requires recalculating the incremental stresses at each internal wrap and adding them to the previous stresses, for each wrap added from the core to the finish diameter. At each step, one has a snapshot of the radial and tangential stress profile at that instant of time and at that current outer diameter.

After the addition of the first wrap, a single calculation for radial and tangential stresses are made for wrap one. After wrap two, calculations are made for wrap one and two and so on to give an arithmetical progression of the number of calculations required. Written as an equation, the number of calculations required are

$$(29) \quad \# \text{ calculations} = \sum_{\text{wrap } i=0}^n i = 1 + 2 + 3 + \dots + n = \frac{n(n+1)}{2}$$

Hence, the number of calculations is approximately proportional to the square of the number of wraps.

The thickness of wraps in the real roll and the thickness of 'wraps' in the wound roll model need not be necessarily equal. However, there are several constraints that must be met when choosing a wrap thickness for wound roll models. The first requirement in that regard is that the number of wraps must be large enough to give a good resolution of the rapidly changing stress gradient, but not so large as to cause excessive computation time or numerical instability. The second requirement is that the WIS profile must be equal for the real roll and the roll model. For example, a 0.001" thick web under 1000 psi WIS, which would give a WIT of 1 PLI, could be modeled by a 0.01" thick web under 1000 psi WIS, which would give a WIT of 10 PLI.

To check whether sufficient wraps are used in a wound model, one needs to run the model using two different wrap thicknesses (same core and finish diameter), and compare the stress profiles. For example, a 0.1" thick wrap (180 wraps and 16,290 calculations) and a 0.05" thick wrap (360 wraps and 65,980 calculations) yield a 3% maximum difference for a particular set of parameters [115]. This indicates that 200 wraps will give sufficient engineering accuracy for that particular set of parameters. This check should be considered when setting up wound roll models. The higher the anisotropy or variation in WIS profiles, the larger the number of wraps which are required to calculate stresses to a given accuracy.

CHAPTER 3

WOUND ROLL MODELS

Overview of Wound Roll Models

Wound roll web stresses, as described in Chapter 1, must be controlled to minimize damage to the product. Additionally, the wound roll stress profiles must be controlled so that the roll will have sufficient structural integrity to maintain its cylindrical geometry despite subsequent handling loads. The purpose of wound roll modeling is to predict web stresses inside the roll as a function of material properties, geometry and WIT (wound-in-tension) profiles. These computer simulations allow wound roll design experimentation to take place off-line without risk to the product. These simulations can be used to find optimum winding conditions which can then be verified experimentally with trials on pilot plant or production winding machines.

Wound roll modeling using mechanics formulations, such as described in Chapter 2, was first developed over three decades ago. Since then, there have been numerous models developed by industrial and academic researchers. While these models generally use the same constitutive equations, there are differences between them in terms of generality, mathematical development, and computational performance. These differences will be explored in this chapter.

The primary difference in the models is an evolution whereby the models have become more general in the behavior that can be described, and thus more representative of real winding. The trend is most apparent in terms of moduli where the isotropic model [131] was superseded by a linear anisotropic model [127], and finally by a nonlinear anisotropic model [132, 133]. Each model is a superset of the previous such that it could describe new behavior in addition to that described by earlier models. Additionally, complex behavior such as stress relaxation [144, 145] and centrifugally induced stresses [150, 151] were also modelled. Current research is focused on extending winding models to the cross direction and describing the behavior of a nip.

Another difference between models is the mathematical techniques used to assemble the constitutive equations into a working set of equations. The equation for the incremental pressure distribution for the addition of a single wrap on the isotropic model is a closed-form equation. However, the anisotropic model produces an integral which can't be solved explicitly, so must be evaluated numerically [127] or by using series approximations [149-153]. Finally, the nonlinear anisotropic model has no closed-form solution but rather is solved as a matrix of finite difference approximations for each layer in the roll, and for each layer added [132, 133].

In the development of the more complex models, some higher order terms are omitted for solution expediency. As will be shown, neglecting terms can have anything from a negligible to debilitating effect on solution accuracy depending on the model and input parameters used. Similarly, though most of the models described here are absolutely rigorous, the choice of different solution techniques results in varying computer performance and accuracy. As will be shown, winding models are ill-conditioned and prone to numerical difficulties. It is easy to find sets of input parameters whose solution time and accuracy varies by several orders of magnitude from one model to the next.

Consequently, the distinct winding models will be checked for rigorously accurate mathematical development, as well as solution performance. Despite the differences in development of the models, one expects that they yield the same stresses for the same set of input parameters. Thus, by comparing the outputs of each of the models for the same set of inputs we can verify the performance of each. Appendix B contains a standardized set of input parameters as well as the outputs from the various models. This close inspection of winding model development and performance have yielded some surprises that will be described in this chapter.

A Simple Linear Isotropic Model

The linear isotropic model is the oldest winding model dating from the late 1950's with Gutterman's work for the US government on magnetic tape winding [131]. Shortly thereafter, similar work was also performed by Catlow and Walls for the textile industry [129]. Since then many other authors have reported results using simple isotropic modeling [134, 135, 146, 147, 154, 179]. Finally, this model was also independently derived by the author for the Beloit Corporation winding studies and serves as the basis for this report [115].

The linear isotropic model has several disadvantages with respect to more modern models because the assumption of isotropy does not well model typical paper and film winding because the ratio of the tangential to radial moduli can approach 1,000 for some materials. Additionally, the linear model often does not run significantly faster than less restrictive models for a given solution accuracy. Despite these limitations however, this model does have unique features which can justify its discussion:

1. It is an ideal introduction to winding models for instructional purposes because of its simplicity, yet it retains a similar development and set of constitutive equations as the more sophisticated models.
2. It is a useful check for the proper behavior of other winding models. If linear isotropic parameters are chosen for a modern model, it must yield the same answers as this simple model. Using this linear isotropic model, a restriction was found on the Yagoda linear anisotropic model. Though Yagoda's formulation is the fastest and most accurate solution for linear anisotropy, it is incapable of solving certain combinations of input parameters including the isotropic case.
3. There may be applications of the winding of thick linear isotropic materials, such as steel or linoleum which might be modeled adequately with a simple model.

The radial and tangential stress distribution for a linear isotropic thick-walled cylinder due to internal and external pressure is given in several handbooks [176], and is also rederived by Roisum from displacement fields [115] as:

$$(30a) \quad \sigma_R = -\frac{r_j^2 r_0^2 (P_j - P_0)}{r_j^2 - r_0^2} \frac{1}{r^2} + \frac{P_0 r_0^2 - P_j r_j^2}{r_j^2 - r_0^2}$$

$$(30b) \quad \sigma_T = -\frac{r_j^2 r_0^2 (P_j - P_0)}{r_j^2 - r_0^2} \frac{1}{r^2} + \frac{P_0 r_0^2 - P_j r_j^2}{r_j^2 - r_0^2}$$

where:

P_j = external pressure (between current outer wrap j , and body of roll)

P_0 = internal pressure (between roll and core)

r_j = (current) roll outside radius

r_0 = roll inner (core outer radius)

The pressure, P_j , between the current outer wrap j and body of the roll is calculated from the winding tension or stress as:

$$(31) \quad P_j = \frac{WIT_j}{r_j} = \frac{h \text{ WIS}_j|_{r=r_j}}{r_j}$$

Equation (31) is a restatement of the outer boundary condition given in equations (28). The variables in equations (30) are generally known with the exception of the core pressure P_0 which can be derived using the definition of core stiffness derived previously (16):

$$(32) \quad E_c = \frac{\sigma_R}{\epsilon_T} \Big|_{r=r_0} = \frac{-P_0}{\epsilon_T @ r=r_0}$$

While the tangential strain in the roll for an anisotropic cylinder is given as (8), the isotropic cylinder is simplified to:

$$(33) \quad \epsilon_T = \frac{\sigma_T - \mu \sigma_R}{E}$$

If we set $r = r_0$ in equations (30), insert into (32) and (33), and solve for P_0 (using Macsyma® on the Symbolics 3650), we calculate the core pressure as:

$$(34) \quad P_0 = P_j \frac{2 r_j^2 E_c}{(r_j^2 - r_0^2)(E + \mu E_c) + (r_j^2 + r_0^2) E_c}$$

Now the stress distribution due to the addition of one wrap of thickness h during winding can be calculated using equations (30) for the stress distribution given the outer pressure from (31), and the core pressure from (34). In other words, the change in the roll's internal stress distribution caused by the addition of a single wrap is calculated for all internal wraps from the core and current outer radii as a function of Young's modulus E , core modulus E_c , the WIT (Wound-in-Tension) and wrap thickness h .

The wound roll model computer program then simply increments the outer wrap j by the 'wrap thickness' h for radii from the core to the finish radius. At each wrap, the program calculates the incremental contribution of that external wrap to all internal wraps and adds the result to the previous values using the principle of superposition. An outline of the computer code to solve this linear isotropic winding model, which is similar to many of the other models, is as follows:

```

input variables
initialize tangential stress array using a function describing the wound-in-stress distribution
increment external wrap j from core to finish radius loop in steps of h
    calculate wound-in-stress at current outer radius
    calculate  $P_j$  from equation (31)
    calculate  $P_0$  from equation (34) and core stiffness equation (22, 23, 26 or 27)
    increment internal wrap i from core to current outer wrap j stress loop in steps of h'
        calculate incremental radial stress from (30a)
        calculate incremental tangential stress from (30b)
        update radial and tangential stresses (new stress = old stress + incr. stress)
    end stress loop
end wrap loop
print final stress distribution

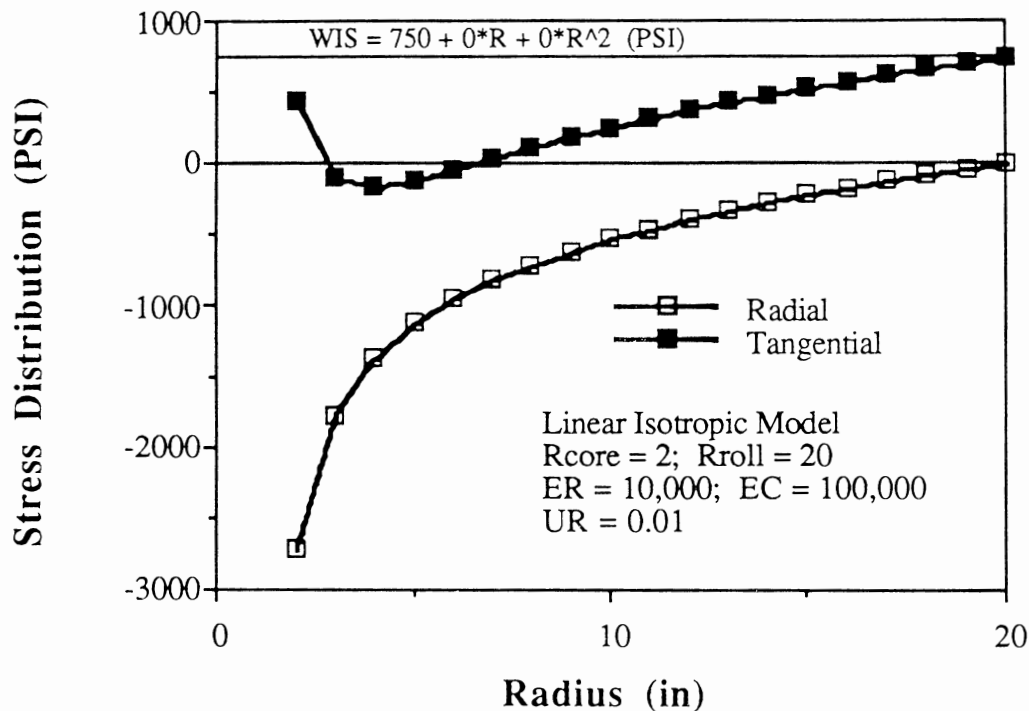
```

There are two stepsize increments for the two nested program calculation loops. The first increment is the outer loop of the program which is incremented from the core radius plus h , to the finish radius of the roll r_n , in increments of the calculation wrap thickness (h). As described at the end of Chapter 2, the choice of calculation wrap thickness (h) is arbitrary and need not equal the real web thickness as long as the WIS (wound-in-stress) is the same for calculation and real web thicknesses. The choice of calculation thickness is a compromise between accuracy and solution time.

Generally as the calculation wrap thickness (h) is decreased, and consequently the number of calculation wraps increases, the solution accuracy will increase. However, the solution time will also increase approximately by the square of the number of calculation wraps as given by (29). Though some models may have numerical instability if the number of calculation wraps is too great, the isotropic model is generally well-behaved in this regard.

The inner program loop is incremented from the core radius to the current winding radius in steps of the print increment in radius (h'). The print increment in radius (h') has no effect on accuracy but only determines the number of radii at which stresses are calculated. For the isotropic model, the solution time will increase inversely proportionally to the print increment in radius (h'). Though the choice of print increment in radius (h') is again arbitrary except that it must be an integral multiple of the calculation wrap thickness (h), for simplicity h' is generally chosen to be equal to h . An example stress distribution for the isotropic model is shown in Figure 14.

Figure 14
STRESS DISTRIBUTION FOR THE ISOTROPIC MODEL



Despite the oversimplifications of the isotropic model, there are several conclusions that can be obtained that will in general hold using more general models:

1. The radial stress at the outside of the roll is always zero because there are no externally applied pressures.
2. The radial pressure is always compressive, and generally becomes more compressive at increasing distances from the roll outside.
3. The tangential stress at the outside of the roll is always equal to the wound-in-stress (WIS) because that was one of the requisite boundary conditions for the solution.
4. The tangential stress, which is initially tensile at the current roll outside, decreases at increasing distances from the roll outside and may become compressive.
5. There are high stress gradients in the vicinity of the core.
6. The simple isotropic model is linear and superposition holds such that doubling the value of a constant WIS profile will double the value of stresses at all wraps. However, the superposition assumption will not be valid for all cases and particularly for the modern nonlinear models.

Linear Anisotropic Models

Anisotropy is a characteristic of some materials which have properties whose values depend on the direction of measurement. In particular, many wound roll materials have Young's moduli (stiffnesses) which are greater in the MD (machine direction) than in the ZD (out-of-plane direction) [56, 57, 115]. Materials such as film can be slightly anisotropic due to manufacturing processes which may pull long molecular chains to a preferred orientation. Paper, which is composed of a complex network of wood fibers, can be highly anisotropic because fibers themselves have a much higher stiffness along their axis than across it, and are generally oriented in the plane of the web. However, even metals which have a very linear stress-strain response as a single web can be anisotropic when measured as a stack property.

Wound roll models simplify the fully anisotropic condition to that of an orthotropy such that there are three independent moduli in the MD, CD and ZD and several Poisson ratios. The three principal axes of the material are mutually perpendicular and closely aligned with the roll. The MD of the web corresponds to the tangential direction in the roll, the CD of the web corresponds to the axis of the roll, and finally the ZD of the web corresponds to the radial direction in the roll. Further simplification results for most models which do not consider variation along the CD. This leaves two moduli, E_R and E_T , and two Poisson ratios, μ_R and μ_T , which describe the behavior of the wraps of material as it is wound into a roll for most of the currently used models.

While E_T can be measured as a single strip in a standard tensile test machine, E_R must be measured as a stack. In both cases, the applied load or stress and the resulting deflection or strain are measured in the direction corresponding to the MD and ZD of the material. The anisotropy ratio of the stack material, which is simply the ratio E_T/E_R , has a large effect on the resulting wound roll stress patterns and can vary from just over 1 to more than 1,000 for typical web materials.

The Poisson ratios describe the strains in one direction resulting from loads applied in another. The Poisson ratio μ_R , sometimes denoted as μ_{TR} , represents the ratio of strain in the tangential direction divided by the strain in the radial direction for loads applied in the tangential direction. Similarly μ_T , sometimes denoted as μ_{RT} , represents the ratio of strain in the radial direction divided by the strain in the tangential direction for loads applied in the radial direction. The effect of Poisson ratios on wound roll stress patterns are usually much smaller than moduli [148], and many materials such as paper have near zero Poisson ratios.

Direct measurement of stack Poisson ratios are extremely difficult in practice [115], and many authors use relationships between more easily calculated properties to indirectly predict these ratios [55, 59, 61, 84]. For example, Hakiel correctly observed that the strain energy constraint

$$(35) \quad \frac{\mu_R}{E_R} = \frac{\mu_T}{E_T}$$

predicts that the two Poisson ratios are not independent [132, 133]. However, it should be noted that these relationships are derived from solid mechanics of ideal materials, whereas stacks are structures composed of often less than ideal materials. Indeed, the application of the constraint to predict one Poisson ratio given the measurement of the other along with moduli has not always agreed with experimentally measured results. Furthermore, most authors do not use this constraint as it reduces the generality of the model and does not simplify the math significantly. However as mentioned earlier, since the sensitivity of winding models to Poisson ratios is slight, the debate over whether to apply these relationships is somewhat academic.

In the next two sections, two linear anisotropic models are discussed which represent the next step in the evolution of winding models. These models by Altmann and Yagoda use the same constitutive equations, share an identical initial development, but use different techniques for solving the winding integral. Consequently, the primary differences are in the accuracy and speed of computation. As will be shown, while Yagoda's model is usually much faster and more accurate, it suffers from a small loss in generality in dealing with small anisotropy ratios and variable WIS (wound-in-stress) profiles.

Altmann Model

The first linear anisotropic winding model was formulated by Heinze Altmann in 1968 [127]. He began with the governing differential equation for winding in cylindrical coordinates assembled from the constitutive equations described in Chapter 2 which are

$$(36) \quad r^2 \frac{d^2 W}{dr^2} + \left(1 - \frac{E_T}{E_R} \mu_R + \mu_T\right) r \frac{dW}{dr} - \frac{E_T}{E_R} w = 0$$

with boundary conditions

$$(37a) \quad E_C = \frac{\sigma_R}{W/r} = \frac{\sigma_R}{\epsilon_T} @ r = r_0$$

$$(37b) \quad \sigma_R = \frac{-WIT_j}{r_j} \quad @ \quad r = r_j$$

where

w = Radial Displacement (in)

r = Radial Location (in)

r_0 = Inner (Core) radius (in)

r_j = Current outer radius (in)

E_C = Core Modulus (lb/in²)

E_R = Radial Modulus (lb/in²)

E_T = Tangential Modulus (lb/in²)

μ_R = Radial Poisson Ratio

μ_T = Tangential Poisson Ratio

σ_R = Radial Stress (lb/in²)

σ_T = Tangential Stress (lb/in²)

WIT_j = Current Winding Tension (lb/in)

The assumed form of the solution is

$$(38) \quad w = A r^\alpha + B r^{-\beta}$$

which can be verified to satisfy the differential equation [115, 127]. The next step is to write the differential equation for the boundaries of the range to the core and the current outside. This will yield two equations to solve for the particular solution constants A and B. Altmann had considerable insight into the nondimensionalization of the elastic and geometric parameters so that the derivation did not become unwieldy. Roisum [115] rederived the solution from Altmann's [127] outline to verify integrity and through this exercise gained appreciation of the elegance of the solution. Later, Roisum used the computer algebra application Macysma to find alternative solution formulations, which though correct were more cumbersome than Altmann's. After considerable algebra, the solution for the radial and tangential stress distribution inside a winding roll for a single wrap of thickness ds is given as

$$(39a) \quad d\sigma_R = - \left(\frac{1 + a r^{-2\gamma}}{r^b} \right) \left(\frac{s^b}{1 + a s^{-2\gamma}} \right) \frac{WIS_s}{s} ds$$

$$(39b) \quad d\sigma_T = - \left(\frac{\alpha - a \beta r^{-2\gamma}}{r^b} \right) \left(\frac{s^b}{1 + a s^{-2\gamma}} \right) \frac{WIS_s}{s} ds$$

where the secondary parameters are defined as:

$$\begin{aligned}
 \Xi_R &= \frac{E_T}{E_R} \\
 \Xi_C &= \frac{E_T}{E_C} \\
 \mu &= \frac{1}{2}(\mu_T + \Xi_R \mu_R) \\
 \delta &= \frac{1}{2}(\mu_T - \Xi_R \mu_R) \\
 \gamma &= \sqrt{\delta^2 + \Xi_R} \\
 \alpha &= \gamma - \delta \\
 \beta &= \gamma + \delta \\
 a &= \frac{\gamma - \mu - \Xi_C}{\gamma + \mu + \Xi_C} \\
 (40) \quad b &= 1 - a
 \end{aligned}$$

and s is the dummy variable of integration from internal radius of interest r , to finish outside radius R . The spatial variables, s , r , and R , are nondimensionalized with respect to core radius to simplify the derivation and condense the formulas. The accretion nature of the wound roll system then is modeled by simply integrating the contribution to the incremental stresses, $d\sigma_R$ and $d\sigma_T$, from the radius of interest r to the finish outside radius R . Additionally, the initial wound-in-stress for each layer, WIS_s , must be added or superimposed upon the stresses caused by layers added above. Thus, the final stress distribution is given as

$$(41a) \quad \sigma_R = - \left(\frac{1 + a r^{-2\gamma}}{r^b} \right) \int_r^R \left(\frac{s^b}{1 + a s^{-2\gamma}} \right) \frac{WIS_s}{s} ds$$

$$(41b) \quad \sigma_T = WIS_s - \left(\frac{\alpha - a \beta r^{-2\gamma}}{r^b} \right) \int_r^R \left(\frac{s^b}{1 + a s^{-2\gamma}} \right) \frac{WIS_s}{s} ds$$

Although this is a closed form expression for wound roll stresses, the integral must be evaluated numerically because b and γ are not integers, and the WIS profile with respect to current winding outer radius will not in general be a simple function. An outline of the computer code to solve Altmann's winding model is as follows, and the code is given in the Appendix A.

```
input variables
calculate intermediate parameters
increment internal radius loop
    goto subroutine integrate lower decade
    goto subroutine integrate upper decade
    calculate stresses
end increment radius loop
print stress distribution

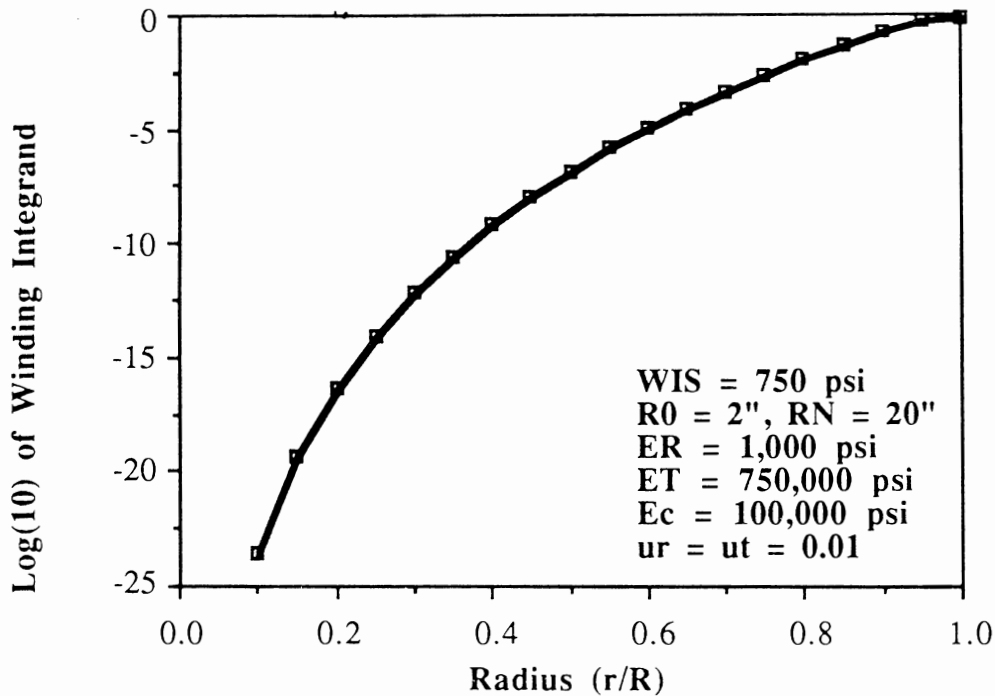
subroutine integrate (from internal radius of interest to finish radius)
    initialize
    integrate loop
        calculate integration panels using Simpson or similar technique
    end integrate loop
return from subroutine
```

The increment for the loop in main program's body determines the interval over which stresses will be calculated and printed, and has no effect on the accuracy of the solution. However, the increment size for the integration subroutine loop does have a tremendous effect on solution accuracy. Several numerical integration techniques were investigated to find an accurate and practical integration method to calculate this extremely difficult integral, and will be discussed in more detail shortly.

Plotting the winding integrand from equations (41) as a function of radius, it becomes apparent why the integral is so difficult to solve with numerical accuracy. As seen in Figure 15, the integrand can easily vary more than 25 orders of magnitude from one end of the range to the other. The gradient is steeper with higher anisotropies and higher finish/core diameter ratios. The steeply varying characteristics of the integrand as a function of radial position is also shared by stresses, strains and displacements due to the addition of a single wrap. This behavior is caused because each layer tends to be self supporting to the pressures from layers above, much as an arch can support external loads without internal support. Consequently, the addition of a single wrap significantly affects only the first few wraps immediately beneath, and diminishes rapidly with depth.

Figure 15

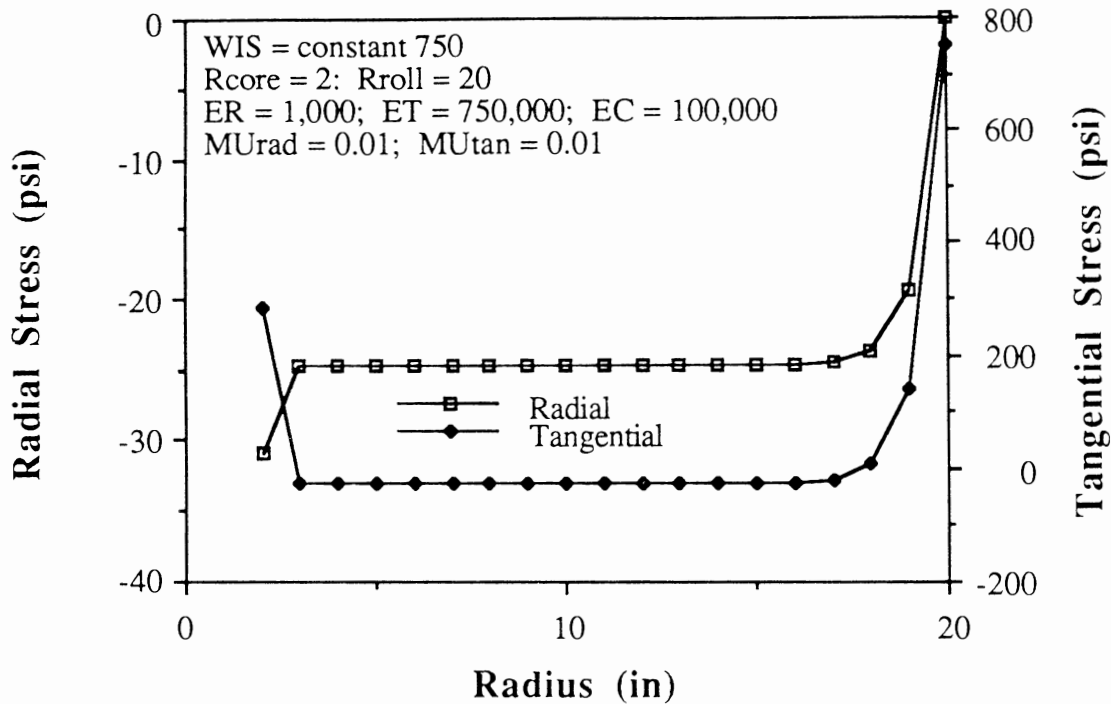
THE WINDING INTEGRAL VS RADIAL POSITION



This rapidly diminishing communication from a layer to those beneath have strong implications for roll structure measurement. First, measurements taken on the roll's surface will be unable to resolve changes made on layers deeper in the roll. Similarly, a large change in wound-in-stress at a particular radial location will be undetectable a short distance away.

Comparing Altmann's winding model described by equations (41) and plotted in Figure 16, and the isotropic model described by equations (30) and plotted in Figure 14, we can investigate the effect on material anisotropy on wound roll stress distributions. This comparison of the winding of anisotropic and isotropic materials, yields the following differences:

Figure 16
STRESS DISTRIBUTION FOR ALTMANN MODEL



1. The magnitudes of the radial stresses for the anisotropic model are much less than for the isotropic model for the same WIS profile.
2. The radial and tangential stress distribution for constant WIS are nearly flat, equal in value in the middle radii of large rolls, and slightly compressive throughout most of the roll. This very near equality of radial and tangential stresses can be used as a quick check of the accuracy of constant WIS linear anisotropic stress calculations.
3. The stress gradients at the core are somewhat less with the anisotropic model than for the isotropic model.
4. Both the isotropic and Altmann models must and do yield nearly identical calculations for stresses using an isotropic set of conditions as seen in Appendix B. However, since anisotropy is a more general and more representative condition of winding, anisotropic models are preferred.

As mentioned earlier, the primary differences in winding models are generality, and numerical performance in terms of accuracy and speed. For the Altmann model, the accuracy and speed of calculation are directly related to the difficulty in numerically evaluating the winding integral, where the integrand can vary by more than 20 orders of magnitude from the core to the outer radius. Several numerical techniques for improving performance were tried and are discussed here.

However, before accuracy can be objectively evaluated, several difficulties must be resolved. First, we must define accuracy. If accuracy is defined in terms of absolute error, then the tangential stresses, which tend to be numerically higher than radial stresses, will tend to appear larger than their real significance. Conversely if accuracy is defined in terms of relative error, then the error will approach infinity near the zero crossing of tangential stresses.

In addition to differences in the error for radial and tangential stress calculations, errors will vary with radial position in a roll. For example, finite difference models such as Hakiel's generally perform poorly for radii near the core where the number of calculation points is smaller. If RMS or another similar measure of error is used to evaluate the entire region as opposed to discrete points, then the effort required to evaluate error becomes quite large. For this simple evaluation however, the relative error is based on the tangential stress at a radius of 5".

The second issue that must be resolved is determining what the 'correct' stress values are which will be used as a reference for the error calculation. One possibility is to vary the grid spacing to find convergence of a model. Unfortunately, though this is a useful check, convergence does not necessarily guarantee correctness. However, if the convergence of stresses in one model agrees quite closely to the stresses predicted by another model for the same input parameters, then the confidence in both models is quite high. This fortunate condition is the basis for this simple error analysis. Specifically, for a wide range of parameters the Altmann model will converge to the stresses predicted by the Yagoda model (to be discussed shortly) to more than 10 decimals of accuracy.

The third issue is that the error depends considerably upon the input parameters used. For example, while most models have numerical difficulty as the anisotropy ratio increases beyond some value such as 1000, the Yagoda model does well at high anisotropies but may not even be able to calculate stresses for low anisotropies. For the following examples, a standard set of input parameters typical of some winding conditions are used and corresponds to those given in Figures 15, 16 and Appendix B.

Finally, stress calculation accuracy and speed also depends on the original source code, the compiler, the microprocessor, as well as the math coprocessor. For example, the ubiquitous but primitive GW basic on the IBM PC has been found unacceptable for many winding models due to numerical overflow of its single precision math. Obviously, speed of computation will improve with compilation, math coprocessor support, as well as processor speed. Due to these and many other difficulties in evaluating accuracy, the following error analysis though objective and representative, is somewhat simplistic.

The most straightforward approach to evaluating the winding integral is to use Simpson's 1/3 rule, and to increase the number of panels to evaluate its effect on accuracy. From Table 2a, we see that the Altmann formulation converges to the Yagoda results if the number of integration panels is high. This gives us high confidence in both the Altmann and Yagoda formulations.

While engineering accuracy of wound roll stresses is easy to obtain with Altmann's model using as few as 100 panels, extreme accuracy is not. For example, if we want to know the stresses at 1 inch locations in the winding of a roll from a 2 inch to 20 inch radius to an accuracy of 1 part in 10E8, we would need to call the integrate subroutine 136 times, and the integrand function 13,600,000 times. Clearly we would like a more efficient method of obtaining a specified level of accuracy. From the large number of panels required for high accuracy, it may be suspected that the winding integral must be unusual because the error term

$$(42a) \quad -\frac{(b-a)}{180} h^4 f^{iv}(\xi)$$

should be very small, and specifically for our case of 100,000 panels equal to

$$(42b) \quad 4.2E-17 f^{iv}(\xi)$$

However since the error is relatively large, the fourth derivative of the integrand must be very large. The high gradients for the winding integral, stresses, strains and displacements create numerical difficulties for winding model calculations.

A classical approach to increase numerical accuracy and/or reduce the number of calculations is to use Rhomberg Extrapolation. With this method for example, a calculation is made at a coarse spacing and then again at a mesh twice as fine. Using these two results, an extrapolation can be made which predicts the calculation result as if it was made with a mesh four times as fine as the original. This extrapolation can be repeated several times. Unfortunately as seen in Table 2b, the winding integral errors actually increase using Rhomberg Extrapolation.

Because the integrand is very steep near the core, it would be reasonable to make the 'mesh' smaller in that region. Since many of the common numerical integration methods require constant space grids, one could divide the integration region into several subregions. Though each subregion would have constant internal spacing, the subregion in areas of steep gradient could have a finer mesh than those which are in areas of moderate gradient. For example, the entire integration region from the radius of interest r , to the outside radius R , could be divided into decades, each with the same number of panels, and the total near 1000 panels. Using this procedure, the 3 decade evaluation would have 334 panels for each of the regions r to $r+0.01(R-r)$, and $r+0.01(R-r)$ to $r+0.1(R-r)$, and $r+0.1(R-r)$ to R . As seen in Table 2c, the two decade integration is the optimum for this case and improves accuracy more than two orders of magnitude.

Other methods were investigated such as adaptive step size integration as well as combinations of methods such as using decade varying panel widths along with Rhomberg Extrapolation. However, the best result obtained was by using Simpson's 1/3 rule for a two decade varying panel width for an accuracy improvement of about 100 times over the unmodified Simpson's integration method. Consequently, this procedure was implemented in the computer coding for the Altmann model given in Appendix A.

Though Altmann pioneered analytical winding with a mathematically correct model, and many subsequent authors use his nondimensionalization scheme, he had errors in his graphs that later stirred criticism. Altmann's figure 1 shows a constant stress region that has a slightly inaccurate value, and more importantly no stress gradient near the core [127]. We can only surmise that the extreme difficulty of accurate numerical calculation of the winding integral with the limited computing resources in the 1960's may have yielded these errors. Furthermore, the stresses at the core might not have been calculated or might have been assumed in error with respect to the large constant stress region.

Table 2a
WINDING INTEGRAL EVALUATION ERRORS
vs # of INTEGRATION PANELS

<u># Panels</u>	<u>% Error for σ_t</u>
10	-204.18
100	-0.41036
1,000	-0.000046342
10,000	-0.0000000047641
100,000	-0.00000000011392

Table 2b
WINDING INTEGRAL ERRORS
vs # of RHOMBERG EXTRAPOLATIONS

<u># Extrapol's</u>	<u>Log10 of relative error </u>
0	-6.33
1	-5.03
2	-5.97

Table 2c
WINDING INTEGRAL ERRORS
vs # of DECADES

<u># Decades</u>	<u>Log10 of relative error </u>
1	-6.33
2	-8.87
3	-8.44
4	-7.91

However, though his calculations and graphs might not have been accurately computed, his mathematical formulation was mechanically sound and without error. Additionally as shown by the more than 10 digit agreement with Yagoda's model, the Altmann formulation can be accurately computed if sufficient care is given to numerical integration. Thus, as illustrated here with Altmann and later with other models, mathematical soundness is necessary but not sufficient to guarantee accurate stress predictions. Numerical considerations are also a requisite part of any winding model development or application. In any case, Altmann's place in winding history is assured for his model has been referenced in more winding papers than any other.

Yagoda Model

Yagoda published a number of works on winding models in the late 1970's [149-153]. However, they have been generally overlooked due to the scholarly nature in which they were written, and due to the intricate math required. Yagoda developed a hypergeometric series evaluation of the winding integral to correct what he believed were errors in Altmann's [127] solution near the core. As shown in the previous section however, Altmann's solution is mathematically correct and the errors in stresses were due to numerical evaluation problems rather than development.

To verify the numerical accuracy of the isotropic and both linear anisotropic winding models, they were each run for several sets of input data, and the results are tabulated in Appendix B. As typified by Table 3 for one of the test cases, the models yield extremely close answers. This close agreement of stress predictions between independently derived models is a benchmark test that is used throughout this thesis to check for proper model operation. However, it appears that Yagoda [152] may not have computed his predecessor's model to check against his own, since differences in the two linear anisotropic models when properly calculated are generally less than a fraction of a percent.

Yagoda [149, 152, 153] begins development of his model where Altmann [127] left off using the same integral formulation

$$(43a) \quad \sigma_R = - \left(\frac{1 + a r^{-2\gamma}}{r^b} \right) \int_r^R \left(\frac{s^b}{1 + a s^{-2\gamma}} \right) \frac{WIS_s}{s} ds$$

$$(43b) \quad \sigma_T = WIS_s - \left(\frac{\alpha - a \beta r^{-2\gamma}}{r^b} \right) \int_r^R \left(\frac{s^b}{1 + a s^{-2\gamma}} \right) \frac{WIS_s}{s} ds$$

with an identical set of dimensionless elasticity parameters

$$\begin{aligned}
 \Xi_R &= \frac{E_T}{E_R} \\
 \Xi_C &= \frac{E_T}{E_C} \\
 \mu &= \frac{1}{2}(\mu_T + \Xi_R \mu_R) \\
 \delta &= \frac{1}{2}(\mu_T - \Xi_R \mu_R) \\
 (44) \quad \gamma &= \left| \sqrt{\delta^2 + \Xi_R} \right| \\
 \alpha &= \gamma - \delta \\
 \beta &= \gamma + \delta \\
 a &= \frac{\gamma - \mu - \Xi_C}{\gamma + \mu + \Xi_C} \\
 b &= 1 - a
 \end{aligned}$$

Next, Yagoda nondimensionalizes the radial and tangential stresses with respect to the wound-in-stress at the core. The remainder of the derivation consists mostly of substituting a hypergeometric series approximation for the winding integral and simplifying. After reducing the expression, the radial and tangential stresses are given by Yagoda as

$$(45a) \quad \sigma_R = -(1 + a r^{-2\gamma}) \sum_{j=0}^M S(r, R, \phi_j) C_j r^{\phi_j}$$

$$(45b) \quad \sigma_T = \sigma_w - (\alpha - a \beta r^{-2\gamma}) \sum_{j=0}^M S(r, R, \phi_j) C_j r^{\phi_j}$$

where the asymptotic solution to the winding integral is

$$(46) \quad S(r, R, \phi_j) = \frac{1}{-(b + \phi_j)} \left[1 - \left(\frac{r}{R}\right)^{-(b + \phi_j)} \right] - \frac{r^{2\gamma}}{2 \gamma a} \sum_{n=2}^{\infty} \frac{(-1)^n}{\left(n - 1 - \frac{b + \phi_j}{2 \gamma} \right) \left[\frac{R^{2\gamma}}{a} \left(\frac{r}{R}\right)^{2\gamma} \right]^n}$$

and the wound in-stress is expressed as polynomial of M+1 terms as

$$(47) \quad \sigma_w = \sum_{j=0}^M C_j r^{\phi_j}$$

Table 3
STRESS DIFFERENCES BETWEEN
YAGODA AND ALTMANN MODELS

WIS=750, ER=1000, ET=750000, EC=100000, UR = 0.01, UT = 0.01

Values are for the Yagoda model and differences are for the Altmann model.

All units in English (inch, PSI).

<u>Dia</u>	<u>Radial</u>	<u>Rad. Difference</u>	<u>Tangential</u>	<u>Tan. Diff</u>
2	-30.874148	0.00000179	286.887777	0.00002686
3	-24.682417	-0.00000023	-24.682417	-0.00000730
4	-24.682417	-0.00000006	-24.682417	-0.00000192
5	-24.682417	-0.00000003	-24.682417	-0.00000102
6	-24.682417	-0.00000003	-24.682417	-0.00000122
7	-24.682417	-0.00000005	-24.682417	-0.00000166
8	-24.682417	-0.00000006	-24.682417	-0.00000196
9	-24.682417	-0.00000006	-24.682417	-0.00000198
10	-24.682417	-0.00000005	-24.682416	-0.00000176
11	-24.682417	-0.00000004	-24.682407	-0.00000139
12	-24.682413	-0.00000003	-24.682276	-0.00000100
13	-24.682366	-0.00000002	-24.680816	-0.00000064
14	-24.681932	-0.00000001	-24.667202	-0.00000037
15	-24.678472	-0.00000000	-24.558613	-0.00000018
16	-24.654383	-0.00000000	-23.802552	-0.00000007
17	-24.505524	-0.00000000	-19.130448	-0.00000002
18	-23.677800	-0.00000000	6.848490	-0.00000000
19	-19.488475	-0.00000000	138.334663	-0.00000000
20	0.000000	-0.00000000	750.000000	-0.00000000

The expression is simplified in the more restrictive case of constant winding tension so that

$M=0$, $\sigma_0 = 0$, and $C_0 = 1$ yielding

$$(48a) \quad \sigma_R = -(1 + a r^{-2\gamma}) S(r, R, \sigma_j) C_j r^{0j}$$

$$(48b) \quad \sigma_T = \sigma_w - (\alpha - a \beta r^{-2\gamma}) S(r, R, \sigma_j) C_j r^{0j}$$

The variable wound-in-stress equation (47) reveals a major limitation of the model as it can only accommodate a polynomial expression. Real winding profiles vary in a noisy manner due to process fluctuations and would be computationally difficult to model as an extremely high order polynomial with terms for each wrap. Another difficulty is the $(b+\phi)$ term in the denominator of equation (46). For the isotropic case, b is zero and ϕ is zero for the first term in the WIS polynomial, so that an undefined division by zero results. Additionally, b can be zero for certain combinations of anisotropic parameters. To circumvent this small problem in Yagoda's formulation, we simply say that if $(b+\phi) < \text{small}$, then the first term in equation (46) can be expressed in the limit as $(b+\phi)$ approaches 0 as $-\log(r/R)$, yielding the isotropic asymptotic solution as

$$(49) \quad S(r, R, \phi_j)_{\text{for } b=0} = -\log\left(\frac{r}{R}\right) - \frac{r^{2\gamma}}{2\gamma a} \sum_{n=2}^{\infty} \frac{(-1)^n}{\left(n-1-\frac{\phi_j}{2\gamma}\right) \left[\frac{R^{2\gamma}}{a} \left(\frac{r}{R}\right)^{2\gamma}\right]^n}$$

A similar problem occurs in the isotropic case for the first infinite series term ($n=2$) of the first WIS polynomial term ($\phi=1$) for equation (49) where $(n-1-(b+\phi)/(2\gamma))$ also goes to zero. Unfortunately, the limit of this term as given by Macsyma is much more complicated. Instead of computing the limit exactly which makes for ugly code, that single term was simply omitted in the computer code if $b+\phi < \text{small}$. Though the stress errors were typically less than 1% of the WIS for the two isotropic cases tested, it prompted a more thorough investigation of Yagoda's proof since he had not called attention to these small difficulties.

Yagoda discarded an entire series of terms [152, eq. 35], which he said could be neglected for practical cases. These terms were reinstalled and found to reduce the errors by nearly 1/2 for the two isotropic parameter sets with lesser effect on a single recalcitrant anisotropic parameter set. Additionally, Yagoda used two other simplifying assumptions [152, eq's 33a & 33b] that were not checked because they were used early in the development of the series solution, and a rederivation appeared formidable.

An outline of the computer code to solve Yagoda's winding model is as follows, and the code is given in Appendix A.

```
input variables
calculate intermediate parameters
increment internal radius loop
    outer summation loop (for number of terms in WIS profile)
        inner summation loop (for infinite series expansion of integral)
        end inner summation loop
    end outer summation loop
end increment radius loop
```

The increment for the outer loop in program's body determines the interval over which stresses will be calculated and printed, and has no effect on the accuracy of the solution. Within this loop, there are two other nested loops. The intermediate summation loop is executed as many times as there are terms in the WIS polynomial profile. The inner summation loop is executed until the remaining terms in the infinite series terms become very small. The only difficulty here is exiting the inner loop before numerical underflow. This underflow occurs due to large exponents, and it is difficult to predict from the value of the current term in the series whether the next term in the series will explode.

One outstanding advantage with Yagoda's solution is that it can be extremely computer efficient for simple WIS profiles. For example, the Altmann solution for the anisotropic case of Table 2 required 100,000 iterations to reach 12 place accuracy while Yagoda's only required one series term except near the core (75 terms at 2", 2 terms at 3"). Additionally, for many sets of input the Yagoda model will calculate stresses to extraordinary accuracies as evidenced earlier by the convergence of Altmann's model. Thus, it is possible for the Yagoda model to calculate stresses to many orders of magnitude greater accuracy, and to do so at a miniscule fraction of the time other models require to achieve even modest accuracy. The disadvantages of the Yagoda model are difficulties with cases of low anisotropy ratios and/or highly variably WIS profiles.

In addition to his conventional winding model, Yagoda also extended his model to include the effects of centrifugally induced stresses [150, 151]. In this work he concluded that the effects of centrifugal forces are small but not negligible. This and other more complex wound roll behavior will be discussed in more detail in Chapter 4.

In summary, Yagoda's model is numerically consistent with the isotropic and Altmann models. The primary advantage of the Yagoda model is extraordinary accuracy and extremely fast calculation time, while the primary disadvantage of the Yagoda model is limitations in the complexity of the WIS profile that can be easily accommodated. Thus, the best application of the Yagoda model is where extremely accurate data needs to be computed quickly to verify other models.

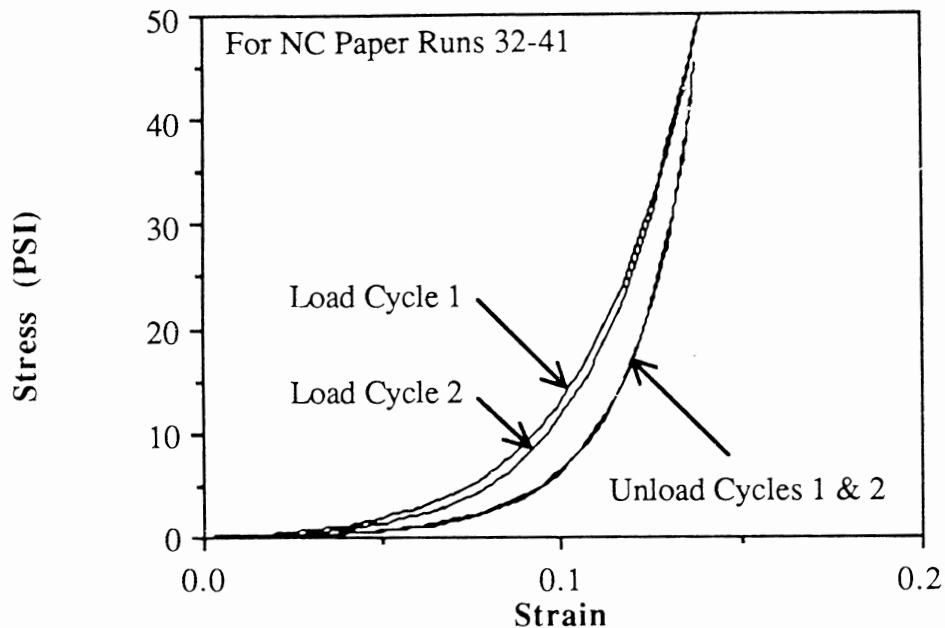
Nonlinear Moduli

The three models discussed thus far, the isotropic, Altmann's and Yagoda's, have all assumed that the material properties are constants. However, material properties are seldom constants, and will vary with load, load history, strain rate, time, temperature, moisture and other factors for a given material. In particular as we will see, the radial or stack modulus E_R will depend strongly on the interlayer pressure σ_R . Moduli are defined as the slope of the stress-strain curve as

$$(50) \quad E_R = \frac{d \sigma_R}{d \epsilon_R} = f(\sigma_R \text{ and other factors})$$

Figure 17 shows the stress-strain curves for one of the materials tested in this project, and typifies most web materials. The first and most important observation is that the stress-strain curves are nonlinear, and consequently the radial modulus is not a constant but rather depends strongly on the stack pressure. The second observation is that the load and unload curves follow different paths, and the area between these curves represents the nonconservative hysteretic energy loss due to a single load-unload cycle. A third observation is that the strain does not return to zero upon unload. This means that the specimen will retain a permanent change in dimension of the same sign as the applied load, although some of this will be recovered with time. Finally, the stress-strain curves 'walks' to the right as a function of loading cycles. However after one full load-unload cycle, the stress-strain curves tend to quickly stabilize. Because of these and other complexities, various procedures and simplifications are used to adequately model a material's first order stress-strain behavior.

Figure 17
NONLINEAR STACK STRESS-STRAIN CURVES



Moduli are indirectly measured using a tensile testing machine equipped with suitable grips or platens. MD and CD moduli are generally tested in tension only, and the specimen strips are mounted in lightly loaded grips. These specimens are typically 1" wide by 4-6" long. To reduce the stress concentration at the grips and consequently reduce the frequency of breaks initiating at the grips, they are either covered with a soft elastomer to spread out the load and increase friction, or the grips have a large radii such as defined by Tappi standards. However, the ZD modulus is only measured in compression as a single ply or stack loaded between two parallel platens.

The platens used for radial or ZD modulus measurement may either be larger or smaller than the specimen stack. The easiest approach, and that proposed by Pfeiffer [79], uses specimens cut somewhat larger than the circular loading platens. With this method, no special cutting or alignment of the specimens is required. However it assumes that the active area is that of the platens, yet there are end effects just beyond the platens as the stack specimens bend away from the stack's center. These end effects may bias the measurement in the direction of a stiffer modulus.

A more difficult approach, is to carefully cut and align specimens into a stack which is smaller than the loading platens. However, whether the specimens are cut individually and collated or sawed as a stack, end effects are still present. If the specimens are cut and collated, they may not be of precisely the same length and width, or may not be precisely aligned, both of which will bias the measurements in the direction of a softer modulus. If the specimens are sawed, the edges of the material may fray or laminate with an unpredictable bias of the modulus measurement.

After the stack specimens have been prepared and fixtured, the tensile testing machine must be set up to compress the stack at a specified strain or load history through one or more cycles. Pfeiffer suggests a strain rate control such that the specimen is loaded to 100 psi over the course of 60 seconds, held at 100 psi for 60 seconds, and unloaded for about 60 seconds [79]. This load history, though by no means a standard, is typical of procedures used by others. However, the maximum load should be selected on the measured or anticipated maximum interlayer pressures for the specific product and process to be modeled. Obviously, rolls of tissue, carpeting or fiberglass insulation will have considerably less pressure than rolls of calendered paper, film or steel. Additionally because of the stabilization of the stress-strain response after the first complete load cycle, it is common to report the results for the second loading curve.

The instrumentation used for moduli measurement are typically strain gage load cells for load measurement and LVDT's for displacement. These load and displacement signals are either recorded on chart paper, or preferably by computer data acquisition which simplifies subsequent data reduction. The tensile test machine, load cells, and displacement measurement must be suitably sized for loads and travel. With stacks typically about 10 square inches in cross section and about one inch high, this translates to a load cell capacities of several hundred pounds and a displacement resolution on the order of 0.001". Care must be taken with larger tensile test machines to avoid overloading the load cells.

The load-displacement data gathered from the tensile tester must be first converted to stresses and strains, and then the derivative must be calculated for the modulus as defined by equation (50). Ultimately however, the data must be converted (curve-fitted) into an expression where modulus is a function of interlayer pressure or stress as required by the nonlinear winding model. The two commonly used curve fits for stack stress-strains are the exponential and the polynomial, and will each be described in turn. It should be emphasized at this time that these stress-strain and resulting modulus expressions are strictly empirical in nature, as there are presently no first principle descriptions of nonlinear stack response.

The exponential curve fit proposed by Pfeiffer is of the form

$$(51a) \quad \sigma_R = -K_1 + K_1 e^{K_2 \epsilon_R}$$

where σ_R is the interlayer stress, e is the base of the natural logarithm, ϵ_R is the radial strain, and where K_1 and K_2 are curve-fitted constants [71 (with changes in nomenclature for consistency)]. The radial modulus can then be calculated for (51a) by taking the derivative as given in (50).

$$(51b) \quad E_R = K_1 K_2 e^{K_2 \epsilon_R}$$

Pfeiffer, Frye and many others in the paper industry attach almost a mystical significance to the K_1 and K_2 constants, particularly in their purported relationship to the propensity to certain roll structure defects. However, there is no published evidence of the significance of these constants. Additionally, though the exponential curve will fit most paper grades and other materials very well, its practical implementation is difficult. First, the $-K_1$ corrective term in (51a), which is required so that the stress is zero at zero strain, adds complexity to the curve fitting procedure. Instead of using a simple fitting program, the exponential fit becomes iterative where K_1 is subtracted from the stress strain data prior to the next iterative fit. Secondly, the formulations (51) are given in terms of radial strains, instead of the stresses in which winding models are typically posed. Thus, a simple modulus expression as a function of interlayer pressure or stress is difficult to achieve.

The polynomial curve fit proposed by Hakiel is of the form

$$(52) \quad E_R = K_1 + K_2 \sigma_R + K_3 \sigma_R^2$$

where the K 's are determined by polynomial curve fitting. While the radial modulus expression is the required input for winding models, the stress-strain curve itself is not particularly useful. Much difficulty can be avoided by performing the derivative (50) numerically on the raw stress-strain data before curvefitting, instead of curvefitting followed by an analytical derivative as used by Pfeiffer's exponential. Though a high correlation fit can often be obtained without the K_3 term, the K_1 term must not be negative because it would not make physical sense. Additionally, the K_1 term may have to be greater than some small positive value because extremely high anisotropy ratios may cause tremendous numerical difficulties with some implementations of winding models.

The radial moduli for this project was tested in a similar fashion to that described above. Specifically, the specimens were cut to 2.5" x 4.0" on a guillotine cutter and collated into stacks approximately 2" tall. The stacks were loaded and unloaded through four complete triangular loading cycles on an Instron programmed in strain rate control from zero to 50 psi, with each complete load cycle taking approximately 6 minutes. Data was acquired with an IBM PC clone using Labtech Notebook software and Metrabyte data acquisition cards. The data acquisition rate was 1/second which gave approximately 150 data points for each load or unload segment.

The first step of data reduction was to average the raw data by 5 to decrease signal noise which would interfere with a good numerical derivative. Secondly, the displacement signal offset was subtracted for each load or unload segment so that the displacement was zero at zero load. Similarly, the tare load of the upper platen was also subtracted off. Thirdly, load was converted to stress by dividing by the 10" cross-sectional area, and displacement converted to strain by dividing by the original stack height. Fourthly, a 2 point central numerical derivative was computed to give the change in slope of the stress-strain data as a function of pressure as indicated by (50). Finally, the resulting modulus/pressure data was curve fitted using the polynomial method given by (52).

The results of the moduli measurement for three of the materials tested for this project are given in Table 4. As seen here, the initial stiffness is considerably greater for the coated board than for the other two materials. More significantly, the strain hardening rate varies considerably between these paper grades. Though the curve fitted moduli expressions are highly correlated with the original data, there is a significant variability between the first and subsequent load cycles. Additionally, it is expected that there will be a significant property variance in many web materials within a single roll, so that the tested sample may not necessarily be representative of the average for that roll. Thus the difficulties associated with hysteresis, creep, property variance and other complex material behavior gives some uncertainty in the radial modulus which is used as a winding model input parameter.

Similarly, the tangential moduli may also possess complexities, particularly for non-elastic materials such as paper, nonwovens, and highly stressed films. For example, most paper grades have nonlinear stress-strain curves, are hysteretic, and have the propensity to creep. Since the tangential nonlinearities are usually much smaller than radial nonlinearities, most winding models have neglected this behavior. However, nonlinear models such as Hakiel's described in the next section can be extended to include more than the predominant radial nonlinearity.

Table 4
RADIAL MODULI

<u>Material</u>	<u>Load Cycle</u>	<u>Radial Modulus (psi)</u>	<u>Correlation (R²)</u>
NC paper	1	17.812 + 33.831*P	0.999
NC paper	2	22.698 + 36.071*P	0.997
NC paper	3	28.483 + 35.062*P	0.990
NC paper	4	34.526 + 35.949*P	0.983
NC paper	calculation	20 + 35*P	
LWC paper	1	23.660 + 51.175*P	0.996
LWC paper	2	42.724 + 54.480*P	0.990
LWC paper	3	24.405 + 57.600*P	0.998
LWC paper	4	32.918 + 58.191*P	0.996
LWC paper	calculation	30 + 55*P	
ctd board	1	61.949 + 112.47*P - 1.2013*P ²	0.998
ctd board	2	65.009 + 118.52*P - 1.3371*P ²	0.997
ctd board	3	74.612 + 114.73*P - 1.2247*P ²	0.994
ctd board	4	79.924 + 119.36*P - 1.3279*P ²	0.997
ctd board	calculation	70 + 115*P - 1.27*P ²	

Some of the nonlinearity in the radial stress-strain curves can be qualitatively explained in terms of the geometry of contact between layers. This begins by noting that there are gaps and incomplete contact between layers. Materials such as paper and nonwovens are by nature rough and porous so that only the peaks of adjacent layers are in contact. Nonporous materials such as film may not be in complete contact due to the entrainment of air during winding as evidenced by a measurable decrease in density of the roll beyond that of the material from which it was wound. Finally, all material have unintentional variations in thickness and deviations from flatness. If these materials are thick enough, bending stiffness can resist complete contact at low interlayer pressures. Despite the various mechanisms of incomplete contact, the result will be similar. As interlayer pressure increases, the proportion of area in contact increases bring more material into compression. Thus, the stack modulus will tend to increase and approach the bulk stiffness of the material as the interlayer pressure and contact area increases. The nonlinearity in the tangential stress-strain curves can be qualitatively explained in terms of the breaking and possible reforming of bonds. In the case of paper, it is the bonds between fibers, and for films it is the bonds between polymer chains.

Hakiel Model

The next step in the evolution of winding models was to incorporate the nonlinear radial modulus. Hakiel [132, 133] was the first to publish such a solution using finite difference techniques, and later Willett and Poesch [186] made incremental improvements to this basic approach. While previous and simpler winding models were able to reduce much of the solution to closed form expressions, the complexities of a nonlinear modulus precluded a predominantly mathematical treatment. Instead, the Hakiel model relies heavily on numerical approximations of the winding differential equation. This numerical approach freed the evolution of winding models from more restrictive descriptions. However as will be shown, this freedom came at the cost of increased computation time and a much greater threat of numerical round-off error and instability.

The constitutive equations and assembly technique are essentially identical to the isotropic, Altmann and Yagoda models. The only significant variation is that the radial modulus, E_R , is allowed to vary as a function of interlayer pressure as indicated in the previous section and defined by equation (50). However as with the previous models, though they are formulated in a similar fashion, the solution technique is very different.

Rather than merely echoing Hakiel's solution, the following derivation will extend the model slightly beyond its original formulation so that the solution is more general. The principle extensions are reducing the constraint imposed on Poisson ratios by strain energy, including higher order derivative cross product terms for better accuracy, and to extend the model to include a nonlinear tangential modulus. It should be emphasized that these deviations from Hakiel's original solution are not corrections, because I have verified his solution to be absolutely correct as formulated by rederiving the solution on a symbolic math application, Macsyma, as well as many numerical checks against other winding models. In addition to these extensions, the nomenclature is changed somewhat from the original publication so that this thesis work is consistent. Finally, since this is currently the best winding model to date, its derivation will be more complete than earlier models.

The radial equilibrium equation of a single 'layer' has been derived as equation (2) in Chapter 2, and given more thoroughly in Altmann's publication [127], and will only be restated here as

$$(53) \quad r \frac{d\sigma_R}{dr} + \sigma_R - \sigma_T = 0$$

The strain-displacement relations for a cylinder have been derived in Chapter 2 as equations (4) and (6) and are merely restated here as

$$(54) \quad \epsilon_R = \frac{dw}{dr}$$

$$(55) \quad \epsilon_T = \frac{w}{r}$$

The stress-strain relations contain the radial and tangential moduli which are now allowed to vary as some function of radial and tangential stresses respectively as

$$E_R = \frac{d\sigma_R}{d\epsilon_R} = f(\sigma_R \text{ and other factors})$$

$$E_T = \frac{d\sigma_T}{d\epsilon_T} = f(\sigma_T \text{ and other factors})$$

However, though the moduli vary directly as some function of stresses and other factors, they will as a consequence vary with radial position because stresses vary with radial position. Consequently, the moduli in the stress-strain relations given by Altmann [127] and equations (7) and (8) are rewritten to emphasize their (indirect) dependence on radial position. Note that because the sensitivity to Poisson ratios is small, and they have been assumed to be constants [148]

$$(56) \quad \epsilon_R = \frac{\sigma_R}{E_R(r)} - \mu_T \frac{\sigma_T}{E_T(r)}$$

$$(57) \quad \epsilon_T = \frac{\sigma_T}{E_T(r)} - \mu_R \frac{\sigma_R}{E_R(r)}$$

Finally, the core stiffness definition derived in Chapter 2 is given again as

$$(58) \quad E_c = \left. \frac{\sigma_R}{w/r} \right|_{r=r_0}$$

Thus, equations (53) through (58) represent the constitutive equations that define the physics of all consistent winding models in general, and this nonlinear winding model in particular. The next steps are to assemble these constitutive equations into a 2nd order winding differential equation.

While the order in which the operations are performed to obtain the differential equation is not unique and will lead to an equivalent expression, the ease of derivation is very dependent on order. Furthermore, the simplest path is not easy to determine until in fact the derivation is complete. Fortunately, symbolic computer algebra can greatly reduce derivation time, reduce the chance of error, provide a log of the derivation, and even convert expressions into computer code. Two applications were used for this and other derivations in this thesis. The first and most powerful is Macsyma running on a Symbolics machine. The second is Mathematica running on an Apple Macintosh which was used for the bulk of derivations for this project. Though Mathematica lacks some advanced mathematical features, is somewhat easier to use and integrates well into report and computer code writing.

Strains can be eliminated from this system of equations by combining equations (54) and (56) as

$$(59) \quad \frac{dw}{dr} = \frac{\sigma_R}{E_R(r)} - \mu_T \frac{\sigma_T}{E_T(r)}$$

and by combining (55) and (57) as

$$(60) \quad w = r \left(\frac{\sigma_T}{E_T(r)} - \mu_R \frac{\sigma_R}{E_R(r)} \right)$$

The displacement, w , can be eliminated by taking the derivative of (60) with respect to r and setting this equal to (59). Although not proved until Chapter 7, the winding differential equation is not dependent of derivatives of E_T , so that it can be regarded simply as a variable whose value must be determined just prior to evaluating the differential equation. Finally, this equation is solved for the derivative of tangential stress as

$$(61) \quad \sigma_T' = (E_R E_T \sigma_R + \mu_R E_R E_T \sigma_R - E_R^2 \sigma_T - \mu_T E_R^2 \sigma_T - r \mu_R E_T E_R' \sigma_R + r \mu_R E_R E_T \sigma_R') / (r E_R^2)$$

The derivative of the tangential stress can be eliminated by solving (53) for the tangential stress and taking the derivative and setting this expression equal to (61). Finally, this equation can be solved for the tangential stress as a function of radial stress and material properties as

$$(62) \quad \sigma_T = (E_R E_T \sigma_R + \mu_R E_R E_T \sigma_R - r \mu_R E_T \sigma_R E_R' + r \mu_R E_R E_T \sigma_R' - 2r E_R^2 \sigma_R' - r^2 E_R^2 \sigma_R'') / ((1 + \mu_T) E_R^2)$$

Now the differential equation can be assembled by inserting the tangential stress expression (62) into the equilibrium equation (53). This expression is then expanded and collected upon the $r^2 \sigma_R''$, the $r \sigma_R'$, and the σ_R terms. Finally, the equation is put in a standard form as

$$(63) \quad r^2 \frac{d^2 \sigma_R}{dr^2} + A r \frac{d\sigma_R}{dr} + B \sigma_R = 0$$

where

$$A = \left(3 + \mu_T - \mu_R \frac{E_T}{E_R} \right)$$

$$B = \frac{\left(-(1 + \mu_R) E_R E_T + (1 + \mu_T) E_R^2 + r \mu_R E_T \frac{dE_R}{dr} \right)}{E_R^2}$$

Next, the boundary conditions at the core and the outside of the roll must be derived. The boundary condition at the core can be solved simply from the system of equations of equilibrium (53), tangential stress-strain (57), and the definition of core stiffness (58) by eliminating the tangential stress and tangential strain. This boundary condition at the core is a derivative such that

$$(64) \quad \left. \frac{d\sigma_R}{dr} \right|_{r=r_0} = \sigma_{R_0} \frac{-E_C E_R + E_R E_T + \mu_R E_C E_T}{r E_C E_R}$$

The outer boundary condition at the current applied wrap is

$$(65) \quad \sigma_R \Big|_{r=r_n} = \frac{-WIT_{r=r_n}}{r_n}$$

There are a few main differences between this derivation and that given by Hakiel [132, 133]. First, he used the strain compatibility equation for cylindrical

$$(66) \quad r \frac{d\varepsilon_T}{dr} + \varepsilon_T - \varepsilon_R = 0$$

instead of the strain displacement relations (54) and (55). However, these expressions are exactly equivalent so that the resulting differential equation will be equivalent.

Another difference which may be significant however, is that a derivative cross product term resulting from the derivative in the equilibrium equation, E_R' , was omitted from the derivation. Since radial modulus is a function of radial pressure which is not a constant, the radial modulus will vary indirectly as a function of radial position. Hence, the E_R' term is nonzero for stacks with nonlinear radial moduli. Looking at the first and last terms in the numerator for B in equation (64), it may be possible that the E_R' term is negligible. This would happen if either μ_R or E_R' were small, or their product with r were small compared with E_R . If the E_R' term is omitted, the expression for A remains the same, but B becomes

$$(67) \quad B = \left(1 + \mu_T - (1 + \mu_R) \frac{E_T}{E_R} \right)$$

However, it will be shown in Chapter 7 that the higher order derivative term should not be dropped for the case of the nonlinear radial moduli with the displacement formulation because it is a dominant term. Therefore, it is conservatively suggested that the full form be retained. Also as will be shown in Chapter 7, a full nonlinear model must include not only the derivative of radial modulus with respect to radius, but also the derivatives of the Poisson ratio terms which were not retained in the previous derivation. Perhaps surprisingly however, the derivative of the tangential modulus need not be included even for nonlinear tangential moduli.

An additional restriction imposed by the Hakiel derivation, which was removed for generality in our derivation, is that of strain energy which states that the moduli and Poisson ratios are related by

$$(68) \quad \frac{\mu_R}{E_R} = \frac{\mu_T}{E_T}$$

It is conservative to not constrain the solution since the strain energy constraint has not been experimentally verified on a single ply of a complex material such as paper, and much less as a stack [186]. Though Hakiel set both Poisson ratios to zero in his analysis and thus the strain energy constraint would not affect his results, it may be significant for other systems. If the strain energy constraint from (68) is also included, the A and B terms of (64) reduce exactly to Hakiel's solution:

$$(69) \quad \begin{aligned} A &= 3 \\ B &= -(g^2 - 1) \end{aligned}$$

where

$$g^2 = \frac{E_T}{E_R}$$

Now that the differential equation given by (64) has been assembled, it must be solved in the region from the core to the current outer radius. Since a closed-form analytical solution to (64) may not be possible for the general case where the A's and B's vary for every internal wrap, numerical solutions must be used. In particular, the finite difference method is used where the derivatives are approximated by numerical differences. Since the finite difference method will be described in more detail in Chapter 7, only a brief overview will be given here.

In the finite difference method, each internal layer is described by a linear algebraic approximation of the differential equation. The equations for all the layers are assembled into matrices which can be solved for the incremental radial stress distribution. From the incremental radial stress distribution, the incremental tangential stresses can be calculated using the equilibrium equation (53). Both radial and tangential incremental stresses are then added to the previously existing stress distributions. This procedure is embedded in a loop which is repeated for every wrap added from the core to the finish diameter.

There are a few decisions that must be made when implementing finite difference computer modeling. This first is the order of the difference approximation, and is typically either a 3 or 5 point central difference. Though both Hakiel [132, 133] and Willett and Poesch [186] used 3 point differences, conventional wisdom indicates that using higher order approximations will improve the accuracy and/or decrease the computer code solution time. However, several comparative runs using both 3 and 5 point differences indicate that the 3 point was significantly more CPU efficient in obtaining a certain accuracy. Not surprisingly as we have seen before, the numerically ill-conditioned nature of wound roll physics seems to defy many standard numerical techniques. Since the 3 point difference has been used by other authors, results in simpler code, and may be more efficient; it may be the preferred order.

Another decision which also affects both accuracy and solution time is grid size or calculation wrap thickness. Although probably not numerically ideal because of the high gradients at the core and outside, all authors to date have used consistently spaced grids because it is much simpler to code. However as described in the end of Chapter 2, the calculation wrap thickness need not equal the real web thickness as long as the value of the wound-in-stress is preserved. The effect of grid size on solution time can be estimated from equation (29), which indicates that solution time is inversely proportional to the square of the grid size. Thus, halving the grid size will quadruple the solution time.

The effect of grid size on solution accuracy is not as easily determined however. It is expected that as a grid is reduced from a coarse size to a finer size that solution accuracy will increase. However if the grid is made ever finer, eventually numerical roundoff errors due to small differences will dominate and accuracy will begin to suffer. Indeed if it is made fine enough, the solution will blow up. Though numerical roundoff errors can be reduced by using double or higher precision, they can't be eliminated.

Figure 18 shows the effect of grid size on the stresses calculated for the Linear Isotropic Standard case (see Appendix B for parameters). As seen here, the solutions for a 0.1" and 0.05" grid give almost identical results. However, as the grid is reduced to 0.02", the tangential stresses begin to become numerically unstable, and at 0.01" both radial and tangential stresses have become unstable. Halving the grid size yet again will cause the solution to completely blow up. Thus, too fine of a grid can actually reduce accuracy.

Figure 19 shows the effect of grid size on the other end of the problem spectrum for the Linear Anisotropic Standard case. As the grid becomes finer, the radial stresses converge to the correct answer. If we were patient enough however, we could also make this set of input parameters also blow up if the grid were reduced sufficiently. One curiosity remaining is why the tangential stresses seem to be unaffected by grid size for this parameter set. This is easily explained by noting that tangential stresses are calculated from the radial stresses and the equilibrium equation. As seen in Figure 19a, the imperfectly calculated radial stresses are too negative, but their slopes are too positive. This coincidental near cancelation of errors occurs primarily for cases of highly anisotropic materials.

One useful trend which can be used to check the proper behavior of winding models occurs for the case of highly (linear) anisotropic materials wound under constant tension which have a large ratio of the finish radius to the core radius. In this case, the radial and tangential stresses will be nearly constant and nearly equal to a half dozen digits through the intermediate diameters of the roll.

Figure 18a
EFFECT OF GRID SIZE ON RADIAL STRESS

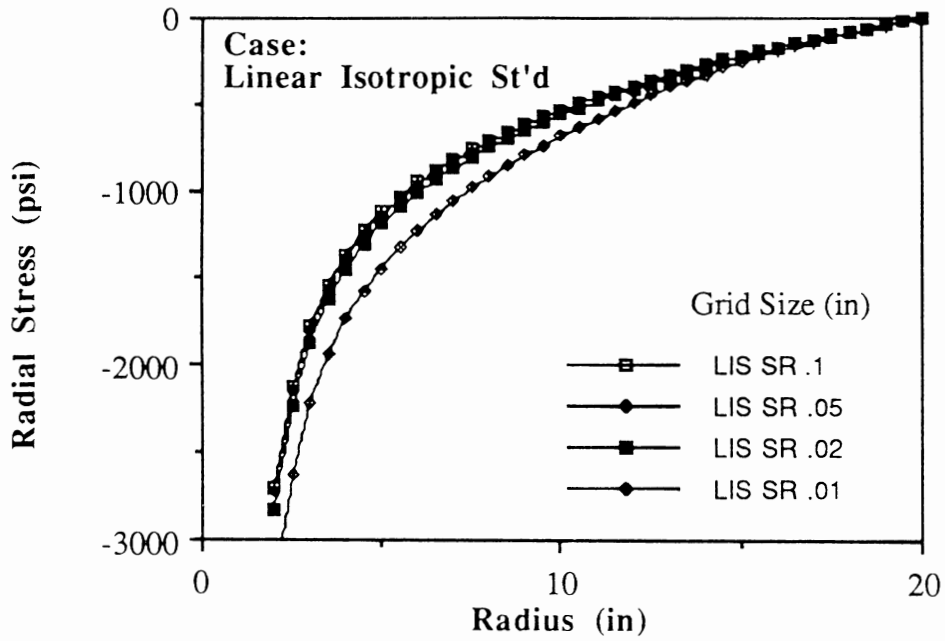


Figure 18b
EFFECT OF GRID SIZE ON TANGENTIAL STRESS

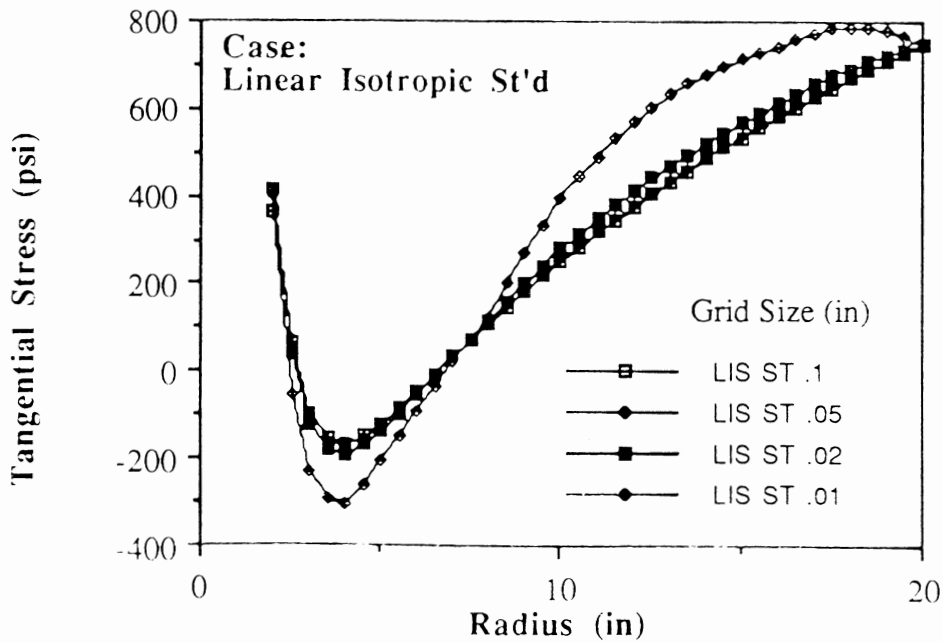


Figure 19a
EFFECT OF GRID SIZE ON RADIAL STRESS

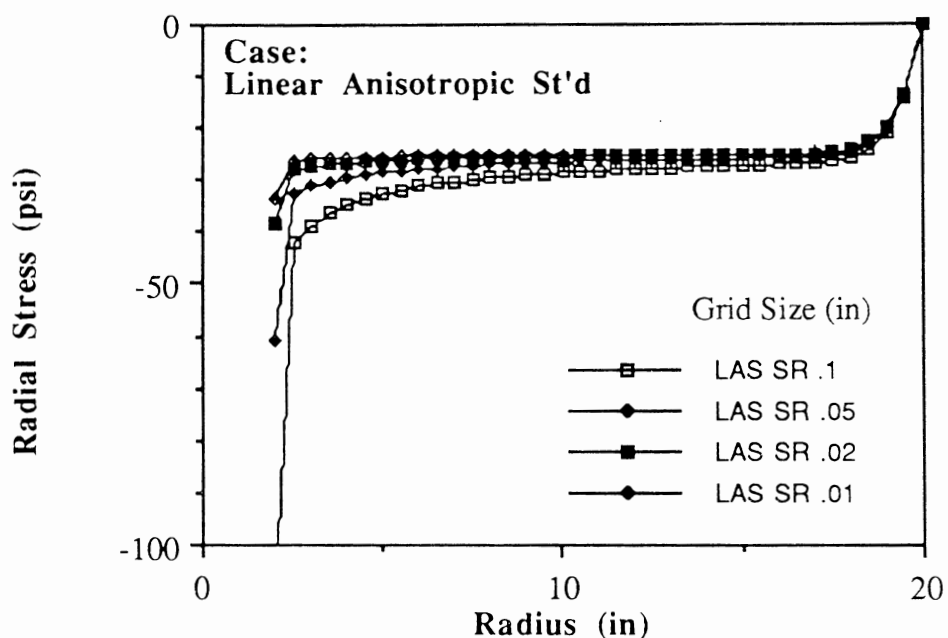


Figure 19b
EFFECT OF GRID SIZE ON TANGENTIAL STRESS

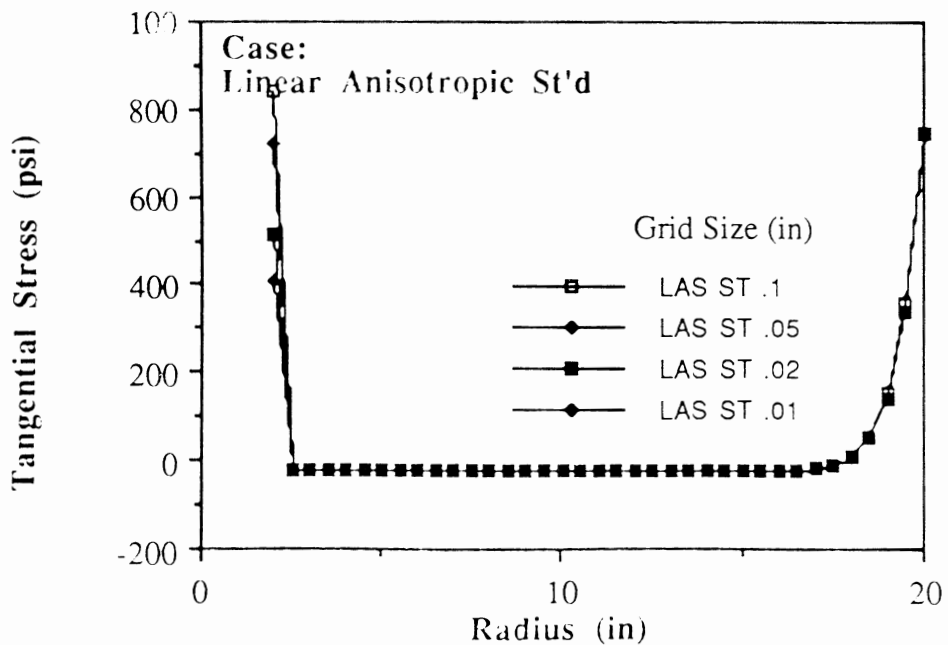
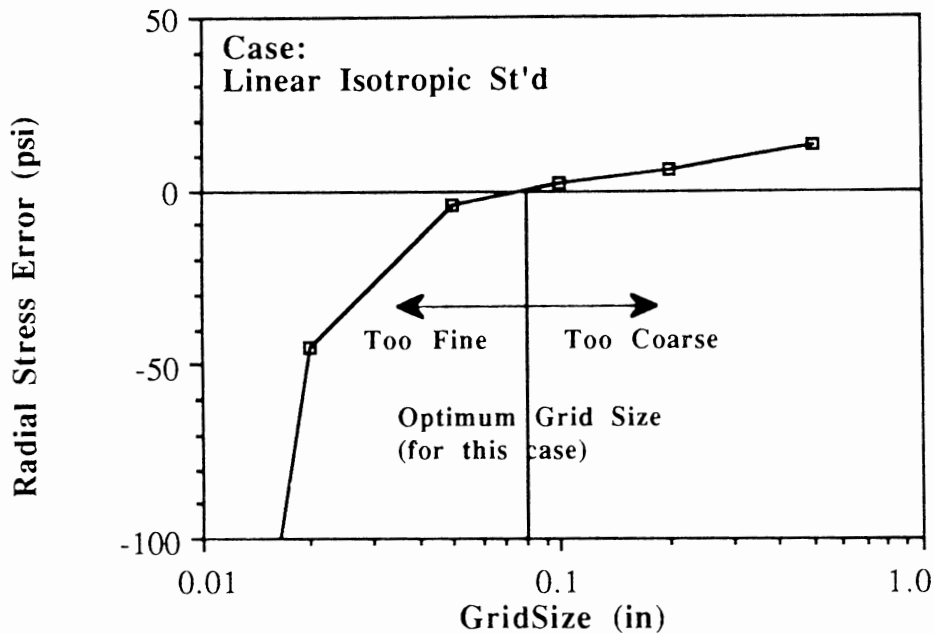


Figure 20
EFFECT OF GRID SIZE ON RADIAL STRESS ERROR



Perhaps a more useful view of the effect of numerical error is to plot it against grid size. This is easily done for cases in which the correct answers are already known because of the existence of independent models such as Altmann and Yagoda. As shown in Figure 20, error is halved as the grid size is halved (quadruple the calculation time). Eventually however, the grid becomes too fine and error increases dramatically from a near zero value due to numerical roundoff. The error graph then consists of two regions. In the coarse region, the error is inversely proportional to the grid size. In the fine region, the magnitude of both the stresses and stress errors increase dramatically with decreasing grid size. Finally, the boundary between the regions should be of near minimal and near zero error.

Though this behavior has not been predicted from first principles error analysis, this trend has been observed in all finite difference formulations of wound rolls models, and for all cases of input parameters that have been run. However, it should be noted that the optimum grid size decreases significantly with increasing anisotropy ratio, and is affected by other parameters. Thus, this observation of error halving for excessively coarse grids can perhaps allow prediction of optimum grid size for cases in which the correct answers are not already known. Also, better values of stresses could be extrapolated for cases in which the optimum grid size results in excessive calculation time.

In summary, Hakiel's winding model is currently the most general and the most useful because of its nonlinear radial modulus capabilities. It is mathematically correct, consistent with previously discussed models, and yields stress values that are very close to the other models as seen in Appendix B, provided that a proper grid size is chosen. However because of the unfortunate effect of numerical approximation, this model should always be run with more than a single grid size (double and halve the expected optimum) to compare results. Finally, a more general formulation would release the strain energy constraint, include the radial modulus derivative cross product, and allow for nonlinear tangential moduli.

Willett and Poesch Model

Two years after Hakiel's model [132], Willett and Poesch [186] published a nearly identical nonlinear winding model. Similarities include not only nonlinear radial modulus capabilities, but also the finite difference solution technique and experimental verification of radial stresses by the axial press test (see Chapter 5). However, though Willett and Poesch were not the first to solve the nonlinear model, they did extend its capabilities somewhat.

First, the initial formulation included stresses and strains due to thermal changes. However, thermal analysis was not investigated in the published examples. Additionally, thermal expansion alone may not be useful unless coupled with a heat transfer model (as will be derived in Chapter 4). Secondly, they developed a novel solution to the difficult problem of Poisson ratio measurement using laser diffraction. From this experiment they concluded that the strain-energy constraint, which gives a relationship between Poisson ratios and moduli, did not hold for the magnetic tape material tested. Finally, they used a SOR (successive over relaxation) solution of the finite difference equation system instead of direct solution by the Gauss method. However, whether SOR improves accuracy or decreases solution time has not been demonstrated.

Though the Willett and Poesch article was generally correct and consistent with other models, two errors were uncovered. The first was a statement that the system of equations is tridiagonal and symmetric. The finite difference equations are tridiagonal only if three point derivative approximations are used, and the system is in general nonsymmetric as will be seen in Chapter 7. Secondly, in their text and their Figure 8 they labeled Altmann's model as isotropic which is rather limiting since it was the first anisotropic model [127]. In summary, the Willett and Poesch model is essentially identical to Hakiel's except strain-energy was not assumed (which is more general) and a different solution technique was used (which has not yet been demonstrated superior).

Pfeiffer Model

Pfeiffer is one of the more prolific winding authors with articles in guiding [48], radial modulus measurement [79], nips [110-112], and particularly roll structure measurement [165-167]. Additionally, he made a foray into analytical modeling of the winding of materials with nonlinear moduli [140, 141]. His novel formulation is based on a strain energy balance between incoming wound-in-tension energy and energy stored in a roll due to the addition of wraps.

This model is formulated from some of the constitutive relations that the previously discussed models use such as equilibrium, and a simplified stress-strain relation, as well as an identical outer boundary condition. However, his model is not consistent with the standard approaches because it does not include a core stiffness parameter and Poisson ratios. Additionally, he constrains the radial stress-strain behavior strictly to

$$(70) \quad \sigma_R = K_1 - K_1 e^{K_2 \epsilon_R}$$

..Though this strictly empirical relationship does indeed work for some materials, it may not necessarily model all materials well. The isotropic and linear anisotropic material cases are two examples, which are well covered in this text, that could not be modeled with Pfeiffer's exponential relationship.

However, there are even more serious questions about the veracity of Pfeiffer's model. First, Hakiel's Figure 8 [133] compares his model with Pfeiffer's using the same data. The resulting difference in radial stress exceeds 10% in some regions, which is far larger than the fractional percent difference between other winding models. Though Pfeiffer later updated his model [141] to correct an equation which had no theoretical basis and claimed that the models yielded the same stresses, this has yet to be independently verified.

Secondly, the shape of the tangential stress profiles are different than obtained by all of the other consistent models. In particular, while the tangential stress profile should have a positive second derivative at the outside (curve is concave up), Pfeiffer's [141 Figure 4] has a negative second derivative. Whether this problem was fixed by the update is also not known. Thirdly, he claims a coarse grid of 100 elements is sufficient to obtain better than 1% accuracy. Typically the other models require several thousand elements to model highly nonlinear cases such as these. Fourthly, a multiplicity of units and incorrect conversion factors given in the article create concern about the care by which the work was prepared.

However, the most damaging critique is given by Penner [139] who shows analytically that Pfeiffer's model is not energy consistent with the Altmann and Hakiel models which are consistent between themselves. We have shown in this chapter that the Isotropic, Altmann, Yagoda and Hakiel models are formulated from the same type of constitutive equations, and from Appendix B that they yield very precise numerical agreement. Consequently, Pfeiffer's model is at the very least inconsistent with these well proven models, and perhaps even incorrect from a mechanics viewpoint.

In summary, though Pfeiffer has numerous achievements in experimental winding, his analytical model is in serious question. First, it is not as general as the Hakiel model and secondly, it is not strictly consistent with all of the other models. Its only advantage is its apparent speed of calculation compared to models other than Yagoda's. Perhaps these inconsistencies will ultimately be shown to be negligible in practice. However, until this has been verified for a range of cases for a particular application, or until the potentially consistent energy formulation is corrected, its usefulness will remain in doubt.

Lekhnitskii Model

Lekhnitskii presents two interesting solutions to the stress distribution inside a pressurized composite ring [137]. Although his solutions to anisotropic rings are not strictly winding models because they are not accretive, they contain all the necessary elements to evolve into winding models provided that the two boundary conditions are included, and that the solution for stress distribution is iterated for wraps added from the core to the finish diameter of the wound roll. Simplistically, this could be formulated in a manner very similar to the Isotropic model presented earlier. However, these formulations will not be performed here as it is beyond the scope of this project. Additionally as will be seen, these formulations may not extend the generalities of winding models beyond their present capabilities.

The first solution is for the radial and tangential stress distribution of a 'roll' composed of layers of concentric rings of identical thickness h (which can be thick) which is pressurized on either or both boundaries. What makes this formulation unique is that each layer can have independently distinct material properties such as moduli. Thus, it could model the winding of composite materials such as tapes with relatively thick adhesives, or variations in properties in the MD which could be discretized to the nearest wrap. Finally the core boundary condition becomes immediately integrated into the solution as it would be nothing more than the inside rings (several are required to meet the constant thickness requirement), where the innermost contained the zero pressure boundary condition.

However, core boundary conditions are already handled by the current winding models, so that no additional capabilities are generated. Similarly, though not widely implemented, the composite material and variable MD properties could be handled by current winding models. The composite material can be modeled as a single wrap with effective material properties calculated from relative thicknesses and individual moduli. The only compromise is that the stress distribution within a single wrap is not directly generated by the winding model. The variable MD properties can also be handled by the finite difference models using lookup tables or formulas. Lookup tables are already required to calculate the nonlinear radial modulus at any particular radius.

The second solution is for the radial and tangential stress distribution of a 'roll' whose material properties vary as a power law function of radial position given by

$$(71) \quad E_R = E_{Rn} r^n$$

where n is an arbitrary real number. Unfortunately, since radial modulus is a direct function of radial pressure and only very indirectly of radial position, this power law relationship may be extremely restrictive.

In summary, while Lekhnitskii's formulations are novel and more closed-form than most, their application may be quite limited. This is primarily because they may provide no more generality than existing models. Consequently, the practical motivation to assemble and extend these solutions into working winding models is missing.

A Tangential Stress Formulation

As mentioned in Chapter 2, all current winding models are described by differential equations which follow the form

$$(72) \quad r^2 \frac{d^2x}{dr^2} + A r \frac{dx}{dr} + B x = 0$$

where x can represent one of five variables which include: displacement, w , stresses, σ_R or σ_T , or strains, ϵ_R or ϵ_T . The only differences are the two boundary conditions and the variable coefficients A and B which depend on the formulation. In this section, this principle will be demonstrated by deriving a tangential stress formulation very much along the lines of the Hakiel radial stress formulation. Furthermore, in Chapter 7 a displacement formulation will also be given.

The tangential stress formulation uses precisely the same set of constitutive equations as the Hakiel model and include equilibrium (53), strain-displacement (54, 55), stress-strain (56, 57) and well as the boundary conditions at the core (58) and current outer surface (65). The only difference is the order in which the equations are assembled. Since the tangential stress formulation results in much longer intermediate expressions, only an outline will be given of the derivation in a table form. Again, the symbolic math application Mathematica was used to increase the efficiency of the derivation and ensure accuracy.

<u>Eq'n</u>	<u>Source</u>
1	equilibrium constitutive equation
2a	radial strain-displacement constitutive equation
2b	tangential strain-displacement constitutive equation
3a	radial stress-strain constitutive equation
3b	tangential stress-strain constitutive equation
4	$w' = 2a$ into 3a
5	$w = 2b$ into 3b
6	$w' =$ derivative of 5
7	$sr' =$ solve 4 equal to 5 for sr'
8	$sr =$ solve 7 into 1 for sr
9	$sr' =$ derivative of 8
10	diffeq = 9 and 8 into 1
11	diffeq = expand and collect sr'' , sr' and sr terms
12	diffeq = reduce to standard form

The differential equation in standard form then becomes

$$(73) \quad r^2 \frac{d^2 \sigma_T}{dr^2} + A r \frac{d\sigma_T}{dr} + B \sigma_T = 0$$

where

$$A = (3*er^2 + der*er*r + 3*er^2*ur - der*er*r*ur - 2*der^2*r^2*ur + er^2*ut + er^2*ur*ut - der*er*r*ur*ut)/(er*(er + er*ur - der*r*ur))$$

$$B = (er^2 - er*et + der*er*r + er^2*ur - 3*er*et*ur + der*er*r*ur + 2*der*et*r*ur - 2*der^2*r^2*ur - 2*er*et*ur^2 + 2*der*et*r*ur^2 + er^2*ut + der*er*r*ut + er^2*ur*ut + der*er*r*ur*ut - 2*der^2*r^2*ur*ut)/(er*(er + er*ur - der*r*ur))$$

and where the typography is simplified such that 'der' for example, is the derivative of the radial modulus with respect to radius, and ur is the radial Poisson ratio etc.

Although the A and B coefficients could be obviously simplified if the radial modulus derivatives were set to zero as in Hakiel's model, the full general form has been retained here. Finally, the core and outer boundary conditions must be derived. Again in an abbreviated outline the core stiffness derivative is derived as:

<u>Eq'n</u>	<u>Source</u>
1	core stiffness definition constitutive equation
2a	radial strain-displacement constitutive equation
2b	tangential strain-displacement constitutive equation
3a	radial stress-strain constitutive equation
3b	tangential stress-strain constitutive equation
4	$w' = 2a$ into 3a
5	$w = 2b$ into 3b
6	$w' =$ derivative of 5
7	$sr =$ solving 4 equal to 6 for sr
8	$st' =$ solving 7 and 2b into 1 for st'
9	set $er'=0$ since it is not req'd as seen from radial stress formulation

$$(74) \quad \left. \frac{d\sigma_T}{dr} \right|_{r=r_0} = -\sigma_{T_0} \frac{E_C(-1 + \mu_R \mu_T) + E_R(1 + \mu_T)}{r(E_R + \mu_R E_C)}$$

Finally, the outer boundary condition is very simply

$$(75) \quad \sigma_T|_{r=r_n} = WIS_{r=r_n}$$

Thus, the tangential stress formulation starts from identical equations and shares a very parallel derivation. Consequently, it has precisely the same generality as the extended Hakiel model since variable wound-in-stress profiles, nonlinear moduli and all the other features are supported. However, there are two minor differences. First, the radial stress is calculated from the tangential stress profile using the equilibrium equation as

$$(76) \quad \frac{d\sigma_R}{dr} = \frac{\sigma_T - \sigma_R}{r}$$

This derivative must be stepped from the outer surface, where the radial stress is known, through all layers sequentially to the core. Thus, the radial stress calculation will accumulate error with decreasing radii. Secondly, the computer solution efficiency will be different from the radial stress formulation.

In summary, the winding differential equation can be described in one of five different mechanics parameters, all of which begin with an identical set of constitutive equations. The differences between these formulations are the coefficients A and B, the boundary conditions, and solution efficiency which will be described in more detail in Chapter 7 where the displacement formulation is derived, computer coded and evaluated. The tangential stress formulation though derived, is not computer coded and evaluated here as it is beyond the scope of this project. The only practical justification to code this formulation would be the possibility of improvements in computer solution efficiency. However, the tangential to radial stress calculation would need to be posed as an integration before the accumulative error problem were eliminated such that computer solution efficiency gains were even possible.

Summary of Winding Models

This chapter has followed the evolution of winding models from the simple isotropic model, to the linear anisotropic models by Altmann and Yagoda, to the nonlinear anisotropic models by Hakiel and others. With the evolutionary trend of increased model generality, the solutions became less closed-form and consequently more reliant on numerical approximations. Unfortunately as a consequence, the computer solution time and the propensity to numerical error also increased.

It has been shown through careful rederivation and comparison of stress output that the Isotropic, Altmann, Yagoda, and Hakiel models are entirely consistent within their range of application. Thus, while the earlier models might have been supplanted by more general models, they have been useful as a cross check of accuracy. Similarly, this close scrutiny has revealed numerous small oversights in the published winding model articles to date. Furthermore, it has been shown that Pfeiffer's model, though accepted for years, is not consistent.

In addition to those articles discussed in detail, there are several others published. These others have not been reviewed here simply because they are not distinct models. For example, Catlow et al [129] and Harland [124, 135] are applications of existing isotropic models, and Wolfeman [146, 147] reiterates the Altmann model. In this strictest sense, the Yagoda and Willett & Poesch models are simply new solution techniques applied to the Altmann and Hakiel models respectively. Thus, the evolution of winding models over the last three decades can be simply classified into three stages: $E_R = E_T$, $E_R \neq E_T$, $E_R = f(\sigma_R)$.

In practice, the choice of model depends on which will perform the required stress calculation as quickly as possible within the required accuracy constraints. Since most real winding situations involve nonlinear radial moduli, the Hakiel model (or variant) would be the preferred choice. However since it is a finite difference model, great care must be taken to make certain that the grid size is not adversely affecting the solution by running the same problem at more than one grid spacing. The only exception to the Hakiel model choice might be the Yagoda model if computational speed and accuracy is at a premium, and where the situation can be adequately modeled with a simple polynomial WIS profile, high anisotropy, and constant radial modulus.

In this chapter, a somewhat idealized model of winding is presented which may not well describe some situations. In the next chapter, more complex roll behavior such as air entrainment, nips, hygroscopic diffusion will be discussed. In some cases, these behaviors have analytical solutions which can be combined with the idealized winding model, while in others the behavior is only qualitatively understood. Additionally, Chapter 7 will present winding models which can be used for the measurement of stresses during winding, as well as developing the finite difference approximations to the Hakiel and other models. Finally, the appendices contain the computer code and calculated stress output for the models discussed in this chapter.

CHAPTER 4

COMPLEX WOUND ROLL BEHAVIOR

Overview of Complex Behavior

The idealized wound roll modeling presented in Chapters 2 and 3 describe the radial and tangential stress distributions as a function of WIS (wound-in-stress) profiles, geometry and material properties. The stress predictions from these models have been frequently verified to accuracies better than 10% [128, 132, 133, 186] using experimental measurements such as thin pressure transducers and the axial press test which will both be described in Chapter 5. Thus, the simplified wound roll models can adequately describe the physics of winding for some cases which are typically the centerwinding of elastic webs wound uniformly with respect to the CD, without slippage and without air entrainment.

However, many real winding situations are complicated by other phenomenon not presently described by the idealized winding models. These phenomenon include external and body forces beyond the WIS boundary condition such as nips [110, 166, 167], centrifugal stresses [150, 151], and gravity. The idealized winding model also simplifies the material description to elastic behavior, yet many materials have significant anelastic behavior such as hysteresis [79], creep, stress relaxation [144, 145]. Furthermore, winding wide nonporous webs at high speeds will entrain air between the layers [188], so that the effective radial modulus is reduced beyond the value given by static testing, and changes with time as air is squeezed out. The idealized models all assume cylindrical geometry, yet real rolls are lobed around the circumference [122], deform around nips, and vary significantly in the CD direction [195]. Deviations from cylindricity can become quite severe if defects such as crepes [109], corrugations, dishing [108] and starring are present. Finally, the strain-displacement relations assume no interlayer slippage, yet smooth low friction webs do slip inside a roll [106].

Some wound roll complications have analytical solutions or empirical treatments. However in most cases, only a minimal subjective understanding exists. Examples of analytical solutions include centrifugal stress [150, 151], and stress relaxation [144, 145]. An example of an empirical treatment is determining WIS as a function of winding tension, nip, and material [166, 167]. However, virtually all of the noncylindricity complications presently have no analytical or empirical methods which can be incorporated into fundamental roll structure stress analysis.

Though most of these complications exists to one degree or another for most winding conditions, the significance can vary widely from negligible to dominant depending of the details of the application. Thus, the first step in analysis is to determine the significance of a suspected complication. In some cases, there are experimental tests designed to quantify behavior. Examples include interlayer slippage which can be quantified by the J-line test [106], air entrainment which can be quantified for films by comparing material and roll densities, and roll shape [173]. However even if the phenomenon is quantified, the significance of its contribution to radial and tangential stress distributions are still not usually determined. Ultimately, the best test for significance is to compare predicted and measured roll stresses.

If a complication is determined to be significant, then its effect must be included in wound roll model analysis. In some cases, the complications can be analyzed separately from the idealized wound roll model. For example, the effective WIS for winders with nips can be determined experimentally [166, 167], and then the idealized wound roll model can be run. Conversely, the effect of stress relaxation can be analyzed after the wound roll model is run [144, 145]. However, in some cases the complication must be analyzed simultaneously with the simplified wound roll model such as the effect of centrifugally induced stresses [150, 151].

The inclusion of this chapter on wound roll complications is justified for at least three reasons. First, they affect the stress distributions beyond that predicted by simple and traditional wound roll models and thus serve as a checklist if discrepancies arise between predicted and measured stresses. Secondly, a simplified wound roll model is an integral part of this project on the measurement of stresses during roll winding, and thus this chapter serves as a list of shortcomings of the approach and suggests future work by others. Thirdly and most importantly however, these complications affect stresses and strains and as a consequence affect roll defects whose minimization is the ultimate goal of all work of this type.

The Effect of a Nip on Wound-In-Tension

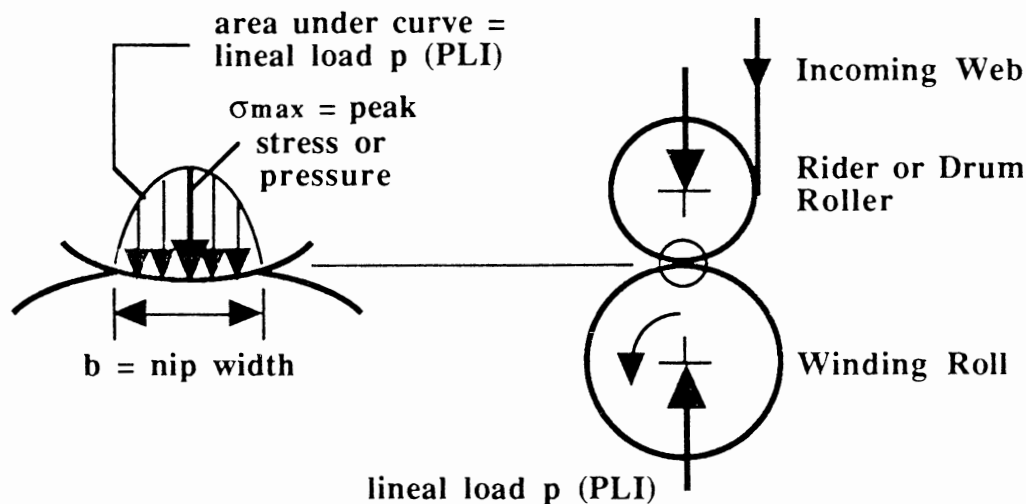
Many rolls are wound in either a surface or center-surface winding configuration such that the incoming web first enters a winding roll under a nip formed by a drum or rider roller. There are several reasons why a nip is used. First, the nip helps exclude air from being wound into the roll on nonporous webs. Second, many large rolls are more practically supported over a drum than through a center shaft which might be prone to excessive deflection due to gravity. Thirdly, a nip can allow a torque differential to be input into a roll if both the winding roll and nipping roller are motor driven. Finally, winding in the presence of a nip increases the WIT (wound-in-tension) beyond the free web tension which allows a somewhat independent choice of web tension for optimum transport through the winder, and WIT for optimum wound roll structure. Thus, WIT can be increased by either increasing web tension, increasing nip, or both.

It is the effect of nip loading on WIT that is most relevant to winding models as it is a required input parameter, and furthermore is one of the more useful control parameters for wound roll optimization. Unfortunately, though web tension and nip loading are easy to measure or determine, their combined effect on WIT is not. Thus in order to use wound roll modeling tools, the WIT as a function of web tension and nip must be determined. An analytical and experimental approach will be described here, as well as their shortcomings.

The analytical approach begins by noting that the stress distribution in a nip may be similar to the Hertzian contact between two parallel cylinders which in its simplest form was solved almost a century ago. Since then, the generality of the contact problem solution has been extended considerably to include such effects as tangential loads due to rolling friction. Much of this work has been performed by J.O. Smith and others of the University of Illinois at Urbana.

Rather than delve into the mathematics of contact solutions which will be shown to be inadequate in determining WIT, only an overview will be given. As seen in Figure 21, the pressure distribution between the relatively hard drum or rider roller and the winding roll is somewhat parabolic in shape. The geometry of this pressure profile is characterized primarily by the contact width, the peak pressure, and the area under the curve which is the lineal nip load. In addition to the stresses at the contact between the two cylinders, there are also stresses inside the wound roll which will be superimposed upon the already existing stress distribution due to winding.

Figure 21
CONTACT PRESSURES IN A WINDING NIP



The principal stresses are both compressive and decrease in magnitude at increasing depth and increasing distance from the centerline of contact [196]. However, the maximum shear stress occurs below the surface at depth of a fraction of the nip width deep. There are several implications of these superimposed contact stresses on wound roll behavior. First, the maximum radial or interlayer stress may be increased by the presence of the nip. This may adversely effect permanent bulk reduction on some materials such as tissue and toweling, and may damage nip sensitive materials such as tapes and carbon type paper. Secondly, if the shear stress is sufficiently large to overcome interlayer friction, slippage may occur which can increase the propensity to wrinkling.

Despite the quantification of stress distributions and the qualitative understanding of trends resulting from analytical contact pressure solutions, the fundamental question of how the nip affects wound-in-tension is still unanswered. Even if the solutions are improved to include anisotropy and rolling friction, this analytical approach falls short because it is an elastic formulation. Thus after the nip has passed, the stress distribution will return to precisely the same state as it was prior to the nip. Consequently, the simple elastic contact solution will leave no residual effect on the roll, which is in opposition to experimental observations that the nip does leave a residual effect [32, 97, 98, 166, 167]. Thus, a useful contact model must be extended to include interlayer slippage and friction. This extension, which is the subject of current research by Dr. J.K. Good at the Web Handling Research Center, is of fundamental importance to predict WIT for use in winding models with nips.

The second primary approach to determining the effect of nip loading on WIT is to measure it. Though there have been numerous attempts at measuring WIT which will be described in Chapter 5, none has been more successful than Pfeiffer's WIT-WOT lab rewinder [166, 167]. This single drum duplex lab rewinder can measure either wound-off-tension on the unwind, or wound-in-tension on the windup section. This is accomplished by wrapping the outer layer of the roll over a load cell tension roller, back over the roll, and out into the sheet run.

Using this rewinder, Pfeiffer experimentally measured the combined effects of web tension and nip loading on WIT. After collecting data from numerous runs, he empirically fit a WIT expression as

$$(77) \quad \text{WIT} = \frac{1}{B} \log\left(\frac{N + A}{A}\right) + \frac{T N}{C + D N}$$

but not > F N

where

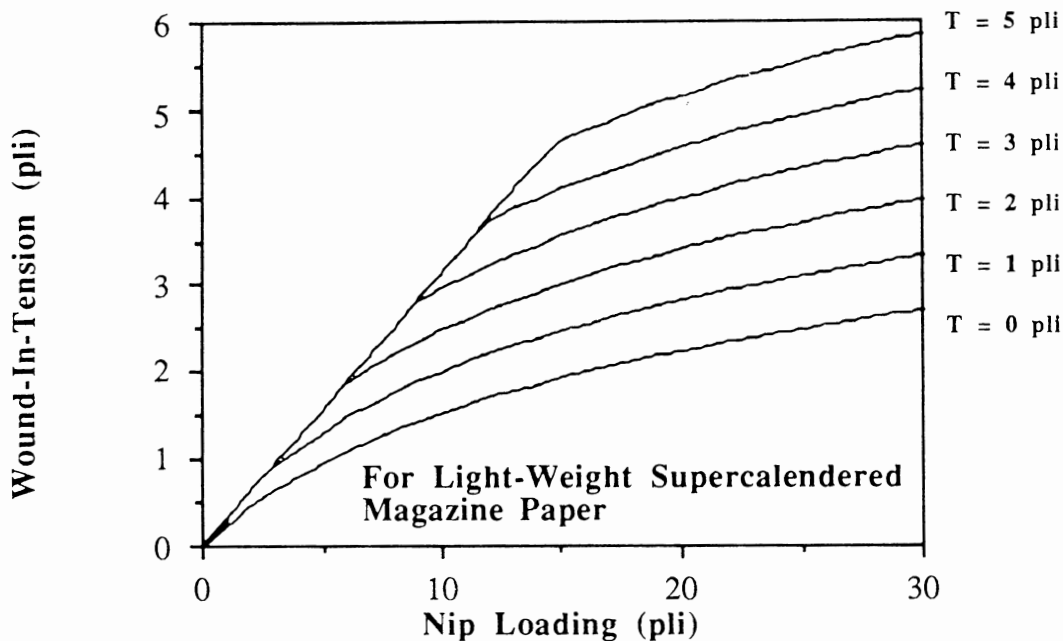
- WIT = wound-in-tension (pli)
- T = web tension (pli)
- and A through F are curvefit coefficients

The resulting coefficients for three grades of paper are given in Table 5, and the WIT as a function of nip loading and tension is shown in Figure 22.

Table 5
WIT COEFFICIENTS FOR 3 PAPER GRADES [166]

<u>Coef.</u>	<u>37.5#/3000ft²</u> <u>calendered kraft</u>	<u>38#/3000ft²</u> <u>lwc magazine</u>	<u>32#/3000ft²</u> <u>newsprint</u>	<u>Units</u>
A	6.99	4.75	17.02	pli
B	0.257	0.736	0.34	1/pli
C	6.35	7.44	17.29	pli
D	1.28	1.34	0.83	none
E	0.584	0.314	0.31	none

Figure 22
EFFECT OF NIP AND TENSION ON WIT



From Pfeiffer's experimental testing, several conclusions can be made.

1. WIT increases with increasing nip loading
2. WIT increases with increasing web tension
3. WIT increases due to web tension are limited by available interlayer friction
4. it may be possible to wind in tension with nip only (without any web tension)

Despite the revolutionary nature of Pfeiffer's work, it has several application limitations. First, the work is entirely empirical without first principles basis. Secondly, because it is empirical, each material must be tested to determine the required coefficients. Thirdly, since there are few winders such as the WIT-WOT, access to obtain this type of data is limited. Fourthly, experimental studies such as this are extremely time-consuming. Fifthly, no effect of torque differential is included in the original work. Finally though not mentioned by Pfeiffer, the coefficients also depend on the diameter of the nip roller and its surface condition. A simple model indicates that the effect of nip on WIT decreases with the square root of drum diameter [102]. Thus, this work would need to be repeated for various nips, tensions and torque differentials, on each material, and for each specific roller.

The effect of nips also affects this project for the measurement of web stresses during roll winding. As will be seen in Chapter 7 and Appendix D, the WIT is increased by increasing the torque differential, nip loading, web tension or a combination. However, this project completely bypasses the difficulty of determining the effect of torque, nip and tension on WIT. Indeed, one of the primary justifications of this project is to determine WIT by simple measurements coupled with winding models. Thus, while the traditional models often require the knowledge of the TNT's (torque, nip, tension) on WIT, this project does not. The reason for the difference is that the traditional models require knowledge of WIT (which depends on the TNT's) as an *input* to the models, while WIT is an *output* from this project's model.

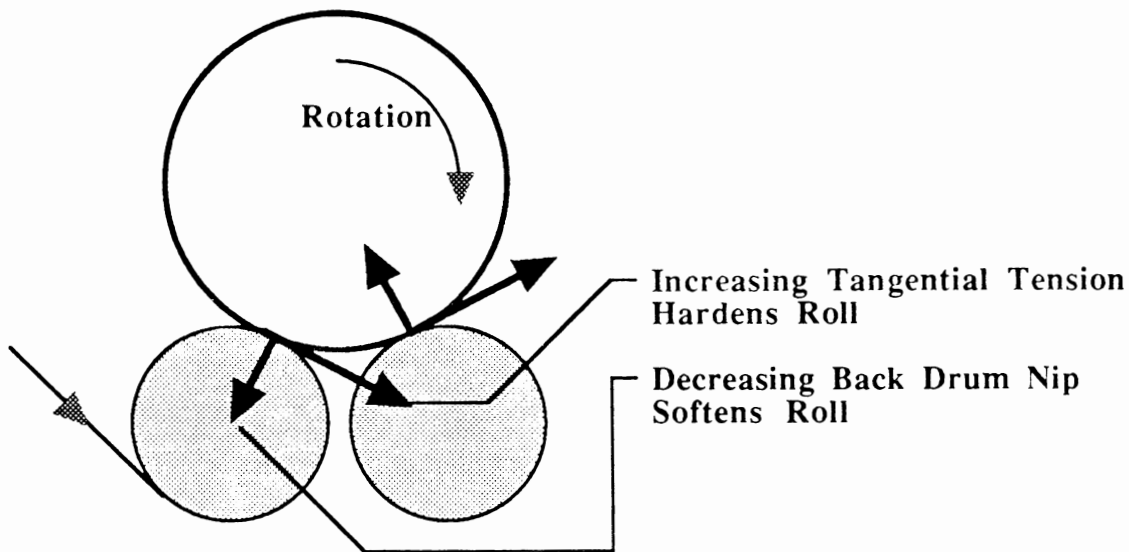
The Effect of Torque Differential on Wound-In-Stress

Just as with nip, torque differential between a winding roll and a roller, or between two nipping rollers also effects WIT. There is a functional difference however, because while nip can only increase WIT, torque differential can either increase or decrease WIT beyond the incoming web tension. However, there is little published work on the effect of torque. Odell found a measurable difference in density as a function of torque differential changes [32]. Hadlock proposed that torque differential be converted by statics to a force on the incoming nip roller that directly adds or subtracts from the incoming tension [102]. Again fortunately, this project can detect changes in WIT resulting from torque differential without specifically modeling the phenomenon.

The Effect of Speed Changes on Torque and Nip

When a surface driven winder accelerates or decelerates, the force to change the speed of the winding roll is often transmitted through the outer layer at the winding nip. In this case, the effective WIT will be changed in a manner not unlike a programmed torque differential. As seen in Figure 23 for a two-drum winder, the tangential load transmitted through the winding nip will tend to cause a hardening of the roll during deceleration. Additionally, the balance of nip loading on both drums changes such that the load on the back drum decreases during deceleration, while the load on the front drum increases. This phenomenon is very similar to the increase in loading on the front tires of an automobile during braking. Despite the back drum nip decrease, the effect of increasing tension on the sheet during deceleration is usually larger in magnitude [32]. However, the details of the drive motor programming on load sharing between the two drums during speed changes will have an effect on the magnitude of the resulting WIT change.

Figure 23
EFFECT OF DECELERATION ON TORQUE AND NIP



The effect of acceleration and deceleration on torque and nip can easily be calculated from kinematics given the acceleration rate, inertia (rewound roll diameter, density), drum geometry and drive motor load sharing. However, the same problem arises as in the previous two sections as to how to calculate WIT from torque differential and nip loading. Thus, once those two issues are resolved, the effect of speed changes on WIT will be easily quantifiable.

Centrifugally Induced Stresses

In addition to changes in speed, rotation of the roll at any speed will alter the stress distribution of the rewinding roll due to centrifugally induced stresses. These centrifugal stresses are superposed onto the already existing roll stresses due to addition of wraps under tension. Just as with the traditional winding models, the centrifugal models use a similar set of constitutive equations, but the equilibrium equation must be supplemented by body forces due to acceleration. There are two centrifugal models which vary in generality as well as solution technique which will be described below. The first is analogous to the isotropic model and has a simple closed form solution, while the second is analogous to the linear anisotropic model and has an exceedingly complex solution which is intimately tied to a traditional winding model.

The isotropic centrifugal model derived by Roisum [115] is based on a closed form solution given by Roark and Young [176] for the radial and tangential stresses in a homogeneous annular disk with a central hole (zero core stiffness) rotating at a constant velocity. These radial and tangential stresses are

$$(78a) \quad \sigma_{Rc} = \frac{3 + \mu}{8} \frac{\rho \omega^2}{386.4} \left(r_k^2 + r_0^2 - \frac{r_k^2 r_0^2}{r_i^2} - r_i^2 \right)$$

$$(78b) \quad \sigma_{Tc} = \frac{1}{8} \frac{\rho \omega^2}{386.4} \left[(3 + \mu) \left(r_k^2 + r_0^2 + \frac{r_k^2 r_0^2}{r_i^2} \right) - (1 + 3 \mu) r_i^2 \right]$$

where

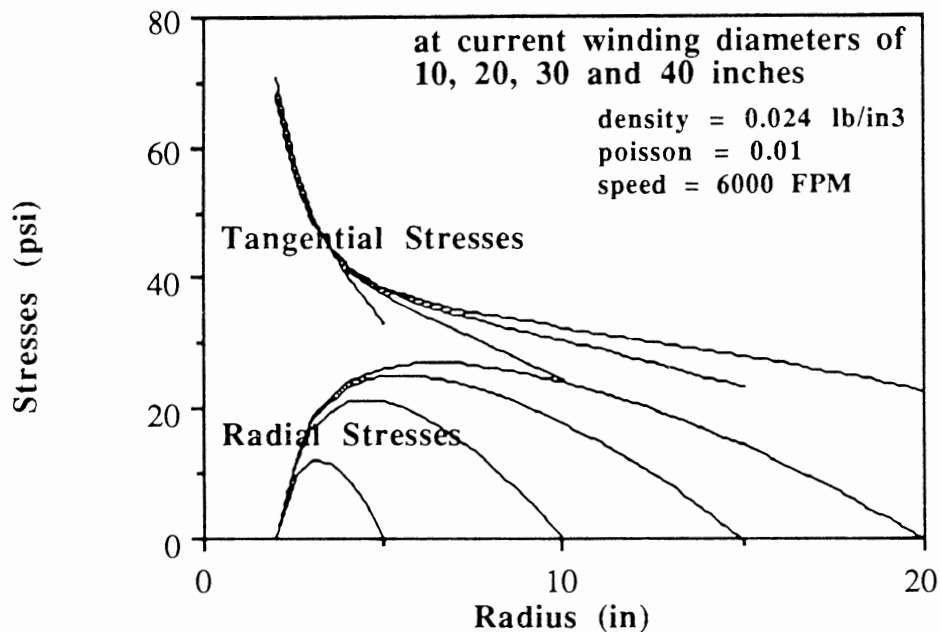
- σ_{Rc} = centrifugal radial stress at an interior radius (psi)
- σ_{Tc} = centrifugal tangential stress at an interior radius (psi)
- μ = Poisson ratio
- ρ = density (lb/in³)
- ω = angular rotational frequency (rad/sec)
- r_0 = radius of core O.D. (in)
- r_i = radius at which stresses are to be calculated (in)
- r_k = radius at current outer surface (in)

and σ_{Rmax} occurs @ $r_i \sqrt{r_0 r_k}$

Just as with the traditional isotropic winding model, the solution is closed form and does not depend on the modulus of the material (except through core stiffness). The stress distribution for a typical paper roll density winding at 6000 FPM is shown in Figure 24. Radial and tangential stresses are tensile throughout the roll, with tangential stresses slightly larger in magnitude. Also as with the traditional winding models, the radial stresses must be and are zero at the outer surface, and are zero at the inner surface if the core stiffness is zero. The peak radial stresses and its radial location occur at an intermediate location. The peak of the tangential stresses however, is at the core (for a zero stiffness core).

The effect of the centrifugal stresses are small but not negligible when compared with the traditional isotropic winding model. Additionally as we have seen from the traditional winding models, we would expect that the magnitude of the radial stresses to decrease and the magnitude of tangential stresses to increase with increasing anisotropy.

Figure 24
CENTRIFUGAL STRESSES - ISOTROPIC MODEL



Though the isotropic centrifugal model is very easy to apply, it does have severe shortcomings. First, the model presented here assumes a zero core stiffness boundary condition although this could be extended much as the isotropic winding model has been. Secondly, the model assumes isotropy which is not representative of most winding cases. Though the trends of the isotropic model will in general hold true for anisotropy, the values of the stresses will be considerably different.

The next step in the evolution of centrifugal models was the anisotropic model developed by Yagoda [150, 151]. The difference between his centrifugal model and his earlier winding model [149, 152, 153] is that the effective WIT changes as a function of rotational speed. This effective WIT, which is input directly into his traditional winding model, is the summation of three terms. The first is the web tension used by all winding models. The second is a slowdown term which occurs due to the decrease in rotational speed as the roll diameter builds even at constant surface speed. The third is a shutdown term caused by a decrease in surface speed. The details of the second and third centrifugal terms were not rederived for this project because they are even more complex than his hyperbolic solution of the traditional winding model. However he did conclude that for the cases tested, that the second and third terms of the centrifugal contributions nearly canceled, so that the net effect of centrifugal forces may be negligible.

Air Entrainment

Another effect of speed on winding is the entrainment of air into the wound roll. As seen in Figure 25, the translation of the incoming web and rotation of the roll drags a boundary layer toward and often into the roll. Additionally as seen from the side view, the distribution can't be uniform across the CD because the air at the edge of the roll will simply leak out. If there were a continuous boundary of air between web layers, there would be no effective interlayer friction and the structural integrity of the roll would be completely lost. This problem can be quite severe when winding nonporous webs such as film, and can severely limit the maximum operating speed of many winders to around 1000 FPM.

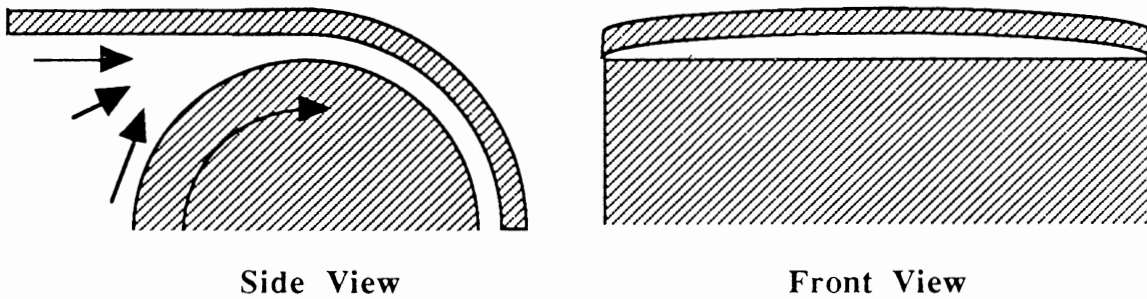
For many winding conditions however, the interlayer air boundary is not complete and is nominally trapped in a parabolic cavity with the ends relatively sealed. However, the distribution is likely to be thicker in low caliper gage bands, and need not necessarily be distributed uniformly around the circumference as evidenced by bubbles under the outer layer on the ingoing side of a nip. Consequently, the distribution of air in a roll in a real wound roll is likely complex.

One of the most effective methods to reduce the amount of entrained air is to wrap the incoming web around a nipping roller, and is standard practice on most nonporous web winders. The amount of entrained air decreases with increasing nip roller load and decreasing nip roller diameter [53]. Many rollers are grooved to increase traction. However, the winding nip roller may need be smooth and cylindrical else there will be unnipped and unrestricted channels for the air to follow into the roll. Additionally, the volume or thickness of air entrained into the roll increases with increasing speed, width, nip nonuniformities, and roll diameter; and decreases with increasing web tension, and web porosity [53]. For relatively incompressible nonporous webs, the volumetric percentage of air entrained into a wound roll can be estimated from

$$(79) \quad \% \text{ Air} = 100 \frac{\rho_{\text{material}} - \rho_{\text{wound roll}}}{\rho_{\text{material}}}$$

However, the volume and distribution changes with time due to end leakage, leakage through porous webs, repeated passage of nips and other changes in loading due to processing and handling.

Figure 25
AIR ENTRAINMENT INTO A ROLL OR ROLLER



The bulk of the analytical work in air entrainment originates from foil bearing theory [197-203]. However, though the inlet region of the foil bearing and winding roll are similar, their exit geometries differ considerably because in the case of the winding roll there is no exit. Additional limitations include incompressibility, no bending stresses, and often the solutions assume an infinitely wide system, so that CD effects are not considered. An interesting addition to traditional foil bearing theory was performed by Tajuddin who appended a simplified rider roll model onto the inlet region of the foil bearing model [53]. However though this model was pioneering, it is similarly constrained to the limitations described above and the rider roll addition also carries many assumptions to make the math tractable. The experimental work in foil bearing air layer measurement includes optical, capacitance and other precision position sensors [204].

Thus, the current state of art in analytical foil bearing theory results in solutions that are simultaneously difficult and simplified beyond useful application to real winding systems. Similarly, beyond equation (79) there has been no published work on the experimental measurement of air layer distributions in a wound roll. However, even if the distribution of air in a wound roll were determined, an equally formidable challenge to incorporate this information into wound roll modeling would need be solved. First, the roll would then be a composite material whose web behavior would be described by quasi-static mechanics equations, and the air layer would be described by time dependent fluids equations. Furthermore, these models should be formulated and solved together because the radial stress-strain distribution would affect the fluid pressure, while at the same time the pressure would affect the radial stress-strain distribution. Despite the difficulties however, the integration of air entrainment into winding models is requisite to their application for many real systems such as the winding of film.

The Cross Direction

Current winding models are accretive descriptions of stresses, strains, and to a lesser extent material properties, that vary in the radial and tangential direction. However, in many real winding conditions the material properties also vary significantly in the CD. In most cases, this is an unintentional result of less than perfect profile control on the machine which produces the web. The most significant CD variations on wound roll structure are usually caliper, tension, and perhaps modulus. However, web CD variations can also be intentional. One example would be discrete labels or stickers arranged in a matrix on a larger flat backing material.

There are several experimental measurements which can profile across the width which include hardness measurements such as the Rhometer, Schmidt Hammer and Bactender's Friend, as well as other measurement principles such as thin pressure transducers and the Cameron Gap. These methods and others will be described in more detail in Chapter 5. There is ample evidence from measurements such as these that a high gradient of profile is correlated to the propensity to certain defects such as corrugations [96, 193].

However, there is very little published analytical work on CD effect on winding. One exception is Spitz's model of the change in the tension profile of a web with a CD caliper variation as it is wound over an incompressible roll [142]. Spitz and others [162, 195] suggest a good measure of CD profile is radius variation

$$(80) \quad RV = 100 \frac{r_{\max} - r_{\min}}{r_{\text{avg}}}$$

where a 1% variation in caliper or wound roll radius would be considered excessive.

However, simplistic CD models such as these are unsatisfying as they are not mechanically consistent with traditional winding models because they lack basic features such as equilibrium and stress-strain equations. If CD effects were properly modeled then the relevant stresses would be radial, tangential, CD as well as the first appearance of shear stresses in winding models. The in-plane shear stresses could perhaps then be coupled to wrinkling models for a prediction of ropes and corrugations.

Hygrothermal Response

Paper taken from a paper machine reel and wound on a winder has a moisture level which is not necessarily in equilibrium with its storage environment. Similarly, film taken from a tenter is often much warmer than the ambient room temperature. Also, many petrochemical webs may contain volatile solvents from their manufacture which may diffuse into the environment with time. In all of these cases, the web and wound roll will take on or give up moisture or heat with time until it reaches equilibrium with its environment. In the case of paper products the equilibrium moisture content will be around 5%, and in the case of film the equilibrium temperature will be around room temperature. The effects of moisture changes on rolls can be quite vivid as evidenced by the innocuous but severe moisture welts or wrinkles occurring on the exterior of overly dried paper rolls.

Due to a high coefficient of hygroscopic expansion of paper, small changes in moisture content will result in large changes in stresses and strains. Similarly, changes in temperature of films and foils will also result in changes in stresses and strains. This can be easily seen from the orthotropic stress-strain relations (7) and (8) when expanded to include hygrothermal behavior as

$$(81) \quad \epsilon_R = \frac{\sigma_R}{E_R} - \mu_T \frac{\sigma_T}{E_T} + \alpha_R \Delta T + \beta_R \Delta C$$

$$(82) \quad \epsilon_T = \frac{\sigma_T}{E_T} - \mu_R \frac{\sigma_R}{E_R} + \alpha_T \Delta T + \beta_T \Delta C$$

However, before these expanded stress-strain relations can be inserted into winding models, the changes in moisture or temperature distributions must first be determined. The following material is based on analysis by Roisum [114] for moisture content of paper and was experimentally verified by weighing a small paper roll over the course of many weeks [118]. However, thermal analysis can be performed identically using this same procedure except that the material properties are thermal instead of hygroscopic expansion coefficients and the distribution is temperature instead of moisture.

Analysis of the hygrothermal response of wound rolls is an example where CD effects must be included because the moisture (heat etc) will diffuse from all exterior surfaces including the faces, the outer surface and possibly the core. The following analysis is based on Fick's Law of Diffusion which is identical in form to the Fourier equation for heat conduction in solids [205].

Assuming isotropy, radial symmetry and no moisture generation, Fick's Law can be written in cylindrical coordinates in r, z and t variables as

$$(83) \quad \frac{\partial^2 C}{\partial r^2} + \frac{1}{r} \frac{\partial C}{\partial r} + \frac{\partial^2 C}{\partial z^2} = \frac{1}{D} \frac{\partial C}{\partial t}$$

where

- C = moisture content (%)
or temperature T in degrees Fahrenheit
- r = radius (in)
- z = CD position (in)
- t = time (sec)
- D = hygroscopic diffusion constant (%/in²/sec)
or thermal or chemical diffusivity

Using a forward finite difference approximation for the temporal derivative and a central finite difference approximation for the spatial derivatives, (83) becomes

$$(84) \quad \frac{(C_{r,z}^{t+} - C_{r,z}^t)}{D \Delta t} = \frac{(C_{r-,z}^t - 2C_{r,z}^t + C_{r+,z}^t)}{\Delta r^2} + \frac{(C_{r+,z}^t - C_{r-,z}^t)}{2 r \Delta r} + \frac{(C_{r,z-}^t - 2C_{r,z}^t + C_{r,z+}^t)}{\Delta z^2}$$

where

t denotes current time

t+ denotes current time plus Δt

+ - subscripts denotes current radius or CD position +- Δr or Δz respectively

Solving (84) for future moisture at node r,z and collecting like terms gives

$$(85) \quad C_{r,z}^{t+} = + \left(\frac{1}{\Delta r^2} - \frac{1}{2r\Delta r} \right) (D \Delta t) C_{r-,z}^t + \left(\frac{1}{\Delta r^2} + \frac{1}{2r\Delta r} \right) (D \Delta t) C_{r+,z}^t + \left(\frac{1}{z^2} \right) (D \Delta t) C_{r,z-}^t + \left(\frac{1}{z^2} \right) (D \Delta t) C_{r,z+}^t + \left[1 - \left(\frac{1}{\Delta r^2} + \frac{1}{\Delta z^2} \right) (2 D \Delta t) \right] C_{r,z}^t$$

Additionally for numerical stability, the last term in (85) must be non-negative. If we let the mesh size be the same in the r and z directions then

for a given mesh size, ($\Delta x = \Delta r = \Delta z$), the maximum time step interval Δt is given as

$$\Delta t_{\max} \leq \frac{\Delta x^2}{4D}$$

or for a given time step interval, Δt , the minimum mesh size Δx is given as

$$\Delta x_{\min} \geq \sqrt{4D\Delta t}$$

Thus, equation (85) defines the solution of moisture distribution of the interior points of the roll in the next time step given the current moisture at the current and adjacent nodes. However in addition to the interior solution, the boundary conditions must also be defined. There are two mathematical possibilities which are a fixed or gradient moisture.

Strictly speaking, the moisture distribution is convective for both moisture and temperature. However in the case of moisture, the convective hygroscopic rate is so large that the outer layer of paper products very quickly reaches equilibrium and is maintained there. This is analogous to a well insulated wall which is near room temperature on the interior, and outdoor temperature on the exterior. However in the case of temperature, both rolls of film and paper often feel warm to the touch, so that a convective boundary condition should be used. Though a convective boundary condition is easy to implement on the above finite difference model, determining the convective constant could be quite difficult in practice.

The computer solution of the model is quite easily performed by predicting the moisture distribution of the next time step based on the current distribution and equation (85). This is implemented in three nested loops. The outer loop merely increments the time and other simple housekeeping. The middle and interior loops scan across the nodes in the r and z directions respectively.

In the following example problem, a 40" long by 40" diameter roll was modeled with a mesh with $\Delta r = \Delta z = 1"$ and $\alpha\Delta t = 0.25$. The initial concentration was uniformly set at C_0 at time $t = 0$ representing either a wet or hot roll. The boundary conditions at all exterior surfaces were set to C_1 at time $t > 0$ which represent drying or cooling.

The results of this example problem showed that the roll which was initially uniformly wet, asymptotically approached a uniformly dry roll after a sufficiently long time. However as seen in Figure 26 for 50 time steps into drying, the distribution of moisture is quite nonuniform. In particular, the roll is drier near the exposed surfaces than in the interior where moisture has yet to be diffused out.

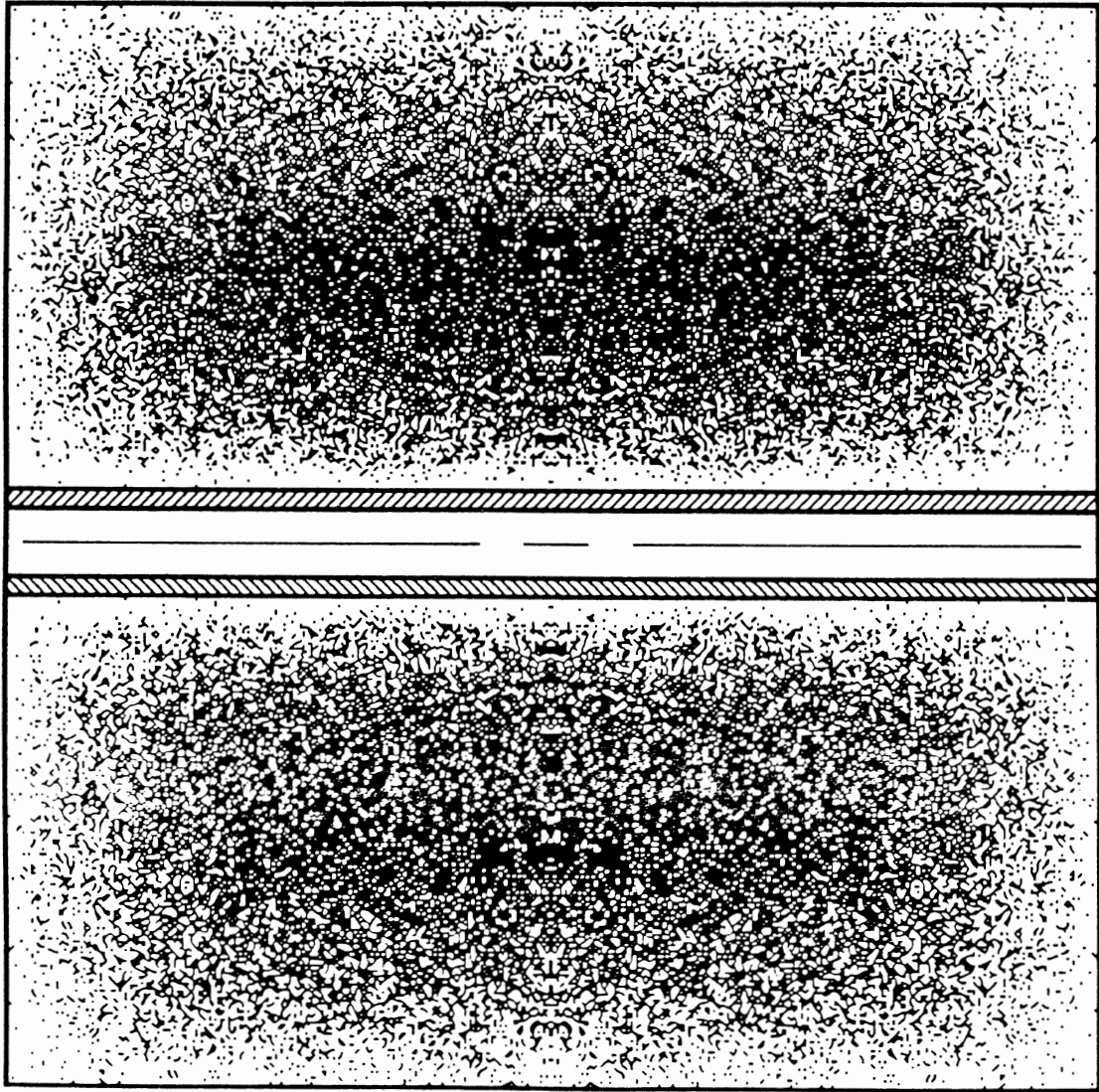
There are several implications of the nonuniform moisture distributions for web handling of materials with nonzero coefficients of hygroscopic expansion. First in the case of drying, the outer edges will have a shorter length than the center which will cause baggy centers. Conversely in the case of wetting, the center will have a shorter length than the edges which will cause baggy edges.

Additionally, there are several implications of nonuniform distributions for winding. First in the case of drying, the outer layers will contract first which may increase radial stresses significantly on the roll's periphery. In the case of wetting, the outer layers will expand first as welts or ridges. Also, cores which have a moisture content in excess of equilibrium will shrink upon drying to the point that some or all radial pressure at the core will be lost [161]. Finally, nonuniform distributions coupled with creep and stress relaxation could result in webs which are permanently nonuniform in camber.

Again, this simple example problem applies identically to nonuniform temperature distributions for cooling of film or foil materials because the constitutive equations are identical. Additionally, this simple analysis can easily be extended to convective boundary conditions, boundary conditions which vary along the face, OD, or core (but not directly with circumferential position with this 2D model), and boundary conditions that vary with time. Also, anisotropic diffusion coefficients can be directly used because the radial and ZD terms in (85) are completely uncoupled. This case could occur with the rolls of laminate materials or film with a significant interlayer air film which acts as an insulator.

The experimental verification of this simple example was easy to perform in the case of moisture whose average value can be determined by simply weighing a drying roll periodically over the course of several months [118]. Additionally from this work, the concept of a time constant was defined which is the time for the moisture content to reach 63% of its final equilibrium value after a step change at the boundary. This time constant concept can be applied to an exposed web in an open draw, a specific location in a roll, or as a bulk property of the roll.

Figure 26
PAPER ROLL MOISTURE / TEMPERATURE DISTRIBUTION
AFTER 50 TIME STEPS OF DRYING / COOLING



Dry or Hot



Wet or Cool

Scale

The time constant of hygrothermal analysis determines if it must be run simultaneous to traditional winding models, or can be decoupled. From the experimental work, it was found that the bulk drying time constant for a 40"x40" paper roll is on the order of one year, though it is somewhat sensitive to roll size and web material. Thus, drying takes place over a much longer period than the winding cycle and can be analyzed separately. Similarly, it was found that the moisture time constant for even a thin paper web exposed on both sides was typically longer than one minute [115]. Thus, the web's moisture content may not change significantly during its time of passage from the unwind to the winder, and thus can be assumed to be that measured on the interior of the unwinding roll.

The changing moisture and temperature distributions are relatively easy to determine by using equation (85). Additionally due to the long time constants, hygrothermal strains can be superposed onto the stress distribution already existing due to winding as a separate analysis step. However, applying the hygrothermal strains to rolls presents a problem because wound roll models describe behavior in the radial and tangential directions while hygrothermal strains occur in all three axes. A simplification would result if these strains were analyzed on a single plane normal to the roll axis such as at the end or center. Then the distribution on that plane could be input into the expanded stress-strain relations.

To solve the resulting hygrothermal stress would involve rederiving a winding model such as Hakiel's presented in Chapter 3 while retaining the hygroscopic and thermal terms, which could be done without difficulty. Next, the expanded model would be solved once for a single system of equations which as the result of superposed hygrothermal radial and tangential stresses. The outer boundary condition for this analysis would be a zero radial stress for there are no wraps added during the process of drying or cooling. Finally, the hygrothermal radial and tangential stresses can be superposed onto the already present winding stresses for a total stress distribution. Notice that this differs from the traditional model, which is accretive, in that the solution for the incremental stresses need on be done once for a given moisture distribution. However, the analysis would need be repeated if the stresses are desired for more than a single time in the drying process. Also, Tramposch gives a similar but more restrictive thermal model [145].

In summary, hygrothermal response can be significant for the winding of many materials where the web is not in hygroscopic or thermal equilibrium with its environment. Hygrothermal distributions are easy to determine using the finite difference solution of the Fourier equation. From these distributions, an expanded traditional winding model can calculate the resulting hygrothermal stresses provided that the distribution is assumed constant across its width.

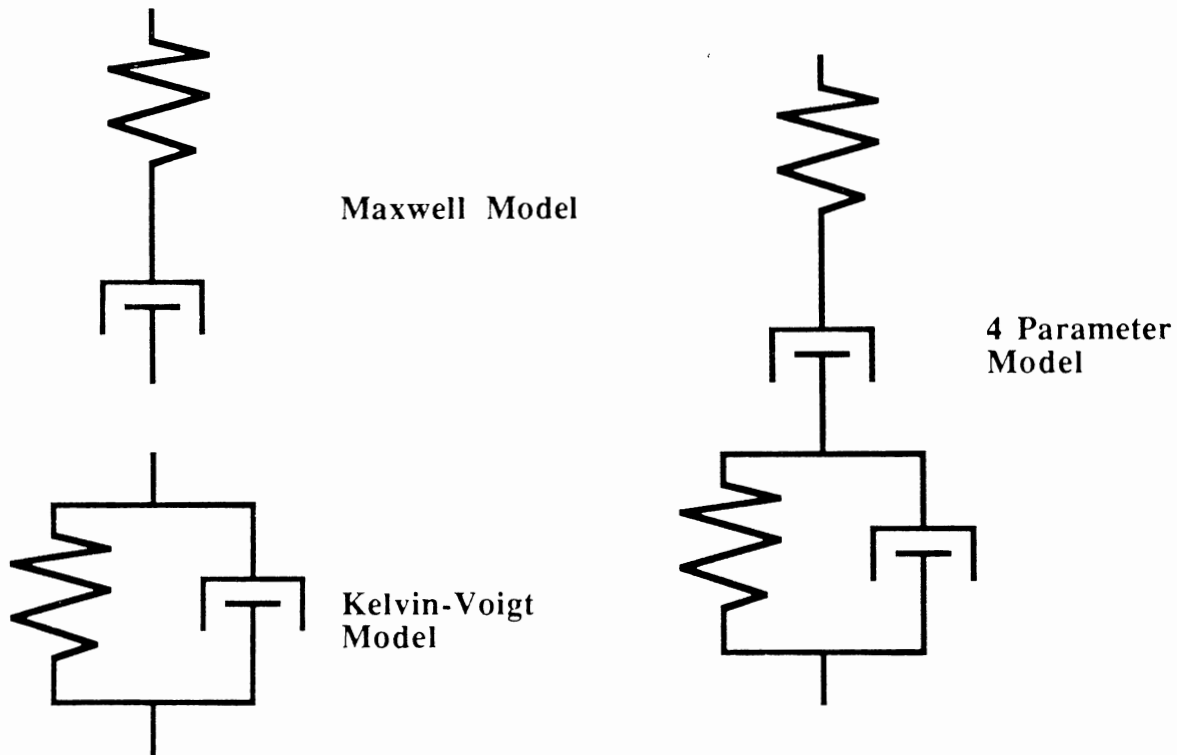
Anelastic Response

All traditional winding models assume that the web material is elastic. This assumption implies that the material will load and unload along the same stress-strain curve. However as seen from Figure 17 in Chapter 3, the load and unload cycles of real materials follow distinctly different paths. Furthermore, the elastic assumption implies that the web material will return to the same shape and length after unloading. However as seen from stress-strain curves of real materials, webs may assume a permanent strain of the same sign as the loading stress after the load has been removed. This behavior is evidenced by baggy lanes on overstretched nonuniform gage materials, changes in registration, flat spots on rolls which were stored on the floor, and permanent loss of thickness or bulk as will be seen in caliper data in Chapter 8. Finally, the elastic assumption implies that no energy is absorbed in a load/unload cycle. Yet if this was true, the coefficient of rolling friction of a wound roll would be quite low, while in fact the rolling friction of some soft materials is quite high.

Clearly, the assumptions of elastic behavior may not model real materials well. There are several viscoelastic models, though they are generally empirical, which are able to represent some of the complex behavior described above. As seen in Figure 27, the most common models are the Maxwell, Kelvin, and 4 Parameter models. All of the models can describe creep and stress relaxation. However, the Maxwell model predicts indefinite amounts of creep under a constant load. Similarly, the Kelvin model is unable to describe partial recovery after load removal. Consequently though much more difficult, the 4 Parameter model is able to better represent real web behavior.

Though much work exists on viscoelasticity, particularly for the Maxwell and Kelvin models, little has been applied to wound roll geometries. However, Tramposch has solved the isotropic [144] and anisotropic [145] stress relaxation of the 4 Parameter model applied to a disk with a zero load outer boundary condition, and an elastic inner boundary condition, under an arbitrary initial stress condition due to winding. Additionally, the model allows for thermal strains for the simple case of a constant initial temperature disk cooling under constant temperature boundary conditions. Though this model is mechanically consistent with the traditional winding models, it is easily the most mathematically complex derivation in winding. Despite the complexity however, analysis such as this is requisite for extending the traditional winding model beyond its simplified elastic assumptions.

Figure 27
VISCOELASTIC MODELS



Interlayer Slippage

Current winding models assume no interlayer slippage in the derivation of the strain-displacement relations for a cylinder. However, there is ample experimental evidence that slippage does occur under some conditions. This includes direct measurement using the J-line [106, 109], rolling cylinders across flat stacks [97, 98, 110], and the increase in WIT with increasing nip load [166, 168]. While interlayer slippage can occur during unwinding and centerwinding, in most cases slippage is significant only in the presence of a nip and is most pronounced on low coefficient of friction materials [106, 108]. Additionally, it has been observed that in both cases of J-lines near the core on a core supported unwind and on the outer surface of a surface nipped windup, that the interlayer slippage is generally in the direction of loosening of the web [106, 108]. The justification for modeling slippage is therefore because it affects the stresses in a wound roll, is not currently described by traditional winding models, and is associated with the propensity to certain defects such as crepe wrinkles [109].

Thus, there is some experimental work which quantifies interlayer slippage based on measurement, such as the J-Line given in Figure 28. Unfortunately, there is no first principle analytical models which can predict the magnitude of slippage, or well determine its effect on wound roll stress distributions. However, there is promising research in this area begun by Dr. J.K. Good at the WHRC using finite element modeling with friction elements between layers. These analytical models when developed would not only predict the magnitudes of slippage, but as importantly determine why slippage occurs in the first place.

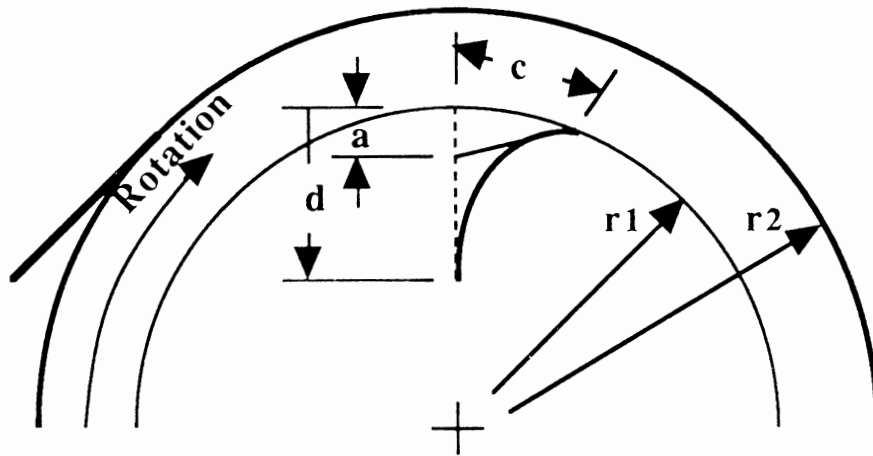
Though analytical models explaining *why* slippage occurs are lacking, a model which explains *how* slippage must have occurred to meet experimental measurement has been proposed by Roisum and is the basis for the following discussion [121]. This model requires two measurements of a J-line geometry as inputs to a slippage function which then yields the distribution of interlayer slippage as a function of depth beneath the roll surface, and as a function of time or added wraps. Additionally, the model can calculate the change in tangential stresses due to slippage.

The model begins by assuming that there is a slippage function which can describe the movement of each layer with respect to the one beneath for each wrap addition during the winding roll. Furthermore, it is assumed that this function moves with the outer surface much as the outer boundary condition of a traditional winding model moves with the outer surface. From these very nonrestrictive assumptions, the entire slippage model can be constructed.

Figure 29 shows a simplified schematic of the application of a slippage function and its effects on the shape of the J-line. For example, with the addition of wrap 'e' the interior layers each move with respect to its underlying wrap by an amount specified by the slippage function. Thus, wrap d's movement is the sum of d with respect to c, c with respect to b and so on. With the addition of wraps f and beyond, the process is repeated again for each revolution, except that the slippage function moves with the surface. Though not necessary, the slippage function chosen here is maximum at the surface and decreases with depth. The result of the addition of numerous wraps with this type of depth decreasing slippage function is that J-line movement which is initially fast, soon stabilizes into the characteristic 'J' shape.

From this schematic, it can be seen that the total movement of any layer at any current outer wrap is the result of two effects. The first is the summation of relative movement of layers beneath for the addition of a single wrap, and the second is the superposition of this movement for the addition of all wraps from the moment the J-line was struck until the specified number of wraps have been added.

Figure 28
J-LINE GEOMETRY



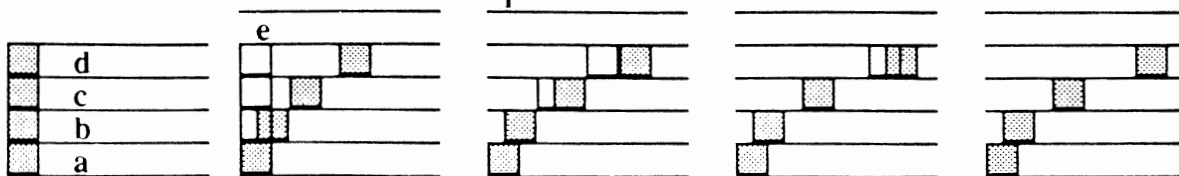
c = max. circum. movement
 c/a = slope of tip

d = depth below J-line tip
 $r1$ = radius when line struck
 $r2$ = radius after winding

Figure 29
SLIPPAGE FUNCTION SCHEMATIC

Schematic Linear Slippage Function, for each revolution:

top layer moves 3 units wrt to 2nd layer
2nd layer moves 2 units wrt to 3rd layer
3rd layer moves 1 unit wrt to 4th layer
no movement below third layer



J-line struck when
 d is top layer

b moves 1 wrt a
 c moves 2 wrt b
 d moves 3 wrt d

b moves 0 wrt a
 c moves 1 wrt b
 d moves 2 wrt d

b moves 0 wrt a
 c moves 0 wrt b
 d moves 1 wrt d

no further
movement as
layers are beneath
depth of influence

Though this can be also be expressed as a double summation for numerical calculation [121], this total J-line movement will be expressed here as:

$$(86) \quad J(d,n) = \int_{w=0}^{w=n} \int_{D=m \equiv \infty}^{D=d+w} j(D) \, dD \, dw$$

where

$j(D)$ = relative slippage function (in/wrap²)

$J(d,n)$ = new position of J-line (in)

d = depth below J-line tip to point of interest (wraps)

D = independent variable of slippage function (wraps)

w = current number wraps added ($0 < w < n$) (wraps)

m = number wraps from point of interest to core

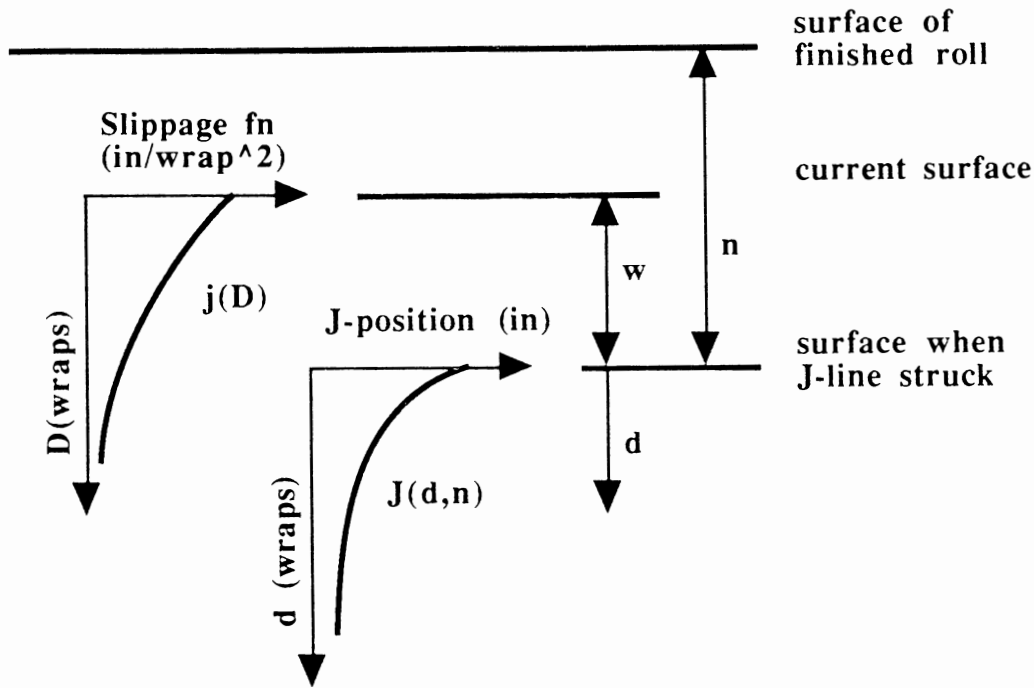
n = total number wraps added since J-line snapped (wraps)

The double integration limits and are better shown in Figure 30. The inner integrand is the slippage function which when computed yields the inches of movement per wrap added as a function of wraps beneath the current outer surface, and follows the current building of the outer surface by wrap addition. The outer integration yields the J-line deformed position as a function of depth below the J-line tip and the number of wraps added. However, the J-line does not move radially outward as does the slippage function.

Thus far, no assumptions have been made whatsoever about the form of the slippage function, only that one exists and depends directly on depth beneath the current surface. However, in order to quantitatively apply the model the form of the function must be determined. Additionally once the form of the function is found, the parameters or constants must be determined for any particular situation.

There may be several approaches to determining the slippage function including first principles modeling and experimental measurement. However, as yet no first principles slippage models have been published. Additionally, direct experimental measurement of the slippage function for a real system may be quite difficult because the slippage between any two adjacent layers will be quite small for the addition of only a single wrap.

Figure 30
SLIPPAGE FUNCTION AND J-LINE



Fortunately, the J-line position itself is easy to measure as it is the double summation of slippage of all layers beneath and for all wraps added. Thus, while the slippage function itself may not be easily measured, several empirical forms can be tried to see which may yield a J-line position which agrees with experimental measurement and observation. In particular, at least three J-line observations must be predicted by the slippage function form. First, the growth of the J-line slewing during *normal winding* must be rapid at first but quickly slow or freeze to a final shape when the J-line is sufficiently below the current outer surface to be under negligible influence from events on the distant outer boundary. Similarly, the growth of J-line slewing under the condition of *no paper addition* such as during a web snapoff and stop must agree with observed real behavior. Finally, the shape of the J-line at any instant will in general have greatest movement at the tip and decreasing to near zero movement at the root. Thus, the requirements of matching the measured J-line shape as a function of revolutions of the rewound roll during normal winding and the case of rotation without adding wraps both constrains and gives confidence to any slippage function which describes these behaviors.

The experimental measurements used for determining the best form of the slippage function and ultimately verifying the model are taken from Lucas [109] and are given in Table 6a. These measurements are made for the same LWC paper grade running on the same winder for both the normal winding and the no wrap addition case, and the J-line shape parameters refer to Figure 28.

Three 2-parameter slippage functions were evaluated and include a constant, linear, and exponential functions. Additionally, the parameters for each of the slippage function forms were solved using a calculus derivation, to be given shortly, and based on the shape measurements given in Table 6a. The 'A' parameter determines the maximum relative slippage between the current outer layer and the one beneath. The 'B' parameter is related to the depth of influence of the interlayer slippage. The relative slippage functions are graphed in Figure 31.

The results of the modeling for normal winding are shown for the three slippage function forms in Figure 32a. Though the slippage functions for each of these cases is very different, the resulting J-lines are very similar. Indeed, they all predict precisely the same maximum tip deflection, c , and the same tip slope, c/a , and have a shape very similar to those generally observed. The only major difference is the depth of influence, which Lucas characterizes by a 'r' parameter [109]. If this was the only test of the slippage function form, the constant model is slightly closer to the appropriate shape and gives a 'r' parameter almost identical to the experimental measurement, though this is difficult to measure accurately.

However, the slippage function form and model must also describe the effects of revolutions without adding wraps, such as after a web snapoff. This is also computed using the same constants A and B as above, and the same equation (85) except that the upper limit of integration of the inner integral is $D=d$ instead of $D=d+w$ because w is zero due to the fact that the current surface is the same as the surface at which the J-line was struck (no web added), and that the upper limit of the outer integral represents revolutions instead of wraps added. The results of the model for the case of a snapoff is shown in Figure 32b. As seen here, the predicted J-line deformation for the three slippage function forms is very different. Clearly, though the exponential model does not predict J-line root quite as well in a normally wound roll, it matches tip slope, a , within about 1% of Lucas's measured values. Additionally, the model predicts 501 revolutions were wound to achieve the shape measured by Lucas, which corresponds to a typical slowdown period for the winder used in that study.

Table 6a
J-LINE SHAPE MEASUREMENTS [109]

<u>Parameter</u>	<u>Description</u>	<u>Normal Value</u>	<u>Snapoff Value</u>
c	max tip movement	0.43"	2.80"
a	tangency of slope at tip	0.23"	0.24"
r	depth of movement	0.42"	0.66"

Table 6b
SLIPPAGE FUNCTION FORMS EVALUATED

<u>Function</u>	<u>j(D) Equation</u>	<u>A (in/wrap²)</u>	<u>B</u>
Constant	A for D<B, 0 for D>B	0.0000730	78.74
Linear	A*(1-D/B) for D<B, 0 for D>B	0.0000494	230
Exponential	A*exp(-D/B)	0.0000366	154

Figure 31
SLIPPAGE FUNCTION PLOTS

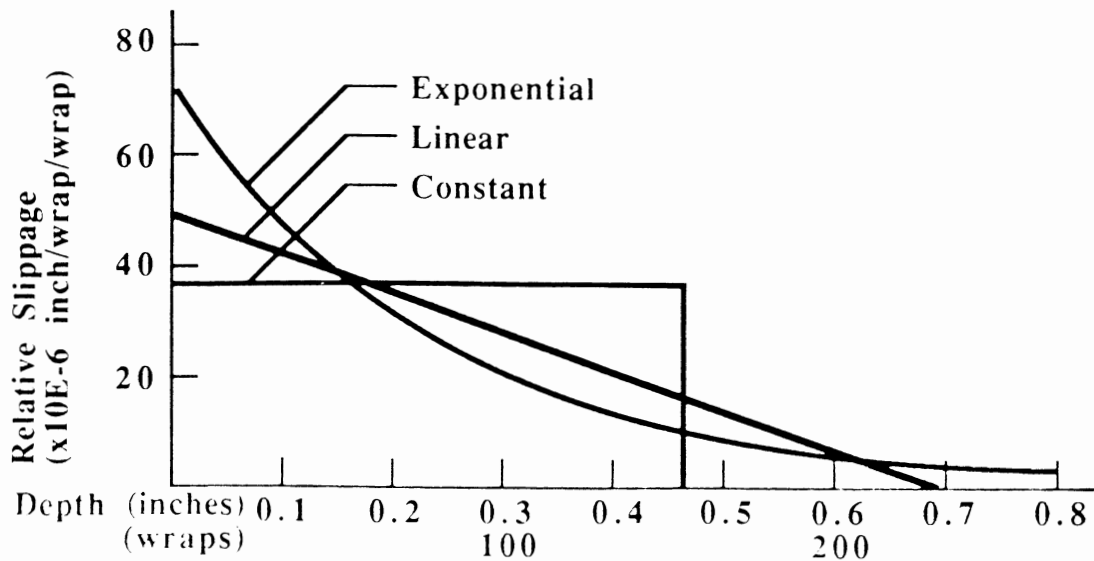


Figure 32a
J-LINE DEFORMATION - NORMAL WINDING

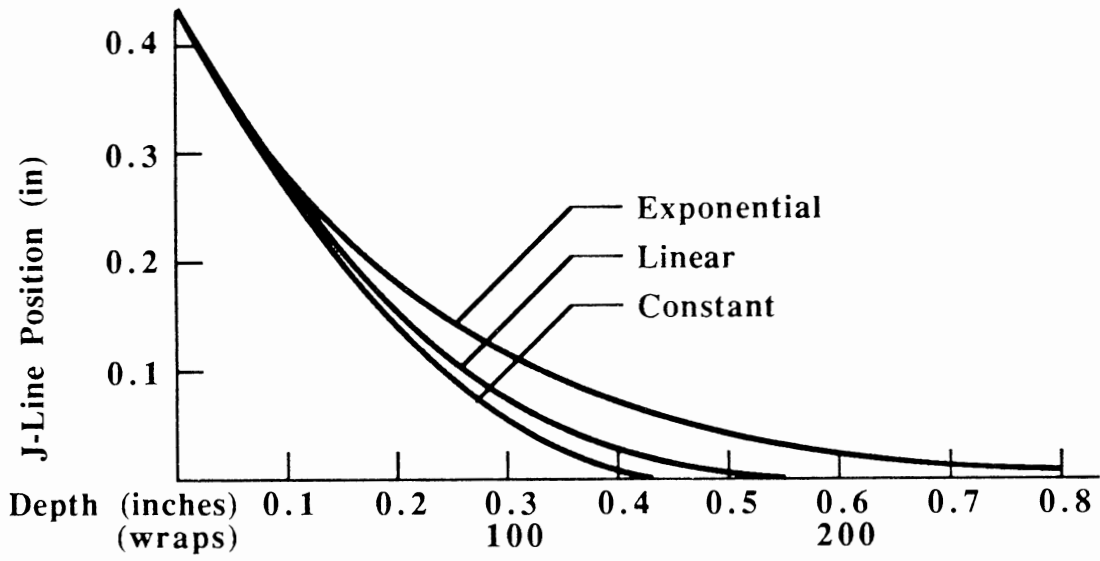
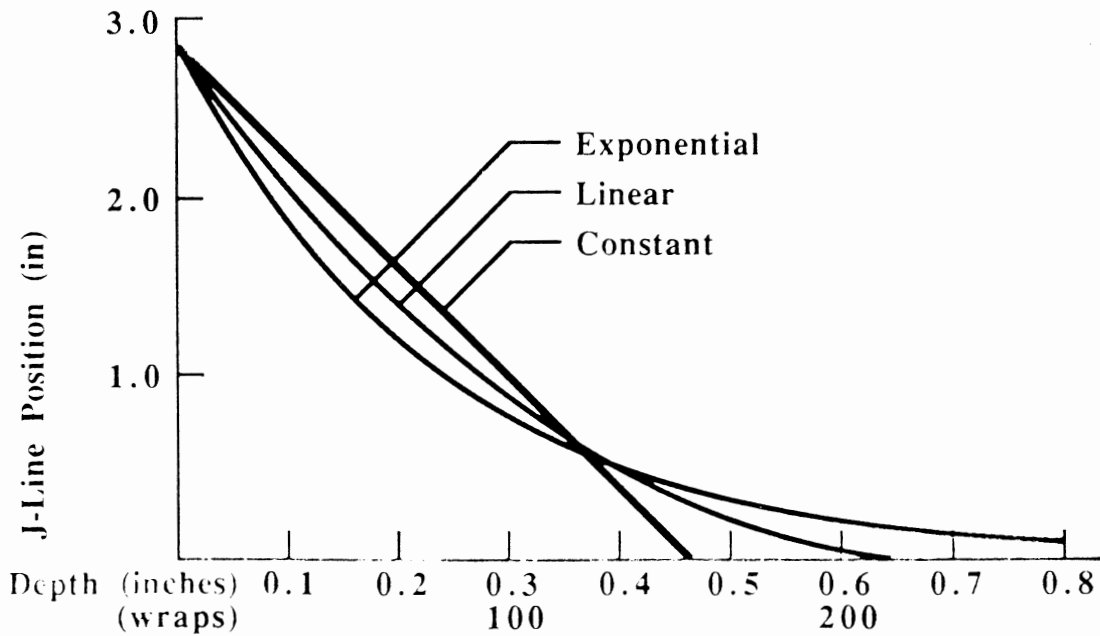


Figure 32b
J-LINE DEFORMATION - AFTER SNAPOFF



One final check on the behavior of the model is to determine if the progression of the J-line movement matches the observation that the movement begins fast but quickly stabilizes. As seen in Figure 33, the J-line progression predicted by the model does indeed show a rapid initial movement followed by stabilization.

The experimental measurements used for the preceding discussion were for J-line deformation of the outer surface due primarily to the passage of nips during winding. However, a similarly appearing phenomenon can occur at the core of a core supported unwind. In both cases, the J-line movement is generally in the direction of loosening which is also the direction of winding or unwinding. However, the shape of the J-line in the case of a core supported winder is slightly different. Again, the relative slippage model was used to try to predict the core J-lines given by Frye [96]. However, the three slippage functions used above did not yield the turn-in of the J-line tip or the indefinite J-line progression which is characteristic of core slippage. However, the model did predict proper core J-line shapes with two small changes, as seen in Figure 34. First, that the slippage function was rectangular. Secondly, that the slippage function moved outward one wrap for every two revolutions.

The progression of J-line movement for any relative slippage function is solved easily by using either a computer program to compute the double summation or by using the integral given in (86). Though there is more generality in the double sum, an analytic slippage function can be solved directly to give many insights into slippage. In particular, the exponential slippage function

$$(87) \quad j(D) = Ae^{(D/B)}$$

can be inserted into (86). Simplification results if the lower limit is assumed to be infinity which corresponds physically to depth of slippage influence which is negligibly small compared to the distance to the core. In this case, the first integration yields

$$(88) \quad J(d,n) = -AB \int_{w=0}^{w=n} e^{\left(\frac{d+w}{B}\right)} dw$$

and finally, another integration yields the deformed J-line shape

$$(89) \quad J(d,n) = AB^2 e^{-d/B} (1 - e^{-n/B})$$

Figure 33

PROGRESSION OF THE J-LINE DURING WINDING

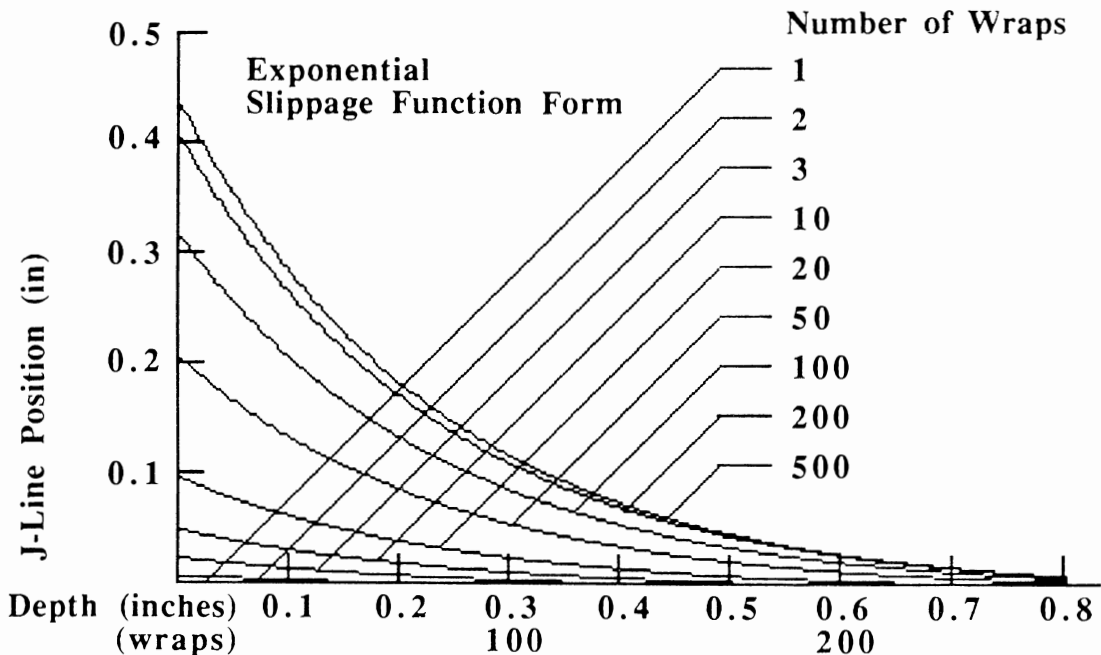
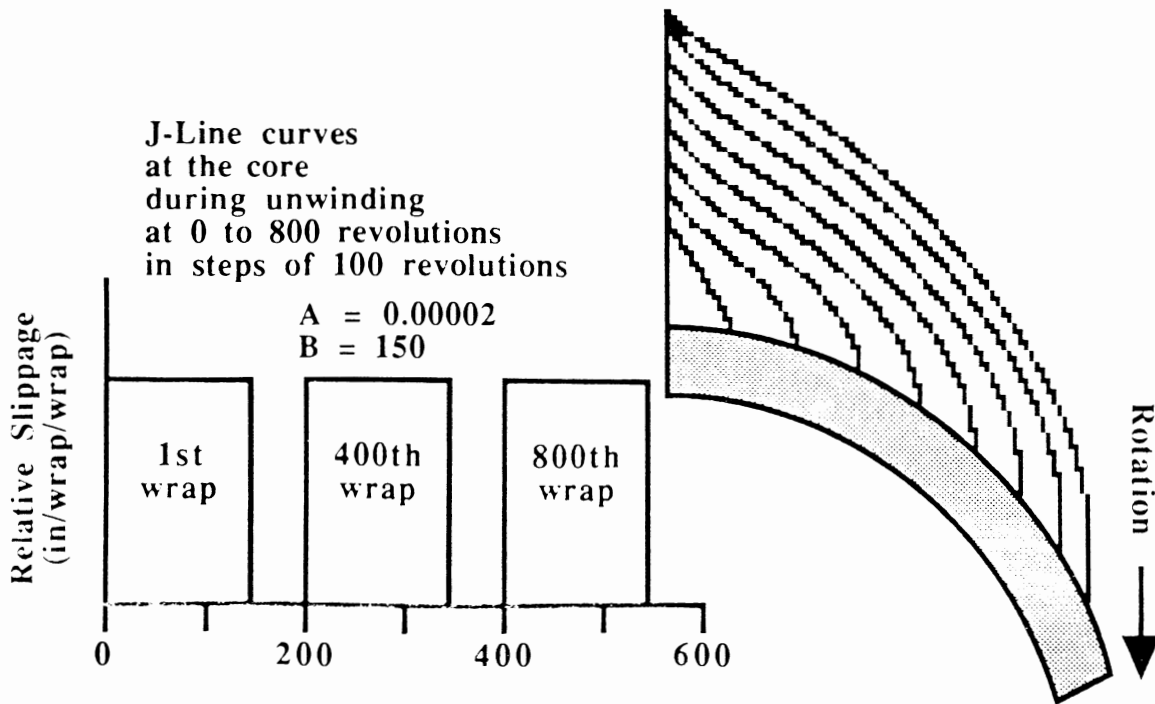


Figure 34

J-LINE SLIPPAGE ON A CORE SUPPORTED UNWIND



Equation (89) can be tested for proper behavior such as

if $n = 0$ then $J = 0$: therefore no movement unless there is wraps or revolutions added

if $n = \infty$ then $J = AB^2 \exp(-d/B)$: therefore movement is bounded

if $n = \infty$ and $d = 0$ then $J = AB^2$: maximum deformation occurs at tip

The slippage parameters A and B can be calculated from measurements of J-line geometry from equation (89) for the exponential form. The maximum tip deflection, c, is calculated for a depth of zero and for a large number of added wraps such that J-line movement is stabilized and is given by

$$(90a) \quad c = J(0, \infty) = AB^2$$

Similarly, the tip slope is calculated for a depth of zero and for a large number of added wraps by taking the derivative of the J-line at the tip and is given by

$$(90b) \quad \text{slope} = t \frac{c}{a} = \left. \frac{d J(d, n)}{d d} \right|_{d=0, n=\infty} = AB e^{-d/B} (1 - e^{-n/B}) \Big|_{n=\infty} = AB$$

where t is the web thickness and c and a are the tip deflection and tangency respectively illustrated in Figure 28. Finally, equations (90) can be solved for the exponential slippage parameters A and B as

$$(91a) \quad B \text{ (wrap)} = \frac{a \text{ (in)}}{t \text{ (in)}}$$

$$(91b) \quad A \text{ (in/wrap}^2) = \frac{c \text{ (in)}}{[B(\text{wrap})]^2}$$

Finally, the J-line movement can also be used to calculate the change in tangential stress due to interlayer slippage for small movements as

$$(92) \quad \sigma_{T\text{slip}} = E_T \epsilon_T = E_T \frac{\Delta}{2 \pi r_1} = \frac{E_T t}{2 \pi r_1} \frac{c}{a}$$

For the large J-line movement given by Lucas [109], and a thickness of 0.003", a radius at which the J-line was struck of 10" and a modulus of 500,000 psi, the resulting change in tangential stress was 44.6 psi which is a small fraction of wound-in-stress. The small effect of slippage on average stresses has also been noted by other authors using different techniques [168].

Several other interesting conclusions result also from this analysis. First, is that the area under the relative slippage curves for any function form must all be equal as they are proportional to the tip slope. Secondly, widely varying relative slippage functions will yield shapes very similar to measured J-line geometries, so that the technique is not very sensitive to uncertainties of the slippage function form. Thirdly no matter what form is chosen, large J-line deflections are predicted by a maximum slippage between the outer and second wraps of only 50 millionths of an inch per revolution.

However, there are limitations to the relative slippage modeling. First, it assumes that the relative slippage function remains significantly constant with time or added wraps, yet friction coefficients, radii and nip loadings do change during roll winding. Secondly, it assumes that the slippage is constant around the circumference as do all other winder models, and thus can only predict average trends. Yet, perhaps the severest slippage problem is crepe wrinkling which results when the slippage occurs abruptly in a narrow circumferential region. Unfortunately, this average relative slippage technique is currently unable to describe circumferential dependence. Also, the relative slippage technique is currently limited to reverse engineering of how movement must have occurred to produce a given J-line geometry. A better understanding would be achieved if the relative slippage was predictable from first principles modeling, which is the subject of current research efforts at the WHRC.

In summary, the relative slippage technique can be used to model the average accumulated movement of every layer for every revolution, and describe the J-line shape provided that slippage as a function of depth is known from either first principles modeling, direct measurement, or from measurement of J-line geometry. The calculation of J-line shape at any time can be calculated most generally from a computer program which keeps track of a double sum for every layer beneath the J-line tip. However analytic relative slippage functions though more restrictive, have closed form J-line deformation expressions which are more convenient. From the modeling, very small relative slippage between any two layers during a single revolution of the wound roll results in large J-line deformations. However, even large J-line deformations represent relatively small changes in the stress state of the roll, provided that the slippage is uniformly distributed around the circumference.

Gravity and External Loading

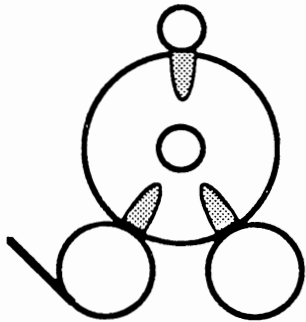
In addition to the winding nip described earlier in this chapter, there are several other loads which can be applied to the wound roll. Several of the more typical loading cases are shown in Figure 35. First, there may be rolling nips aside from the winding nip. In the case of the two drum winder, there are also nips at the rider roll and front drum. Additionally, there is an internal rolling nip between the core and inner layers which can be considerably larger in magnitude than external nips for large core supported rolls. There is strong evidence that all rolling nips can lead to interlayer slippage at the core [96] as well as at the outside [106, 109]. Additionally, there is strong evidence that in addition to the winding nip the other rolling nips can also effect WIT changes beyond that produced by the web tension and winding nip [97, 98, 168].

However, several loading cases commonly occur during storage or handling which affect internal web stress distributions that are not uniformly distributed around the circumference. These loads to produce permanent set may be relatively low and act for a long time, or high and act for a short time. An example of a low load acting for a long time is rolls lying on the floor or in storage racks which have the tendency to retain flat spots. These flat spots induce web flutter and tension surges which may impair productivity of the process served by the unwind [120, 122]. Rolls stored in a core supported stand also take on an eccentric set which similarly affects subsequent processing. Consequently, many rolls are supported on end which considerably reduces anelastic deformation.

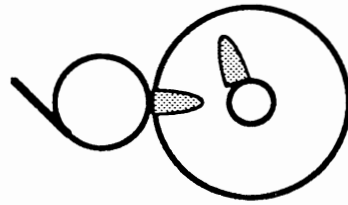
Conversely, if the loads are high enough they need only act over a short period to induce permanent changes in shape and stress distributions. One example is the grab truck which squeezes the roll on opposite sides of the OD [173]. Another example, which is common in roll handling equipment, is stopping a moving roll with roll stops that are too stiff. Though both low loads for long periods and high loads for short periods both affect roll stress distributions nonuniformly, there is a difference. The impact or grab truck squeeze loading is much more likely to trigger starring type defects.

Currently, there is little published analytical work describing the superposition of circumferentially nonuniform loading on wound roll stresses. Though finite element modeling may address some aspects of the problem, the analysis is inherently very nonlinear due to contact loading against a curved surface and anelastic behavior. However, there is some experimental work on roll shape profiling which can help diagnose the causes and quantify effects of nonuniform loading [173] which will be discussed further in Chapter 5.

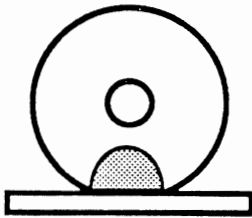
Figure 35
TYPICAL EXTERNAL LOADS



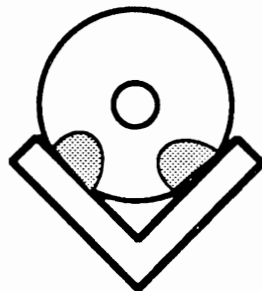
3 Rolling Nips on
2-Drum Winder



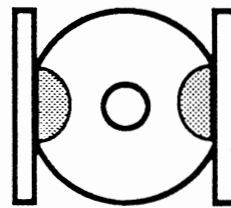
2 Rolling Nips on
Core Supported Surface Winder



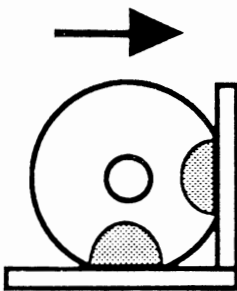
1 Point Storage



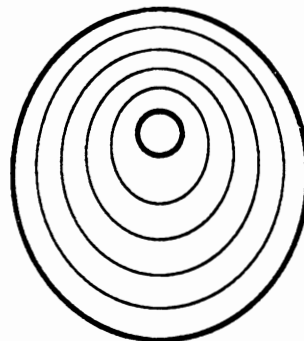
2 Point Storage



2 Point Grab



Impact Against Stop



Core Support Deformation

Roll Defect Theory

Though minimizing roll defects is the principal goal of the science of analytical and experimental winding research, very little has been published in this area. What little does exist comes primarily from experimental studies such as the correlation between caliper or hardness gradients and wrinkle or burst defects [96], and the minimum radial pressure at the core required to avoid loose cores [161]. The reasons for the dearth of roll defect theories may be due to application dependence, complexity, lack of either understanding or confidence in winding principles, or simply that the state of the art has yet to mature to meet its ultimate goal. Whatever the reason however, in this section some simple roll defect theories will be proposed which are assembled from established mechanics principles.

The simplest failure theories state that materials will fail if the stress exceeds the ultimate strength, or more conservatively the yield strength of the material. The stresses imposed on the material are the superposition of both the traditional wound roll model stresses and more complex behavior such as external loading at nips or hygroscopic stresses. Since the wound roll system is highly anisotropic, there will be failure criteria in both the radial and tangential directions. Additionally, many materials have different yield magnitudes in tension and compression. Thus, no fewer than four boundaries exist for the stress profile, and each will be discussed in turn.

$$(93a) \quad \sigma_{R,r} > \sigma_{R \text{ compressive yield}} \quad \text{for all } r$$

The radial pressure must not exceed the yield pressure of the material which may lead to permanent loss of bulk for soft materials such as tissue, or cause breakdown of constituents such as with carbonless paper, or cause extrusion of components such as with tape adhesives, or cause wringing of layers together such as with films. In the absence of external loading and other complexities, the location of the maximum radial pressure as seen in the figures from Chapter 3 for the typical WIS profile and high core stiffnesses is at the outer core radius. If external loading due to core support is also included, the maximum radial pressure at the core is further increased due to the core/roll nip. However, in many cases the external loading at the roll periphery may dominate due to excessive nips, heavy rolls lying on their periphery or rolling impact.

$$(93b) \quad \sigma_{R,r} < \sigma_{R \text{ tensile yield}} \quad \text{for all } r$$

The maximum interlayer tension non-adhesive materials can withstand inside a wound roll is less than or equal to zero. However, adhesive materials can withstand some interlayer tension if it is less than the strength of the adhesive bond. In the absence of unusual complexities, the maximum interlayer tension will occur on the bottom side of the core/roll nip for heavy core supported rolls for which Hussain suggests a minimum 50 psi pressure for newsprint [161]. However, the interlayer pressure may also go to zero on either side of a heavy nip as evidenced by bubbles of entrained air which may cause wrinkling and creasing if the bubble goes through the nip unevenly or suddenly.

$$(93c) \quad \sigma_{T,r} > \sigma_{T \text{ compressive yield}} \text{ for all } r$$

There is a lower limit on tangential stress to avoid buckling or compressive yielding. The location of the minimum tangential stress for typical WIS profiles and high core stiffness occurs at the core radius. However, the tangential stress can often be compressive throughout all but the outer radii of the roll.

$$(93d) \quad \sigma_{T,r} < \sigma_{T \text{ tensile yield}} \text{ for all } r$$

Finally, the upper limit on tangential stress avoids web breaks or tensile yielding. The location of the maximum tangential stress in almost all cases is at the roll OD and is equal in magnitude to the WIS. However in addition to the traditional wound roll stresses, drying or cooling may superpose even greater tangential tensions upon the material [114].

These failure theories are somewhat simplistic as the material is under biaxial stress, where the stress in one direction affects failure in the other. In materials science, more advanced failure theories include the superposition of these two directions such as in maximum shear, octahedral shear, distortion energy and Von Mises stresses. Additionally, materials science also includes other more complex failure theories such as fracture and cumulative damage due to fatigue. However, a more relevant interaction of winding stresses occurs for starring or buckling failures where the compressive tangential stress promotes instability and the compressive radial stress promotes stability.

These failure theories thus far discussed are based on stresses and material failure. However, there are several roll structure requirements based on deflection that also must be met. For example, the winding of wide rolls on slender cores may result in excessive bowing of the core due to its own weight or external nip loading [11]. Another core example is that the ID of the core must not expand under load beyond the stroke of expandable shafts.

Other deflection based failures can result if there is any interlayer slippage deflection due to external loading. The simplest example is that the interlayer pressure and friction must be high enough to unwind a roll which is braked through the core without interlayer slippage. In this case, the interlayer frictional torque must be greater than torque applied to the unwind or centerwind by web tension at all radial locations.

$$(94) \quad 2 \pi l r^2 \mu \sigma_{R,r} > r_{OD} * WIT \quad \text{for all radii } r$$

The failure modes described above are those for which a simple mechanics description exists. Unfortunately, there are numerous other failure modes for which even classification and appellation are ambiguous [99]. Though these are often very application dependent and are often more of a material defect nature than strictly winding, they are nevertheless a very important aspect to the economics of winding.

Furthermore though there are numerous failure modes, there are few controllable parameters. As discussed in Chapter 1, process constraints often exist which preclude varying such things as machine geometry and material properties to optimize winding. Indeed, the only general controllable variable is the WIS profile which depends on the TNT's (torque, nip, tension and speed), each of which has its own constraints. Thus, the number of failure modes far exceeds the number of variables which can be controlled. The results of this mismatch of problems and solutions is that in general roll defects can't be eliminated and the best one can hope for is the reduction in their number and severity.

The science of optimizing winding then becomes one of minimizing a penalty function which is quantified as the sum of the products of the cost of a defect and the frequency of occurrence for each defect type as a function of the controllable variable(s). In other words, the defects must be quantified and their net effect minimized through multivariate nonlinear optimization with constraints. Though Blaedel devoted his thesis to developing 'A Design Approach to Winding a Roll of Paper', his contribution was merely to outline the necessary tools as he did not apply the technique to a real or even simulated winding system.

In summary, the goal of the science of winding is to minimize defects. In simple cases of material limit based failures and simple winding systems, many of the tools are already in place to minimize a single defect type at a time. However, true optimization awaits additional quantitative developments in the description of more complex roll behaviors, and more comprehensive roll defect theories.

CHAPTER 5

ROLL STRUCTURE MEASUREMENT

Background

The ultimate goal of roll structure measurement is to determine if visually undiscernible defects are present in a roll so that it may be rewound or culled, and future defects prevented by appropriate changes in controllable parameters. It is believed that if measurements are too low that the roll will not have sufficient integrity to survive subsequent handling. Conversely, a high measurement might indicate the potential for bursts and other damage by overstressing the material. Additionally, the desirable profile is often believed to be harder at the core and tapering smoothly to a softer finish, and uniform across the width [102]. An abrupt change in the profile as a function of diameter or width are presumed to indicate the potential for starring and corrugations respectively.

Many publications have evidenced the cause and effect relationship between changing the TNT's (Torque, Nip and Tension) of winding and a resulting change in some roll structure measurement. Unfortunately, there is very little published data to support the widely held belief that roll defect prediction can be made from roll structure measurements. If better quantitative relationships between roll structure measurement and roll defects are established, then it would be appropriate to consider designing the structure of a roll such that defect frequencies are reduced. Blaedel outlined such an approach using penalty factors and optimization routines, though he did not actually implement the concept [128].

Roll structuring is the profiling of the TNT's of winding as a function of roll diameter such that the roll is wound tight enough to survive loads during winding, handling, shipping and unwinding; but not so tight as to damage the material. The concept of roll structure measurement and control to optimize winding and to minimize defects evolved slowly in a parallel development with winding machine controls [90]. Recent microprocessor technology evolution has also influenced roll structure measurement, especially for the density analyzer and for data acquisition.

The evolution began with winders that were only equipped with a weighted strap brake on the unwinding roll to crudely set web tension. At this time, roll structure measurements were made by operators who struck rolls with short wooden clubs known as backtender's sticks to sound roll tightness or hardness. Though roll hardness as measured by a billy club is not a fundamental roll structure property and lacks quantitative definition, it is nonetheless useful and omnipresent at most winders.

In the 1950's and 60's, pneumatic control of unwind brakes for web tension, rider roller nip load, and electric drive control of drum torque differential gave operators the ability to vary the setpoint TNT's (torque, nip, tension and speed) as a function of current diameter to optimize the wind [90]. Simultaneously a better understanding of the relationship of TNT's to roll quality evolved from observations that varying these control parameters produced observable effects in roll hardness. Consequently, a proliferation of inventions were designed to quantify roll structure or hardness profiles which included tests such as the gap test, and instruments such as the Rhometer. Though the need for good roll structure measurement methods is as strong as ever, one of the few concepts to appear in the last two decades was the density analyzer which is a computer based instrument which measures ingoing web length and roll rotation. The density analyzer development parallels the application of PLC and other computers to control TNT setpoints.

There are many measurement methods that have been used to attempt roll structure profiling. Most of these methods are based on either hardness such as the Rhometer and Schmidt Hammer; or friction such as the core torque, pull tab and Smith Needle; or strain such as the Cameron Gap test. Furthermore, all present methods will either profile across the width of the roll or with diameter but not both, so that a complete three (or more) dimensional picture of winding is very difficult to obtain [169, 171]. The impact hardness testers will profile across the width, but only at the current outer diameter unless the roll is unwound and measured at various diameters. The remaining methods will profile as a function of diameter, but will only give an effective average of variations across the width. Since the TNT's are usually programmed as a function of diameter instead of width, roll structure measurements profiled as a function of diameter are better suited for determining optimum control setpoint functions. Conversely, profiling across the width is better suited for diagnosing problems with CD (Cross Direction) nonuniformities in the web and winding machine.

Since roll structure measurement has been invention driven, there is a blurring of definitions such that hardness, density and tension are used almost synonymously, though conversion and direct comparison between these different units of measure are not usually possible. Only those units that are closely related to the fundamental roll structure parameter of web stresses such as the gap test and WIT can be converted. Though in principle it would be possible to convert interlayer pressure profiles and density profiles to WIS profiles if supplemented by winding models, this has not been done.

Despite the wide variety of measurement techniques available, methods based on the fundamental parameters of web stresses are confined to special lab studies because of immense practical difficulties. Furthermore, only the density analyzer is able to monitor roll structure with any semblance of online measurement automation. Clearly there is a need for a fundamental roll structure measurement method than can operate in a production environment as well as a lab. This unfulfilled need for a good winding measurement is the impetus for this thesis work, which is the marriage of analytical modeling with an extension of density analyzer hardware.

In this chapter, the various roll structure measurements based on hardness, pressure, strain and other means will be discussed. Though there are more than a dozen methods, most have been only applied for special research studies. Thus in addition to their principles of operation, application and limitations will also be described. The interested reader will find a more thorough treatment of roll quality measurement by Roisum [169, 170]

Rhometer

Quantification of roll hardness became possible with the invention of the Rhometer in 1965 by Pfeiffer. The principle of operation of the Rhometer, shown in Figure 36, is analogous to an electronic version of the backtender's stick where hardness of the roll is judged by the magnitude of the rebound. The handheld Rhometer contains a small trigger activated striker which is instrumented with an accelerometer. After the striker is released, the peak impulsive deceleration of the striker hitting the rewind roll is converted by electronics into a reading displayed on a meter. The meter is graduated into 'Rhos' where $1 \text{ Rho} = 3 \text{ G's}$ (acceleration of gravity). The value of the reading is related to an integration of the interlayer pressure of the outer inch or so of material. Further improvements to the original design by Beloit's Wheeler division incorporate a traversing carriage drive for automatically profiling hardness across a roll or set of rolls, strip chart output, and modernized electronics.

Rhometer sales are about equally divided between paper and film, but is more predominant in the United States than elsewhere. Despite the Rhometer's popularity, it does have several drawbacks. It is sensitive to operator technique, so that variations are seen between different operators, and beginners have difficulty in obtaining consistent readings due to slight variations in the way it is held. Also, the Rhometer has an undesirable sensitivity to grade and roll diameter. Dense grades such as supercalendered paper and film read higher than more compressible grades for identical WIS values. Additionally, the Rhometer will read higher on small diameter rolls than larger rolls. Though the Rhometer is not based directly on the fundamental roll stress parameter, the readings are more sensitive to roll structure changes than many other measurements [169, 171]. Additionally, the Rhometer is one of the few measurements that have been correlated to roll defects. Burns showed that a 100% Rhometer screening would flag about half of the rolls containing bursts, which made it a useful go/nogo quality control tool despite its high rate of false positives [156].

Schmidt Hammer

The Paper Roll Hardness Tester, also known as the Schmidt Hammer and Schmidt Concrete Tester, is also an impact tester. This handheld device is composed of a spring loaded plunger/hammer which is pressed against a roll causing a compression of the spring, as seen in Figure 37. When depressed sufficiently, the spring is released causing the plunger to strike the roll and rebound [159]. The magnitude of the rebound is recorded on a mechanical pointer scale as well as on an optional strip chart. This device, marketed by Testing Machines Incorporated, was used originally to measure concrete hardness and later modified to measure roll structure. The Schmidt Hammer has been used to diagnose paper manufacturing process problems which result in hardness variations across the width [193].

Though both the Rhometer and the Schmidt Hammer are both handheld hardness testers, there are several differences. The Rhometer measures peak deceleration while the Schmidt Hammer measures a parameter more closely related to the coefficient of restitution. While the Rhometer is prevalent in the United States, the Schmidt Hammer is the preferred method in European paper mills. Most importantly however, the Schmidt Hammer has been tested to give poor resolution of sensitivity to roll structure changes on some grades [169, 171]. Due to their handheld convenience, the Rhometer, Schmidt Hammer and the Smith Needle which will be described shortly, are the only roll structure measures that are commonly used in production.

Backtender's Friend

While the Rhometer and Schmidt Hammer are suitable for cross machine hardness profiling, the Backtender's Friend marketed by Accuray profiles hardness as a function of roll diameter as well as CD position. The Friend is a traversing carriage mounted wheel which rides on the rewinding roll. The wheel has a sensor button on the periphery which bumps the roll once per revolution and records the value of the impact. The carriage moves the wheel sideways to profile across the width of the building reel. Sensor signals from the Friend are recorded and processed by a computer and displayed on a video monitor which plots hardness as a function of CD position for every traverse of the sensor.

The Friend's extremely high price compared to the handheld hardness testers reflect the additional capacity to do limited control of supercalender air showers, which is its primary application. The Friend's computer takes inputs from the wheel hardness sensor and sends output corrections to electrically operated cooling air shower valves. In CD positions where the hardness is relatively low, the Friend will add additional cooling of the supercalender roll, so that the caliper is increased at that point. Bonazza in a four month study concluded that installation of the Friend reduced culled rolls by about 44% [155].

In addition to the extremely high price, the Friend has several other practical limitations. The sensor wheel and carriage are bulky, so that packaging would be quite difficult on many winders. The contacting nature of the sensor wheel would be objectionable to many materials that are delicate or pressure sensitive. The basic principle of hardness measurement is not yet related to the fundamental parameters of wound roll stress, so that first principles application is precluded. Finally, the resulting roll structure profile plots appear noisy, so that resolution is likely to be quite low. The development of practical modeling or measurement which simultaneously describes both the radial and CD remains as elusive as ever.

Figure 36
THE RHOMETER ROLL HARDNESS TESTER

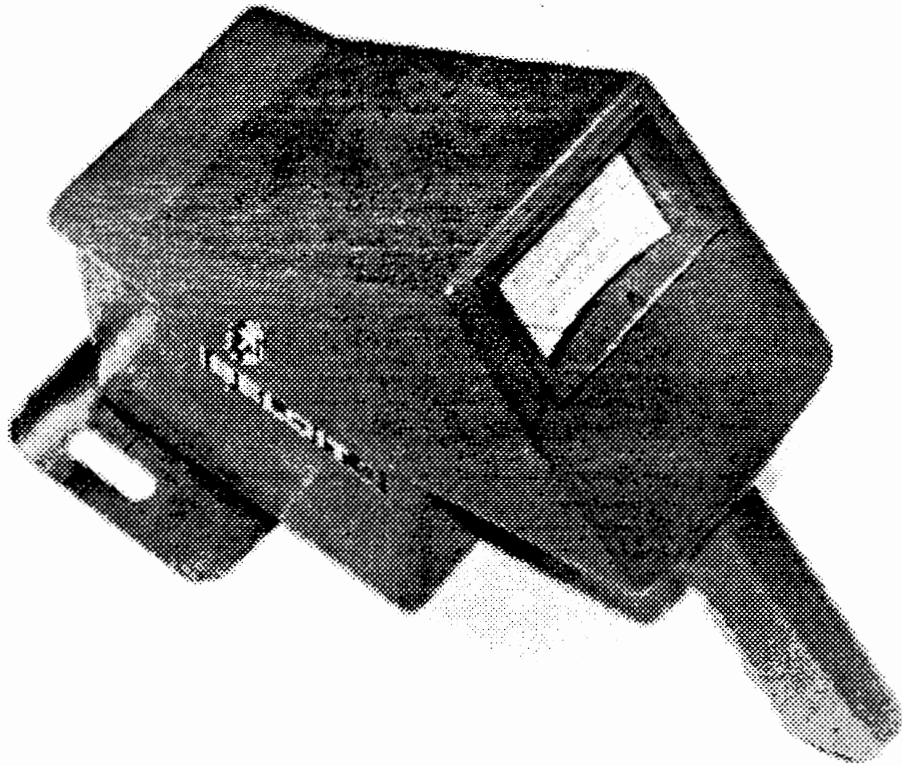
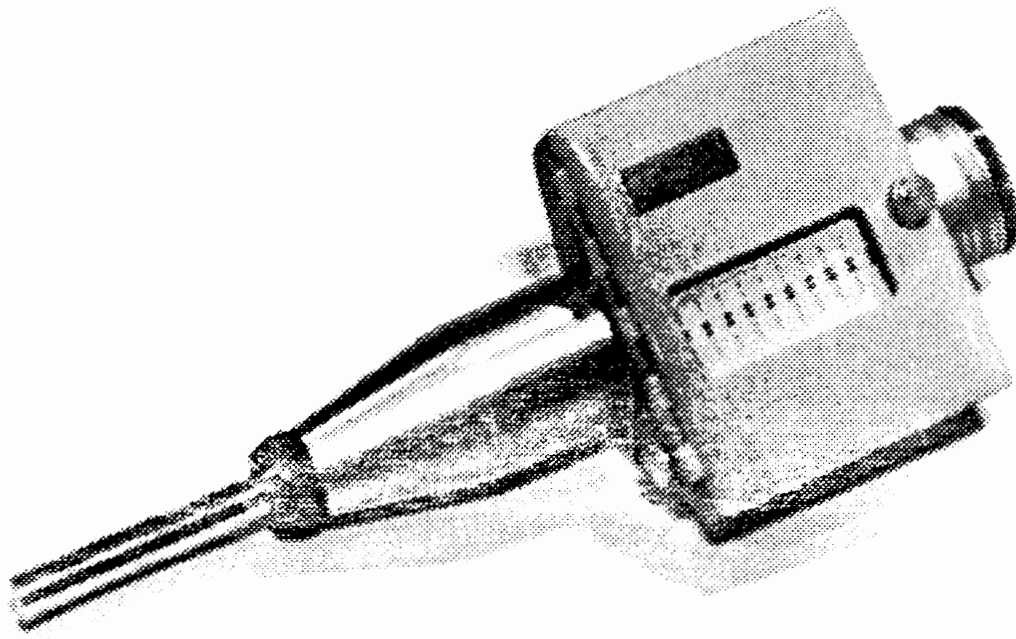


Figure 37
THE SCHMIDT ROLL HARDNESS TESTER



Smith Needle

Of the several friction based measurements of interlayer pressure, the Smith Needle is the only method that is commonly used in the production environment. The Smith Needle, more formally known as the Smith Roll Tightness Tester, is presently marketed by Testing Machines Incorporated. The Smith Needle is a handheld device that consist of a spring loaded needle indenter which is penetrated between the layers of paper on the roll of paper as seen in Figure 38. The Needle has a spring loaded flange which insures the tester is held perpendicular to the roll end and has a dial indicator for registering the tightness reading. The needle is attached through a spring to the dial indicator movement.

The principle of operation of the Smith Needle is to measure the force required to penetrate a needle to a constant depth of about 1/2" into the face of the rewound roll. This force is the sum of the web/needle friction plus the force required to separate the layers of paper, both of which are determined in part by the radial stress in the roll at the point of measurement. However, the values given by the instrument are not force but arbitrary units peculiar to this device. Because the Smith Needle reading is dependent on friction, measurements have a large variability and are dependent on the material. The Smith Needle is supplied in two versions: Model A for medium roll hardness, and Model B for high roll hardness.

Although the Smith Needle is easily able to profile roll structure as some function of interlayer position and radial position, it has a few drawbacks. As mentioned earlier it is friction dependent, so that comparisons between grades can't be made. Additionally, the Smith Needle and other friction based devices have large scatter in readings due to friction variations, so that many readings are required to given statistical confidence to the results. Finally, the Smith Needle can be considered a destructive measurement for some lightweight grades because the needle may nick the web edge during penetration, which may cause the web to break when it is unwound.

Core Torque Test

The core torque test was developed by Hussain in 1977 as a quality control test to identify whether a winding start was tight enough, so that sufficient paper/core friction was developed to allow for unwinding without core slippage [161]. As seen in Figure 39, the test requires only a torque wrench fitted with a keyed steel core plug.

Figure 38
THE SMITH ROLL TIGHTNESS TESTER

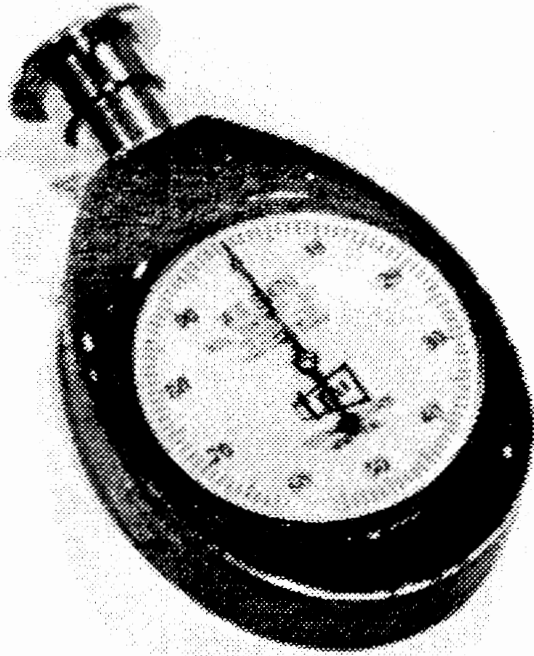
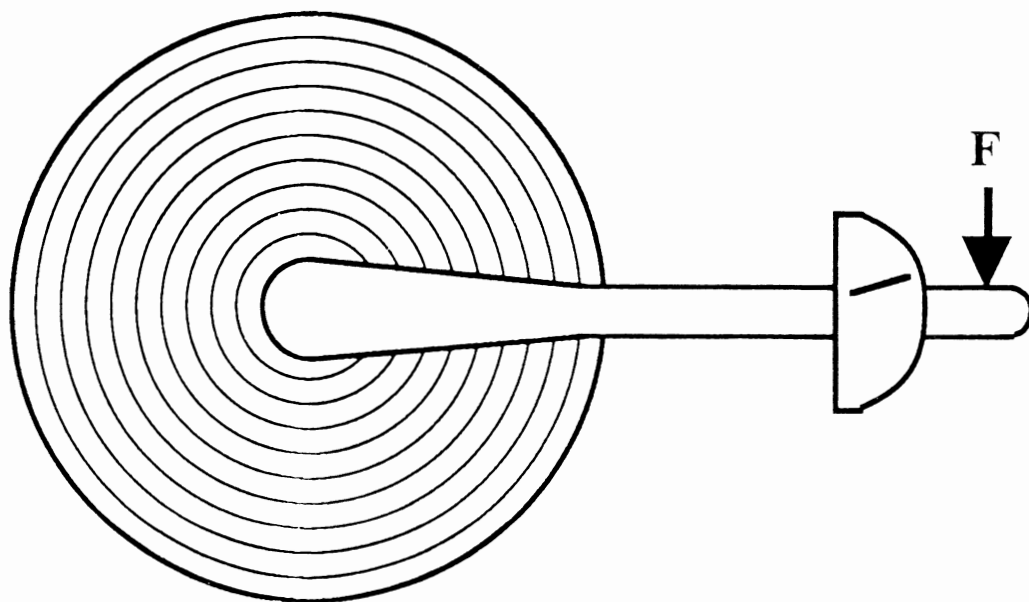


Figure 39
THE CORE TORQUE TEST



The torque required for core slippage is measured, and can be converted to radial stress at the core by the following formula

$$(95) \quad \sigma_R = \frac{2 T}{\pi \mu L D^2}$$

where

σ_R = radial stress at the core (lb/in²)

T = torque to slip (in-lb)

μ = coefficient of static friction between core and material
(0.3-0.4 for paper on fiber cores)

L = length of core (in)

D = outer diameter of core (in)

Hussain indicated for newsprint that a minimum radial stress should be 15 psi for fiber cores and 50 psi for steel cores, which was also verified by measurements of cores equipped with strain gages. He also had determined that core diameter variations, which have a large effect on core pressure for conventional two drum winders, should be no more than 0.015". Though the core torque test is simple and reliable, it does have several drawbacks. The test is likely to yield different values corresponding to torque in the tightening and loosening direction of the wind. Additionally, the method must consider that a fiber core may initially test well, but due to subsequent drying and shrinkage much of the core pressure may be lost. Also, there is a practical difficulty in manually applying enough torque to cause slippage on long and/or large diameter cores. Most importantly however, the core torque test yields only a single data point corresponding to the average radial pressure at the core, and as such can't be used for profiling.

Pull Tab Test

The pull tab test involve winding thin steel or plastic tabs into the roll at various diameters. After the roll has stopped, the force required to remove the tabs can be measured with a force gage as seen in Figure 40. Interlayer radial pressure can then be calculated from the removal force, coefficient of friction, and area of the tab [138, 157]. Improvements in the test are seen if the tabs are encased in an envelope with less variation of friction coefficient than the material to be tested. This test is potentially hazardous when inserting tabs into a winding nip, is very time-consuming, can yield noisy data, and may disrupt the winding geometry and stresses with the insertion of the tabs. As a consequence, its application is limited.

Figure 40
THE PULL TAB TEST

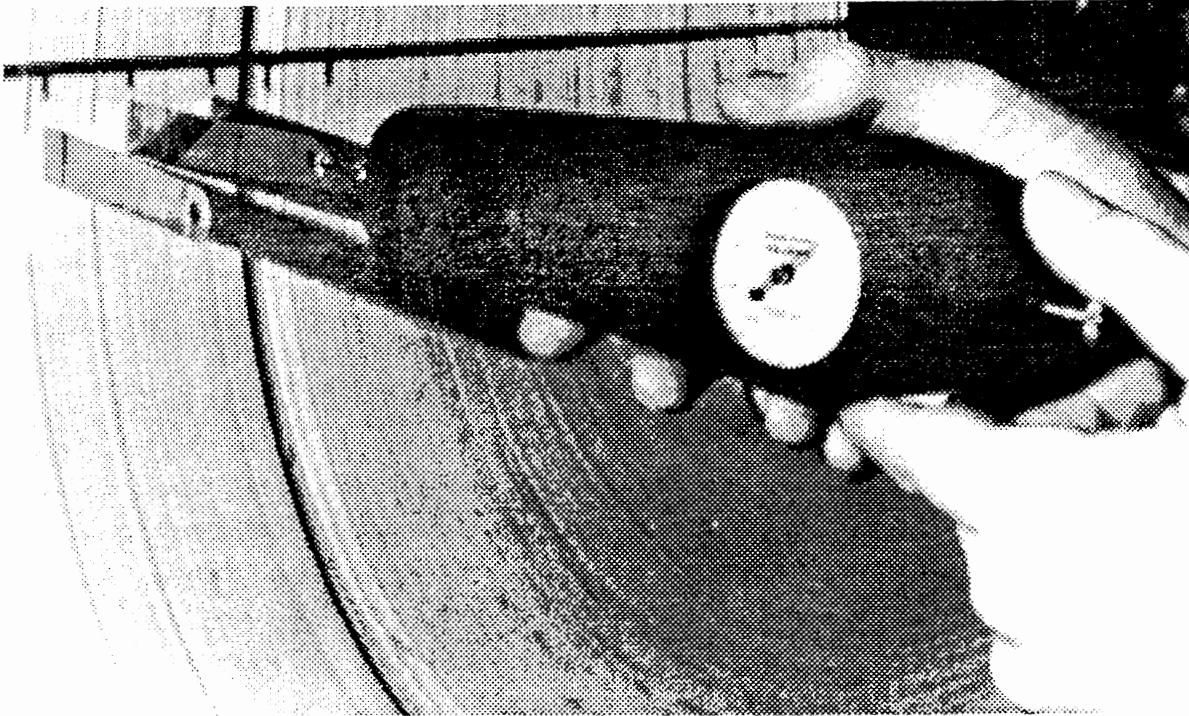
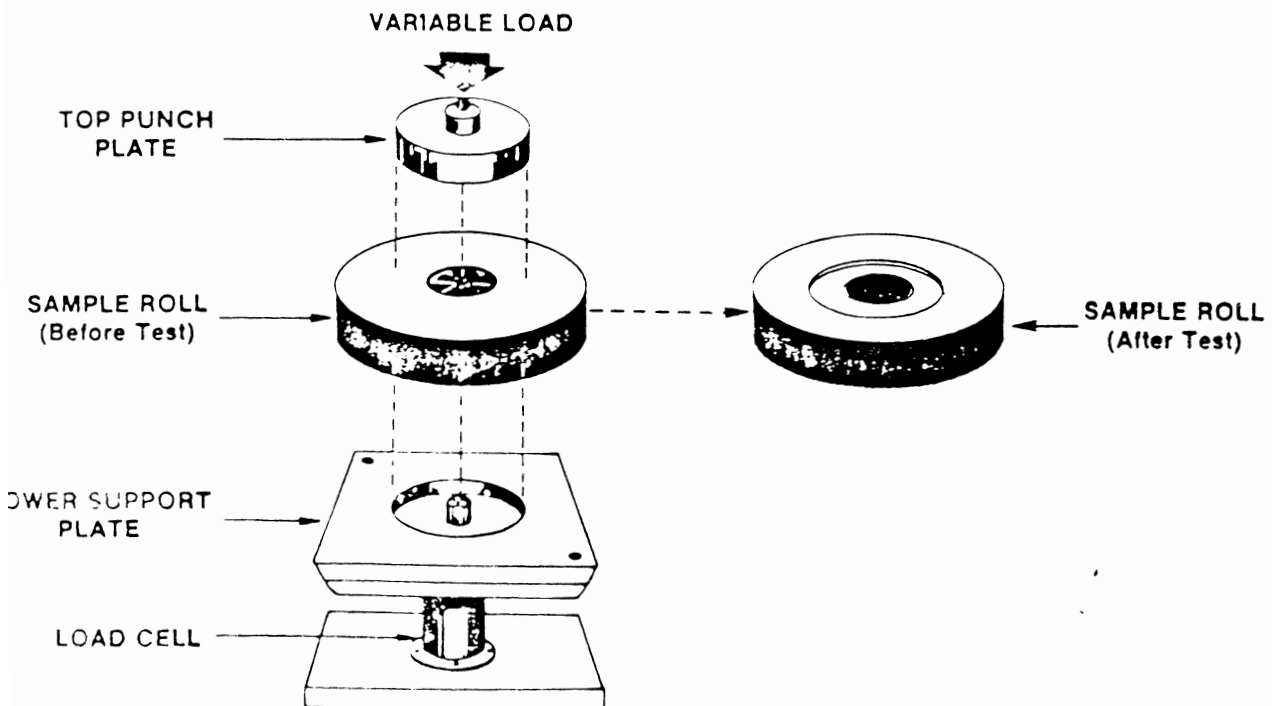


Figure 41
THE AXIAL PRESS TEST



Axial Press Test

Another test that can profile interlayer pressure by friction measurements similar to the pull tab test is the axial press test. In this test, a male and female die are placed concentrically on the two faces of the roll and loaded in a press as seen in Figure 41. Radial pressure can then be calculated from the force required to slip (telescope) the roll axially, the diameter of the dies, and the coefficient of friction between material. This test, developed by Hakiel, is even more involved than the pull tab but will yield less noisy data because of the much larger measurement area [132, 133, 186].

Thin Pressure Transducers

Pressure transducers that are thin and flexible may be wound into the roll for a direct measurement of interlayer pressure. Pressure transducers of suitable geometry that have been wound into a roll include capacitance gages, resistance gages, strain gage load cells and piezoelectric film. The capacitance gage is a compressible ($\mu \ll 0.5$) dielectric sandwiched between thin brass plates. As the pressure is increased, the plate separation decreases and the dielectric constant increases which can be measured with a capacitance meter. Miniature soil pressure transducers, which are capacitance gages, were first used by Hussain to measure interlayer pressure in 1968 [160]. Subsequently, Blaedel [128] and Wolfemann [147] both used these gages to verify linear anisotropic winding models. The procedure is similarly involved as the pull tab test such that the gages must be calibrated under static loading inside a stack. Additionally, the gages can have an undesirable sensitivity to curvature which must be taken into account.

Resistance gages are a thin matrix of carbon potted in an elastic binder which are screen printed onto a thin plastic sheet with electrical leads. As the thin composite is loaded under pressure, the matrix compresses which decreases carbon separation and consequently resistance which can be measured at the leads. Force Sensing Resistors (FSR's) are a trade name for one particularly successful formulation which has reduced the undesirable cross sensitivity to loading in other axes, temperature, moisture and other factors [163]. Thin strain gage load cells or pressure transducers are also available which have been wound into rolls, but are somewhat thicker than other alternatives, and are not flexible in bending. Finally, piezoelectric (Kynar brand) film has also been wound into rolls. Unfortunately, the piezofilm has such a short time constant that it is more suitable for dynamic measurements such as transient pressures going through a nip than longer measurements such as interlayer pressure during winding.

Acoustic Interlayer Pressure Measurement

Although acoustic measurements are frequently used for web elastic moduli measurements [55-57, 64, 68, 72, 76, 81, 85] and occasionally on free span web tension [71], its application to interlayer pressure measurement has been limited. In most cases, the acoustic measurements make use of the fact that the time of flight of a sound wave through a material is dependent on elastic moduli and material stress [157]. Pfeiffer used this approach in 1966 for one of the first measurements of interlayer pressure profiles in a roll [165]. He began by measuring sonic velocity through a stack loaded into compression. The time of flight of the acoustic wave from the transducer on one end of the stack to a pickup on the other was measured as a function of compressive pressure. Later, he outfitted a rewind roll with an acoustic transducer at the core and a pickup which could be set at various radii. From the stack calibration, and the time of flight measurement inside the roll, he inferred compressive pressure profiles as a function of radial location.

As novel and inventive as this approach was, Pfeiffer's results are not corroborated by later analytical and experimental stress profiles. The compressive pressure profile, though approximately correct in value, has a shape that is inappropriate. He further compounded errors by calculating the tangential stress distribution as a derivative of the pressure distribution. Though analytically correct, the process of taking a derivative of noisy and uncertain data yields even greater problems. Even today, pressure measurements can seldom be made with sufficient accuracy that would allow tangential stress calculations. This is but one of many examples where winding authors have not independently verified their analytical and experimental efforts, thus care must be taken when interpreting their conclusions.

Caliper Method

The average caliper of a stack of material can be measured as a function of interlayer compression in a tensile test machine. This caliper versus pressure curve can be used to infer pressure inside a roll at various radii if the radial distance spanned by a known number of layers is carefully measured. This procedure has several difficulties that render the results questionable. First, the stack is measured under uniaxial stress while the roll is under biaxial stress. If the material has a nonzero μ_R , the tangential stresses will affect the radial deflection. Secondly, layers are difficult to count and radial span is difficult to measure. Thirdly, the method will not work well in areas near the core and outside where the stress gradients are high. Most importantly however, this method assumes uniform caliper which is seldom a good assumption to make.

Cameron Gap

Of the many measures of tangential stress or strain, the Cameron Gap is the only method that is commonly used in the production environment. The Cameron Strain test, more commonly known as the Cameron Gap test, has been used to analyze roll structuring for more than 25 years, and was adapted as a Tappi standard test in 1963 (174). This test requires only a sharp knife to slit the outer layer, a fine scale or magnifying reticle to measure the gap, and a flat tap to measure roll circumference. From these measurements, tangential strain can be calculated as

$$(96) \quad \epsilon_{T@r=r_z} = \frac{\text{Gap Width}}{\text{Circumference of Roll}}$$

The Gap test is one of the few based on a fundamental stress or strain parameter. The strain can easily be converted to stress by multiplying by the materials tangential modulus of elasticity. The Tappi standard indicates a maximum allowable strain of 0.21-0.23% be used as an acceptance criteria for 40 lb publication paper. This corresponds to about 1,000 psi wound-in-stress or about 30% of the ultimate strength of the sheet. Though this test is fundamental, is a Tappi standard, and used by several authors, there are several problems. First, the measurement is extremely difficult to make with accuracy, especially at small diameters [169, 171]. Secondly, the test yields only a single data point corresponding the average strain at the outer diameter. Consequently, to profile a roll as a function of diameter, the entire roll would have to be slabbed down and destroyed. Additionally, in the process of severing a layer, slight stress redistributions in the roll occur due to the relief of the pressure supplied by that outer layer.

Slit Roll Face

The radial location of the tangential paper stresses transition from tension to compression (about 15% of the way from the outer surface) can be inferred by slitting the roll face radially with a sharp razor from the core to the outside. At radial locations where the tangential stresses are tensile, the slit will open, and where compressive, will tend to close. This seldom used method is both destructive, approximate and also redistributes the stresses in the roll in the measurement process.

Radially Drilled Holes

Holes drilled radially into a roll of paper from the outside to the core are initially circular in shape. If the roll is slabbed down, paper stresses are released which will cause the initially circular holes to take an elliptical shape [168]. This change in shape represents the tangential strains in the paper roll after it was wound and could be converted to stresses provided that Poisson ratios were near zero. The major diameter of the holes are difficult to measure accurately, and the test is obviously destructive.

Strain Gages

Strain gages though ubiquitous in structural measurement, are very difficult to apply for wound roll stress measurement. Hussain used strain gages bonded to the inside of a core to measure the effect of increasing pressure due to wrap addition [161]. However, since the cylindrical wraps quickly become self supporting of external pressure, the core measurement shows increasing pressure for the addition of only a couple inches of radial addition of the web. Hussain also bonded strain gages directly to the web prior to winding to measure changes in tangential stress as a function of wrap addition [160]. Finally, Rand and Eriksson also bonded strain gages to the web and observed the circumferential stress changes as a function of circumferential location going through a nip, and as a function of diameter [168]. Strain gages must be calibrated when bonded to web because the stiffness of the gage and web are comparable. Furthermore, bending, cross loading, adhesive bonding, and gage leads limit this approach for stress measurement strictly to involved lab studies.

J-Line

The J-Line test measures the extent of interlayer slippage at the core or outside of a roll as a function of winding or unwinding revolutions. The test, illustrated in Figure 42, involves snapping a radial line on a winding or unwinding roll with a chalked line [106, 109]. As the wind progresses, the initially straight line may quickly skew in the direction of the wind but will slow and eventually freeze after several revolutions [157]. J-Line movement is usually associated with nip rollers or core supported rolls on grades with low friction coefficients such as LWC paper. The magnitude and angle of the deformed line tip provides a quantitative measure of strain changes due to slippage [121]. Though the average change in strain is usually small, the slippage may occur abruptly in a single layer, which might indicate a possible crepe wrinkle. A more detailed discussion of interlayer slippage is given in Chapter 4.

WIT-WOT Rewinder

The WIT-WOT (Wound-In-Tension, Wound-Off-Tension) rewinder is a single drum duplex laboratory winder designed and built in the 1960's for Pfeiffer's classic works on tensions during winding [166, 167]. The principle of operation of both the WIT and WOT loops is that the outer layer of the roll is passed over load cells for tension measurement prior to entering and exiting the roll respectively. As seen in Figure 43, the unwind section is composed of a brake whose torque is determined by the free web tension setpoint and the web tension load cell. The windup section is a speed controlled drum with the surface winding nip provided by loading cylinders.

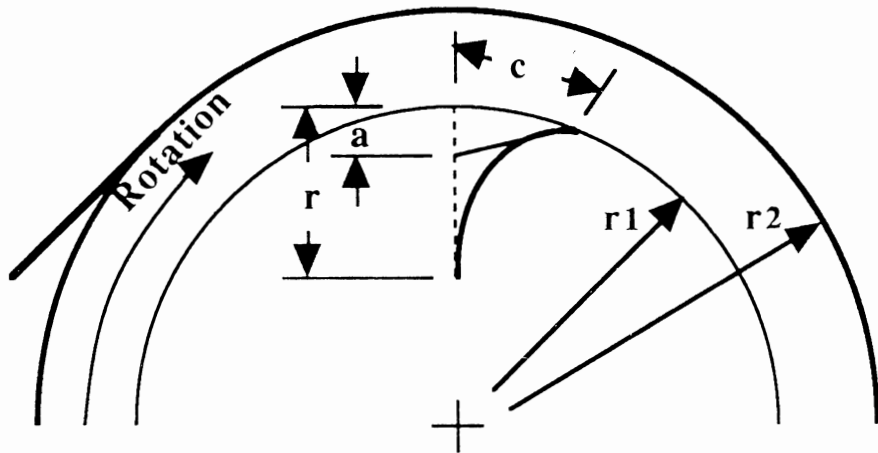
Pfeiffer and others demonstrated that the WIT-WOT winder is able to measure tensions with great resolution, even to the point of resolving variations in a single wrap due to a splice. However, though the WIT and WOT profiles for a single roll have a very similar shape, the WOT tension can be much lower than the WIT. Whether this is due to differences in the two tension loops or whether this is a reflection of anelastic behavior such as creep and stress relaxation, or whether some fundamental problem exists remains to be determined. Since the tension profiling must be done at extremely low speeds (<200 FPM) due to air entrainment, and there are only a few of these winders in the world, this measurement approach is definitely limited to specialized lab studies.

However, rewinders of any type may be used for detailed and careful testing of rolls in a mill environment. As the roll is unwound slowly, it can be profiled across its width and at various diameters to give a complete three-dimensional picture of the roll's structure. For example, a Rhometer could take readings at one inch increments across the width of the roll and at one inch diameter increments as the roll is unwound. Additionally, this rewinder testing can be augmented by other test methods as well as close visual inspection.

X-Ray Tomography

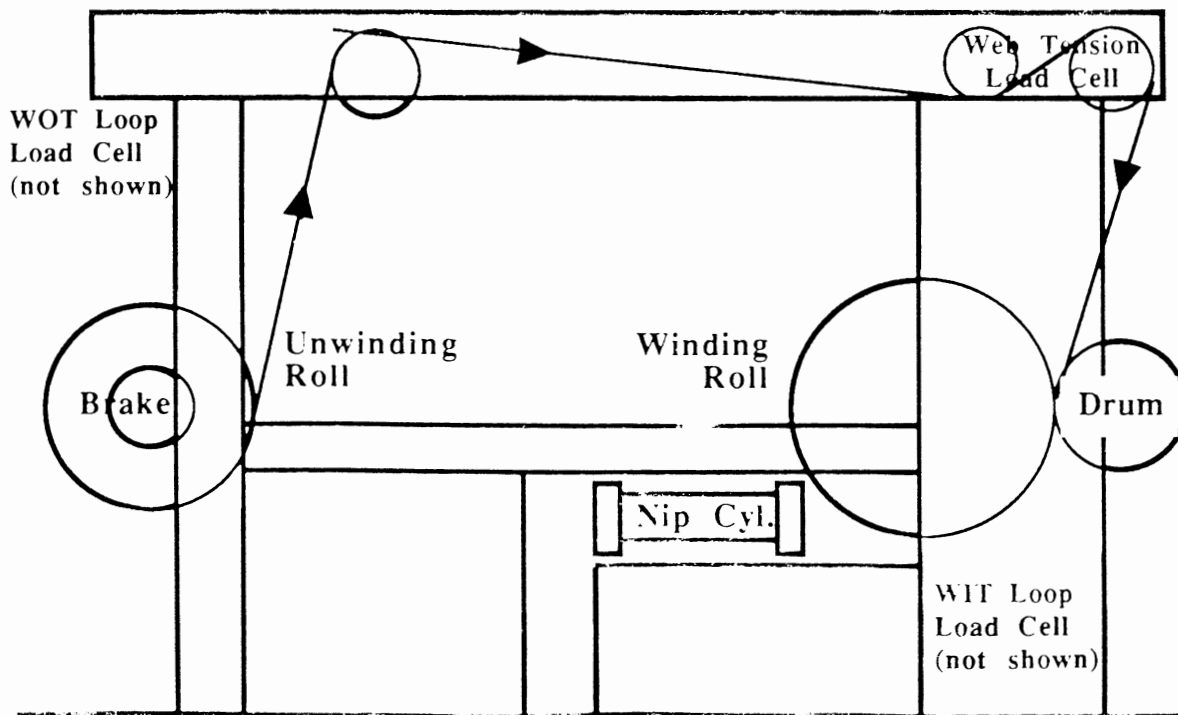
Computerized X-ray tomography has been used on rewound rolls to attempt to discern roll defects and profile [164]. Though this method was sensitive to basis weight variations, the correlation of tomography readings to defects or roll structure profile were not established.

Figure 42
THE J-LINE TEST FOR INTERLAYER SLIPPAGE



c = max. circum. movement r = depth of influence
 c/a = slope of tip r_1 = radius when line struck
 r_2 = radius after winding

Figure 43
THE WIT-WOT REWINDER



Roll Shape Profiling

One of the fundamental assumptions in wound roll models is that the roll is cylindrical such that it has a constant radius at each layer as a function of circumferential and CD position. The circularity assumption comes into play in the equilibrium equation, while variations about CD position not currently modeled for the most part. Though rolls are not perfectly cylindrical as measured by several methods, the effect on wound roll model accuracy has not been established.

Radii as a function of circumferential location has been measured in winding rolls for the purpose of estimating forcing functions for wound roll vibration using cam followers attached to LVDT's or by a pantograph mechanism inserted into the core and swung around to trace the roll's periphery [173]. The shape of the roll as a function of circumferential position can then be described by using a Fourier approximation as [120, 122]

$$(97) \quad r(\theta) = r_0 + r_1 \cos(\theta + \theta_1) + r_2 \cos(2\theta + \theta_2) + \dots = r_0 + \sum_{i=1}^{\infty} r_i \cos(i\theta + \theta_i)$$

where

$r(\theta)$ is the radius at circumferential location θ

r_0 is the nominal or average radius

r_i is the i th contribution of sidedness

i is the sidedness number

θ is the circumferential location

θ_i is the phase relationship of sidedness

Not only does the shape of the roll affect surface winder vibration, it also causes periodic free web tension transients during unwinding [120, 122, 158]. Additionally, the roll's shape may be altered due to handling loads such as the two point radial squeeze of clamp trucks and other loading conditions described in Chapter 4 [158].

In addition to profiling radius as a function of circumferential location, a profile as a function of CD position may be obtained by a device described by Quint [162]. The CD profiler consists of a stand to hold a roll and a pair of caliper arms mounted on a traversing carriage. The caliper arms ride on cam followers on opposite diametral locations on the roll and separation of the arms is measured by a LVDT as the arms traverse down the axis of the roll for a profile of diameter as a function of CD position. Quint claims from this study that a caliper nonuniformity as small as a few millionths of an inch can affect roll performance. However, the method received little attention and is no longer used.

Nip Width and Pressure

In addition to the thin pressure gages described earlier, there are other methods better suited to nip width and/or pressure measurement. Indeed, nip width can often be large enough to be conveniently measured by a simple ruler. If not, there are several kinds of nip impression papers that will determine the shape of the contact between two cylinders. These nip impression papers contain encapsulated dyes which break open under a specified pressure. For example, Beloit Manhattan manufactures a nip impression paper that is something like carbon paper. Similarly, Fuji film is a more capable nip impression paper which can give a quantitative indication of the magnitude of the nip pressure at any location by measuring the color intensity of the dye with a special optical meter.

The application of these papers is to determine the width of the nip as well as its shape which should nominally be rectangular. However, the pressure distribution of real calender or winder nips varies tremendously across the width such that it is not unusual to have contact over less than half of the length of the nip. Deviations of the contact shape from rectangularity are used to diagnose problems such as caused by misalignment, loading nonuniformity, deflection, roller diameter differences, and web caliper differences.

However, these products do have several application problems. First if nip width is to be measured, the paper must be inserted into a disengaged nip which is then engaged. Secondly, the activation pressure of the products are undesirably sensitive to temperature, moisture and cross loading such as shear. Thirdly, they have a limited activation pressure range such that the low pressure at the periphery of the contact will not activate the dye so that the nip is actually wider than measured. Finally, the measurement is difficult and possibly dangerous to perform under actual running conditions so that its application is usually limited to static tests.

Once nip width is measured and total lineal load determined by measurement or calculation, then peak nip pressure can be estimated. This is based on the solution to the Hertzian contact between two parallel isotropic cylinders [115]. Though real nips are often complicated by such things as anisotropy, sandwiched materials, or tangential loads such as rolling friction, the pressure profiles still remain approximately parabolic. Thus

$$(98) \quad \sigma_{\max} \cong 1.277 \frac{p}{b}$$

where σ_{\max} = peak pressure near center of nip (psi)

p = lineal load (pli)

b = contact width (in)

Summary

Several methods of roll structure measurement have been described here. Additionally, all of Chapter 6 will be devoted to the density analyzer as it is the most modern of the roll structure measurement methods and that upon which this project is based. Despite the number of measurements available however, most have only been applied on a few occasions for specialized research studies and are unsuitable for production monitoring. Even of those that are used in the production environment, their application is generally sparse and irregular at best. Only on a fraction of all winders are rolls monitored regularly with instruments.

Desirably, an ideal roll structure measurement would be one that is sensitive, easy to apply, profiles with both diameter and CD, and directly based on the fundamental parameters of web stresses. Unfortunately, none presently exists which meets all of these criteria. Indeed, most of the methods fall short in several characteristics. Thus selection for any application is a compromise [169, 171]. The need for a good fundamental roll structure measurement, was the impetus for this thesis project. Of the desirable characteristics, this project meets all but the profiling with respect to CD. Additionally, this is the only new roll structure measurement method developed in more than a decade.

CHAPTER 6

THE DENSITY ANALYZER

Density

Web density in an unloaded condition, along with caliper (thickness) and basis weight (weight/area) are properties that have been monitored for quality control in the paper industry for many decades. Low densities of less than 0.01 lb/in^3 are desired for tissue and toweling where bulk (inverse of density) and absorbency are important. Conversely, high densities of more than 0.042 lb/in^3 are desired for LWC (lightweight coated and supercalendered) where the sheet is filled with clays and other materials to provide a dense and smooth printing surface. The density for a typical grade of paper is about 0.024 lb/in^3 but may range as much as a factor of two, while film is similar at typically 0.034 lb/in^3 but has a much smaller variation. Density can be calculated from basis weight and caliper as

$$(99) \quad \rho = \frac{b}{c}, \text{ where}$$

$\rho =$ density (lb/in^3)
 $b =$ basis weight (lb/in^2)
 $c =$ caliper (in)

However, basis weight is usually given in units peculiar to a material such as $\text{lbs}/3000\text{ft}^2$ for paper and $\text{lbs}/1300 \text{ ft}^2$ for board, and caliper may be given in mils (0.001").

Long before the density analyzer instrument was invented, it was noted that the density of a web material increased with increasing ZD loading. In particular, high wound-in-tensions produced high interlayer pressures and consequently an increase in density that could be discerned with careful measurements of roll diameter and weight. In 1967, Ulyanov patented a density meter consisting of a tab inserted between layers of the roll which was connected to a LVDT for measurement of radial deformation as additional layers were added during winding [37]. However, this crude device gave density only at a single data point as a function of added wraps, and was not suitable for production measurements.

In the 1970's, winding literature began to use the term density synonymously with wound-in-tension. This included an article in 1970 by Shvetsov who compared the density of wound rolls to the unstressed density of the parent material [36]. He defined a density index as

$$(100) \text{ density index} = \frac{\rho}{\rho_0}$$

where

$$\begin{aligned} \rho &= \text{rewound roll density (lb/in}^3\text{)} \\ \rho_0 &= \text{unstressed material density (lb/in}^3\text{)} \end{aligned}$$

He found this density ratio to vary from 0.80 to 1.09 for more than 600 rolls of paper tested from several mills and proposed this measure be used for roll quality control. A similar approach is used to estimate the amount of air wound into rolls of impermeable material such as plastic film given in equation (79). In 1979, Hewinson obtained an United States Patent for a winding machine design, which was claimed to control wound roll density at a predetermined value, by winding inside a loop of belt which controlled the circumference of the rewinding roll [23].

However, it was not until 1980 that the first practical measurement method for density became available with the invention of a computerized roll density analyzer. This development was headed by Eriksson of the Swedish Newsprint Research Center and funded by a consortium of three corporations [19-21]. Since then, machinery builders such as ASEA [14], Beloit Corporation [17, 18], General Electric [31], Jagenberg, Voith [16] and Wartsila, as well as paper companies such as Abitibi Price [30], Champion International, Norpac, St Regis Paper, and Tasman Pulp & Paper [32] have developed similar instruments.

Today there are scores of density analyzers in use on paper mill reels, winders, rewinders and unwinds throughout the world. Some of density analyzers are portable PC's [17, 18, 30], while others are permanently mounted in benchboards or control cabinets [14, 16]. Since its invention, most of the improvements in the density analyzer have been incremental such as faster computers, higher count encoders and a better coupling of encoders to the rotating roll and roller. The most novel development attempts included closed loop control of density to a target value (unsuccessful), caliper compensation schemes [16] (questionable), and changing from diameter based to length based sampling [17] (practical) for monitoring several rolls simultaneously on duplex winders.

Density as a Roll Structure Analysis Tool

While the density analyzer may not be the most common method of roll structure measurement, its performance is by far the best documented in public literature. Eriksson showed the effect of torque, nip and tension on wound-in density; the relationship between wound-in and wound-off density of roll after long term storage; and the effect of wrap sample size [19-21]. McDonald showed correlation between Rho hardness and density; the effect of calendering (caliper) on density; and the effect of torque on density [30]. Odell's study was the most complete detailing the effect of source paper machine; the effect of torque, nip, tension, speed, acceleration; splices; and set location on the parent log to the density profile at the winder [32]. Similar studies were performed later by Granlund [22], Komulainen [25, 26], and Holmer [24]. Additionally, several less technical papers also proclaim the virtues of the computerized roll density analyzers [15, 27, 28, 33].

These many studies usually confirm the following conclusions about density

1. Density profiles follow those of other roll structure measurement methods including the Rho hardness, Smith Needle, and wound-in tension.
2. Density is increased with increasing torque, nip and tension.
3. Wound-off density is equal or slightly greater than wound-in density after a period of storage.
4. Density increases during acceleration, decreases during deceleration and drops abruptly if the winder is stopped for a splicing operation.
5. Density has an undesirable sensitivity to changes in caliper or basis weight [16, 18, 30, 35]. As discussed later in this chapter, this cross sensitivity problem can be eliminated by supplementing density measurements with caliper measurements.

Despite limitations of the density measurement, which will be discussed later, the density analyzer possesses most of the attributes of an ideal roll structure measurement [169, 171]. These include profiling with respect to diameter for diagnosing required changes in the TNT's, recording capabilities, nondestructive testing, ease of use, and moderate cost. Perhaps the two greatest advantages however, are the relatively high resolution of roll structure changes, and the ability to be implemented for automated on-line production measurements. For these reasons, this measurement serves as a platform for development of the stress measurement device invented for this thesis work.

Theory of Operation

The density analyzer, as seen in Figure 44, consists of a winder or unwind, two incremental rotary encoders, pulse counters, and a microcomputer. One encoder is used to measure web footage and is mounted on a roller or drum which travels at web speed. The length of web run during the sample can be calculated as

$$(101) \quad l_i = \frac{\pi d_d p_{d,i}}{ppr_d}$$

where

- l_i = incremental length for sample i (in)
- d_d = drum roller diameter (in)
- $p_{d,i}$ = drum roller encoder pulses for sample i
- ppr_d = drum roller encoder pulses per revolution

Similar to gear calculations, the current rewind roll diameter can be calculated from the ratio of the pulses of the two encoders as

$$(102) \quad d_{r,i} = d_d \frac{p_{d,i}}{p_{r,i}} \frac{ppr_r}{ppr_d}$$

where

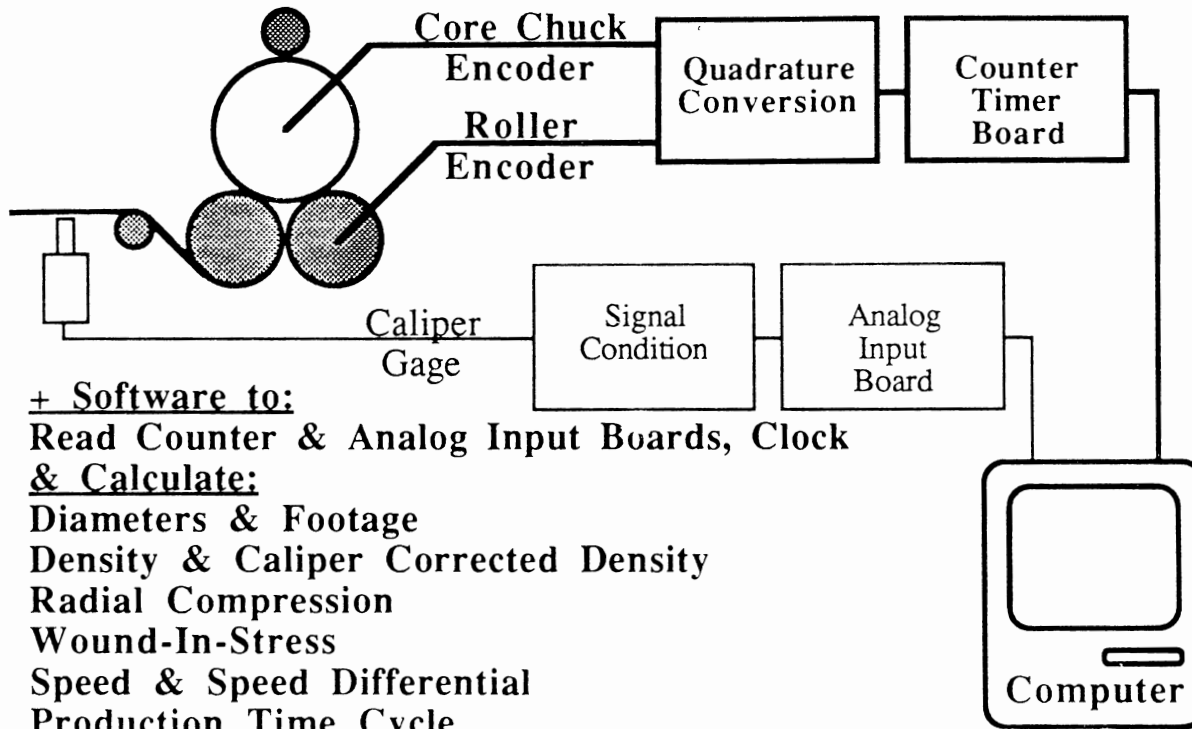
- $d_{r,i}$ = rewind roll diameter (in)
- d_d = drum roller diameter (in)
- $p_{d,i}$ = drum roller encoder pulses for sample i
- $p_{r,i}$ = rewind roll encoder pulses for sample i
- ppr_r = rewind roll encoder pulses per revolution
- ppr_d = drum roller encoder pulses per revolution

However, the number of wraps, n , of material added during the sample interval is usually fixed prior to running as

$$(103) \quad n = \frac{p_{r,i}}{ppr_r}$$

where n is typically an integer near 100 for typical web materials.

Figure 44
THE DENSITY ANALYZER



Also, web surface speed can be calculated using elapsed time between samples as

$$(104) \quad s_i = \frac{l_i}{t_i}$$

where

- s_i = surface speed during sample i (in/sec)
- l_i = incremental length during sample i (in)
- t_i = time elapsed during sample i (sec)

which can be used for winding productivity analysis. Finally, with the addition of more encoders, accurate speed differentials can be computed between any two rollers or drums equipped with encoders.

The pulses generated by the two or more encoders are counted by counter data acquisition boards and passed to the computer for calculation. One of the encoders, typically the rewind roll, serves as a timer for sample acquisition. In this mode, the number of pulses representing a desired wrap count is loaded into the rewind roll counter at the start of every sample. As the roll is winding, the rewind roll encoder pulses are counted down from the preset value and the drum roller encoder pulses are counted up from zero. When the rewind roll counter reaches zero, the contents of the drum roller counter are latched and passed to the computer. Then, the rewind counter is set to the preset wrap count and the drum counter is zeroed to start the acquisition cycle anew. At each sample, length, speed, density and other parameters can be calculated as a function of current rewind roll diameter.

The number of wraps in a sample interval selected by the operator has a large effect on the performance of the density analyzer. If the wraps are set high, the noise of the density profile as a function of wound roll diameter will be reduced but will have so few data points that changes of short duration may be missed. Conversely, if the wraps are set low, the plot will become so noisy that interpretation becomes difficult. Most density analyzers operate with large wrap counts corresponding to about one inch of diametral increase between samples which yields fewer than 40 data points for the density versus diameter plot of a typical paper roll.

The Density Calculation

Wound roll density, as its name implies, is nothing more than the weight of material wound into a given volume. The derivation of wound roll density begins with simple definitions for density, weight and volume.

$$(105) \quad \rho = \frac{\text{weight}}{\text{volume}}$$

$$(106) \quad \text{weight} = (\text{length}) (\text{width}) b$$

$$(107) \quad \text{volume} = \frac{\pi}{4} (d_i^2 - d_{i-1}^2) \text{width}$$

where

b = basis weight (lb/in²)

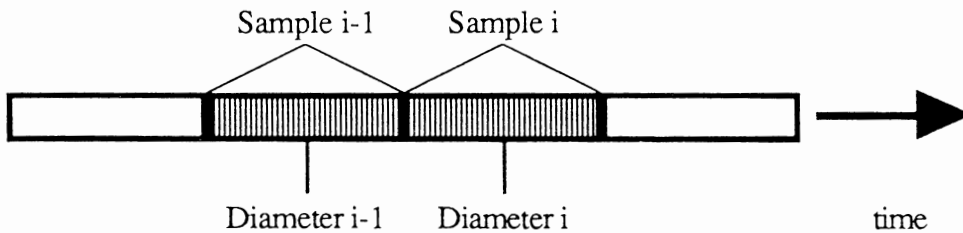
d_i = diameter of current sample

d_{i-1} = diameter of previous sample

Solving equations (105-107) simultaneously for density and eliminating weight and volume yields

$$(108) \quad \rho = \frac{4 b (\text{length})}{\pi (d_i^2 - d_{i-1}^2)}$$

Though diameter in particular, as well as other variables in general, are constantly varying, the average properties are determined over an entire sample and attributed to the midpoint of the sample as seen below.



Though (108) could be calculated from results of (101-103), it is advantageous to calculate density directly from measurements. Solving equations; (101) written for the average of diameters at sample i and $i-1$, (102) written twice for diameters i and $i-1$, and (103) simultaneously for density yields

$$(109a) \quad \rho = \frac{2 b n^2 ppr_d}{d_d (p_{d,i} - p_{d,i-1})} \quad (\text{no caliper correction})$$

The constants in the equation (109) are; n which is the predetermined and fixed number of wraps during a sample and termed 'wrapcount'; ppr_d which is the pulses per revolution of the drum roller encoder; and d_d which is the drum diameter. These constants are all easily determined with great precision and will not contribute significantly to uncertainties in the density measurement.

A pseudo-constant in equation (109) is the basis weight b , which is almost always assumed to be a constant, but in reality varies due to web manufacturing fluctuations. As seen from equation (99), any changes in either unstressed material density or unstressed material caliper will change the basis weight, which changes the density reading or calculation.

Caliper Sensitivity and Correction

This cross sensitivity of density to caliper or basis weight changes has been documented, but not widely appreciated. McDonald [30] showed that calendering of paper increased density values over that of the uncalendered source material, and similar observations have also been made by Voith [16]. The easiest way to see the effect of caliper changes is to wind a roll composed of one or more webs with different gages that are spliced together. The roll seen in Figure 45 has a sudden caliper drop of about 8% over the diameter range of 30-34", which results in a similar increase in density of 8% over the same diameter range. Similar results have been obtained by Roisum in previous work [35].

The danger in diagnostics of density plots without caliper information is that a change such as illustrated in Figure 45 could be misinterpreted as resulting from events caused by the winding machine, such as changes in the TNT's. In this example, the forces and loads of the winding machine on the web remained approximately constant. However, the stresses were increased due to a reduction in material thickness over which the forces acted.

In order to make the diagnostics of density plots more reliable, it is desirable to separate the effects of material and machine. One way this can be accomplished, developed by Baum [18] and Roisum [35], is to caliper correct density calculations. Density can be caliper corrected if thickness measurements are made simultaneously with diameter and length measurements from the encoders. From equation (99) basis weight can be calculated from a measured (and assumed constant) unstressed material density, a measured thickness, and inserted into the density calculation equation (109a) yielding

$$(109b) \rho = \frac{2 \rho_0 c n^2 p p r_d}{d_d (p_{d,i} - p_{d,i-1})}$$

A vivid demonstration of the effects of caliper variation on density was performed by Scott Baum of Beloit who programmed the loading on a calender to vary with during the course of processing rolls. This varying load cause a variation of caliper as high load permanently compacted the paper more than lower loads. As seen in Figures 46 and 47 for a step and ramp change respectively, the uncorrected density follows inversely with changes in caliper. However with caliper correction using equation (109b), the density profiles become relatively flat corresponding to the expected and desirable near uniform roll structure that was programmed into the TNT's of the winder for those runs.

However, caliper correction also works well on normal variations of caliper resulting from manufacturing process fluctuations. Figure 46 shows a comparison of density and caliper corrected density on a single roll which has a significant MD variation in caliper. Though the caliper corrected density still contains some caliper information, the plot shows a considerable reduction in 'noise'. With caliper correction, the effect of changes in winding machine forces stands out more clearly, so that interpretation becomes more reliable. In this example, the profile is a sudden step drop in the TNT's at a 20 inch roll diameter superimposed on the typical smile profile of two-drum winders.

As mentioned earlier, the caliper corrected density is most closely related to the *loads* imposed upon the web, while the uncorrected density is most closely related to the *stresses* imposed upon the web. It might be tempting to conclude from this that the uncorrected density has the closest correlation to the stresses predicted by the traditional analytical winding models. However, this is not so because the winding models assume a constant caliper, so that any caliper variations must be normalized out just as the caliper corrected density has been. The best way to view this is that the radial stress boundary condition is the load (ie caliper corrected density) divided by the current outer radius.

In this discussion there has been the implicit assumption that the density and wound-in-stresses are related in a stronger fashion than simple statistical correlation that has been well demonstrated. For example, perhaps there exists some conversion function between stresses and density based on first principles modeling. As will be indicated the end of this chapter and shown in the next, by extending the traditional winding models it is possible to calculate density profiles from WIS profiles and material properties. However, there would be little practical impetus to do so because stress models contain more information than density profiles, so that information would be lost in the conversion. Additionally, caliper corrected density like information can be converted to stresses from strictly first principles modeling and is the basis of this project. A new roll structure measurement, radial compression, will be described in the next chapter which has many advantages over the corrected and uncorrected density calculations and is a direct input to the outer boundary condition of the stress calculation model.

In conclusion, the traditional density calculation will show the combined effects of both TNT changes and caliper changes, so that the separate contributions of each may be extremely difficult to determine. A better approach is to monitor caliper to determine gage consistency of the material being wound, from which changes required in the upstream manufacturing can be determined. Then use the caliper corrected density (or better yet the radial compression from Chapter 7) profile to diagnose roll structuring effects, from which changes in the TNT's and other winding machine parameters can be determined.

Figure 45
EFFECT OF CALIPER ON DENSITY

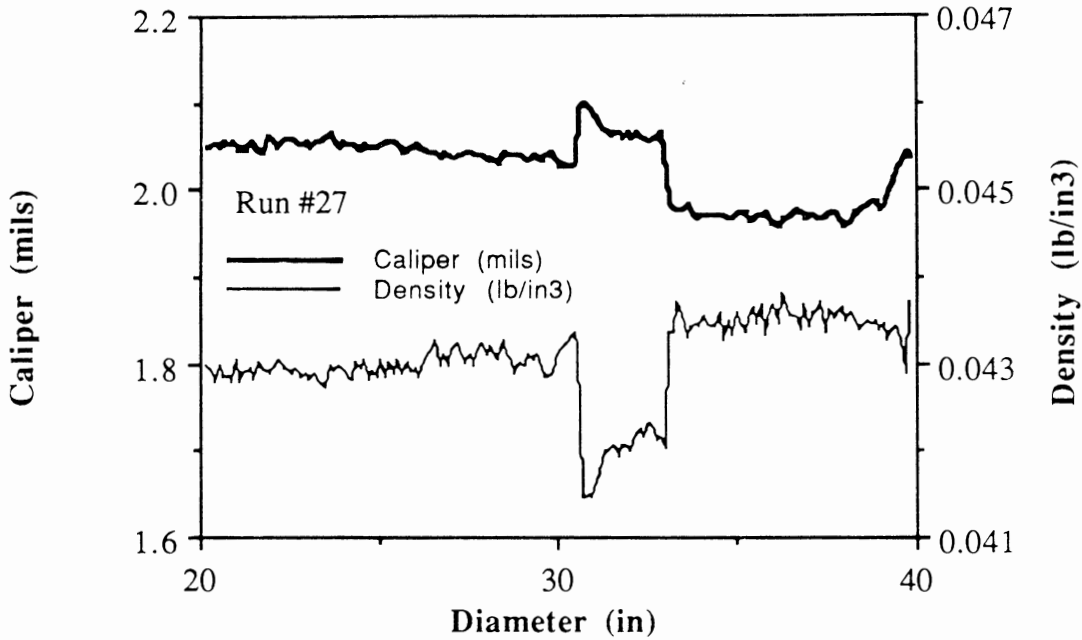


Figure 46
EFFECT OF CALIPER CORRECTION ON DENSITY

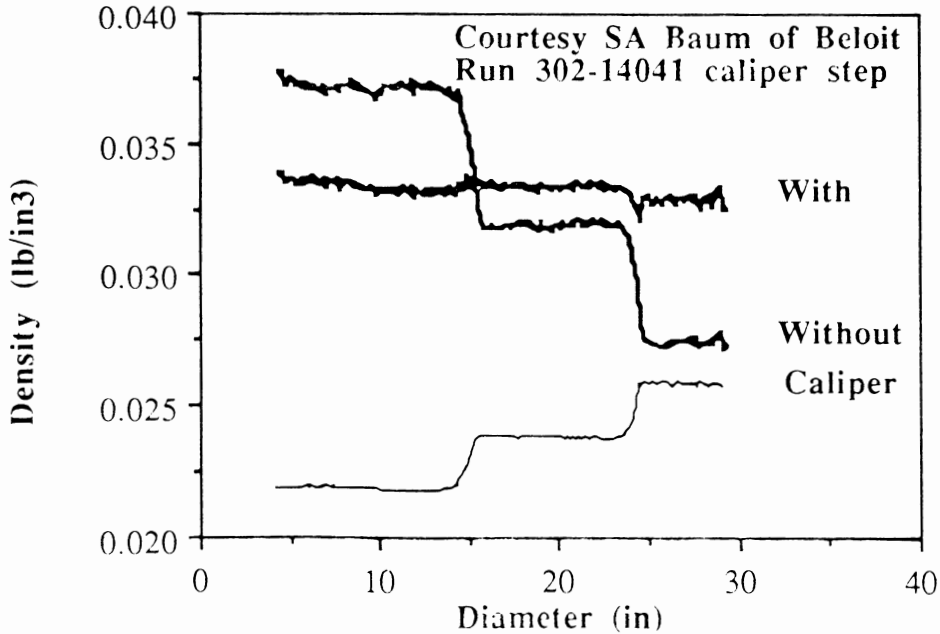


Figure 47
EFFECT OF CALIPER CORRECTION ON DENSITY

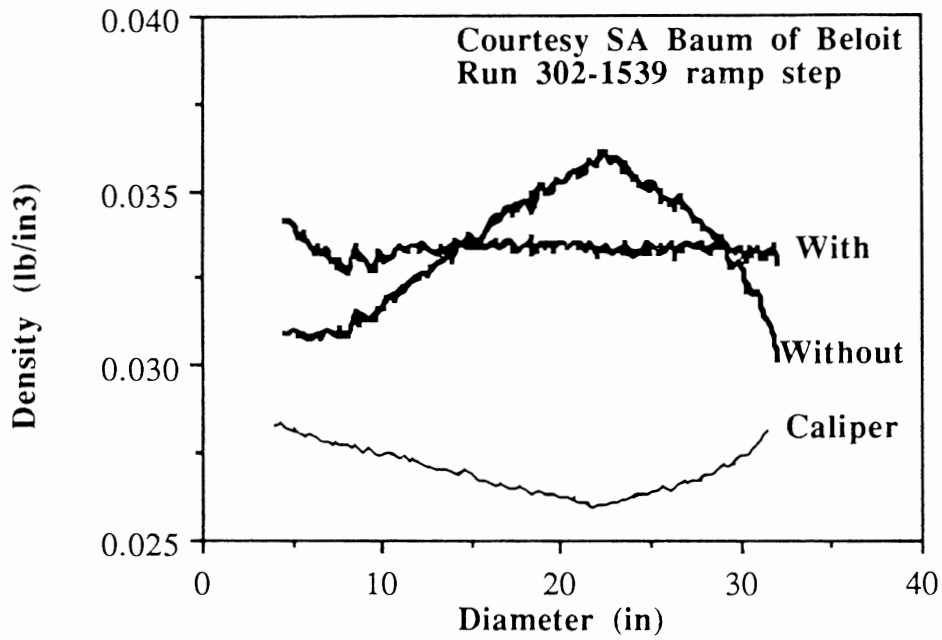
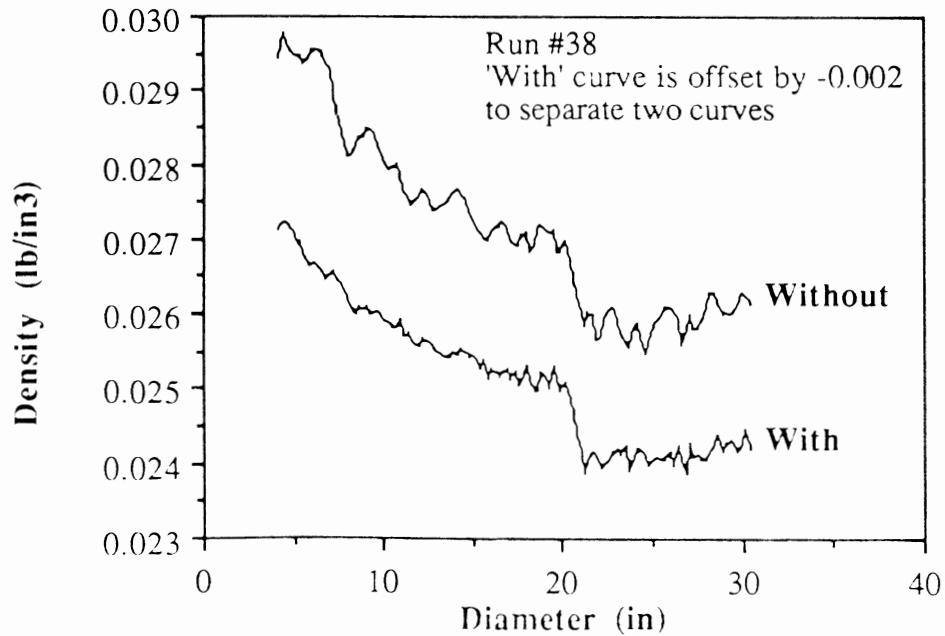


Figure 48
EFFECT OF CALIPER CORRECTION ON DENSITY



Raw Density Data

The raw data from the drum roller encoder as a function of sample number is a straight line whose value at any point is proportional to the current rewinding roll diameter as determined by equation (102) and illustrated in Figure 49. If the hardware is operating properly, the plot will be a featureless line which would intersect the origin of zero pulses at a zero rewind roll diameter.

However, there can be rare hardware errors where the sample may be double triggered which gives a zero count for a sample as shown for sample number 2150. Similarly, the trigger may skip a beat which would give a value twice the expected. These physically impossible readings which occur perhaps once in every thousand or ten thousand samples, cause a total disruption in the density calculation for two consecutive samples. Fortunately, these events are easily detected through statistics. If the significance of the spike by the Z-test exceeds 3σ or 99.9%, this value may be replaced by the expected value. More conservative criteria include removing data that has a probability of less than $1/2n$ of occurring where n is the number of samples. The most conservative is Chauvenet's principle which allows the removal (replacement) of a single data point if its deviation ratio exceeds the standard deviation ratio.

Finally, the data set may contain a series of consecutive errant values if the winder is stopped in the middle of a set such as occurs during a snapoff and splice. In this case, it is not generally possible to correct raw data in that region because the data before and after the stop are not synchronized. Therefore, the density profile must be calculated to the last good point before the stop, and again from the first good point after the stop to the end of the roll. Though the raw data can't be easily spliced across such an event, the calculated density can be.

Density as a Derivative

In qualitative terms, density is a measure of the compaction of the material being wound during a sample. Alternatively, a density profile represents a radial growth pattern of roll diameters during consecutive samples as illustrated in equation (108). However, density can also be viewed in its relationship to the raw encoder data by noting that it is inversely proportional to the difference in drum pulses between consecutive samples as seen in equation (109). As seen in Figure 50, the difference in drum pulses between consecutive samples can be a noisy signal which varies about a small positive mean and may contain numerous spikes. The degree of noise is primarily related to the sample size interval set by the operator, as measured in inches of radial growth.

Figure 49
RAW DENSITY DATA

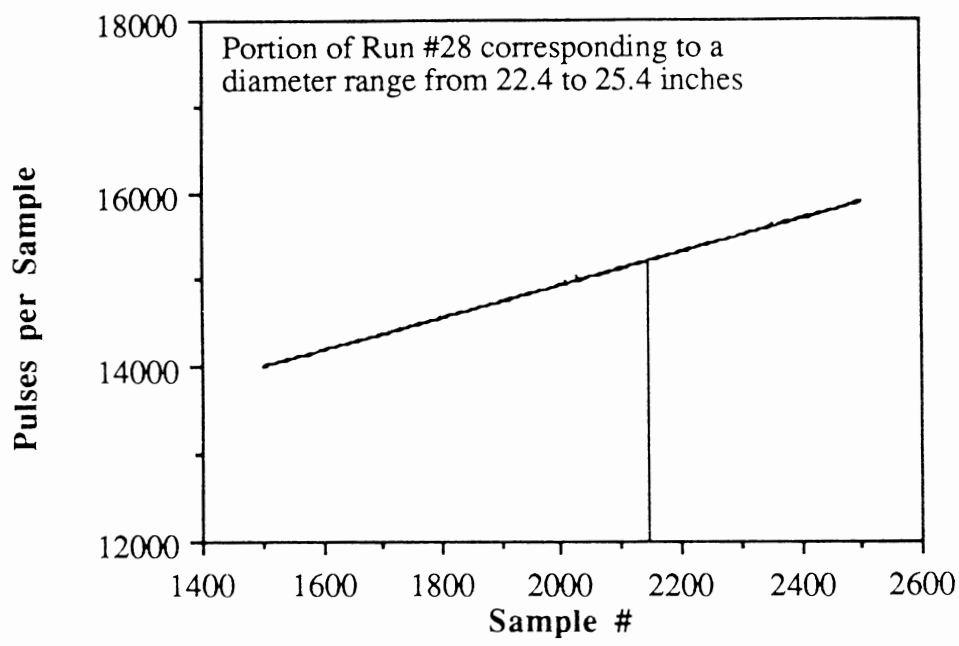
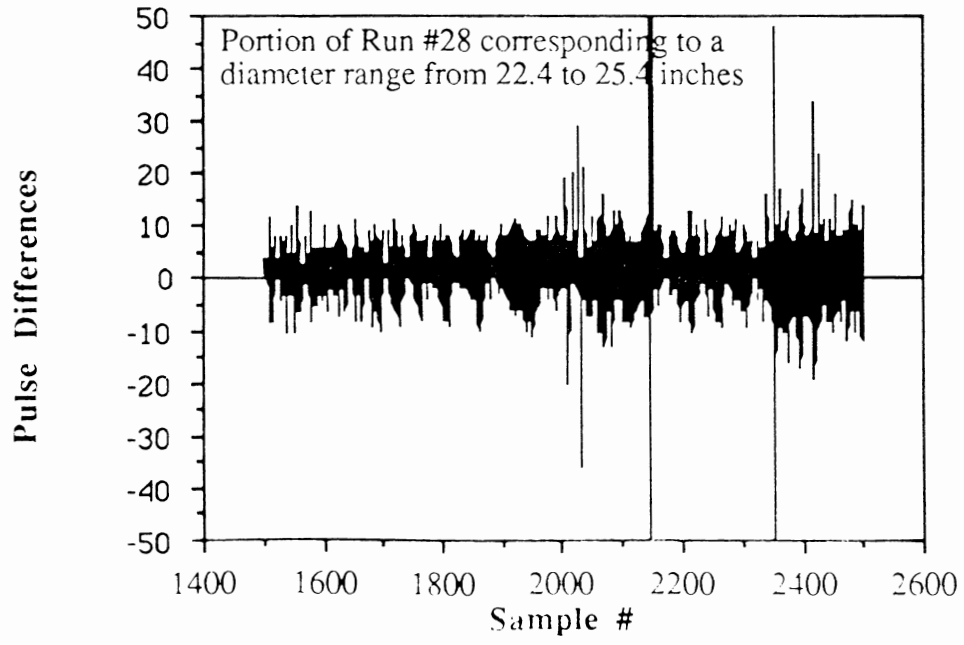


Figure 50
DENSITY DERIVATIVE



Density is inversely proportional to the pulse difference between consecutive samples from equation (109), and the pulse difference is effectively the first derivative of the raw pulse data, which can be seen by writing the first derivative as a two point backward finite difference approximation.

$$(110a) \text{ 2 pt. approx.} \quad \left. \frac{dp}{ds} \right|_{s=s_i} = \frac{1}{h} (p_i - p_{i-1}) + \frac{1}{2} h f''$$

where

p = pulses

i = sample number

h = base point spacing (=1 for this examples)

$(1/2)hf''$ = leading error term

The reason that pulse differences, and as a consequence the density, can be very noisy is because these calculations are derivatives of data, and taking derivatives of data increases variation. From classical numerical analysis, we can increase the accuracy by either decreasing the base point spacing (sample size), or by using higher order derivative approximations such as

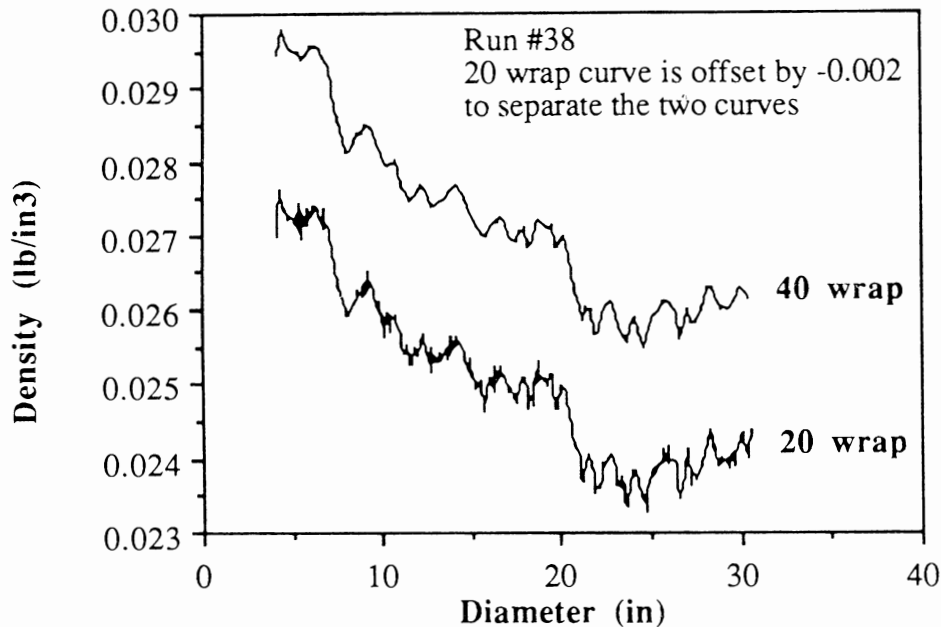
$$(110b) \text{ 3 pt. approx.} \quad \left. \frac{dp}{ds} \right|_{s=s_i} = \frac{1}{2h} (p_{i+1} - p_{i-1}) - \frac{1}{6} h^2 f'''$$

$$(110c) \text{ 4 pt approx.} \quad \left. \frac{dp}{ds} \right|_{s=s_i} = \frac{1}{2h} (2 p_{i+1} + 3 p_i - 6 p_{i-1} + p_{i+2}) - \frac{1}{12} h^3 f''''$$

and so on. Unfortunately, both decreasing base point spacing and higher order derivatives increase noise considerably, so that this approach is not useful.

In practice, noise reduction for pulse difference and density calculations are best achieved by summing raw data over a sufficiently large diameter increment. The one wrap original data sampling size can be increased by summing to give a 20 or 40 wrap effective sample size as shown in Figure 51. The higher the effective wrap size, the less noise in the resulting plot, and the fewer the resulting plotted data points. So effective wrap size is an operator selectable parameter which trades profile resolution for measurement resolution. Depending on the quality of instrumentation, the material, the winder, and operator preference, effective wrap size may vary from as little as 0.05" to more than 1.0" on the diameter. Higher resolutions can be obtained by higher count encoders that are tightly coupled without backlash to the roll and roller, web grades with high friction coefficients that minimize interlayer and roll/roller slippage, and grades with uniform caliper profiles.

Figure 51
EFFECT OF SAMPLE SIZE ON DENSITY



Density Noise Reduction

The character of pulse difference or density noise can be studied using statistics to describe the data distribution. As seen in the histogram of Figure 52, most of the data roughly fits a normal distribution about a mean corresponding to the average density. In addition, there are three outliers on the negative side and one on the positive side that correspond to spikes in the data, but are not well described by a Gaussian distribution. However, removal of these moderate sized outlying spikes (not to be confused with the much larger spikes occurring with double or missed samples) and replacement with their expected value did not have a significant effect on density noise because their overall contribution was small. Even if the strength of this clipping filter was increased so that more and more outliers are replaced by the local mean, the effect on density noise was minimal until nearly all values were replaced by the local mean, which is the same as data smoothing. Smoothing was also tried, but gave a disagreeable rounding or slurring of the data if applied with sufficient weight to have an effect.

Another approach attempted to find a dominant frequency in the spectral content that could be removed with a notch filter. However as seen in Figure 53, the pulse difference data contains no dominant frequency components that would be eligible for removal.

Figure 52
HISTOGRAM OF PULSE DIFFERENCES

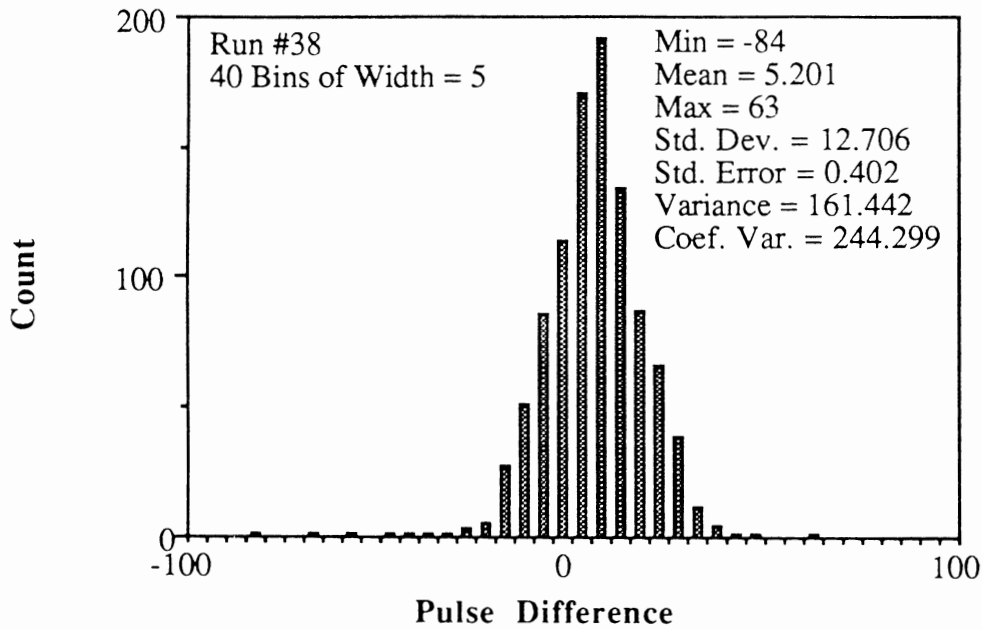
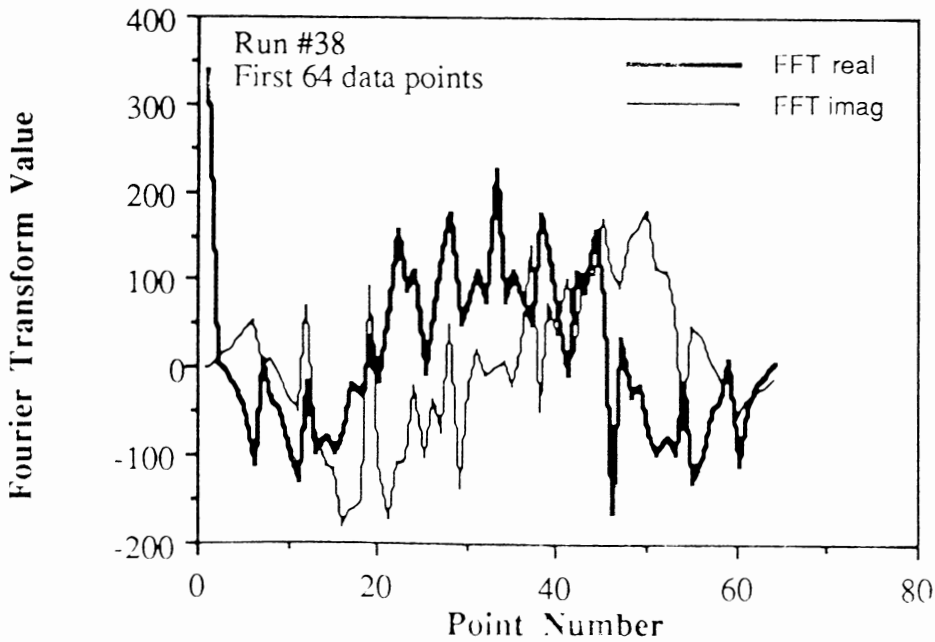


Figure 53
FOURIER TRANSFORM OF PULSE DIFFERENCES



However, another noise reduction technique that did perform well was the digital low pass filter applied after the density calculation in the following loop,

```
PRINT "LOW PASS DIGITAL FILTER"  
TEMP = DENS(1)  
FOR Q% = 3 TO NUMSAMPLE%  
    DENS (1) = [DENS(Q%) + DENS(Q%-1) - TEMP*(1-2*LOPASS)] / (1+2*LOPASS)  
    TEMP = DENS(Q%)  
NEXT Q%
```

where DENS(Q%) is the calculated density array for effective sample number Q% of NUMSAMPLE% total samples, TEMP is a temporary variable, and LOPASS is the filter strength which was set at about 2 for an optimum.

After several combinations of noise reduction techniques were tried in various orders, the following procedure seemed to give the highest profile resolution with the least noise:

1. Double or missed samples are removed and replaced with a local mean.
2. Samples are summed to about 0.1"-0.5" effective diameter difference
3. Density or caliper corrected density is calculated.
4. Resulting density values are run through a digital low pass filter.

Sizing Density Data Acquisition

The design of density data acquisition systems are restricted by hardware limitations of computer memory, computer speed, encoder counts, encoder speed, counter speed and the winder itself. Thus, the data acquisition system must be optimized for each class of applications determined primarily by the nominal thickness of material, the maximum rewind roll size and winder speed. Consequently, a system designed for a carpet winder whose rolls may have only a few dozen wraps must be sized differently than for a system on a paper machine reel which may have more than 10,000 wraps. Fortunately, the useful range of a particular system is usually wide enough to accommodate most of the wound rolls produced on a particular winder. Additional range can be easily obtained by switch selectable quadrature processing of encoder pulses, and setup parameters in the software application.

In this section, a system sizing example will be given for a series of runs made for this project. The design goal of this project was maximum accuracy and resolution, while winding speed was reduced as there were no production pressures in the lab environment. However, designing for wide potential application did include using the ubiquitous IBM PC-AT compatible microcomputer and commonly available data acquisition equipment even though more capable equipment exists at higher cost and reduced availability. In particular, the following input parameters are used for runs numbered 32-41:

minimum core outside diameter = $d_{0,\min} = 4.0''$
 maximum rewind roll outside diameter = $d_{n,\max} = 30.0''$
 drum roller diameter = $d_d = 24.0''$
 minimum material caliper = $c_{\min} = 0.003''$
 minimum computer memory sample array size = $s_{\min} = 10,000$
 maximum count before overflow of counter or storage = $\text{cnt}_{\max} = 65,536$
 maximum winder speed = $v_{\max} = 50.0$ inches/sec
 maximum encoder or counter frequency = $f_{\max} = 1,000,000$ hz (encoder)
 maximum data acquisition sample rate = $R_{\max} = 4$ hz

The first consideration in sizing the system is the number of raw data samples that can be stored in computer memory, which determines the minimum wrap sample size.

$$(111) \quad n_{\min} = \frac{(d_{n,\max} - d_{0,\min})}{2 c_{\min} s_{\min}} = \frac{(30 - 4)}{2 \times 0.003 \times 10,000} = 0.433$$

It is convenient to set the wrap parameter to a convenient value, which may preferably be an integer. If this was a production application, and in anticipation that the minimum caliper will be somewhat less inside a roll due to interlayer pressure, the wrap count might be set to 1.0 to extend the range of smaller caliper and/or larger maximum roll diameters. However to maximize the resolution of this research project, a wrap count of $n = 0.5$ was used.

Now the rewind roll encoder count must be sized such that overflow is avoided. From equation (103), the maximum roll encoder pulses per revolution can be determined.

$$(112) \quad \text{ppr}_{r,\max} = \frac{\text{cnt}_{\max}}{n} = \frac{65,536}{.5} = 131,072$$

However, accuracy considerations of the rewind roll encoder are not necessarily correlated to increasing the encoder pulses per revolution, ppr, as with the drum roller encoder. This is because the roll encoder serves as the timing mark for the start and end of sampling, so that consistency of timing is the controlling parameter for accuracy. Though higher count encoders will generally have better timing consistency (usually plus or minus one pulse error), the once per revolution index pulse will have similar or better consistency than the raw pulses, multiplied pulses or quadratured pulses. Indeed, applications where the sample size is an integer number of wraps could use an extremely fast photoswitch with a once per revolution target in place of an encoder. For example, the Automatic Timing & Controls model number 7062AFRN4X4NLX photoswitch has a response of 15 μ s [18]. At a high wound roll rotational frequency of 20 hz, the resolution of this photoswitch would be equivalent to a 3,333 ppr encoder, and at lower speeds the performance would be even better. Though there are no significant cost differences, the advantages of compact packaging, flexible target positioning and a smaller number of pulses makes fast photoswitches a viable alternative to rewind roll encoders. For this project however, a single channel of a 2500 ppr encoder with a 10x multiplier was used yielding $ppr_r = 25,000$.

Next, the drum roller encoder must be sized so that its counter will not overflow at large rewind roll diameters. Using equations (102) and (103), the maximum drum roller encoder ppr can be sized as

$$(113) \quad ppr_{d,max} = \frac{d_d}{d_{r,max}} \frac{cnt_{max}}{n} = \frac{24}{30} \frac{65536}{.5} = 104,858$$

For these runs, two channels of a 2500 ppr encoders with 10x multipliers were fully quadratured (x4) for an effective pulse rate of 10,000 ppr.

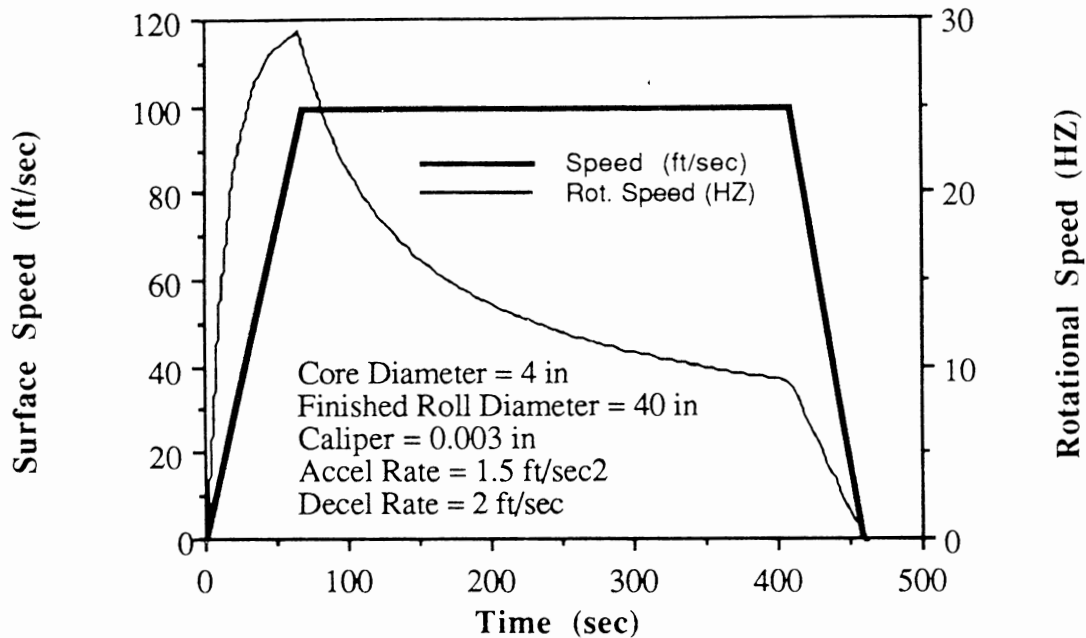
There are speed limitations for both encoders, both counters and the computer data acquisition system that must be considered. The limitations are based on the maximum rotational frequency of the drum roller and rewind roll. As seen in Figure 54, winders may have a simple surface speed profiles composed of acceleration, run and deceleration segments. The maximum ppr of the drum roller encoder is then determined by the minimum of the encoder or counter frequency, maximum speed and drum roll diameter as

$$(114) \quad ppr_{d,max} = \frac{\pi d_d f_{max}}{v_{max}} = \frac{\pi (24) 1,000,000}{50} = 1,508,000$$

The lesser of the pulse rates from equations (113) and (114) must be used.

Figure 54

REWOUND ROLL SURFACE AND ROTATIONAL SPEED



The rewind roll encoder rotational speed is somewhat more complicated than the surface speed as seen in Figure 54, due to ever increasing roll diameters. The maximum rotational frequency for the simple speed profile occurs at the end of the acceleration segment. To calculate this maximum frequency, the diameter at the end of acceleration must first be calculated from core diameter, caliper and acceleration rate as

$$(115a) \ t_{\text{accel}} = \frac{v_{\text{max}}}{\text{accel}}$$

$$(115b) \ l_{\text{accel}} = \frac{1}{2} t_{\text{accel}} v_{\text{max}}$$

$$(115c) \ d_{r,\text{fmax}} = \sqrt{\frac{4}{\pi} l_{\text{accel}} c + d_0^2}$$

$$(115d) \ \text{ppr}_{r,\text{max}} = \frac{\pi d_{r,\text{fmax}} f_{\text{max}}}{v_{\text{max}}}$$

Similar to the drum roller encoder, the lesser of the values of equations (112) and (115d) must be used for the rewind roll encoder pulse rate.

Finally, the maximum sample frequency of the data acquisition/computer/software system must not be exceeded by setting the wrap count too small. This can again be calculated from the diameter at the top of acceleration and the surface speed.

$$(116) \quad n_{\min} = \frac{\pi d_{r,\max} R_{\max}}{v_{\max}}$$

In the case of wrap count, the greater of the values predicted by equations (111) and (116) must be used.

From this design procedure, maximum resolution is achieved by sizing the wrap count small such that available computer memory is filled as much as possible during a run on a large diameter roll of thin caliper. This resolution allows easier detection and replacement of errant data values. However, since averaging would always be required at such small sample sizes, it may be practical to consider cascading counters and storing data as long integers. For example, a 32 bit integer takes twice the memory as a 16 bit integer but could store 32,000 times the number of counts. Maximum accuracy is achieved by increasing the drum roller encoder pulse rate such that the array storage at a large rewind roll diameter is near overflow.

Another way in which memory storage could be optimized would be by storing differences in pulses between consecutive samples instead of the pulse counts themselves. These differences are much smaller, could be nested two per (integer) byte, and are all that are needed for the density calculation. However, there is a practical issue of calculating diameter that requires the raw count. One way this could be accomplished is by storing the first sample as a raw count and the remainder of the samples as count differences. From this data, the raw count at any sample could be reconstructed as the sum of the first raw count plus the sum of count differences to the sample being calculated. However, if there were a hardware problem such as a missed or double sample, or a web break and splice, the raw counts and consequently diameter may not be reconstructed reliably.

Finally, the data acquisition throughput rates can be increased by using an interrupt driven minimal background data acquisition task of high priority coupled through a circular buffer to a calculation and display foreground task of lower priority. In this mode, samples are acquired immediately on rewind roll encoder countdown, while calculation and display takes place as CPU time permits. Thus, the sample rate can be as fast as the minimal data acquisition task rather than the entire requirements for processing a sample. A more detailed discussion of hardware and software is given in Chapters 8 and 9 respectively.

Density and Stress

Though there have been many publications showing an empirical or statistical correlation between density and stress, there is only a single article by Penner which tries to establish a fundamental link between these two measures [139]. In this article, Penner postulates that the increase in density can be calculated as the radial strain on the outer layer as it is added under tension. From this he calculates a simple equation linking WIS to density changes given radial and tangential moduli as well as current outer radius.

Unfortunately, this novel effort while yielding plausible results is neither general, mechanically consistent, nor correct. The conversion is not general because the relation assumes linear anisotropic moduli. The conversion is not mechanically consistent because no core stiffness is included. However, the most serious problem is that the density is assumed to change strictly due to the radial strain in the outer layer. However as seen from equation (108), the density calculation is based on a change of diameters which has two components. The first is an increase due to the addition of a web wrap of a given caliper under no stress. The second is the superposition of the deformations caused by the addition of the web wrap under stress. The deformations include not only the outer layer but all layers beneath as well.

However, density can be calculated from WIS and an extension to winding models as follows. First, the incremental radial and tangential stresses due to a single wrap are calculated for all the individual wraps in the roll using a traditional winding model. Second, the radial strain for each individual wrap can be calculated from the incremental stresses and the radial stress-strain equation (7). Third, the incremental radial deflections of each individual wrap can be calculated from the strain-displacement relation equation (4). Fourth, the deformation of the outer surface due to stresses is calculated as the sum of all the individual wrap radial deflections. Fifth, the new diameter is equal to the old diameter plus the caliper of the wrap added, plus the sum of the wrap radial deflections. Finally, the density can be calculated from the change in diameters.

It is also possible to calculate stresses from density as well by doing something like the above procedure in reverse. However, a much better approach will be detailed in Chapter 7 which bypasses the density calculation and uses diameter and caliper data supplemented by a winding model. From the diameter and caliper data, radial compression can be calculated will be used directly as the outer boundary condition of the model.

Summary

The density analyzer has been described in such detail here because it is one of the more useful winding measurements and serves as a platform for this project. This chapter has given a thorough derivation of the density parameter based on pulse counts from encoders attached to the rewinding roll and roller traveling at web speed. Additionally, a design procedure has been outlined as components need to be selected for a particular application. Finally, common data faults such as double triggering and noise have been described along with solutions where known. Further information about density can be found in Chapter 7 which details an extension to the measurement of stresses, Chapter 8 which describes hardware, Chapter 9 which describes software, Appendix C which gives computer program listings, and the extensive Bibliography.

The density analyzer, in a procedure given by Roisum, was shown to be able to statistically resolve roll structure changes better than most other methods [169, 171]. In addition to the Backtenders Friend, it is the only roll structure measurement presently available which can operate unattended in a fully automatic fashion. Finally, because of its simple, small and rugged components, the density analyzer can be easily configured for most winders. Thus, the density analyzer is currently one of the best roll structure measurement devices due to its sensitivity, automation, and application as both a research and production monitoring tool.

The only serious density limitations are its units of measure which are not directly related to the fundamental parameters of web stresses, undesirable cross-sensitivity to caliper changes, a floating reference due to the basis weight input, and the inability to profile with respect to the CD. It is the first three of these four limitations that this project will address. This is done by supplementing the density like information with caliper and incorporating it into an extended winding model.

CHAPTER 7

A NEW WINDING MODEL FORMULATION

Why a New Approach is Needed

Most winding models use a similar formulation of a second order differential equation with two boundary conditions that are written and solved in an accretive or iterative manner as wraps are added from the core to the finish diameter. The differential equation is determined primarily by material and geometric properties, the core boundary condition by core stiffness, and the outer boundary condition by an assumed wound-in-stress. Unfortunately, the wound-in-stress profile is rarely known for real winding systems except for two rather limiting situations of a centerwinder equipped with caliper and tension measurement, or a unique lab rewinder called the WIT-WOT [166,167]. As a consequence, useful application of winding models is not only limited by the lack of analytical roll defect theories and roll structure design criteria, but also by the lack of knowledge of the wound-in-stress which is a vital input to the winding models. Hence while winding models have given some useful insights, their application remains for the most part an academic exercise.

If the winding model could be reformulated such that all necessary inputs were relatively easy to obtain, useful application could be immediate even without roll structure optimization algorithms. This could be accomplished by comparing stress distributions of rolls that are judged acceptable with those that are rejected, where the judgement may be made by roll structure measurements, statistics, empirical approximations or simple subjective observation. This comparison of stress distributions between rolls would be as a function of both controllable parameters such as wound-in-tension, and uncontrollable parameters such as material properties. With such knowledge, one can adjust controllable parameters such that the stress distribution approaches that of rolls deemed to be acceptable.

More specifically, if the winding model can take many of its inputs from online measurement during winding, the inferred stress distribution can be used as a roll quality monitor. Furthermore, if computations can be made accurately and quickly, a computer could adjust controllable inputs in closed loop control so that the inferred stress distribution closely matches a target stress profile. Finally, when roll structure optimization routines are developed [128], the reformulated winding model could serve as the nucleus of a control strategy that can enhance the quality of winding to the accuracy of the measurements, and to the degree which the model reflects real behavior. Thus, reformulating the winding model in terms of inputs that can be measured online could revolutionize winding through quality control measurement, simple control, and optimized control.

Another major benefit of a new winding model is that it enables the development of the first practical measurement of stresses for research or production quality control. Though there are other methods described in Chapter 5 that can also measure stresses, they all have rather severe limitations of either sensitivity or ease of application [169, 171]. However, the new measurement model is sensitive, automated and easily applied on most winders or unwinds.

Overview of the New Model

The primary difficulty with present winding models is that the outer boundary condition of WIS (wound-in-stress) is often difficult to determine for many real winding conditions. Reformulation of winding models, which presently assume a WIS profile, to a method where required parameters can easily be measured involves recognizing that all current winding models are determined systems. These systems are composed of constitutive equations which can be assembled and reordered, so that the physics of the wound roll is described by a second order differential equation. As seen in Chapter 3, the constitutive equations can be reordered, so that equivalent differential equations for the determined system can be written in terms of stresses, strains or displacements. In each of these formulations, both the inner and outer boundary conditions vary with the formulation.

Presently, the traditional winding models are written in terms of radial stress which requires a known radial stress boundary condition at the outer surface which is computed from the WIS using equation (28a). However, this new model can reformulate the same constitutive equations into a differential equation written in terms of displacements. The advantage, as will be seen, is that the boundary condition at the outer surface can be obtained from density-like measurements of diameter supplemented by caliper. Thus, the reformulation to a new and easily measured boundary condition is the essence of this work.

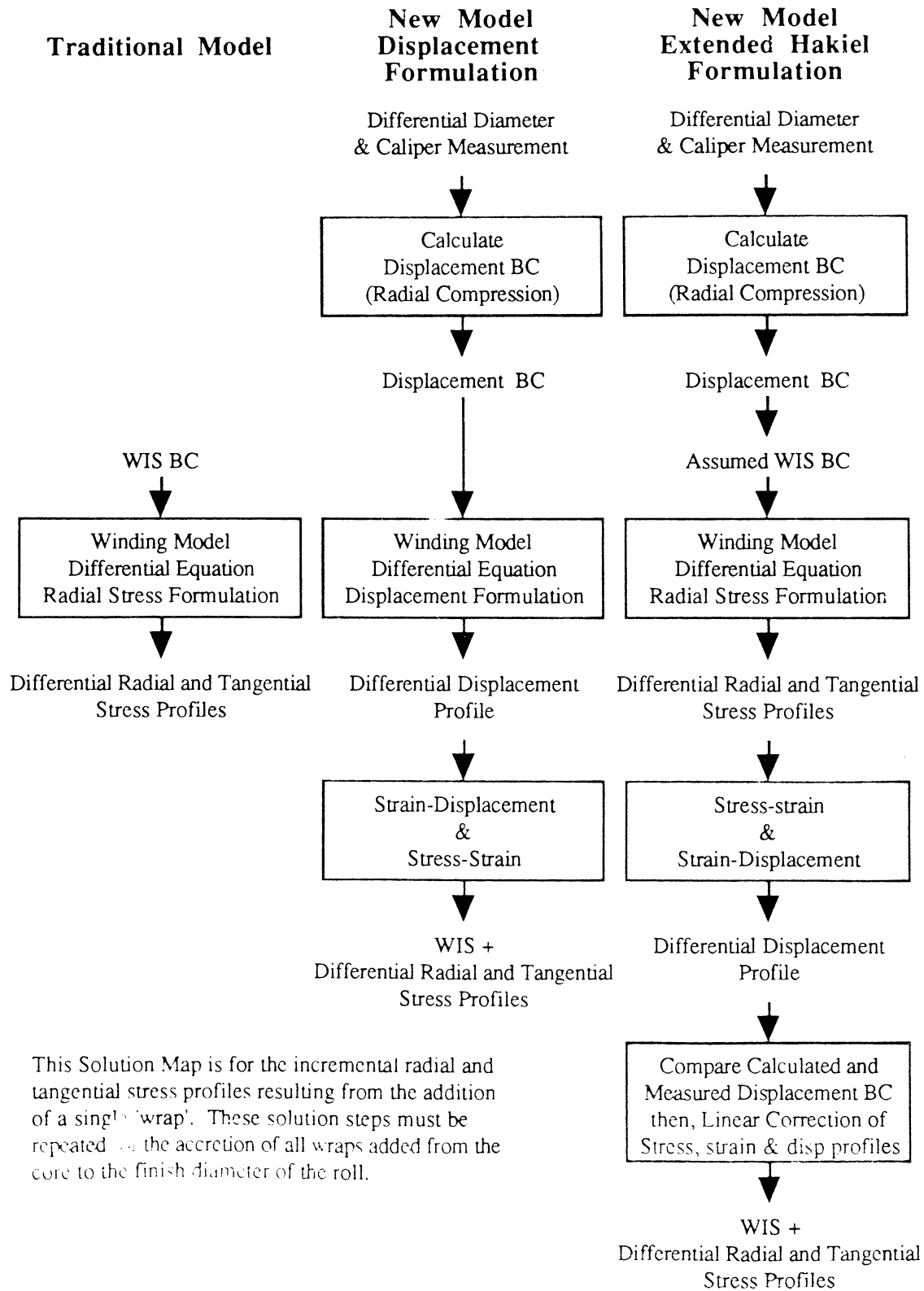
However in addition to the reformulation, this new model requires a more complete solution to the physics of a wound roll than traditional models. This is because in addition to radial and tangential stresses which both approaches yield, the new model also requires that strains and displacements be solved as displacement in particular is intimately tied to the outer boundary condition. Thus the new approach is a superset of traditional models.

Another difference between the traditional and the new approach is the direction of the solution. Present models begin with an *input of a WIS* profile and output calculated radial and tangential stress profiles. However, the new model begins with an input of a displacement profile from diameter and caliper measurements and *outputs a WIS* profile with the radial and tangential stress profiles resulting as intermediate calculations. Thus in a certain sense, the new approach is a solution of an extension of the traditional winding models in reverse.

In this chapter, two complete, correct, independent and mechanically consistent solutions of the measurement of stresses during winding are given. The first solution, the Displacement Formulation, was primarily written in terms of displacement as it is in the closest form to the measurable boundary condition, and stresses are calculated at the final step. The advantage of this approach is simplicity. However, the Displacement Formulation will be shown to be computationally time-consuming as extremely small grids are required to obtain a required accuracy for highly nonlinear and/or anisotropic materials. Thus a more practical and efficient solution needed development, which resulted in the Extended Hakiel Formulation which though more complicated, has a greater computational efficiency. Even so, several new numerical techniques are needed as the Extended Hakiel Formulation requires more calculations than the conventional Hakiel model. Both formulations will be discussed in detail in this chapter.

A comparison of the solution steps for the traditional, Displacement Formulation and Extended Hakiel Formulation is given in Figure 55. As evidenced here, the new models are more extensive than the traditional model as in addition to stresses, the strain and displacement fields must also be calculated. Though the new models require more steps, these additional calculations are not very involved because they are based directly on the constitutive equations which are much simpler to solve than the differential equation which is at the heart of every winding model. However it must be stressed that despite the different appearances of the solutions, they are all mechanically consistent in every way as they result from the same constitutive equations. Consequently, the new models share the identical set of assumptions and limitations as the traditional winding models.

Figure 55
SOLUTION MAP OF WINDING MODELS



However, the new approach has one very distinct difference from traditional models in that it is more than just a model. Rather, it is a methodology for measuring stresses using any consistent winding model given diameter and caliper measurements. Consequently beyond the immediate implementation of this new approach, the future benefits are that it is both flexible and extensible. It is flexible because it cares not what sensor technique is used to measure diameter and caliper, only that they are available. Furthermore, it cares not what winding model is used, only that it is mechanically consistent.

Thus, this methodology can grow to accommodate both improvements in measurement as well as winding models. If the measurement of diameter or caliper could be made more accurately by lasers for example, it could be directly input into the stress measurement algorithm. Similarly, if winding models are extended to include anelastic behavior or air entrainment, this methodology can be applied provided that the model is mechanically consistent and is thus able to calculate strains and displacements in addition to stresses. Finally, this methodology is one of the few technologies that directly connects analytical and experimental winding sciences as discussed in Chapter 1.

To summarize, the measurement of stresses during winding takes diameter and caliper measurements and outputs WIS, radial, and tangential stresses. The calculation is based on the physics of wound rolls which describe how the outer radius must grow due to the addition of wraps and deform due to the addition of these wraps under a wound-in-stress. Though the measurement of stresses is indirect, so are many other common methods. An analogy is a spring scale which takes deflection as its input and outputs a force, where the calculation is the familiar spring equation.

The remainder of this chapter begins with the description of the new outer boundary condition which is the essence of this new technique. This new outer boundary condition can be nondimensionalized to Radial Compression which can be a stand-alone technology and has many advantages over the density calculation. Next, the constitutive and differential equations for both the Displacement Formulation and Extended Hakiel Formulation are assembled and solved. These sections include derivations of the finite difference approximation of differential equations as well as their solution technique. Finally, the measurement of stress methodology is evaluated by comparing the outputs of the two new models with synthesized and real WIS data. Additionally, a more extensive treatment of sensitivity analysis is given in Chapter 10 and the appendices contain both computer code and output for the new model.

A New Outer Boundary Condition

The outer boundary condition of current winding models requires a force, tension or stress measurement as a function of winding radius. This force measurement is extremely difficult to accomplish in practice, even in a laboratory environment. After considering numerous alternative measurements of some characteristic of the outer boundary, diameter or radius might be a prime candidate because of its ease of online measurement to high accuracy using encoders and the density analyzer approach. Since there is no closed form equation relating roll radii to WIS, the constitutive equations must be reformulated and reordered in terms of displacements instead of the customary radial stress under the outer wrap.

The boundary condition for this new approach to winding models begins by noting how a roll grows with the addition of a single wrap, which is modeled traditionally as a hoop. This growth from one diameter to another is the superposition of two effects. First, the roll will tend to increase in radius by the thickness of the wrap added. Secondly, the roll will tend to deform inward as the addition of a wrap under tension will increase the incremental radial stresses of all layers in the roll due to the additional interlayer pressure. As seen schematically in Figure 56, the compaction is greatest for the outer layers and rapidly decreases with depth. Subjectively, the rapidly decreasing compaction with depth is due to the self supporting nature of the rings. Quantitatively, this decrease is directly due to the incremental radial stress profile which also decreases rapidly with depth.

The new boundary condition is easiest to understand if the effects of caliper addition and roll deformation are separated into two steps. Figure 57 shows a general diagram of a roll with j wraps, upon which will be added the k^{th} wrap. Focusing on the k^{th} wrap, if it is first added in an unstressed condition, as in the center diagram, the roll would then assume a diameter of $r_k = r_j + c_k$. However, as wrap k is added under a wound in tension, a pressure is developed between wrap j and wrap k . As a consequence, the thickness of wrap k is reduced from c_k to $c_k(1 + \epsilon_{R,k})$. Similarly, the incremental interlayer pressure increases will cause all wraps under wrap j to decrease in thickness, thus radius r_j will decrease to r_j' and so on. The core, which is the foundation of the wind, will also decrease slightly in radius in response to increasing radial compression. Thus, each of the layers of the roll as well as the core will experience an incremental decrease in thickness due to the incremental increase in interlayer compression as quantified by winding models and illustrated in Figure 56.

However, though the distribution of layer compaction or deformation will need to be eventually solved, at this time the outer boundary condition is of greatest importance. The essential observation that can be made from the new boundary condition illustrated in Figure 56 is that the displacement of the outer radius of the roll tends to increase by the thickness of the added wrap, c_k , and simultaneously decreases by an amount w_k due to summation of the incremental compaction of all layers, w_k . Though the roll would tend to increase its radius by c_k , any positive WIS on wrap k will reduce the radial increase by $-w_k$. Thus, from the figure,

$$(117) \quad r_k = r_j + c_k + w_k$$

where w_k is defined as positive outward, but will be negative for real winding systems. Rearranging the terms and noting that sample sizes for data acquisition and grid sizes for model calculations need not necessarily be the same as wrap or caliper thickness, we can rewrite the outer boundary condition, equation (117), into its final form as

$$(118) \quad w_k = (r_k - r_j) - \sum_{n=1}^N c_{k,n}$$

where

- w_k = the stress induced radial displacement of outer 'wrap' k (in) defined as positive outward
- r_j = radius at sample j (in) after addition of wrap j
- r_k = radius at sample k (in) after addition of wrap k
- Σ = summation of the number of real wraps corresponding to a N wrap data acquisition or calculation sample size
- c_k = the unstressed caliper of the N wraps comprising sample k (in)
- r_j' = radius to sample j (in) after addition of a wrap k

Thus, the outer boundary condition has been reformulated from wound-in-stresses, which are difficult to determine, to a radial displacement w_k . The relevance of equation (118) is that the terms of the right hand side can be measured easily during winding or unwinding. The radii r_j and r_k can be measured with great accuracy using incremental encoders and equation (102). The caliper, under web tension, can be measured with various sensors in the sheet run just upstream of the winding roll.

The application of the new measurable boundary condition, the radial deformation of the roll's outer surface given by (118), is immediate for the Displacement Formulation which is written in terms of radial displacement. However, other differential equation formulations can also make use of the boundary condition, albeit more indirectly. For example, another way the boundary condition can be obtained is to sum up the individual compactions of all the individual layers as well as the core. This results from constitutive equations given in Chapter 2 such as the incremental radial strain displacement with its finite difference approximation

$$(119) \quad \epsilon_{R,i} = \frac{dw}{dr} = \frac{w_i - w_{i-1}}{h}$$

If the radial strains are summed for each individual layer from the core to the current outer surface then

$$(120) \quad w_k = w_0 + h \sum_{i=1}^k \epsilon_{R,i}$$

which says that the radial deformation of the outer surface is equal to the core deflection, w_0 , plus the average thickness multiplied by the sum over all layers of their incremental radial strains. The core stiffness definition, given as equation (16) in Chapter 2 can be solved for the core deflection as

$$(121) \quad w_0 = \frac{r_0 \sigma_{R0}}{E_c}$$

The final form of the deflection of the outer surface is obtained by inserting the core deformation equation (121) and the anisotropic radial stress-strain relations into equation (120) yielding

$$(122) \quad w_k = \frac{r_0 \sigma_{R0}}{E_c} + h \sum_{i=1}^k \left(\frac{\sigma_{R,i}}{E_R} - \mu_T \frac{\sigma_{T,i}}{E_T} \right)$$

Thus, equation (122) can be used to calculate the deformation of the outer surface due to the incremental radial and tangential stresses obtained from conventional winding models. One application of (122) is for the Extended Hakiel Formulation where an assumed WIS is adjusted until the measured (118) and calculated (122) incremental outer deformations are equal.

Caliper Cautions

The application of the new boundary condition requires both a careful measurement of diameter and caliper, and a clear understanding of what caliper means. Careful measurement is a requisite because as seen in (118), the calculation for deformation is subject to numerical errors resulting from what is known as small differencing. In other words, the radius difference, deformation and caliper are all extremely small compared with the radius. Thus, small uncertainties in measurement will have a large effect of the deformation calculation. Additional information on caliper measurement can be found in Chapter 8.

The second requisite is that the caliper used in that equation is a stack property which is the arithmetic average distance between layers in a stack which is *completely unstressed*. This is a direct result of the superposition, illustrated in Figure 57, of the stress induced radial deformations onto the radial growth due to the addition of the thickness of an unstressed web. Typically however, caliper is measured in real systems under a state of biaxial loading. First, the caliper measured on a free span of a web processing line is under a state of MD tension which is required for web transport. Secondly, all contacting caliper gages and even some non-contacting gages exert a ZD compressive load upon the web in the measurement area.

Fortunately however, caliper measured under biaxial loading can be converted to the unstressed caliper required by (118) using simple stress-strain relations for the linear anisotropic case. This begins by noting that when a web is under stress, it experiences a through-thickness strain and change of caliper as

$$(123) \quad c_{\text{stressed}} = c_{\text{unstressed}} (1 + \epsilon_R)$$

where in this case, ϵ_R represents the through-thickness strain. Solving equation (123) for unstressed caliper and inserting the stress strain relation (7) gives

$$(124) \quad c_{\text{unstressed}} = \frac{c_{\text{stressed}}}{\left(1 + \left(\frac{\sigma_R}{E_R} - \mu_T \frac{\sigma_T}{E_T}\right)\right)}$$

The two contributions to the biaxial load are the ZD measurement pressure σ_R , and the free web MD tension induced stress σ_T which is the web tension divided by caliper. Depending on the application and material, one or both of these terms can be quite significant. Though the web tension contribution to thickness changes for the paper used in this project's experimental validation are not significant because the poisson ratio is near zero, the ZD pressure contribution can't be neglected because of the soft radial modulus.

However, the nonlinear radial modulus of typical materials poses a problem for the direct application of (124) because the stiffness is a function of pressure. Fortunately, this is easily addressed by using radial stress-strain curves to calculate the change in radial strain for a stack initially at a ZD measurement pressure as it is completely unloaded. This radial strain is equal in magnitude and opposite in sign as the radial strain given by loading from zero to the measurement pressure. This value can be obtained directly from stress-strain curves such as given by Figure 17, or indirectly from the radial modulus. For this project, the ZD caliper measurement sensor imposed a ZD pressure of 7.3 psi. This caused a theoretical radial compaction due to a caliper gage measurement pressure of 8.8%, 6.9% and 2.7% for the NC, LWC and coated board respectively. However, even this caliper correction is somewhat simplistic in that there are some bending stiffness edge effects around the periphery of the gage area that reduce the deformation due to gage load. Thus, the actual corrections needed will be smaller than predicted by the simplistic approach described above.

Thus, the caliper read by the gage may be significantly lower than the unstressed thickness of the web and consequently must be properly accounted for. This is especially important in light of the fact that the compression due to interlayer pressures and the pressure due to caliper gage measurement may be of similar magnitude. Thus, the importance of this correction cannot be overstated. Even the author who derived these corrections did not apply them at first, until the resulting radial compression and stress calculations yielded nonsense which was traced back to a serious oversimplification of taking the caliper readings at face value. The moral here is that instrument calibration and proper operation is not enough, one must understand what the instrument readings actually imply. In the case of contacting caliper measurements, the load applied by the gage affects the readings such that actual thickness is underestimated.

Radial Compression

While wound roll stresses are the ultimate goal of this project, their computation is relatively complex and time-consuming. Additionally, some quality control programs may not need the fundamental parameters of stresses to simply discriminate relative changes in the winding roll. Indeed, nearly all of the most common roll structure measurement methods use arbitrary monotonically increasing scales such as Rho, Schmidt, Smith and density, which cannot be directly related to stresses. Therefore, it would be appropriate to determine if some simple intermediate parameter based on the existing measurements of diameter and caliper might suffice in lieu of more complicated stress calculations.

One possibility would be the radial displacement of the outer surface during winding as given by equation (118). In some ways, this is an ideal simple parameter because it easily calculated, and is very closely related to the WIS. This relationship is monotonic because increasing the WIS will increase the inward radial deflection for any combinations of input parameters. Additionally, since the outer boundary condition singly drives the solution for WIS, there is obviously a close relationship. Thus, radial displacement profiles will match closely in shape, though not scale, the other roll structure profiles such as hardness, and tension.

However, radial displacement does have two drawbacks as a roll structure method. The first, though relatively minor, is that the values of radial displacement are extremely small numbers which may not be intuitive to many of the operators who might use such a system. More important however, the value of radial displacement depends on caliper and sample size. For small samples, radial displacement is directly proportional to the radial difference between consecutive samples. Thus, a 20 wrap sample will deflect twice as much as a 10 wrap sample for a given caliper. Similarly, a 10 wrap sample on thicker material will deflect more than on a thinner material. Thus, radial displacement has an undesirable cross sensitivity to caliper and sample size.

A simple solution to this problem is to nondimensionalize the radial displacement with respect to either caliper or measured differences in radii between consecutive samples. Furthermore, if this value is changed in sign so that positive WIS yields a positive calculation, as well as multiplied by 100 to express as an intuitive percent, we now have an ideal, simple, and intuitive calculation. This new parameter, called Radial Compression, which is derived from minor manipulations of the new outer boundary condition, is simply calculated as

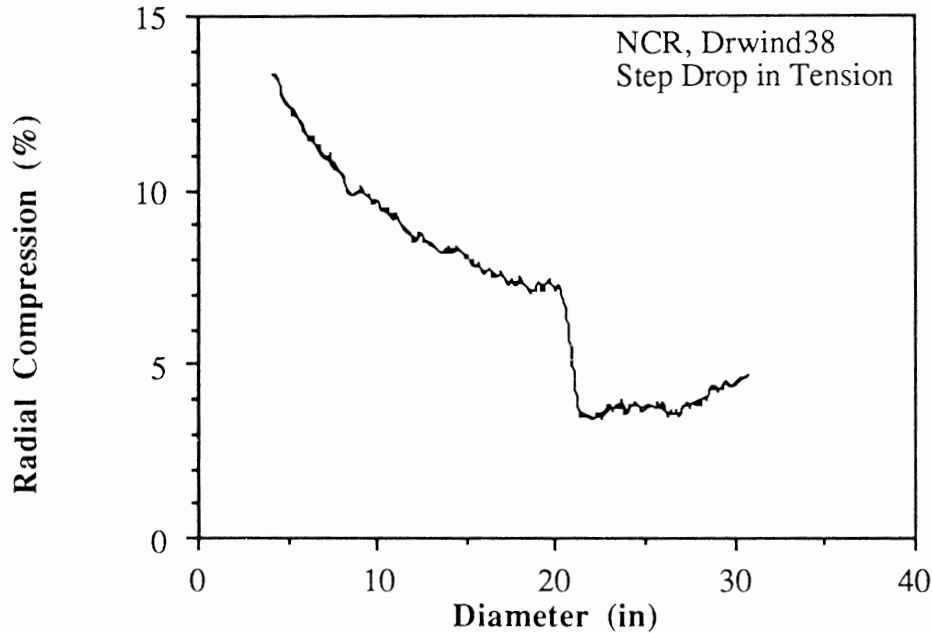
$$(125) \quad \text{Radial Compression} = \mathfrak{R}_k = (100\%) \frac{2 \sum_{n=1}^N c_{k,n} - (d_k - d_j)}{2 \sum_{n=1}^N c_{k,n}}$$

As seen in equation (125), the Radial Compression calculation is derived directly from easily obtained measurements. The numerator is nothing more than the negative of the displacement boundary condition given by (118), while the denominator is the nondimensionalization by the measured caliper of the sample. The 2's in the numerator and denominator simply convert from radii to diameters, and the 100 multiplier gives percent. The nondimensionalization by caliper is not to imply that the compression takes place strictly within the sample zone as is assumed by the simplistic density calculation. As indicated in Figure 56, the compression though greatest at the OD extends to the core.

An example of a Radial Compression profile of a roll wound with a step decrease is shown in Figure 58. This figure shows the typical smile shaped profile of two-drum winding upon which is superposed a step reduction in the TNT's. What is striking about this figure is the extremely small spatial resolution of displayed points and the absence of measurement noise. These desirable characteristics are not shared by any current roll structure measurement method. Though Radial Compression has a distant ancestry in the density analysis, it has several distinct advantages.

1. Radial Compression accounts for caliper variations which increases the resolution of the measurement tremendously. As will be shown in Chapter 10, the statistically measured improvement in roll structure resolution is one to two orders of magnitude over currently used methods!
2. Radial Compression requires no web properties to be input by the operator, but rather measures all quantities needed after the system is initialized for encoder counts and roller diameters. Conversely, basis weight is a required operator input for density giving the resulting calculations a floating reference depending on the value given for basis weight.
3. Radial Compression has no zero offset. Thus while Radial Compression is zero for $WIS = 0$, the density will be the unstressed density of the materials which can vary from 0.01 to 0.05 lb/in³ for paper grades alone.

Figure 58
A RADIAL COMPRESSION PROFILE



4. The Radial Compression values are typically a few percent which is intuitively easier to relate to than the small ϵ' imals given by density.
5. Is closely related to the fundamental properties of stresses, as it is a nondimensionalization of the outer boundary condition which drives the stress solution.

In conclusion, while Radial Compression was not the ultimate goal of this project of measuring stresses during winding, it was a very fortunate intermediate outcome. It is in many ways an ideal production quality control measure because of its extreme sensitivity, ease of measurement and calculation, and the intuitive nature of the scale. Thus while it may not satisfy some research needs, its application in a production environment can justify its development. Finally even if stresses are the ultimate roll structure measure, the Radial Compression calculation is not in vain as it is a nondimensionalization of the outer boundary condition for the two models given in this chapter. Additionally, Radial Compression provides a quick check of data integrity before length stress calculations are performed.

The Displacement Formulation

As indicated earlier, two stress calculation models were developed. The first given here is the Displacement Formulation which is the simpler of the two, but as we shall see suffers from numerical calculation difficulties. This model is derived by first writing the winding differential equation in terms of displacements because the outer boundary condition is already in terms of displacements, although the core boundary condition will need reformulation. Next, the finite difference approximations are developed and the matrix solution technique selected. Finally, the model is run using simulated data to evaluate accuracy, numerical difficulties and sensitivity.

Though this particular model is of more academic interest because numerical difficulties preclude practical application for many real systems, several interesting points about winding models in general will be discovered. First, that while the radial stress gradient must be included in the derivation, the tangential gradient does not appear. Second, the technique of simulating data sets can indirectly verify models over parameter ranges that can't be accommodated by other models. Thus, Hakiel's model was independently verified for nonlinear radial moduli which are not covered by other models such as by Altmann and Yagoda.

As indicated in Chapter 2, winding models must obey the constitutive equations for the physics of the wound roll. However as indicated in Chapter 3, the constitutive equations can be assembled in different orders to result in second order winding differential equations written in terms of stresses, strains or displacements. Thus, the Displacement Formulation begins with the constitutive equations

equilibrium

$$(126) \quad r \frac{d\sigma_R}{dr} + \sigma_R - \sigma_T = 0$$

from the radial strain displacement (4) and stress-strain (7)

$$(127) \quad \frac{dw}{dr} = \frac{\sigma_R}{E_R} - \mu_T \frac{\sigma_T}{E_T}$$

and from the tangential strain displacement (6) and stress-strain (8)

$$(128) \quad w = r \left(\frac{\sigma_T}{E_T} - \mu_R \frac{\sigma_R}{E_R} \right)$$

Solving (128) for tangential stress yields

$$(129) \quad \sigma_T = \frac{\mu_R r E_T \sigma_R + E_R E_T w}{r E_R}$$

Inserting (129) into (127) and solving for radial stress yields

$$(130) \quad \sigma_R = - \frac{E_R \left(r \frac{dw}{dr} + \mu_T w \right)}{r (\mu_R \mu_T - 1)}$$

The first derivative of the radial stress with respect to radius can now be obtained from (130). However, care must be taken here as to what terms of the equation may vary directly or indirectly with radius which will result in cross product terms that have been omitted by previous authors (see Chapter 3). Since radial modulus varies directly with interlayer pressure, it will also vary indirectly with radial position. Therefore, it must be regarded as a variable for the purposes of taking the derivative. However, the Poisson ratios are assumed to be constants for simplicity and because the winding models have a demonstrated insensitivity to these material properties. Note that the derivative does not include tangential stress so that the derivative cross product is not a parameter of the wound roll physics as is the radial modulus derivative. Thus because all formulations are equivalent, the radial modulus gradient must be included in any derivation (of nonlinear radial modulus models) while the tangential modulus gradient need not.

The next intermediate steps in the derivation will not be included in entirety because of their lengthy expressions. They were solved using a symbolic math application, Mathematica, running on an Apple Macintosh. In outline form, the derivative is performed on (130) as indicated above. Next, the radial stress equation (130) is inserted into the tangential stress equation (129). This tangential stress result, as well as the derivative of radial stress from (130) and finally the radial stress expression (130) are all inserted into the equilibrium equation given by (126). Finally, the winding differential equation written in terms of displacements is reduced to standard form so that

$$(131) \quad r^2 \frac{d^2 w}{dr^2} + A r \frac{dw}{dr} + B w = 0$$

where

$$(131a) \quad A = 1 + \mu_T - \frac{E_T}{E_R} \mu_R + \boxed{\frac{r}{E_R} \frac{d E_R}{dr}}$$

$$(131b) \quad B = \frac{-E_T}{E_R} + \boxed{\frac{\mu_T r}{E_R} \frac{d E_R}{dr}}$$

and the terms enclosed in the boxes represent the higher order terms resulting from taking the derivative of the radial stress expression given by (130). It is interesting to note that if these terms are deleted for the case of linear anisotropy, then the coefficients reduce to exactly those given by Altmann [127]

$$(131c) \quad A = \left(1 + \mu_T - \frac{E_T}{E_R} \mu_R \right)$$

$$(131d) \quad B = \frac{-E_T}{E_R}$$

The next question, one of practicality, is whether these higher order terms are significant for nonlinear radial moduli models. While it is difficult to make generalizations because of the wide variety of material properties for real winding systems, several test cases indicated the following. First, the higher order terms are only needed for nonlinear models. Second, the high order terms seem to be small for Hakiel's radial stress formulation [132, 133]. However, the high order terms may be quite significant for the displacement formulation for nonlinear radial moduli. In particular, the high order fourth term given by (131a) can be of the same order of magnitude as the first and third terms. Without its inclusion, nonlinear radial moduli cases weren't calculated properly.

Finally, the differential equation given by (131) and the coefficients given by (131b & c) hint at numerical difficulties that will be demonstrated shortly. First, the displacement field has a much higher gradient than the radial stress field as indicated best by the derivative given in (127). High gradients increase the propensity for numerical approximation and roundoff errors. Secondly, the inclusion of yet another significant derivative term, the high order radial modulus derivative in (131a), can pose problems because numerical derivatives increase numerical noise.

Since the critical outer boundary condition has been reformulated from stresses to radial displacements, the core must also be reformulated to displacements. This begins with the definition of core stiffness is given from Chapter 2 as

$$(132) \quad E_c = \frac{\sigma_R}{w/r} \Big|_{r=r_0}$$

The strain-displacement equations (4) and (6) combined with the stress-strain relations (7) and (8) can be combined to solve for the first derivative of the displacement at the core in terms of E_c , material properties, and displacement at the core as

$$(133) \quad \frac{dw}{dr} \Big|_{r=r_0} = \frac{-w(-E_c + \mu_T E_R + \mu_R \mu_T E_c)}{E_R r}$$

This core gradient boundary formulation in terms of a displacement field can't be solved directly, but will be ultimately solved as a finite difference formulation.

Finite Difference Approximations to Differential Equations

Although there are other methods for solving differential equations, one of the simplest and most general method is perhaps the finite difference approximation first applied to winding models by Hakiel [132, 133]. In this method, the first and second derivatives are approximated by difference equations. The first derivative for example is approximated by the difference in values (rise) between two neighboring points divided by the grid spacing (run) which is analogous to slope. This is an example of a two point forward difference approximation of the first derivative. Additionally, the coefficients depend on the base point about which the derivative is computed. Finally, there are higher order approximations using more points to compute the approximation even more accurately. The approximations can also be derived for second and higher derivatives. Tables 7a and 7b give the finite difference approximations for the first and second derivatives using from two to five points.

Table 7a
1ST DERIVATIVE FINITE DIFFERENCE APPROXIMATIONS

$$\left. \frac{df}{dx} \right|_{x=x_i} = \frac{1}{m! h} \sum_{i=0}^m a_i f_i + E$$

where: f = function of x
 x_i = base point about which the derivative is calculated, with equal base point spacing h
 m, a_i = coefficients
 E = leading error term

	i	a_0	a_1	a_2	a_3	a_4	E
Two point ($m=1$)	0	-1	1				$-1/2 h f''$
	1	-1	1				$1/2 h f''$
Three point ($m=2$)	0	-3	4	-1			$1/3 h^2 f'''$
	1	-1	0	1			$-1/6 h^2 f'''$
	2	1	-4	3			$1/3 h^2 f'''$
Four point ($m=3$)	0	-11	18	-9	2		$-1/4 h^3 f''''$
	1	-2	-3	6	-1		$1/12 h^3 f''''$
	2	1	-6	3	2		$-1/12 h^3 f''''$
	3	-2	9	-18	11		$1/4 h^3 f''''$
Five point ($m=4$)	0	-50	96	-72	32	-6	$1/5 h^4 f''''''$
	1	-6	-20	36	-12	2	$-1/20 h^4 f''''''$
	2	2	-16	0	16	-2	$1/30 h^4 f''''''$
	3	-2	12	-36	20	6	$-1/20 h^4 f''''''$
	4	6	-32	72	-96	50	$1/5 h^4 f''''''$

Table 7b
2ND DERIVATIVE FINITE DIFFERENCE APPROXIMATIONS

$$\left. \frac{d^2f}{dx^2} \right|_{x=x_i} = \frac{2}{m! h^2} \sum_{i=0}^m a_i f_i + E$$

where: f = function of x
 x_i = base point about which the derivative is calculated, with equal base point spacing h
 m, a_i = coefficients
 E = leading error term

	i	a_0	a_1	a_2	a_3	a_4	E
Three point ($m=2$)	0	1	-2	1			$-1 h f'''$
	1	1	-2	1			$-1/12 h^2 f''''$
	2	1	-2	1			$1 h f'''$
Four point ($m=3$)	0	6	-15	12	-3		$11/12 h^2 f''''$
	1	3	-6	3	0		$-1/12 h^2 f''''$
	2	0	3	-6	3		$-1/12 h^2 f''''$
	3	-3	12	-15	6		$11/12 h^2 f''''$
Five point ($m=4$)	0	35	-104	114	-56	11	$-5/6 h^3 f''''''$
	1	11	-20	6	4	-1	$1/12 h^3 f''''''$
	2	-1	16	-30	16	-1	$1/90 h^4 f''''''$
	3	-1	4	6	-20	11	$-1/12 h^3 f''''''$
	4	11	-56	114	-104	35	$5/6 h^3 f''''''$

On the the first decisions that must be made on finite difference approximations is the order of the approximation. As seen in Tables 7, the error terms given in the last column decrease in size as the number of points used in the approximation are increased. However, the increase in accuracy comes at a cost of longer computing time per derivative. Typically, the net computing time should decrease with increasing order of approximation. However, both the Displacement Formulation and Hakiel model computed faster to a given accuracy for the cases tested using a 3 point rather than a 5 point approximation. Although the 3 point approximation was ultimately selected for application because of speed and simplicity, both are included here for completeness.

Once the order of the approximation is selected, the finite difference approximations are substituted into the derivatives of the winding differential equation. Then, like terms are collected. The simplest example will be demonstrated here for the internal layers of the Hakiel model. From Table 7a for the three point central difference approximation ($m=2, i=1$), the first derivative is approximated as

$$(134a) \left. \frac{d\sigma_R}{dr} \right|_{r=r_j} = \frac{(-1)\sigma_{R,j-1} + (0)\sigma_{R,j} + (1)\sigma_{R,j+1}}{2h}$$

Similarly from Table 7B for the three point central difference approximation ($m=2, i=1$), the second derivative is approximated as

$$(134b) \left. \frac{d^2\sigma_R}{dr^2} \right|_{r=r_j} = \frac{(1)\sigma_{R,j-1} + (-2)\sigma_{R,j} + (1)\sigma_{R,j+1}}{h^2}$$

The derivative approximations (134) are then inserted into differential equation given earlier

$$(135) \quad r^2 \frac{d^2\sigma_R}{dr^2} + A r \frac{d\sigma_R}{dr} + B \sigma_R = 0$$

to give

(136)

$$r^2 \left(\frac{(1)\sigma_{R,j-1} + (-2)\sigma_{R,j} + (1)\sigma_{R,j+1}}{h^2} \right) + A r \left(\frac{(-1)\sigma_{R,j-1} + (0)\sigma_{R,j} + (1)\sigma_{R,j+1}}{2h} \right) + B \sigma_{R,j} = 0$$

Finally, the terms are multiplied out and collected on common radial locations of $j-1$, j and $j+1$ as

$$(137) \left[\frac{r(2 - A h)}{2 h^2} \right] \sigma_{R,j-1} + [B - 2 r^2] \sigma_{R,j} + \left[\frac{r(2 + A h)}{2 h^2} \right] \sigma_{R,j+1} = 0$$

This equation represents the finite difference approximation for the winding differential equation written in terms of radial stress for the j^{th} layer. Similar equations must be written for all of the other layers in the current roll size. These will be assembled into a linear system of equations in matrix form as

$$(138) [\mathbf{A}] \{\mathbf{x}\} = \{\mathbf{B}\}$$

where

$[\mathbf{A}]$ = a square matrix composed primarily of coefficients of the finite difference approximation of the winding differential equation, written in terms of displacements (or stresses or strains)

$\{\mathbf{x}\}$ = a column matrix of unknown displacements (or stresses or strains) for each layer

$\{\mathbf{B}\}$ = a column matrix containing the displacement (or stress or strain) outer boundary condition which forces the solution

This system of equations will be assembled as shown in Figures 59 where the first layer corresponds to row 1, and the outer layer corresponds to row n . However, the layers adjacent the core and the outside posed even additional complications for both the 3 and the 5 point approximations. First in addition to the differential equation, they must also contain the finite difference approximation of the boundary conditions. The inner layers must incorporate the core stiffness, E_c , boundary condition and the outer layers will incorporate the boundary condition of a known displacement (stress or strain) at the outer surface. Second, the order of the approximation must decrease near the core and outer layer as well as the point about which the derivative is computed, so that the resulting matrix retains either the 3 or 5 wide bandwidth. As a consequence, the inner and outer layers use a forward and backward difference respectively, instead of the central difference used for the intermediate layers. The structure of the resulting 3 point system is shown in Figure 59a. Though more complicated, a 5 point approximation to the winding differential equation can also be derived as well for the internal layers and is shown in Figure 59b.

Figure 59a
3 POINT WOUND ROLL EQUATION SYSTEM

$\begin{matrix} 1 & 2 \\ 1 & 2 & 3 \\ & 2 & 3 & 4 \\ & & 3 & 4 & 5 \end{matrix}$	<p>Solution for a n wrap roll in terms of:</p> <ol style="list-style-type: none"> 1. Stresses 2. Strains 3. Displacements 	$\begin{matrix} Y_1 \\ Y_2 \\ Y_3 \\ Y_4 \\ \\ Y_i \\ \\ Y_{n-4} \\ Y_{n-3} \\ Y_{n-2} \\ Y_{n-1} \end{matrix}$	$=$	$\begin{matrix} 0 \\ 0 \\ 0 \\ 0 \\ \\ 0 \\ 0 \\ 0 \\ 0 \\ c_1 * Y_n \end{matrix}$
$i-1 \quad i \quad i+1$				
Models:				
1. Linear	$n-5 \quad n-4 \quad n-3$	Y_{n-4}	$=$	0
2. Anisotropic	$n-4 \quad n-3 \quad n-2$	Y_{n-3}	$=$	0
3. Nonlinear Anisot'c	$n-3 \quad n-2 \quad n-1$	Y_{n-2}	$=$	0
4. Others	$n-2 \quad n-1$	Y_{n-1}	$=$	$c_1 * Y_n$

Figure 59b
5 POINT WOUND ROLL EQUATION SYSTEM

$\begin{matrix} 1 & 2 & 3 \\ 1 & 2 & 3 & 4 \\ 1 & 2 & 3 & 4 & 5 \\ & 2 & 3 & 4 & 5 & 6 \end{matrix}$	<p>Solution for a n wrap roll in terms of:</p> <ol style="list-style-type: none"> 1. Stresses 2. Strains 3. Displacements 	$\begin{matrix} Y_1 \\ Y_2 \\ Y_3 \\ Y_4 \\ \\ Y_i \\ \\ Y_{n-4} \\ Y_{n-3} \\ Y_{n-2} \\ Y_{n-1} \end{matrix}$	$=$	$\begin{matrix} 0 \\ 0 \\ 0 \\ 0 \\ \\ 0 \\ 0 \\ 0 \\ 0 \\ c_2 * Y_n \\ c_1 * Y_n \end{matrix}$
$i-2 \quad i-1 \quad i \quad i+1 \quad i+2$				
Models:				
1. Linear	$n-6 \quad n-5 \quad n-4 \quad n-3 \quad n-2$	Y_{n-4}	$=$	0
2. Anisotropic	$-5 \quad n-4 \quad n-3 \quad n-2 \quad n-1$	Y_{n-3}	$=$	0
3. Nonlinear Anisot'c	$n-4 \quad n-3 \quad n-2 \quad n-1$	Y_{n-2}	$=$	$c_2 * Y_n$
4. Others	$n-3 \quad n-2 \quad n-1$	Y_{n-1}	$=$	$c_1 * Y_n$

Equation (137) gives the coefficients of three of the eight distinct terms used in the 3 point matrix system, while the five point approximation has 20 distinct terms. Additionally, the terms are dependent on the formulation so that a set must be generated for both the displacement and radial stress formulation. Though these derivations are not particularly difficult, they can be somewhat lengthy. Therefore, all derivations for the finite difference approximations were performed using a symbolic math package, Mathematica by Wolfram Research, running on the Macintosh II. Additionally, Mathematica can convert resulting equations into code for the C and Fortran computer languages, so that computer code generation is automated, accurate, and expedient. Tables 8 give the coefficients for the 3 and 5 point formulations of both the displacement and radial stress formulation.

Notice that the coefficients are nearly identical except for near the core. This is the result of the fact that the structure of both differential equations are identical, only the A and B coefficients are different and are found in equations (131) and (63) respectively for the displacement and radial stress formulations. However, the core boundary condition also depends on formulation, hence the difference for the finite difference approximations on the first few layers. In the derivation of the coefficients of Tables 8, the matrix solution does not solve directly for the core displacement or radial stress and must be calculated as a subsequent step. The justification for this approach is simply to keep the numbering of matrix rows and web layers the same without using a zero row pointer which is not supported by some computer languages. However, one could just as easily have the core displacements come directly from the matrix solution by merely rearranging the equations slightly.

Once the matrix coefficients have been determined, they must be coded into a computer program which calculates the values of the A and B coefficients (which are not constants in the case of nonlinear moduli), then calculates and assembles the matrix coefficients into memory, and finally solves for the unknown solution vector of either incremental displacements or radial stresses. This incremental solution must be embedded into a loop which iterates for the winding from the bare core to the finish diameter of the roll. Accumulated current stresses are calculated simply as the superposition of the previous stress state plus the incremental stresses calculated from the current solution iteration.

Table 8a
MATRIX COEFFICIENTS - 3 PT DISPLACEMENT FORMULATION

<u>Row</u>	<u>Col</u>	<u>Expression</u>
1	1	$(b \cdot \text{core} \cdot h^2 + 2 \cdot a \cdot h \cdot r - 4 \cdot r^2 - 2 \cdot \text{core} \cdot r^2) / (\text{core} \cdot h^2)$
1	2	$(-(a \cdot h \cdot r) + a \cdot \text{core} \cdot h \cdot r + 2 \cdot r^2 + 2 \cdot \text{core} \cdot r^2) / (2 \cdot \text{core} \cdot h^2)$
i	i-1	$(r \cdot (-(a \cdot h) + 2 \cdot r)) / (2 \cdot h^2)$
i	i	$b - (2 \cdot r^2) / h^2$
i	i+1	$(r \cdot (a \cdot h + 2 \cdot r)) / (2 \cdot h^2)$
n-1	n-2	$(r \cdot (-(a \cdot h) + 2 \cdot r)) / (2 \cdot h^2)$
n-1	n-1	$b - (2 \cdot r^2) / h^2$
		$c1 = -(r \cdot (a \cdot h + 2 \cdot r)) / (2 \cdot h^2)$
		$\text{core} = (-2 \cdot \text{ec} \cdot h - 3 \cdot \text{er} \cdot r_0 + 2 \cdot \text{er} \cdot h \cdot \text{ut} + 2 \cdot \text{ec} \cdot h \cdot \text{ur} \cdot \text{ut}) / (r_0 \cdot \text{er})$
		$w_0 = (-4 \cdot w_1 + w_2) / \text{core}$

Table 8b
MATRIX COEFFICIENTS - 5 PT DISPLACEMENT FORMULATION

<u>Row</u>	<u>Col</u>	<u>Expression</u>
1	1	$(6 \cdot b \cdot \text{core} \cdot h^2 - 2 \cdot a \cdot h \cdot r - 3 \cdot a \cdot \text{core} \cdot h \cdot r + 6 \cdot r^2 - 12 \cdot \text{core} \cdot r^2) / (6 \cdot \text{core} \cdot h^2)$
1	2	$(r \cdot (a \cdot h + 6 \cdot a \cdot \text{core} \cdot h - 3 \cdot r + 6 \cdot \text{core} \cdot r)) / (6 \cdot \text{core} \cdot h^2)$
1	3	$(r \cdot (-2 \cdot a \cdot h - 9 \cdot a \cdot \text{core} \cdot h + 6 \cdot r)) / (54 \cdot \text{core} \cdot h^2)$
2	1	$(r \cdot (-(a \cdot h) + 3 \cdot r)) / (3 \cdot h^2)$
2	2	$b - (a \cdot r) / (2 \cdot h) - (2 \cdot r^2) / h^2$
2	3	$(r \cdot (a \cdot h + r)) / h^2$
2	4	$-(a \cdot r) / (6 \cdot h)$
i	i-2	$-(r \cdot (-(a \cdot h) + r)) / (12 \cdot h^2)$
i	i-1	$(2 \cdot r \cdot (-(a \cdot h) + 2 \cdot r)) / (3 \cdot h^2)$
i	i	$b - (5 \cdot r^2) / (2 \cdot h^2)$
i	i+1	$(2 \cdot r \cdot (a \cdot h + 2 \cdot r)) / (3 \cdot h^2)$
i	i+2	$-(r \cdot (a \cdot h + r)) / (12 \cdot h^2)$
n-2	n-4	$-(r \cdot (-(a \cdot h) + r)) / (12 \cdot h^2)$
n-2	n-3	$(2 \cdot r \cdot (-(a \cdot h) + 2 \cdot r)) / (3 \cdot h^2)$
n-2	n-2	$b - (5 \cdot r^2) / (2 \cdot h^2)$
n-2	n-1	$(2 \cdot r \cdot (a \cdot h + 2 \cdot r)) / (3 \cdot h^2)$
n-1	n-3	$(a \cdot r) / (6 \cdot h)$
n-1	n-2	$(r \cdot (-(a \cdot h) + r)) / h^2$
n-1	n-1	$b + (a \cdot r) / (2 \cdot h) - (2 \cdot r^2) / h^2$
		$c2 = (r \cdot (a \cdot h + r)) / (12 \cdot h^2)$
		$c1 = -(r \cdot (a \cdot h + 3 \cdot r)) / (3 \cdot h^2)$
		$\text{core} = (6 \cdot \text{ec} \cdot h(1 - \text{ur} \cdot \text{ut}) + 11 \cdot \text{er} \cdot r_0 \cdot \text{er} \cdot h \cdot \text{ut}) / (18 \cdot \text{er} \cdot r_0)$
		$w_0 = (w_1 - w_2 / 2 + w_3 / 9) / \text{core}$

Table 8c
MATRIX COEFFICIENTS - 3 PT RADIAL STRESS FORMULATION

<u>Row</u>	<u>Col</u>	<u>Expression</u>
1	1	$(b \cdot h^2 + 2 \cdot a \cdot \text{core} \cdot h \cdot r - 2 \cdot r^2 - 4 \cdot \text{core} \cdot r^2) / h^2$
1	2	$(a \cdot h \cdot r - a \cdot \text{core} \cdot h \cdot r + 2 \cdot r^2 + 2 \cdot \text{core} \cdot r^2) / (2 \cdot h^2)$
i	i-1	$(r \cdot (-(a \cdot h) + 2 \cdot r)) / (2 \cdot h^2)$
i	i	$b - (2 \cdot r^2) / h^2$
i	i+1	$(r \cdot (a \cdot h + 2 \cdot r)) / (2 \cdot h^2)$
n-1	n-2	$(r \cdot (-(a \cdot h) + 2 \cdot r)) / (2 \cdot h^2)$
n-1	n-1	$b - (2 \cdot r^2) / h^2$ $c1 = -(r \cdot (a \cdot h + 2 \cdot r)) / (2 \cdot h^2)$ $\text{core} = \text{ec} \cdot \text{er} \cdot r0 / (2 \cdot \text{ec} \cdot \text{er} \cdot h - 2 \cdot \text{er} \cdot \text{et} \cdot h - 3 \cdot \text{ec} \cdot \text{er} \cdot r0 - 2 \cdot \text{ec} \cdot \text{et} \cdot h \cdot \text{ur})$ $\text{sr0} = \text{core} \cdot (-4 \cdot \text{sr1} + \text{sr2})$

Table 8d
MATRIX COEFFICIENTS - 5 PT RADIAL STRESS FORMULATION

<u>Row</u>	<u>Col</u>	<u>Expression</u>
1	1	$b - (a \cdot r) / (2 \cdot h) + (6 \cdot a \cdot \text{core} \cdot r) / h - (2 \cdot r^2) / h^2 - (18 \cdot \text{core} \cdot r^2) / h^2$
1	2	$(r \cdot (a \cdot h - 3 \cdot a \cdot \text{core} \cdot h + r + 9 \cdot \text{core} \cdot r)) / h^2$
1	3	$-(r \cdot (a \cdot h - 4 \cdot a \cdot \text{core} \cdot h + 12 \cdot \text{core} \cdot r)) / (6 \cdot h^2)$
2	1	$(r \cdot (-(a \cdot h) + 3 \cdot r)) / (3 \cdot h^2)$
2	2	$b - (a \cdot r) / (2 \cdot h) - (2 \cdot r^2) / h^2$
2	3	$(r \cdot (a \cdot h + r)) / h^2$
2	4	$-(a \cdot r) / (6 \cdot h)$
i	i-2	$-(r \cdot (-(a \cdot h) + r)) / (12 \cdot h^2)$
i	i-1	$(2 \cdot r \cdot (-(a \cdot h) + 2 \cdot r)) / (3 \cdot h^2)$
i	i	$b - (5 \cdot r^2) / (2 \cdot h^2)$
i	i+1	$(2 \cdot r \cdot (a \cdot h + 2 \cdot r)) / (3 \cdot h^2)$
i	i+2	$-(r \cdot (a \cdot h + r)) / (12 \cdot h^2)$
n-2	n-4	$-(r \cdot (-(a \cdot h) + r)) / (12 \cdot h^2)$
n-2	n-3	$(2 \cdot r \cdot (-(a \cdot h) + 2 \cdot r)) / (3 \cdot h^2)$
n-2	n-2	$b - (5 \cdot r^2) / (2 \cdot h^2)$
n-2	n-1	$(2 \cdot r \cdot (a \cdot h + 2 \cdot r)) / (3 \cdot h^2)$
n-1	n-3	$(a \cdot r) / (6 \cdot h)$
n-1	n-2	$(r \cdot (-(a \cdot h) + r)) / h^2$
n-1	n-1	$b + (a \cdot r) / (2 \cdot h) - (2 \cdot r^2) / h^2$ $c2 = (r \cdot (a \cdot h + r)) / (12 \cdot h^2)$ $c1 = (r \cdot (a \cdot h + 3 \cdot r)) / (3 \cdot h^2) \cdot \text{sr}[z]$ $\text{core} = (\text{ec} \cdot \text{er} \cdot r) / (6 \cdot \text{ec} \cdot \text{er} \cdot h - 6 \cdot \text{er} \cdot \text{et} \cdot h - 11 \cdot \text{ec} \cdot \text{er} \cdot r - 6 \cdot \text{ec} \cdot \text{et} \cdot h \cdot \text{ur})$ $\text{sr0} = \text{core} \cdot (-18 \cdot \text{sr1} + 9 \cdot \text{sr2} - 2 \cdot \text{sr3})$

Though this outlines the essences of the solution technique, there are several caveats to be aware of. First, the A and B coefficients are not constants that can be calculated once at the beginning of the program if any of the material properties vary with radius. For example, with nonlinear radial moduli the coefficients must be calculated on an individual basis every time they are used based on the current accumulated radial stress at any particular radial location. Furthermore, calculation of the coefficients is based on the previous stress state, and applied for calculating the current stress state. Using old data in new calculations is inherent in many finite difference formulations and does not usually pose a problem if the mesh is fine enough. However, the A and B coefficients given by (131) and (63) contain an anisotropy ratio E_T/E_R which can result in a division by zero error for the roll outside where $\sigma_R = 0$ if the radial moduli curvefit yields a zero stiffness at a zero pressure.

Secondly to save memory, only the nonzero banded coefficients of the square A matrix are stored in memory, so that careful bookkeeping is required. Thirdly, because of the fine mesh often required for high anisotropies to maintain solution accuracy and the iterative nature of winding solutions, great care must be taken to optimize the matrix solution technique. Though Willett and Poesch claimed that the A matrix is symmetric [186] which gives a faster solution, this is definitely not the case as seen in the coefficients of Table 8. A fast solution technique for the 3 point approximation is the Tridiagonal algorithm, and for the 5 point approximation is a modified Gauss routine which only solves in the banded nonzero portion of the equation system.

Fourthly, the differential solution is embedded in a general loop which can only be started from the 4th wrap addition for the 3 point approximation and the 6th wrap addition for the 5 point approximation. Therefore, the accumulated stresses must be calculated for the first few wraps which do not fit into the general equation structure shown in Figures 59. There are a couple of approaches that could be used to address this problem. First, a closed form expression could be derived for the stresses for each of the first few wraps. However, this expression would be extremely unwieldy, especially for the 5 point approximation. A simpler approach is to estimate the accumulated stresses for the first few wraps, then go into the main solution loop, and finally correct the stress state on the first wraps by high order extrapolation from wraps immediately above. In any case, the first few wraps should not have a significant effect on the final roll solution which is composed of thousands of wraps.

Fifthly, tangential stresses can be calculated from the equilibrium equation and radial stresses using either incremental values and superposition, or at the very end after the final radial stress state is determined. For the traditional winding models, there is no need for tangential stress information until the end. Consequently, it is preferable to avoid accumulated error incurred by solving the equilibrium equation for every wrap by rather calculating tangential stresses only once at the end of the solution. However, tangential stresses are required for the Displacement and Extended Hakiel displacement to stress models, as tangential stress effects radial displacement through the Poisson ratio. Therefore, incremental tangential stresses must be calculated for every wrap for the purposes of displacement field calculations only. However, the final tangential stress state is not calculated from the superposition of these incremental stresses, but rather from the final radial stress state and the equilibrium equation.

Finally, it is very important in all finite difference approximations to check whether the grid is fine enough so that a specified level of accuracy is obtained. As seen in Figures 19 of Chapter 2, Hakiel's model can be sensitive to grid size. This is even more so for the more complicated displacement to stress models as we will see in the next and other sections.

On every iteration of the Displacement Formulation, the displacement field for every wrap in the current roll is solved. However, this displacement field must be used to calculate the more useful incremental radial and tangential stresses, and in particular the WIS at the current outer layer. The incremental radial stress and tangential stress equations can be derived from a simultaneous solution of the stress-strain (7, 8) and strain-displacement equations (4, 6) as

$$(139a) \quad \sigma_R = \frac{E_R \left(r \frac{dw}{dr} + \mu_T w \right)}{r (1 - \mu_R \mu_T)}$$

$$(139b) \quad \sigma_T = \frac{E_T \left(\mu_R r \frac{dw}{dr} + w \right)}{r (1 - \mu_R \mu_T)}$$

where the derivative of the displacement field is calculated as a 3 point or 5 point central difference for intermediate layers, and as a forward difference for the core layers, and as a backward difference for the outer layers as given by the formulas in Tables 7. Finally, the WIS is calculated from the radial stress under the outer layer and the boundary condition (28a) as

$$(139c) \quad \text{WIS}_{r=r_n} = r_n \sigma_{R, r=r_n}$$

In summary, the finite difference approximation and matrix solution technique can be used to solve a wide variety of problems including all formulations of winding models. The coefficients of the matrix terms result from the finite difference approximation to the derivatives in the winding differential equation which are assembled, multiplied out and collected upon like radial locations. Though higher order approximations are generally most efficient for solving many problems, the winding differential equations seem to be best solved using 3 point approximations. The resulting matrix system is solved for all wraps in the current roll yielding incremental stresses, strains or displacements. Finally, the solution is repeated for all wrap additions from the core to the finish diameter and total accumulated values can be calculated either from superposition of incremental results or as a final step.

However, there are many caveats that must be kept in mind for a robust and efficient solution. Additionally, radial displacement to stress formulations require solution steps beyond that of traditional winding models. In particular, the Displacement Formulation requires radial and tangential stresses as well as WIS to be calculated from the displacement field. In the next section, the Displacement Formulation will be evaluated for accuracy and sensitivity using simulated displacement data.

Simulating Displacement Data for Model Evaluation

Once a displacement to stress winding model has been computer coded, it must be tested for accuracy and sensitivity. Conventionally, this would be done by taking on-line measurements as inputs to stress calculation routines and then verifying the output by independent measurements using some other technique. Although this can and will be done, this would entail the simultaneously debugging of both the data acquisition and the winding model portion of this complex system. A surer approach would be to first debug these components separately, then as a system. The check for proper operation of the data acquisition hardware was already performed by verifying that the proper rewinding roll diameters are displayed. Then the Radial Compression, which is closely related to the boundary condition driving the winding model, is calculated to demonstrate sensitivity to roll structure changes as well as insensitivity to measurement noise.

However, to check the proper behavior of the displacement to stress model would require a 'perfect' input data set, so that any resulting problems would belong strictly to the model rather than the input. Since real measured data is flawed, and especially so for the noisy environment of winding nonuniform webs, another approach is needed. The solution to this dilemma is to create a near perfect but artificial set of displacement data using extensions to already existing winding model.

A schematic of a method developed to calculate a radial displacement data set which is used to evaluate the displacement-to-stress models is shown in Figure 60. Data simulation begins by picking a set of input parameters to as inputs to one of the conventional winding models. Then, the stress-strain and strain-displacement relations are used to calculate the incremental radial strains on each layer. The incremental displacements, which is equal to radial strain multiplied by thickness, for each layer is summed to give a radial displacement at the roll's outer surface. Additionally, the core deflection must also be calculated and added to the layer deformation.

The equations used to extend the conventional winding models to calculate displacements come very simply from the constitutive equations for winding. The incremental deformation of a single layer can be calculated simply from the radial stress-strain relation (7) and the definition of strain as

$$(140) \quad \Delta w_i = h \epsilon_{R,i} = h \left(\frac{\sigma_{R,i}}{E_{R,i}} - \mu_T \frac{\sigma_{T,i}}{E_{T,i}} \right)$$

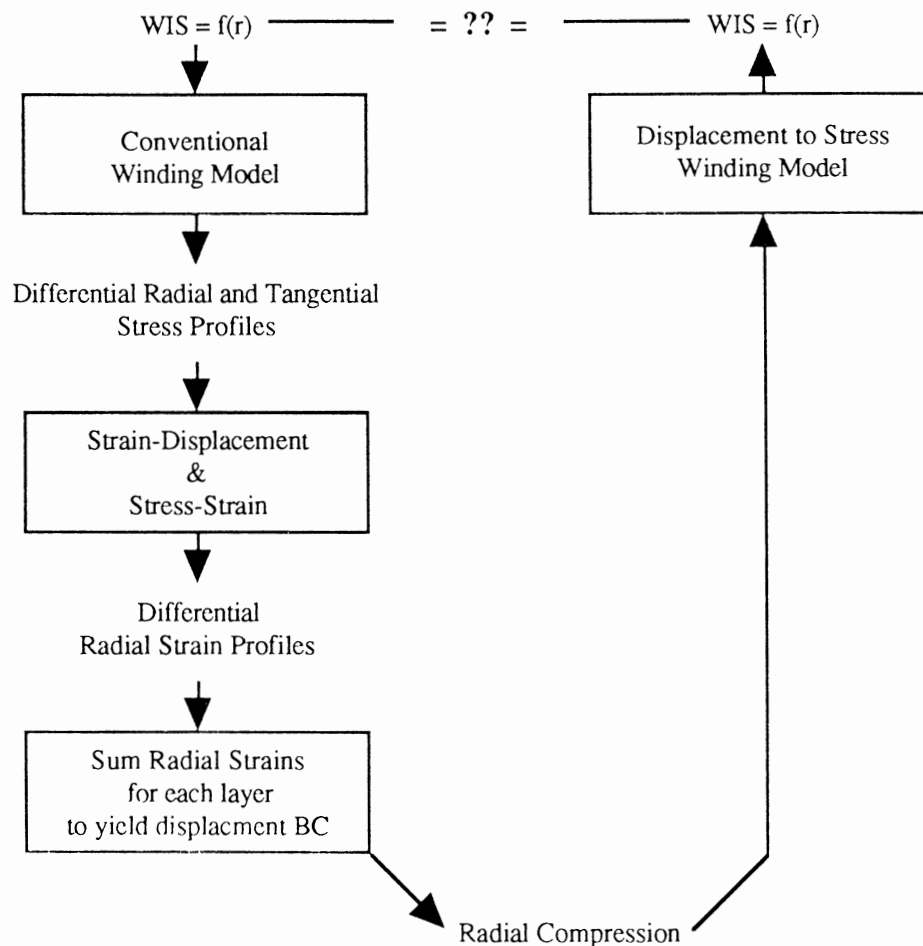
The core deflection is calculated directly from a rearrangement of the core stiffness definition (16) as

$$(141) \quad w_0 = \frac{r_0 \sigma_{R,0}}{E_c}$$

Finally, the total deformation at the outer surface of the roll is simply the sum of the individual layer deformations plus the core deformation

$$(142) \quad w_n = \frac{r_0 \sigma_{R,0}}{E_c} + \sum_{i=1}^n h \left(\frac{\sigma_{R,i}}{E_{R,i}} - \mu_T \frac{\sigma_{T,i}}{E_{T,i}} \right)$$

Figure 60
DISPLACEMENT DATA SIMULATION
TO CHECK STRESS MODEL



This displacement data set, which is an output of extensions to conventional winding models, is then used as inputs for the new displacement-to-stress models. The WIS calculated by the new models, using the same geometry and material properties, should be equal to the WIS originally input into the conventional winding model. If this WIS as a function of radius agreement holds for several widely varying test cases, then one can be reasonably confident that not only is the new model consistent and correct, but also the conventional model as well. Even the smallest of errors in the long serial chain would cause a difference between input and calculated WIS profiles. Thus, the new models can be debugged and screened for proper operation before subjecting them to the uncertainties of real data from a new measurement technique.

The input parameter sets, given in Appendix B, used to test conventional winding models were also used to evaluate the displacement-to-stress models. As seen in Figure 61a, the total error accumulated by all the serial calculations were less than 1% for most of the radius range for three of the input sets. This is well within most engineering requirements and lends confidence that the algorithms are correct. This is especially so because the LAT case is one in which all input parameters are nonzero and different, and the WIS profile is nonlinear. However as seen in Figure 61b, a moderately anisotropic input set requires a small grid size even for the 5 point derivative used here. Though a 3 point derivative requires about an order of magnitude smaller grid size, the net computing time was similar, and in both cases was much longer than calculating a conventional winding model with the same input parameters.

Next, nonlinear radial moduli test cases were run. At first there was not the expected agreement between input and calculated WIS. After considerable searching this was traced back to the missing high order terms given in equations (131). Then agreement to engineering accuracy was obtained, but only for the low anisotropy ratio of 20 corresponding to the NAT case. Additionally, the calculation time for this case exceeded one day for a fast PC based engineering workstation. Thus, the much greater calculation time required to obtain a reasonable accuracy for the high anisotropy ratio of 30,000 for the real data obtained on the soft NC paper was deemed impractical.

The qualitative explanation for the numerical convergence difficulties of the Displacement Formulation could be as follows. First, the higher order terms in the displacement formulation are significant for nonlinear radial moduli, and dominant for some input cases. Thus, the coefficients of the displacement differential equation contains numerical derivative calculations, and with it an expected propensity for numerical error. Secondly, the displacement field has a greater gradient than the radial stress field of conventional winding models causing the matrix system of equations to be even more ill-conditioned and thus prone to numerical roundoff errors. Finally, the displacement to stress calculations contain yet another numerical derivative that must be calculated.

In summary, the Displacement Formulation is mathematically consistent with other winding models and is verified with simulated displacement data to yield WIS values within engineering accuracy for 5 of the 6 input test cases. However, the formulation contains calculations that are far more numerically unstable than conventional winding models. Thus while the model is rigorous, it may not have practical application because of the extremely long computation time required for nonlinear and/or highly anisotropic properties that characterize most real web materials. Thus, the Extended Hakiel Formulation given in the next section was developed, so that stresses could be calculated more practically.

Figure 61a

WIS ERROR - DISPLACEMENT FORMULATION

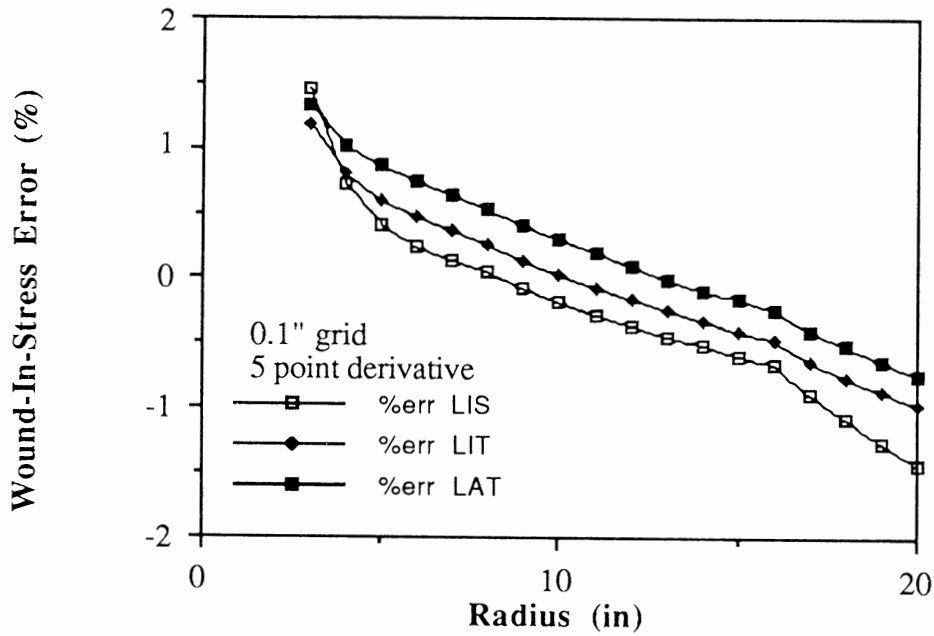
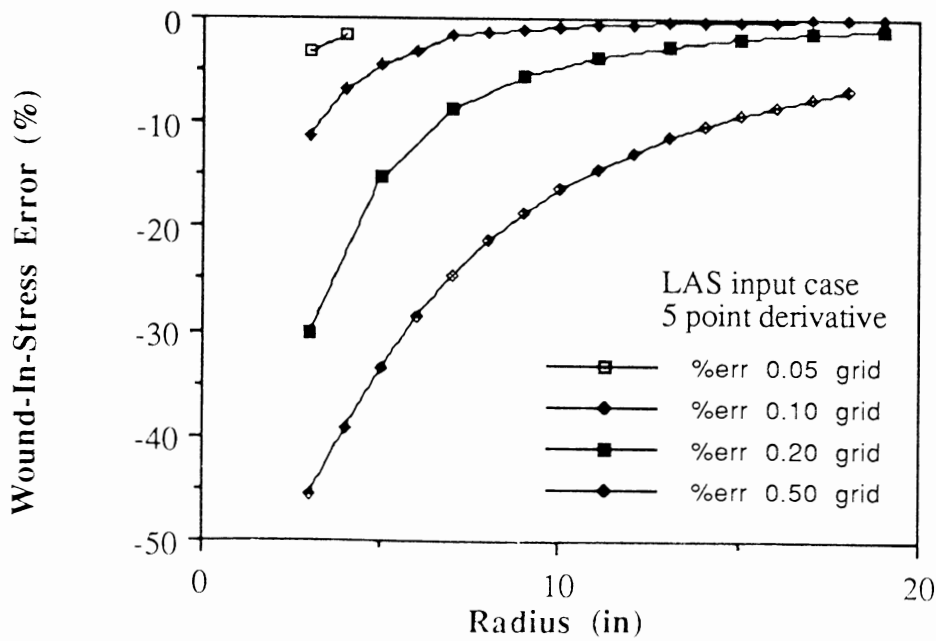


Figure 61b

WIS ERROR - DISPLACEMENT FORMULATION



Extended Hakiel Formulation

Since the more straightforward Displacement Formulation was not able to compute highly nonlinear or anisotropic data in a practical amount of time, another approach was needed. Since Hakiel's model [132, 133] is currently the most general and has been subjected to numerous analytically and experimental verifications, it was chosen as the foundation for an alternative displacement to WIS model. However, it needed to be extended considerably from its origins in order to give the more complete solution required by this new approach. First, radial strains and deformations would need to be calculated, so that the measured deformation at the outer boundary could be used. Secondly, the solution steps needed reordering, so that instead of WIS being an input to the model as in Hakiel's work, it would be the output of this new approach.

The solution to computing the deformation at the outer boundary is not difficult as the incremental radial and tangential stresses can be used to calculate radial strains at each layer with the help of the radial stress-strain relations (7). Then the change in thickness for each layer can be calculated from the radial strains and the wrap thickness. Finally, the deformation at the outer surface is the sum of the change of thicknesses of each layer in the roll plus the core deflection. The astute reader will recognize this as precisely the same method used to simulate displacement data given in a previous section. Thus, the incremental deformation at the outer roll surface due to the addition of a single wrap given by equation (142) is repeated here as

$$(143) \quad w_n = \frac{r_0 \sigma_{R,0}}{E_c} + \sum_{i=1}^n h \left(\frac{\sigma_{R,i}}{E_{R,i}} - \mu_T \frac{\sigma_{T,i}}{E_{T,i}} \right)$$

The solution to reordering the formulation so that WIS becomes an output instead of an input is also not difficult. We recognize that though the moduli may be nonlinear and the accretive nature of winding is very nonlinear, the solution of all traditional winding models is linear within a single solution step for the addition of a single wrap [132, 133]. This can be seen from the matrix system of equations resulting from the finite difference approximation. For example, given

$$\begin{aligned} & [A] \{x\} = \{B\} \\ \text{then} & \quad [A] \{x'\} = \{B'\} \\ \text{if} & \quad B'_i = c B_i \quad \text{and} \quad x'_i = c x_i \quad \text{for all } i \end{aligned}$$

In other words, doubling the WIS forcing function contained in $\{\mathbf{B}\}$ will double the incremental radial stresses $\{\mathbf{x}\}$. Thus, the incremental radial stresses are proportional to the WIS. In fact, all stresses, strains and displacements are similarly proportional to WIS because the constitutive equations are also linear. However, there are two cautions to bear in mind. First, though incremental linearity is exactly true for constant moduli, linearity is approached for nonlinear moduli only if the incremental stresses are much smaller than the accumulated stresses so the coefficients of the $[\mathbf{A}]$ matrix do not change significantly from one wrap to the next. This will be the case if the mesh is made sufficiently small. This assumption is also shared by Hakiel's solution technique [132, 133] but can be mitigated by using an iterative solution technique such as SOR used by Willet and Poesch [186]. Secondly, accumulated linearity is only true for constant moduli [132, 133].

This proportionality between stresses, strains and displacements as a function of WIS can then be used to reorder the WIS from an input to an output as follows. First, a WIS is assumed. Next, the displacement at the outer surface, $w_{n,\text{calculated}}$ is calculated from an extension of Hakiel's (or any other legitimate winding model) as indicated in the schematic of Figure 55. Finally, all stresses, strains and displacements are corrected using the proportional linearity property of the incremental solution given the calculated and measured displacements. Thus for example,

$$(144) \quad \text{WIS}_{\text{actual}} = \text{WIS}_{\text{assumed}} \left[\frac{w_{n,\text{measured}}}{w_{n,\text{calculated}}} \right]$$

An outline of the solution steps for the Extended Hakiel model, whose code is given in Appendix C, is as follows.

```

initialize program
read displacement data from disk file,  $w_{n,\text{measured}}$  calculated from (118)
approximate solution for first 3 layers (for 3 pt derivative)
loop from layer 4 to finish radius of roll
    assume a WIS based on the previously calculated WIS
    calculate incremental radial stresses from Hakiel's model
    calculate incremental tangential stresses from equilibrium equation (2)
    calculate and sum displacements to give  $w_{n,\text{calculated}}$  from (142)
    correct incremental radial, tangential and WIS stresses by (144)
    accumulated stresses = previous stresses plus incremental stresses
end main loop
recalculate accumulated tangential stresses from equilibrium equation (2)
print and save the solution

```

Accelerating the Solution

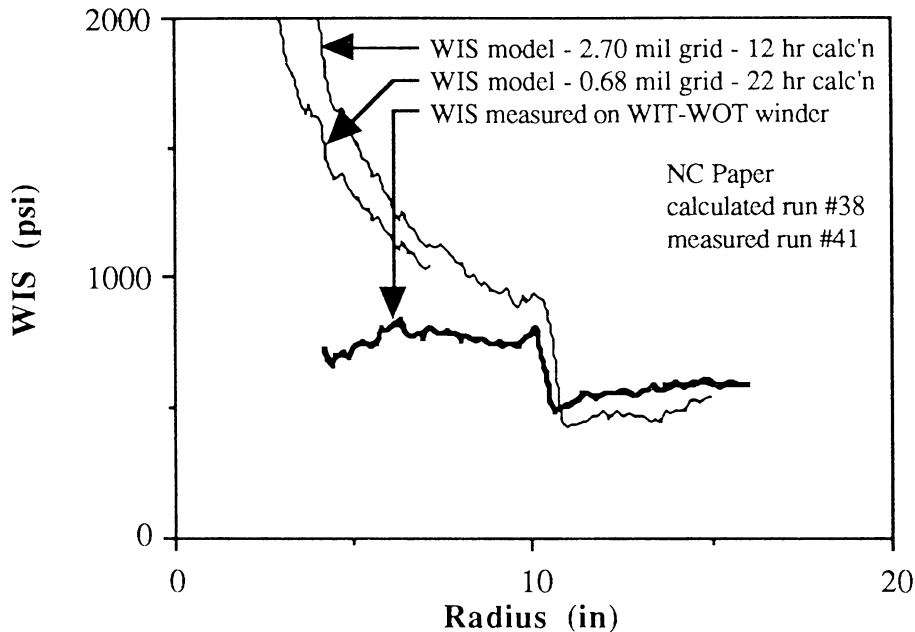
Before applying the Extended Hakiel Formulation to a real data set, a couple of pre-checks should be made. First, the Extended Hakiel Formulation was checked using several simulated data sets as indicated in Figure 60. The results were very uninteresting as the stress agreement was generally better than 4 digits. However, this check is not as useful for the Extended Hakiel Formulation as it was for the Displacement Formulation. This is because while the data simulation and Displacement Formulation are very different and independent by nature, the data simulation and the Extended Hakiel Formulation share a highly parallel development. However, it does give confidence to proceed as the data simulation using either extensions of Altmann's or Hakiel's models checked using either the Displacement or Extended Hakiel Formulations.

Secondly, Hakiel's original (or any other equivalent traditional) winding model should be used to roughly estimate the mesh size required for maximum solution accuracy. As cautioned by Figures 18 and 19 as well as many other places elsewhere in this text, all runs of winding models should be checked for convergence as a function of varying mesh size. If the mesh is made too coarse the accuracy will suffer. Conversely, if the mesh is made too fine numerical instability can result. The optimum mesh size and resulting accuracy depends upon many factors such as the order of derivative approximation, the independent variable chosen for the winding differential equation, and the anisotropy ratio. As the anisotropy ratio increases, the optimum mesh size decreases which results in lengthy solution times.

Since the most disabling feature of the Displacement Formulation was the inability to compute highly nonlinear and anisotropic cases in a reasonable time, the most difficult of the real winding data cases was tackled first. The NC paper had an incredibly high anisotropy ratio at a near zero interlayer pressure of $E_T/E_R|_{p=0} = 600,000/20$ or 30,000. Additionally, the NC paper also had a radial modulus that was also very nonlinear and varied from 20 psi at zero interlayer pressure to 1740 psi at 50 psi interlayer pressure.

Using the Extended Hakiel Formulation described in the previous section, the WIS calculated from the new model and density-like measurements was compared with WIS measured on the Beloit WIT-WOT winder and are shown in Figure 62. The comparison between the new model and measured results shows clearly that the new model does indeed predict stresses well for radii larger than 10 inches. Though there are differences between predicted and measured stresses, they are less than 15% for larger radii. The source of these differences is difficult to pinpoint but could be attributed to approximations in the model, errors in the WIT-WOT, material property uncertainty, or stress relaxation.

Figure 62
WIS FOR TENSION DROP - CALCULATED VS MEASURED



Additionally from Figure 62, we can see that the solution seems to require an even finer grid to converge to the proper stresses near the core. Unfortunately, the estimated computation time to even complete the 0.68 mil grid computations to the outside is about 100 hours. Though computing this highly nonlinear run would be out of the question for the Displacement Formulation, we are still faced with the difficulty of speeding up the solution of the Extended Hakiel Formulation, so that the fine meshes required for highly nonlinear systems can be computed in a practical amount of time.

Consequently, two techniques for solution acceleration were developed which can be applied not only to this model, but most other winding models as well. The first technique is based on the observation that the incremental stresses and strains become vanishingly small as a function of depth from the current roll surface. Thus rather than explicitly solving for all layers in the roll, only the outer layers that are sufficiently affected by wrap addition are modeled. Secondly, though meshes need to be fine to capture the high gradients, a complete solution is not needed for every layer addition because the effect of the addition of layer $n+1$ on a roll is very much like the addition of layer n . Thus, we can use the solution for layer n to approximate the effects of the next few layers without explicitly solving for them.

Justification for the first technique for solution acceleration based on explicitly solving only the outer region of a roll can be seen in Figure 63. As seen here, the incremental radial stresses are largest at the current roll outside and taper rapidly with depth. Additionally, the depth of significant incremental radial stress contribution is very dependent on the anisotropy ratio such that high ratios will result in a very small depth of influence. Since many web materials have anisotropy ratios between 1,000 and 10,000, one can see from the plot that the depth of significant influence is relatively small. Though it is difficult to see from the graphs, the significance at a 2" depth is in the 2nd and 8th digit respectively for the 1K and 10K anisotropy ratios. At a depth of 5", the significance is incredibly small and is in the 5th and 21st digit respectively for the 1K and 10K anisotropy ratios. At a depth of 18" and for a 10K anisotropy ratio, the significance is miniscule and occurs in the 155th digit! No wonder wound roll mathematics are so ill-conditioned. Thus, below a certain depth the incremental stresses become so small that explicit solutions in those depths is both wasteful and can contribute to numerical problems due to the orders of magnitude of difference of values across the matrix system.

Implementing the depth limited solution is quite simple. The solution begins as usual from the core until the current radius grows to more than the significant depth. Then, the solution only solves the outer (depth deep) layers with an approximate inner boundary condition. This approximate inner boundary condition is a core radius equal to the current radius minus the significant depth, and the core stiffness equal to the current radial modulus at the layer which is the significant depth below the current surface. The only difficulty is determining what the significant depth might be for nonlinear materials. An initial estimate can be made by varying the core stiffness from zero to infinity to see how far out it significantly influences the stresses. However, a more rigorous check is to perform sensitivity analysis on the significant depth as will be given in Chapter 10.

The depth limited solution is no different in principle as varying the grid size so that it is fine in areas of high gradients and values, and lower elsewhere. However, the depth limited solution is far more straight forward to implement. The advantages of the depth limited solution is tremendous as it reduces solution time from approximately the square of the number of grid points in the roll to proportional to the number of grid points in a roll. Thus for example, while halving mesh size will quadruple the solution time for conventional solutions, it will only double the solution time for the depth limited solution.

Figure 63
INCREMENTAL RADIAL STRESS VS DEPTH AND E_T/E_R

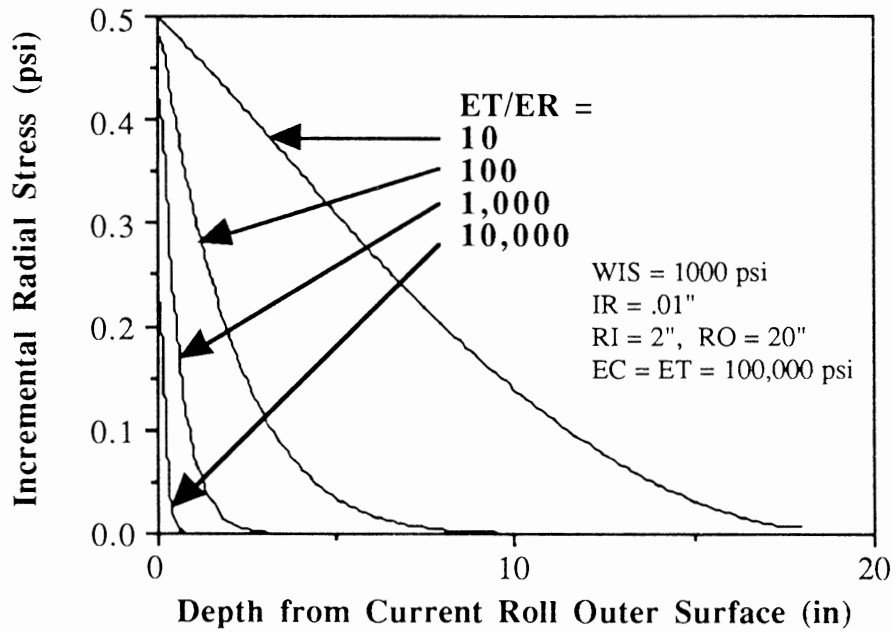
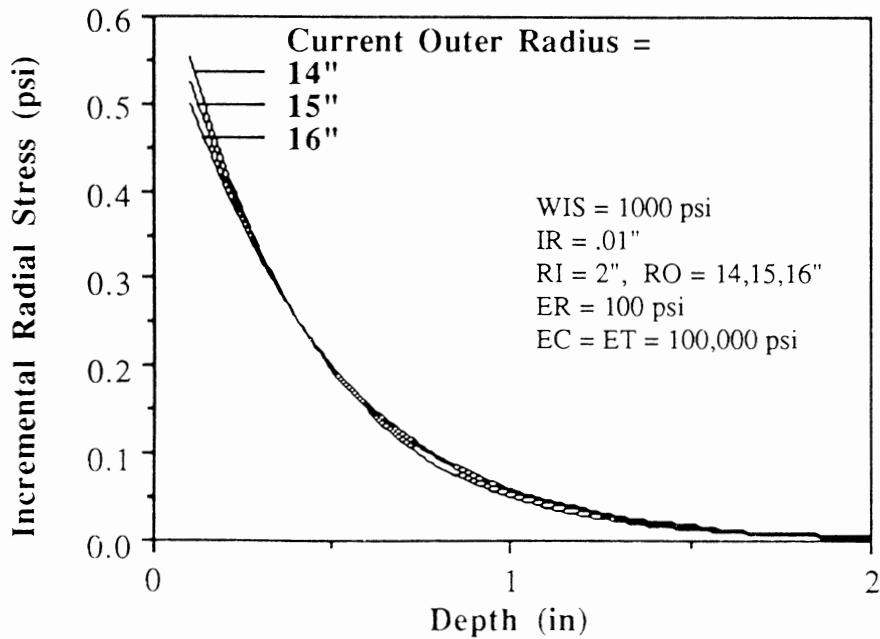


Figure 64
INCREMENTAL RADIAL STRESS VS DEPTH AND RADIUS



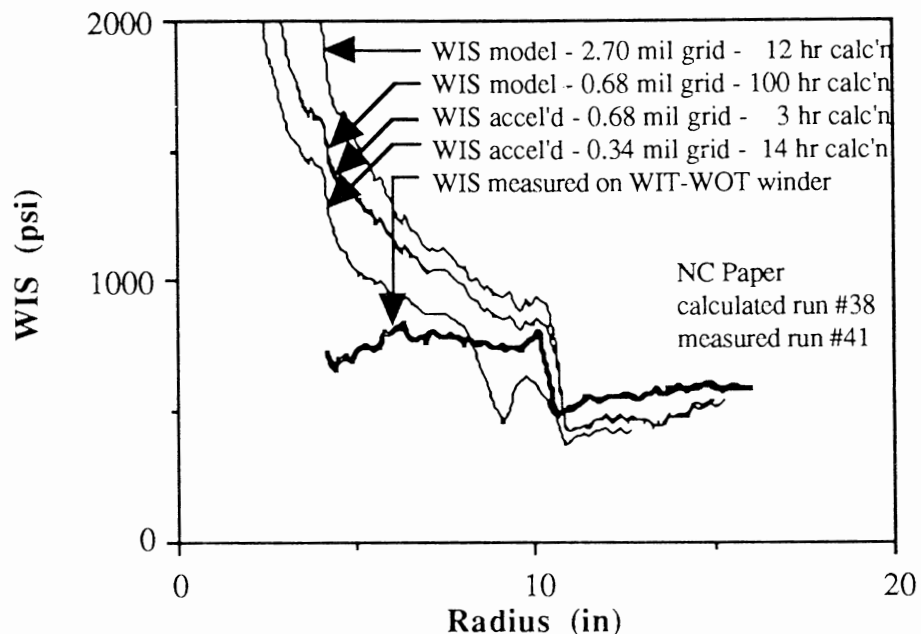
The second technique to accelerate solution times is based on the observation that the incremental radial stresses do not vary significantly as a function of current radius (or radius ratio) for small changes in current outer radius. As seen in Figure 64, the incremental radial stress distribution does not vary much for even current outer radii more than an inch apart if all other parameters are similar.

Thus for example, we can use the incremental radial stress explicit solution for 15.000" current radius to predict the solution for current radii of 15.001" and so on to perhaps 15.020". This is done simply by sliding the incremental solution outward one wrap for every wrap added, and then adding the incremental solution to the previous accumulated stresses to yield the current accumulated stresses. This is equivalent to using a coordinate system based on depth beneath the current outer surface and which follows it with wrap addition. This solution replication is repeated until the approximation errors become significant at which time an explicit solution is again required. As with the depth limited solution, the solution replication acceleration is not used until the roll diameter becomes sufficiently large. Again, sensitivity analysis is required for each set of input parameters to determine how many times the replication can be performed before solution accuracy is compromised. The advantages with replication are again tremendous because a conservative 20 times replication on a 0.001" grid spacing may reduce the solution time yet another order of magnitude beyond the improvements achieved by the depth limited solution acceleration.

Several aspects of the application of the depth limited and replication solution acceleration techniques are shown in Figure 65. First, all solutions converge to very closely to the WIT-WOT measured WIS for radii greater than 10". Secondly, WIS near the core converges in all solutions toward the measured WIS as the mesh becomes finer, indicating that the wraps near the core require yet even a finer mesh to converge. Thirdly, the conventional and accelerated solutions lie almost on top of each other indicating that the acceleration technique need not compromise accuracy. Fourthly, the savings in computer solution time are enormous. For a 0.34 mil grid, the accelerated solution computes in 14 hours where a conventional solution would require 770 hrs, or more than 50 times as long.

Despite the many orders of magnitude better solution response for the accelerated Extended Hakiel Formulation over the Displacement Formulation, some problems still exist. First, the solution at the 0.34 mil grid became temporarily unstable at a radii range of 8-10 inches. This corresponds to 7 hours into a calculation which is about 10,000 grid points above the core. Clearly this highly nonlinear and anisotropic case is presenting formidable numerical difficulties.

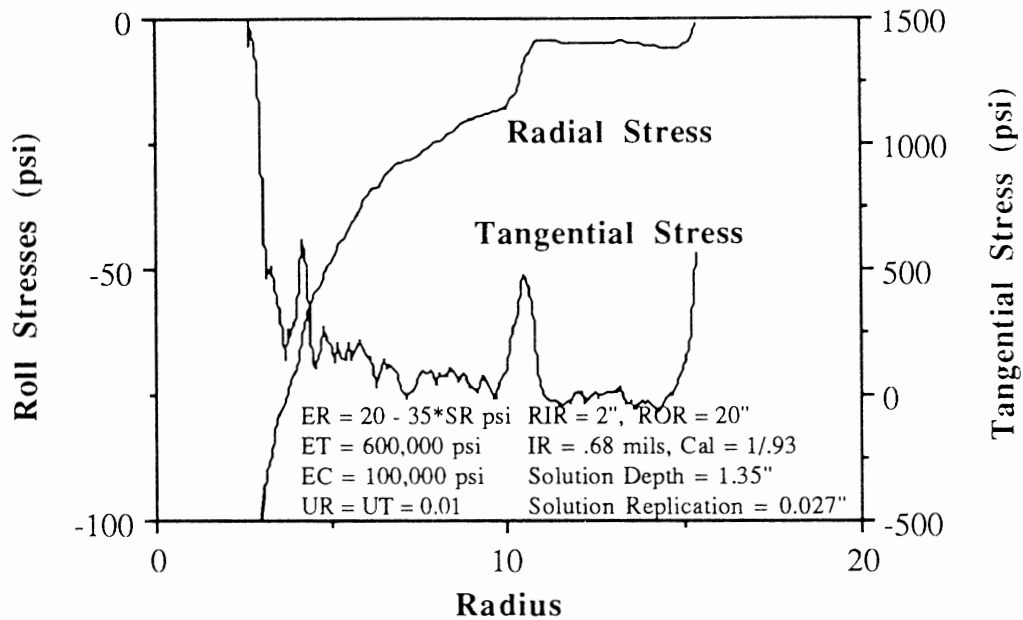
Figure 65
WIS - CONVENTIONAL AND ACCELERATED SOLUTIONS



Secondly, the WIS predicted by the model has considerable error near the core which might have arisen from several sources. First as mentioned several times, the grid should be even finer yet for this particular run, which would yield an undesirably long computation. Secondly, the real core stiffness is likely to be much lower than the theoretical. This results from the data acquisition instrumentation which was not able to take data immediately from the first wrap of the core, but rather useful data begins only after a few hundred wraps. Thus, the real core with many wraps of web is much softer than the theoretical bare core, which inflates the model's prediction of WIS. Finally and most importantly, and for reasons yet unknown, the density, radial compression (Figure 58) and WIS model reflect acquired data which begins at extremely high values. This characteristic is shared by all runs with the NC paper grade, but not with any of the other runs on other grades.

As mentioned previously, the new displacement to stress winding model is more complete than traditional winding models. As seen in Figure 66, the new model can predict body stresses just as traditional winding models. Though these stresses were not experimentally verified, they are realistic based on measurements on similar rolls, and result directly from Hakiel's model given the WIS predicted by the new model. Consequently, in addition to body stresses, the new model also predicts WIS, strains and displacements. In other words, the complete mechanics description of roll winding physics.

Figure 66
PREDICTED ROLL STRESSES - RUN #38



Additional Experimental Validation

In addition to the WIT-WOT experimental validation on the NC paper just described, validation for the other two grades tested will also be presented here. The next radially stiffer material tested was the LWC (lightweight coated magazine grade) paper. Figure 67a shows the WIS predicted on one run and compares with that predicted by Pfeiffer's classic WIS formula [166]. The agreement between the new model and the Pfeiffer empirical formula is remarkably close except near the start of the calculation run. Again though the body stresses were not measured, the stresses calculated from the new model and shown in Figure 67b are quite reasonable in that LWC is among the tightest wound of paper grades and may have interior interlayer radial pressures of 50-100 psi.

Figure 67a

WIS - CALCULATED VS PFEIFFER EQUATION

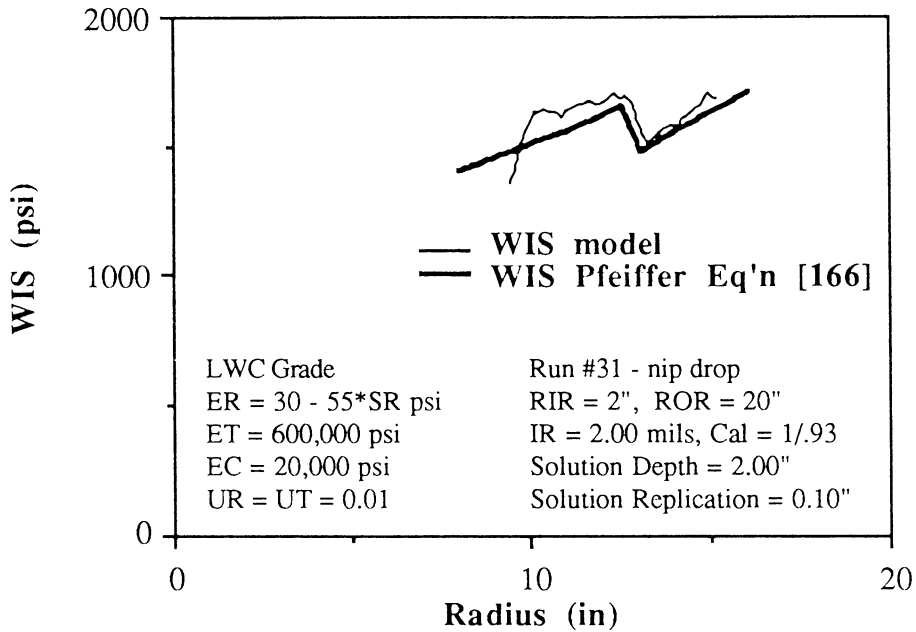
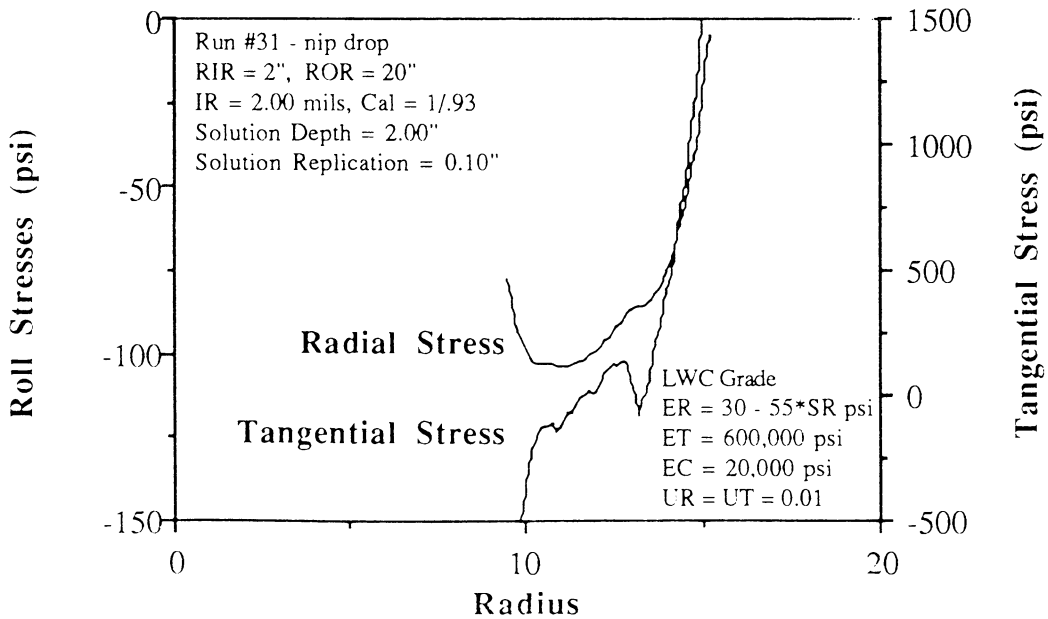


Figure 67b

PREDICTED ROLL STRESSES - RUN #31



Several other observations can be made from this run. First, note how the moderate change in WIS due to the nip drop at a 13" radius caused only a tiny change in radial stress (because it results from an integration) and a large change in tangential stress (because it results from a derivative). Second, note that the optimum mesh size for this material is coarser than the mesh size for the previous run whose material had a higher anisotropy ratio. This conclusion is consistent with all other finite difference formulations of wound roll models. Thirdly, some difficulty was experienced modeling this particular run which has an undesirably high sensitivity to the mesh size as will be shown in Chapter 10. Fourthly, this run illustrates starting the new displacement to stress model after considerable material has already been wound. This was necessitated by the fact that the initially high rotational speed of the rewind roll outran the data acquisition equipment until the roll had built to a 9" radius as described by equation (119). Thus, even though useful data was not obtained from the very start of winding, the new model still can be applied. The only additional difficulty is choosing an equivalent core stiffness for the beginning of the data which minimizes the size of the beginning tail. This equivalent core stiffness is approximately the radial modulus on the layer corresponding to the beginning data. Just as with starting the model at the core however, the calculation error is highest at the beginning where there are fewer grid points to represent the rapidly varying stress gradients.

The last experimental validation run presented here is for the stiffest material tested, which is the coated and calender food board (similar to milk carton material). The WIS predicted by the new model is compared with WIT-WOT measurements in Figure 68a. As seen here, the predicted and measured stress distributions are very close in magnitude, but the predicted WIS values are noisier. This additional noise results primarily from the data acquisition measurements rather than from the model itself. The spike at a 21" radius was caused by a splice in the material. The simple lap splice used on the roll is more than twice the nominal thickness of the material (2 time the caliper plus the splice tape thickness). This splice when run into the winding roll caused a very audible pounding which lasted for dozens of wraps. It is likely that the data spike, which was seen on every thick splice, may result from the splice temporarily upsetting either the caliper measurement due to the sudden lift, or the diameter measurements by the pounding which may have caused interlayer slippage on this low coefficient of friction material. However, the greatest source of the measurement noise is simply that the material is so stiff that the resulting radial deformations are so small that they are near the limit of the resolution of the instrument's ability to measure. Again, though the body stresses were not measured as they result directly from Hakiel's already verified model, they are realistic.

Figure 68a
WIS FOR NIP DROP - CALCULATED VS MEASURED

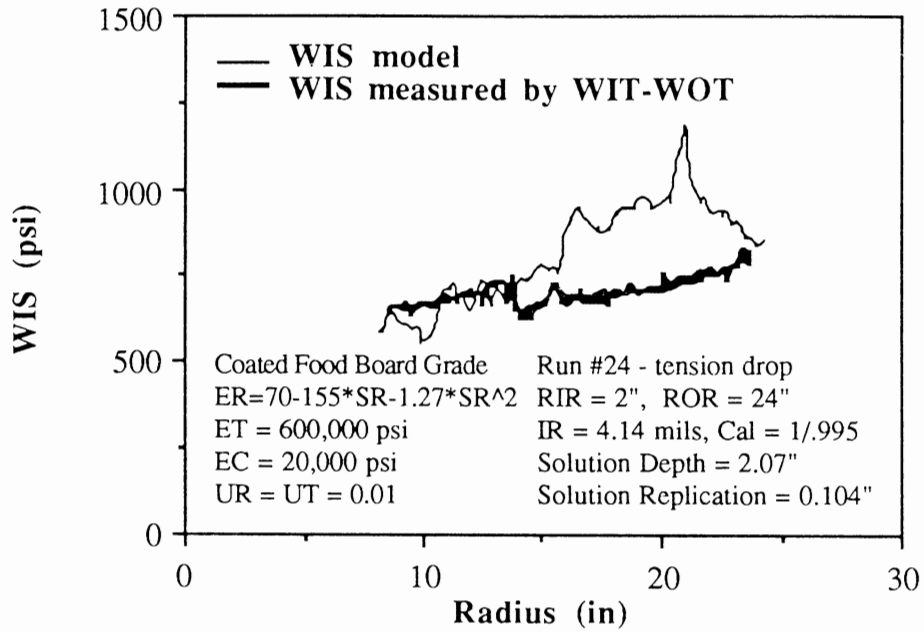
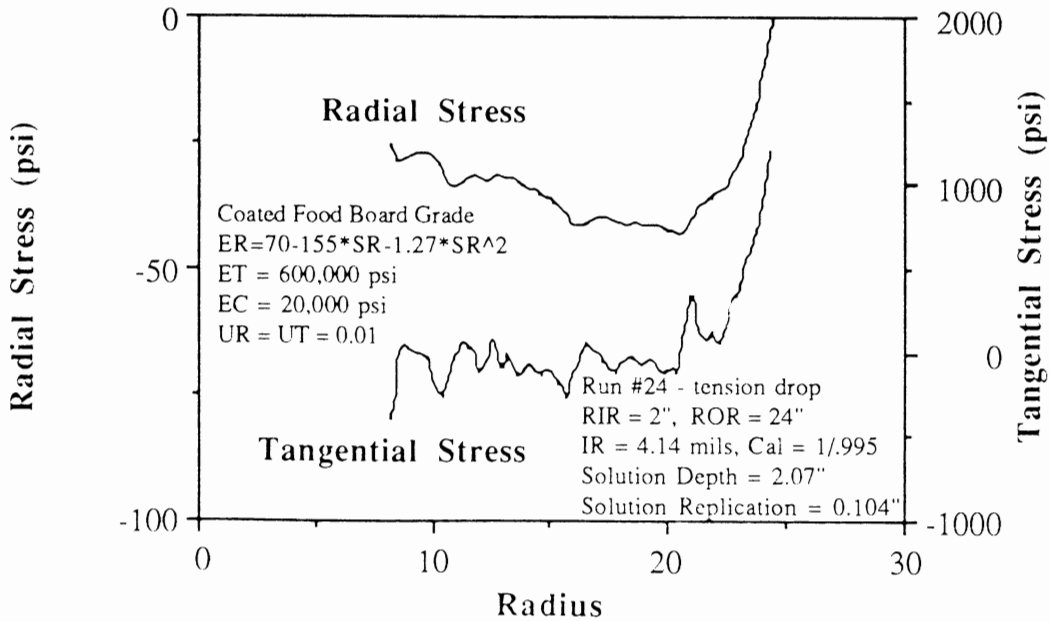


Figure 68b
PREDICTED ROLL STRESSES - RUN #24



Conclusion

This chapter has presented three different methodologies for reducing data obtained from density-like measurements of roll diameter and web thickness. The first of which was radial compression which has the tremendous advantage of extremely fast computation. Additionally, the radial compression parameter, as will be shown in Chapter 10, has improved the resolution of roll structure measurements more than one order of magnitude beyond the best currently available. Finally, the radial compression parameter was shown to be directly related to the boundary condition of the new wound roll models as it is simply the nondimensionalization of the deformation of the outer surface of the roll due to wrap addition.

Since the ultimate goal of this project is to obtain stress calculations from roll deformation measurements, the physics of the wound roll must be assembled into a differential equation from the constitutive equations. The first and simplest of the two deformation to stress models was the Displacement Formulation which was advantageous because the measured deformation of the roll's outer surface is simply the displacement boundary condition which could be directly input into the Displacement Formulation. This model was verified to be consistent with the Linear, Altmann, Yagoda and Hakiel models by creating simulated data as inputs to the new model. Unfortunately, the winding differential equation based on displacements is even more ill-conditioned than other assemblages of the same constitutive equations. Consequently, practical application of the Displacement Formulation is limited by the extremely fine mesh, and the consequently long computation time required for highly nonlinear and anisotropic systems.

The second of the deformation to stress models was developed by extending Hakiel's (or any other consistent model) to calculate and sum the strains and displacements on each layer. The Extended Hakiel Formulation was validated with simulated data, WIT-WOT measured data, and with Pfeiffer's empirical equation. This validation was performed for widely varying systems including data simulated from the standard parameters given in Appendix C, as well as real data from three very different paper grades. Though agreement was generally close, there are difficulties. First, materials with extremely high nonlinearity or anisotropy ratios are difficult to compute in a reasonable length of time, and accuracy is worst nearest the core. At the other end of the range, materials that are radially stiff present data acquisition measurement difficulties due to the extremely small deformations that must be resolved.

Finally, the scope of the issues of the data acquisition equipment required to make the measurements, and the new model to process the measurements, are so wide that there are numerous opportunities for problems. Indeed as we will see in the next chapter, it is difficult to merely define what thickness means for some materials, much less to measure it. And thickness is just one of the many measured quantities required to implement this new model! Similarly, Chapter 4 contains numerous caveats that may present additional complexities that are not currently included in wound roll models. Though this new model has been more carefully verified than most both analytically and experimentally, implementation in a production environment is not for the faint of heart.

Additional supporting material required for this new system can be found in the following chapters. Chapter 8 describes the hardware and instrumentation which was used to prototype this new system. Chapter 9 describes the minimal computer software required for the data acquisition and data preprocessing. Additionally, the computer code used for data acquisition, data preprocessing and the new model is given Appendix C. Chapter 10 details a sensitivity analysis of both the data acquisition measurements and the new deformation to stress model. Finally, Chapter 11 describes in more detail some of the system implementation difficulties which could be the subject of future work.

CHAPTER 8

DATA ACQUISITION HARDWARE

Introduction

The roll structure measurements of density and caliper corrected density described in Chapter 6, as well as the new measurements developed by this project of Radial Compression and Wound-in-Stresses described in Chapter 7, all share the common requirement of roll diameter and web thickness measurements. These roll structure techniques do not stipulate how diameter and caliper must be measured, and there are certainly many ways of doing so. However, these methods require that the diameter and caliper inputs be made with extreme precision, moderate speed, and in some cases in a noncontacting manner. Thus, only a few of the many methods for geometric measurement will be practical and suitable for these roll structure techniques.

This chapter will describe the winding equipment as well as diameter and caliper measurement methods which were used to prototype this project. The winding equipment is a state-of-the-art high speed two drum lab winder. The encoders and their signal processing for diameter measurement are a conventional approach for density analyzers, however effort was made to increase precision beyond that of typically available equipment. However, the noncontacting air-floated LVDT gage adapted for measuring caliper was a novel, precise, and economical alternative to the conventional approaches to on-line caliper measurement which are typically very expensive. Also included is a discussion of the difficulties and subtleties of defining and measuring the thickness of thin web materials which have a relatively large surface roughness such as paper and textiles. Finally, the setup, calibration, performance, difficulties, limitations and alternatives of this prototype are discussed in detail, so that similar and perhaps even more successful systems can be developed by others. Observations of previous experiences on similar density analyzer systems by the author and others will also be included as appropriate.

The data acquisition system to measure stresses during winding as defined by this project will minimally include; a winder equipped with an encoder coupled to a roller traveling at web speed and an encoder (or an extremely fast switch) coupled to the core, core chuck or core shaft; at least two programmable counters; a caliper gage; an analog input card; a computer; and software. There are numerous configurations that could be assembled to perform the data acquisition, and the optimum configuration may well vary between applications. For this project prototype however, component selection and system design was based on the criteria of accuracy, flexibility, and availability. It is likely that any production versions of this system may choose criteria of simplicity and robustness of operation at the expense of accuracy or flexibility.

Since the stress measurement calculation system is serial in nature, the overall performance of the system is no better than the weakest component. For example, a million pulse per revolution encoder may not outperform modest count encoders if the coupling between the winding roll and its encoder has more backlash than one millionth of a revolution. Similarly, interlayer slippage inside the wound roll, slippage between the rewind roll and the encoder roller, drift in the caliper gage, or erratic response to data acquisition interrupts (latency) all contribute to stress measurement noise. Therefore, great care must be used to build a system which can measure the small diameter differences and caliper to the resolution required to determine wound roll stresses.

The duration of the experimental portion of this project was quite short, and preceded the completion of the analytical portion of this project by nearly a year. Software programming began in November 1988 for a class project in Digital Data Acquisition and Control, and system installation and startup took place at Beloit's R&D facility in Rockton Illinois during December 15-20, 1988. After installation, the measurement system acquired diameter and caliper measurements from December 20-29 on more than 30 rolls of papers of four different grades including two grades of LWC (light weight supercalendered magazine), heavy coated board (milk carton stock) and NC (similar to bond).

Aside from the winding measurements, material properties were measured at Beloit's R&D facility using industry standard equipment, with the exception of radial modulus which has no test standard and was performed on a MTS tensile tester at OSU. The results of these test measurements are included in the appendices and elsewhere in the thesis.

The Winder

The Beloit R&D two-drum winder, shown in Figure 69, is a precision pilot plant machine such that roller cylindricity, alignment and eccentricity are within a few thousandths of an inch. Additionally, the winder is equipped with modern and capable sensors for tension, speed and motor loads; and controls which include PLC's and a digital electric drive. The flexibility of the control system, partially shown in Figure 70, is such that any reasonable torque, nip, tension and speed profiles as a function of rewound roll diameter can be easily programmed. Additional support services including an instrumentation shop, a machine shop, a paper test lab, and a large stock of paper rolls made this facility a near ideal environment for prototype development. Table 9 gives a brief summary of the characteristics of the two-drum winder

Table 9
BELOIT TWO-DRUM LAB WINDER SPECIFICATIONS

Speed	0-10,000 FPM	Width	48 inch face
Drive Motors	(2) 40 HP drums (1) 60 HP unwind	Roll Diam.	4-60 inch
R.R. Nip	0-15 PLI	Drums	(2) 24" with .75" gap
Tension	0-10 PLI	Spreader	D-bar
PLC	Allen Bradley	Set Change	Fully automated
		Drive	Reliance DCM

Figure 69
TWO-DRUM WINDER AT BELOIT R&D

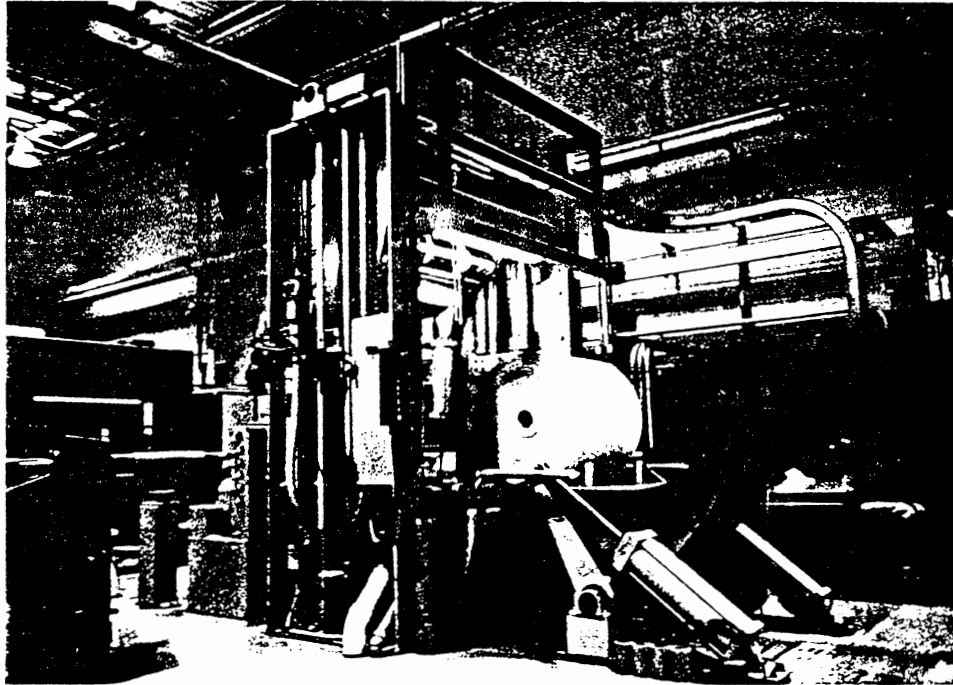
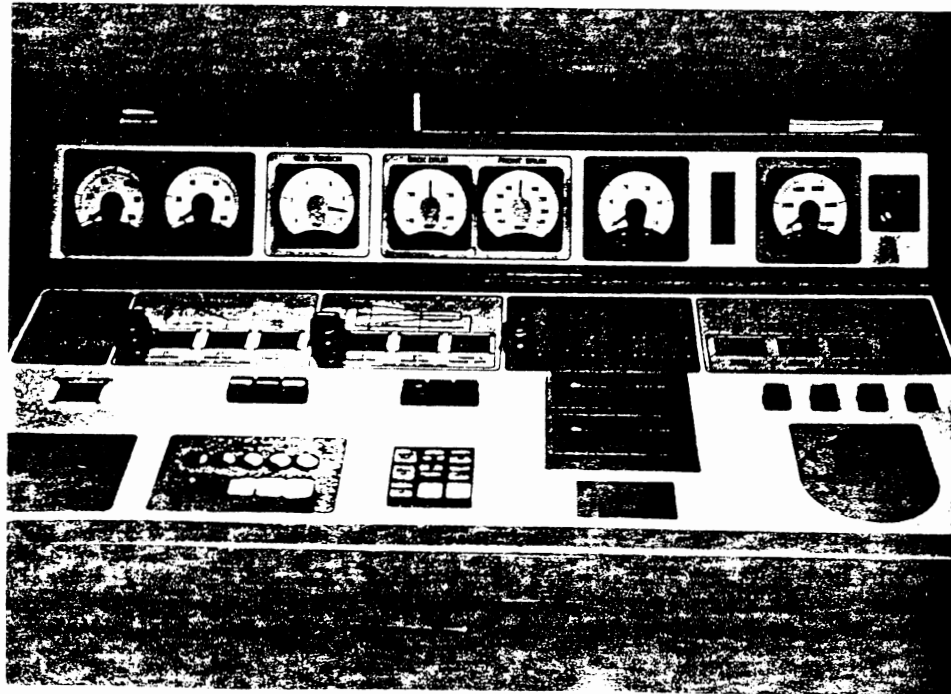


Figure 70
WINDER BENCHBOARD



Incremental Encoders

Encoder count and wrap count for the stress measurement system must be sized for each application as given in Chapter 6 for the density analyzer, and will not be repeated here. To summarize, the rewind roll encoder pulses per revolution must be as high to increase system accuracy, but not so high as to overflow counters, computer memory, or exceed the frequency limit of either the encoders or the counters.

The ratio of the roller encoder pulses divided by wound roll encoder pulses times a constant, given in equation (102), over some wrap sample interval, gives the average roll diameter during that sample. Thus, encoder pulses and analog caliper measurements determine the radial displacement boundary condition for this stress measurement system, as given by equation (118). Since there are two differences, one between consecutive diameter samples, and another of the caliper measurement, data integrity is highly dependent on both pulse and caliper accuracy as will be further discussed in Chapter 10.

One obvious way to increase the diameter measurement accuracy is to increase the number of pulses per revolution, and commercial encoders with nearly 10 million pulses are readily available. However, there are other considerations that make more modest encoders a better choice. High count encoders are more expensive, have lower maximum rotational speeds, and may exceed counter frequency limitations. Also, high count encoders require more memory and computer time to process the data. Additionally, though increasing encoder count rate will increase diameter resolution, it will do so following the law of diminishing returns as other sources of noise such as slippage begin to predominate. Early experiences showed that encoders with less than 1,000 ppr (pulses per revolution) adversely effected data integrity, while Baum showed that encoders more than 5,000 ppr gave little additional benefit [18].

However, the design goal of this project placed high emphasis on accuracy, at the expense of winding speed and computer processing time. Thus, an encoder system was selected which had 100,000 ppr capabilities as seen in Figure 71 and Table 10. Additionally, the desire of flexibility to explore various configurations led to a 2,500 line per revolution encoder, with an external 10X multiplier, and switch selectable quadrature of 1, 2, or 4X multiplication. Thus, by simple switch setting, or changes in connections, many different effective pulse rates can be obtained as given in Table 11.

Figure 71
ENCODER WITH EXTERNAL MULTIPLIER

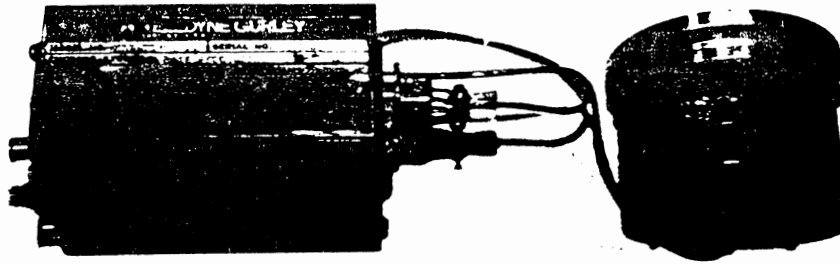


Table 10
ENCODER SPECIFICATIONS

(All encoders were manufactured by Teledyne Gurley of Troy, New York)

	<u>Runs 1-31</u>	<u>Runs 1-31</u>	<u>Runs 32-41</u>
Location	Back Drum	Core Chuck	Back Drum & C.C.
Model	8225-2500-CQSG	8225-100-CDSG	8335-2500-CBQA
Multiplier			HRB-IE
PPR (max.)	10,000	400	100,000
Output	TTL	TTL	TTL
	Square Wave	Square Wave	Square Wave
Freq. (max. kHz)	400	400	250

Table 11
EFFECTIVE PULSE RATES

(for a 2 ch., 2500 line encoder, with index pulse, 10X multiplier and quadrature)

<u>Pulses per Rev.</u>	<u>Index</u>	<u>Multiplier</u>	<u>Quadrature</u>
1	X	-	-
10	X	10	-
2,500	-	-	1
5,000	-	-	2
10,000	-	-	4
25,000	-	10	1
50,000	-	10	2
100,000	-	10	4

Another consideration for accurate diameter measurement is that the encoders are closely coupled to their roll or roller without any play or backlash. Since encoders are fragile, a compliant coupling is needed to isolate them from misalignment forces. The coupling used for this project was a spiral coil type supplied by the encoder vendor, however, a short piece of rubber tubing may also work well. However, this tubing must be short and stiff to avoid torsional vibration between the encoder and its roller. Similarly, torsional vibration can occur between a drive motor which is connected to a drum roller through a long inshaft. Since the torque of a motor varies as the rotating fields interact, the system can be forced into a two mass (motor and drum), single spring (inshaft) vibration mode.

Encoders connected to a core chuck present another problem because the chuck may roll or wobble erratically inside the slightly larger core, even if the core and chuck are keyed together. Solutions to chuck/core slippage are application dependent, but may include expandable chucks or shafts, higher axial loading of the chuck against the core, or a small tapered metal 'spear' on the chuck which penetrates the end of a capped or uncapped fiber core, as was used for this project. Since packaging of the wound roll encoder can be difficult on production machines, an extremely fast noncontacting photoswitch or proximity switch may be a better choice (see Chapter 6). Since photoswitches are smaller than encoders, and can be mounted at some distance from the harsh environment of a rotating chuck, system reliability might be increased for production environments.

Finally, accurate diameter measurements minimize slippage between the web and the encoder. If the roller is in a free web span, it should be of low inertia, freely turning, and grooved to reduce air entrainment. However, the best location for this encoder is coupled to a winding drum, as was done for this project, or to a nip roller which travels at the same surface speed as the winding roll. Some benefit may be achieved by using encoders on each of the two drums on a two-drum winder, and averaging the results. It is interesting to note that this configuration has shown that even with drum torque differential control, as opposed to drum speed differential, the drums travel at slightly different speeds.

One additional form of slippage that reduces diameter measurement accuracy is interlayer slippage inside the wound roll, otherwise known as J-line deformation [106]. Though interlayer slippage is easy to detect by striking a radial line on a winding roll, and observing whether the line bends, it is very difficult to reduce. This type of slippage occurs more frequently for lightweight, low friction materials wound with a nip roller such as LWC (light weight supercalendered), newsprint, and films. Fortunately, the accuracy of the system may not suffer noticeably because moderate J-line movement is calculated to have a minimal effect on wound-in-stress [121]. However, the erratic stick-slip nature of slippage may mean a decrease in measurement resolution due to increased noise.

A final method of increasing diameter measurement accuracy is to increase the wrap count sample size. Though this method is highly successful, there is an unavoidable trade-off between measurement noise, and the number of data points in the wound roll profile. For example, a 20 wrap effective sample size (acquired sample size times averaging) will have only half as many points in the resulting roll structure measurement profile, but the profile will be about 1/4 as noisy.

The integrity of the encoder-counter-computer system can be checked in three ways. The easiest is by benchtop testing of an encoder driven by a variable speed motor. The index pulse or additional photoswitch is used to simulate the wound roll encoder, while the two encoder channels are used to simulate the roller encoder. Proper operation is seen as identical roller counts for a fixed wound roll sample size. Another test of the system can be performed after installation by measuring the diameter of a core which is rotating in contact with a drum or nip roller, but without winding any material being wound onto the core. Proper operation is seen as a series of very closely calculated diameters. Finally, the most demanding test is to calculate radial compression or density from measurements made during winding. Even the smallest problems will show as extremely noisy plots, or contain spikes which indicate a sampling error.

Quadrature Conversion

Typically, encoders provide two channels of output pulses, A and B, that are offset in phase by 90 degrees as seen in Figure 72. One common application of the two channels is to determine direction of rotation by detecting which pulse train leads the other. More important for this project however, the two pulse trains can be combined into a single output of four times the single channel output of the encoder through the process of quadrature. This will give a higher effective pulse count, and resulting improvements in diameter measurement accuracy.

Though encoder manufacturers provide quadrature conversion products, these generally give a non-adjustable times four multiplication. While this may be perfectly acceptable for a production model with a limited application range, more flexibility would be desirable for a laboratory prototype. Consequently, a custom quadrature conversion circuit box, partially shown in Figure 73, was designed with a dipswitch selectable X1, 2, and 4 multiplications. The circuit combines the A and B input channels into a single output channel using XOR gates, Schmidt triggers, and other simple electronic components. The maximum output frequency rating is adjustable through a resistor setting which determines the width of output pulse, and is nominally about 500 kHz.

Another feature provided by the custom quadrature circuit board is electrical isolation of the computer's counter card from the encoder's signal lines. This isolation is accomplished by standard LED/photodiode pairs in series with all inputs to the circuit board. Though this type of protection might not be needed in a lab environment where wiring is simple, industrial controls are considerably more complex, with increasing chances of miswiring high voltage sources into the TTL level of personal computers. Though not implemented on this particular project, analog and digital IO (input/output) also should be isolated. Typically, isolation amplifiers will provide overload protection for delicate computer equipment from machine sensors and industrial controls, as well as providing common mode rejection, and reducing ground loop problems.

Other electrical design considerations for encoder selection are the type of output. For this project and other similar applications, TTL level square wave output with line drivers may give better reliability for high count encoders in electrically noisy environments. Additionally, cable runs should be short, shielded, and avoid proximity to sources of electrical noise such as high voltage connections to electric motors. As indicated by these discussions, reliable data acquisition design for industrial applications are more difficult than for the lab, because of the many additional electrical design considerations.

Figure 72
ENCODER PULSE TRAINS

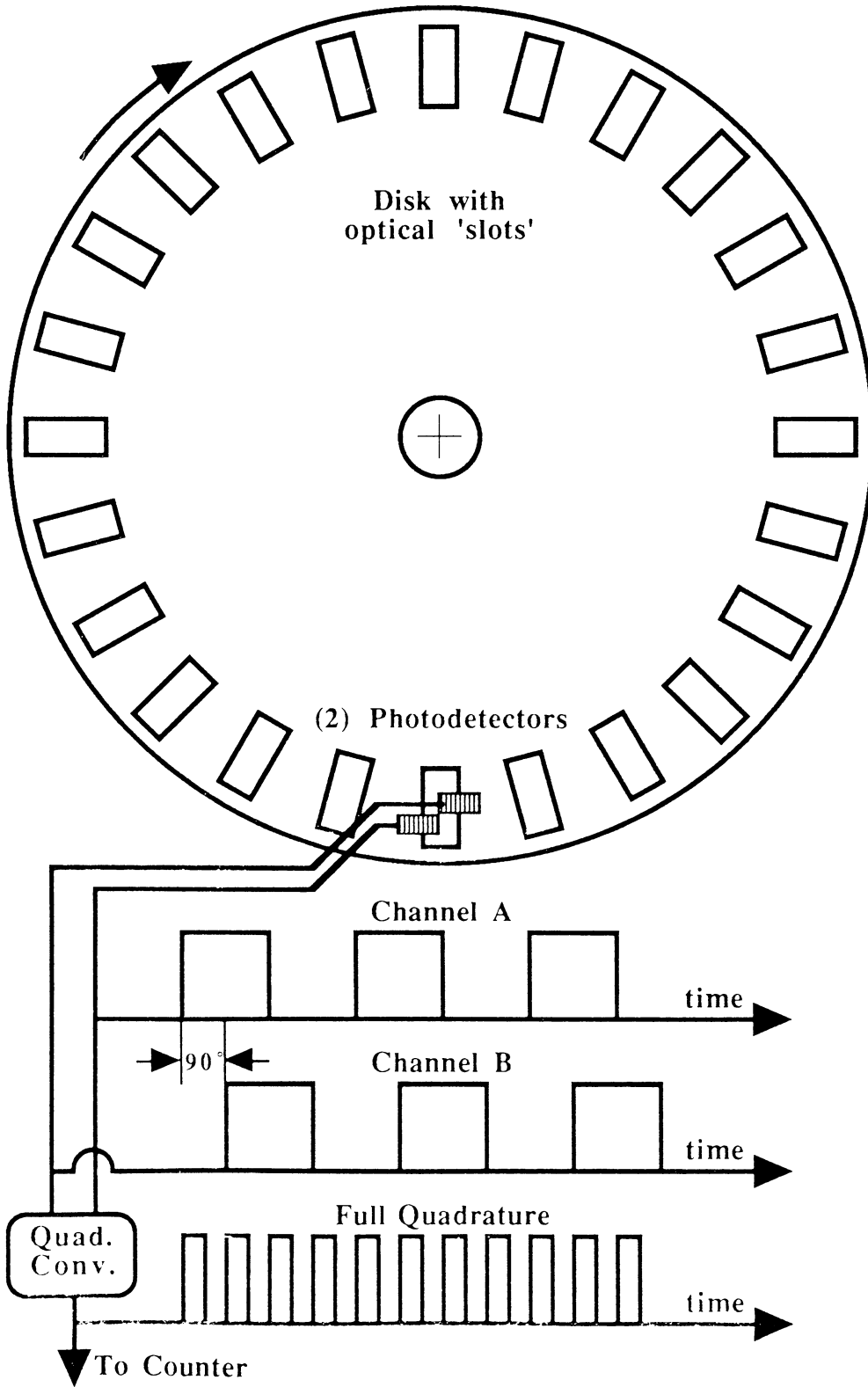
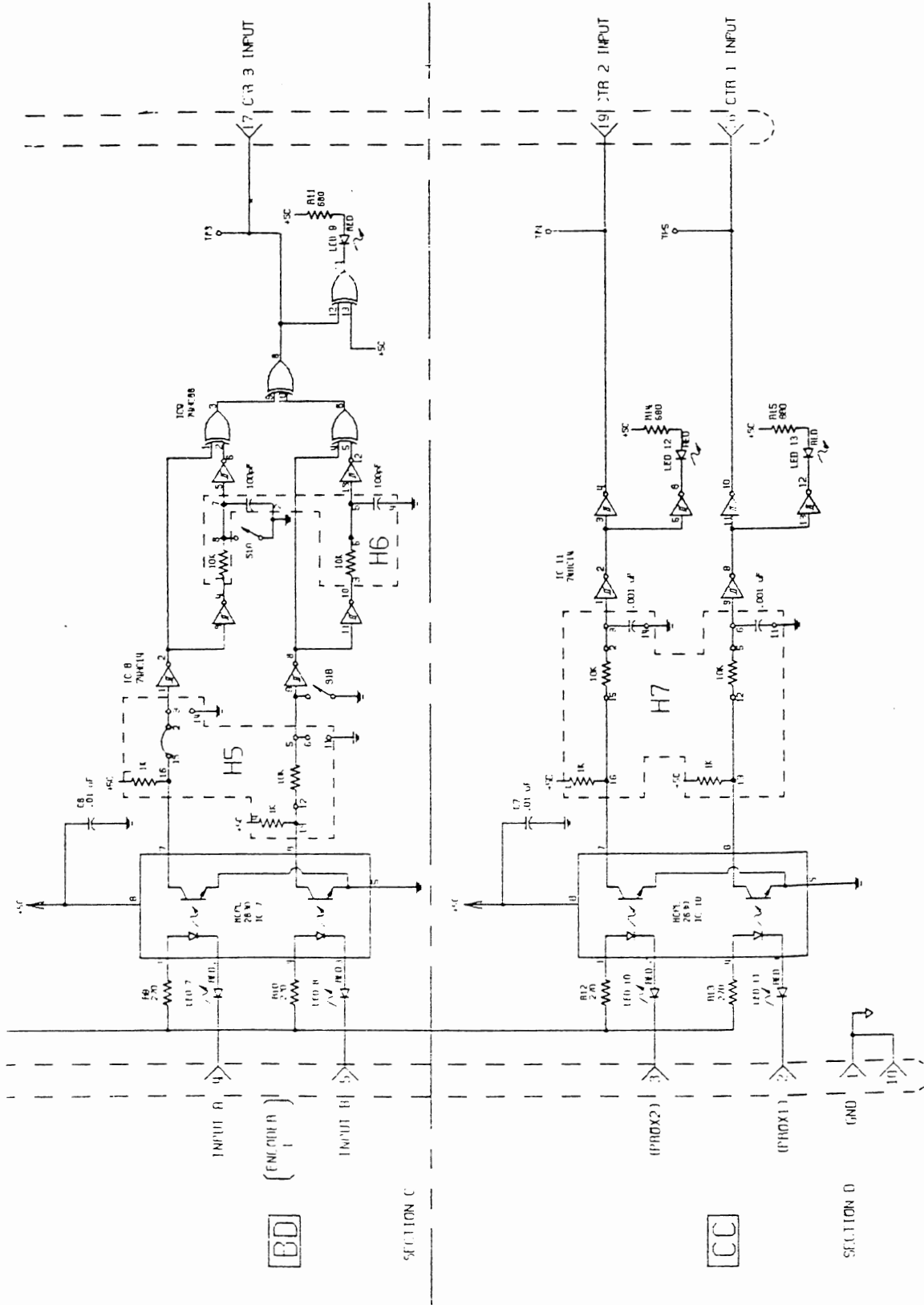


Figure 73
 QUADRATURE CONVERSION AND ISOLATION CIRCUIT



Counter Data Acquisition

Pulses from both the roll and roller encoders must be counted over some sample wrap count and passed to the computer for storage and calculation. Though other configurations are possible, typically the rewind roll encoder serves as the timekeeper for the start and end of each sample, while only the roller encoder pulses are passed to the computer. Consequently, a minimum of two counters are required, where the first counts until the preset wrap count value is reached, and the second accumulates counts until a full sample signal is received by the first. At that time, the contents of the second counter are passed to the computer, and both counters are reset for the next sample. The computer then calculates the average rewind roll diameter over that sample from equation (102); where the roller count is the variable, and the wrap count and roller diameter have been preset prior to run.

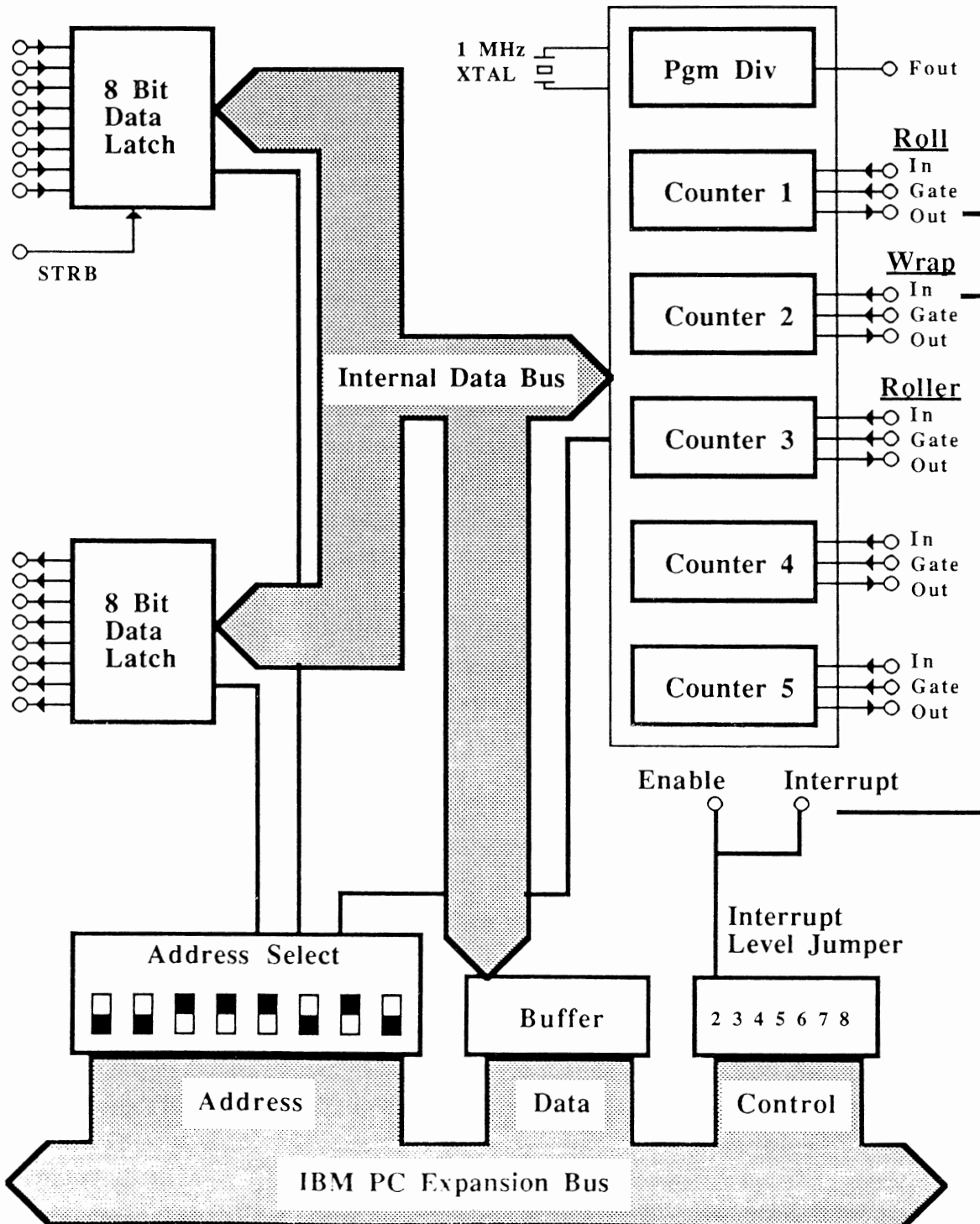
Thus, counter board selection must include at least two counters, but they can't be independent because the end of the roller encoder count is determined by the roll encoder. Additionally, due to the extremely high frequency of incoming pulses and the criticality of not missing even a single pulse, sample latching and some sample processing must be done on the counter board, because computer IO and CPU processing time is greater than the few microseconds between pulses. Further demands that are placed on counter board selection by high count encoders are the high requirements for maximum frequency and count values. Given these requirements, the Metrabyte CTM-05 Counter/Timer board for the IBM PC series microcomputer was chosen for this application. This board has tremendous programming and configuration flexibility, giving it wider capabilities than most counter boards. Also, its small size and very modest price make it nearly ideal for many PC based counting, timing or frequency data acquisition applications. A brief summary of the CTM-05's specifications are shown in Table 12, and its block diagram schematic in Figure 74.

Table 12

METRABYTE CTM-05 COUNTER BOARD SPECIFICATIONS

Counters	(5) 16-Bit	<u>Programmability</u>
Frequency	to 7 MHz	Up/Down & Binary/BCD counting
Clock	1 MHz	Frequency Output
Input Port	8 Bit Latched	Triggering and Gating
Output Port	8 Bit Latched	Count and Gate Source
Software	10 Basic Programs	One-Shot or Continuous Outputs
	+ 3rd party	Alarm Comparators

Figure 74
 METRABYTE CTM-05 BLOCK DIAGRAM SCHEMATIC



Numerous configurations are possible with the CTM-05 board due to its extensive programmability. Each of the five counters is initialized with a 16 bit (2 byte) command code which determines such things as whether it will function in an upcount or downcount mode, count source, and count output. Additional flexibility is obtained by how the DB-29 connector is wired, as well as any interconnections between counters. For example, it may be desirable to cascade two counters so that the effective maximum count prior to overflow increases from 16 bits (65,536) to 32 bits (4,294,967,296). Thus, cascading could allow extremely high pulse rate encoders to be used for a modest doubling of memory storage space from integers to long integers, and a less than doubling of the time for passing values from the counter card to the computer. Cascading counter #3 to counter #4 could be done either by physically wiring the output of #3 to the input of #4, or by sending the appropriate initializing software command code.

Additionally, more than one CTM-05 card can be used simultaneously for cascading many high count encoders, provided that the address and interrupt vectors are different. As mentioned earlier however, the law of diminishing returns and the weakest link serial nature of the system makes it doubtful that any detectable improvement in accuracy would be achieved beyond 100,000 ppr unless the entire winder and data acquisition system was redesigned to much tighter tolerances.

For this prototype, counter #1 was used for the rewind roll encoder, counter #2 for the sample count, and counter #3 for the roller encoder. Cascading was not needed for the prototype system on the rolls tested using 100,000 ppr encoders. However, a small increase in encoder rate, roll diameter; or decrease in caliper or available memory, would have required cascading to avoid overflow.

Counter #1, which takes its inputs from the rewind roll encoder, serves as the timekeeper for samples and is initialized at the beginning of each sample to a value corresponding to the number of pulses for the desired wrap count, which is given in equation (103). It is configured in a downcount mode, so that it counts backward from the initialized wrap count pulse value towards zero. When counter #1 reaches zero, it sends an output which triggers several events that take place entirely on the CTM-05 counter board. First, its output is used to increment the sample counter #2 by one. Secondly, its output latches the current count in the roller counter #3, and immediately resets counter #3 to zero. Thirdly, counter #1 is reset to the wrap count pulse value. Finally, counter #1's output sends an interrupt to the PC, so that an interrupt driven data handling routine could be triggered. Although interrupt driven software was not used for this project, it has been for prior projects, and has many advantages that will be discussed later.

Counter #2, which serves as a sample counter, has the simplest configuration. It is initialized to zero only once at the start of every data acquisition run. During each data acquisition run, it merely counts the output from counter #1, which increments at the end of every sample. The purpose of this counter is to allow a polling mode of data acquisition, so that a new sample can be detected as an increase of one in counter #2's contents. Additionally, it also can detect a missed sample as an increase of more than one in its contents between consecutive polls.

The use of counter #2 is superfluous for interrupt driven software, except that it can more directly determine if samples have been missed. However, even though missed or double counted samples are very damaging to data, they are extremely rare for well designed systems. There are two principle ways in which a sample can be missed. The first is if the system is misdesigned, so that the computer does not have time to read and process a value during the time it takes for samples to be produced. From equations (111), (115) and (116), this can happen for sluggish processing on small wrapcounts during the top of acceleration when the rewrap frequency is maximum. The second way a sample can be missed is if pulses are dropped by the hardware, which is an electrical design issue.

Counter #3's contents, which is the roller encoder pulses during a sample, is the essence of the diameter calculation, and is the only value that needs to be passed to the computer for storage and calculation. At the beginning of every sample, counter #3's contents are initialized to zero; and at the end of every sample, the current contents are latched by the output of counter #1. The latched contents are read by the computer either on interrupt, or when the next polling of counter #2 indicates a new sample is present, depending on which mode the data acquisition software is written in.

Despite the modest complexity of counter processing, almost all of the work is done on the counter board itself, which not only frees the computer from low level housekeeping, it also increases the potential throughput of the counter board. Thus, after the appropriate control commands have configured each of the counters prior to run, the board is nearly self sufficient. The only minimal duties of the computer during data acquisition are to merely read the contents of the counters, which must be passed as two bytes per counter through the bus. Even the computer IO is assisted by the CTM-100, which provides buffering of inputs and outputs so that the computer can process them as CPU time becomes available.

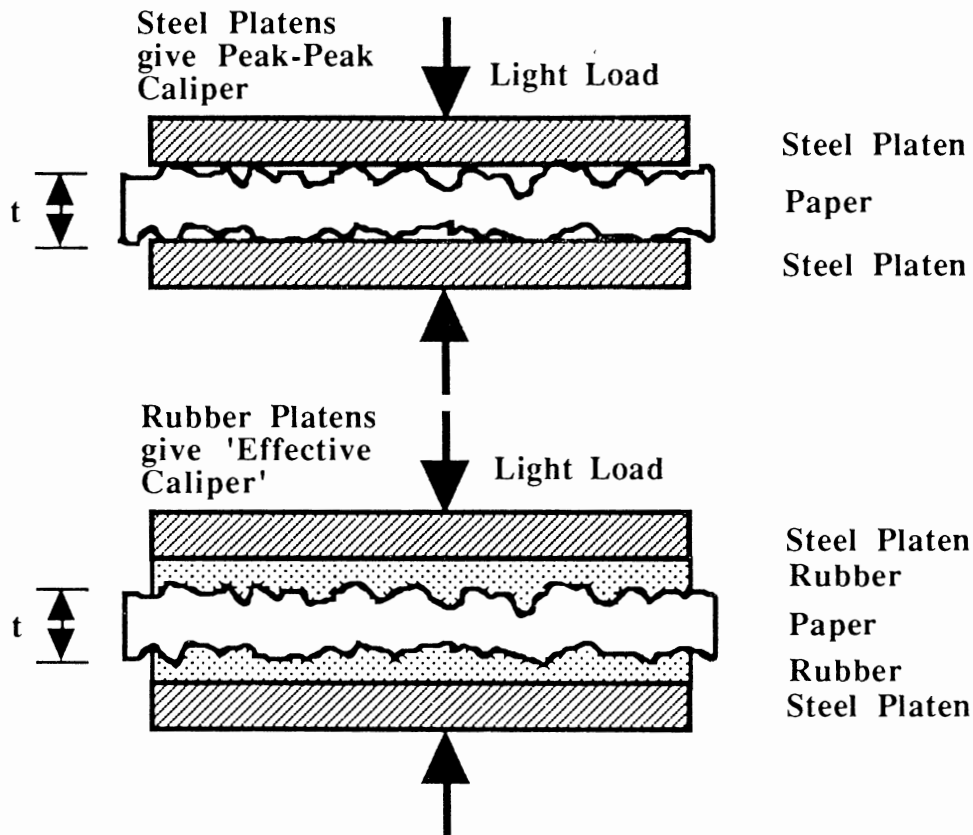
Off-Line Caliper Measurement

Aside from rewound roll diameter, caliper is the other on-line measurement required to predict wound roll stresses, which start with the new displacement boundary condition given by equation (118). As with diameter, caliper must also be measured with great accuracy due to the differencing nature of the model formulation. Caliper measurement can in general be made off-line by testing discrete samples in a lab, or on-line with sensors located in a free span of a web processing machine. For the purposes of this prototype however, on-line measurements are required for the winding of webs that vary even slightly in thickness with time or MD position. Even so, off-line caliper measurements are still required to calibrate or check the accuracy of on-line measurements.

Simple off-line measurements of caliper can be made with a precision (0.0001" or better) micrometer. To improve the accuracy of the reading, it is common to measure the thickness of a small stack of material and divide by the number of sheets. Dedicated lab caliper gaging instruments will improve the accuracy and consistency even more by providing a precise loading of the web between precision steel platens, and by having higher resolution position sensors, as seen in the top of Figure 75. Though there are many different instruments for measuring web thickness, the technology itself is generally a mature one, where procedures and standards have been in effect for decades [73, 74, 77, 175-180]. For example, TAPPI test T411 specifies a motor-operated micrometer applying 7.3 ± 0.3 psi over two circular platens of 0.62-0.64 inch diameter, which are parallel to each other within 0.00005 inch [175]. This test, written in 1926 and only updated four times since, serves as design specifications for caliper gages produced by Emveco, Thwing-Albert, TMI and others [77].

While caliper measurement of most films is straightforward, paper and other materials with porous or rough surfaces present an additional complexity of the very definition of thickness itself. The difficulty is similar to the definition of surface roughness, which can be specified by peak-peak, RMS, waviness, or in many other ways. The Institute of Paper Chemistry, recognizing the need for a better measure of thickness for rough grades, developed a rubberized platen caliper gage [89]. As shown in the bottom of Figure 75, the soft rubber conforms to many of the surface peaks and valleys, giving a better approximation of thickness than does the peak-peak values of the steel platen gages. Other caliper gaging methods include mercury pycnometric displacement, and an effective thickness concept solved from simultaneous bending and extensional stiffness measurements [179, 180].

Figure 75
PEAK-PEAK AND EFFECTIVE CALIPER



Though the effective thickness of rough materials may be better described using methods similar to IPC's Rubber Platen caliper gage rather than using a steel platen, a more representative measure might be to account for how the layers of web stack against each other in a wound roll. Thus, instead of a web against steel or a web against rubber, a web against web caliper measure may more accurately reflect the wound roll. The Tappi test T500, though designed for measuring the thickness a stack of paper in books, uses just such a concept [175]. In this test, approximately one inch of paper is loaded between parallel steel platens under a pressure of 36.3 ± 1.4 psi, which is a considerably higher load than Tappi's test T411 and IPC's gage.

Though each of these different methods are repeatable and internally consistent, they unfortunately give caliper values that can easily vary more than 10% between the methods [89]. Since a thorough evaluation of caliper measurement is considerably beyond the scope of this project, only an opinion can be offered for the most suitable off-line testing for this project. This would combine the best features of several techniques. First, procedures and specifications of the T411 standard, which is more thoroughly described than other methods, would improve the consistency and resolution of the method. Secondly, a stack of material similar to T500 would best approximate wound roll behavior, and reduce uncertainty with a larger sample size than the single sheet methods. Thirdly, modifying T500 to rubberized platens would minimize end effects of the top and bottom layers by giving the platens a compliance closer to what might be seen in a wound roll. Finally, the loading would be cycled from zero to perhaps about 100 psi and down to zero over two cycles, to quantify the unloaded caliper, as well as the hysteretic nonlinear stress-strain stack modulus E_R as described in Chapter 3. For this project however, much of the verification of the on-line caliper gage was performed using a TMI #449-27 caliper gage. Since this instrument conforms to the loading of 7.3 psi guideline of T411, the loaded caliper is somewhat less than the unloaded caliper and depends on the stack modulus of the material. The unloaded caliper must be calculated from equation (124) or by extrapolating down the stress-strain curve as indicate in Chapters 3 and 7.

On-Line Caliper Measurement

While off-line measurement may be useful for quality control and calibration, on-line caliper measurement is required for the measurement of stresses, as defined by this project, for any material whose caliper varies significantly with time or MD position, with respect to its anticipated ZD deformation inside a wound roll under interlayer pressure. The first commercial on-line caliper gages were based on changes in magnetic reluctance between a coil and a steel platen that are separated by the web [77]. Miller and Springer of the Springer Corporation used this principle for a contacting gage, where a coil attached to a puck loaded the web against the platen by about 0.19 psi. This sensor has an unusually high resolution of 10 μ inch. Unfortunately, it is a contacting sensor which could scratch or mark many grades of film or paper. A similar variable reluctance sensor is the Calmike by Indev Incorporated [73]. With this sensor however, the web is floated on each side on an airfilm of about 100 μ inch thickness, by a blower connected to the coil and platen which supplies a 20 in H_2O pressure. Though this sensor is noncontacting, its accuracy is considerably less for two reasons. First, the airfilm is large and can be effected by web speed and roughness. Secondly, if the sensor halves are connected to two different cross machine beams for CD profiling, caliper readings will vary with changes in relative displacement caused by changes in mechanical or thermal loads to the two beams.

In addition to caliper, basis weight, moisture, and elastic moduli can also effect wound roll stresses. Basis weight sensors are as prevalent on paper machine equipment as caliper gages. Though basis weight does not enter into this winding stress model, it does enter the density analyzer through equation (46). Basis weight, which is mass per unit area, is most commonly measured by the absorption of beta particles through the web produced by a radioactive source. Web moisture not only affects basis weight, but hygroscopic diffusion may cause changing stresses and strains for many materials, such as paper and textiles, which increase in length with increasing moisture. Web moisture is measured by the absorption of certain wavelengths of infrared energy. Finally, on-line modulus and poisson ratio measurement by acoustic methods, developed by the Institute of Paper Chemistry, are starting to be used in production environments [56, 57, 68, 77].

The Schaevitz Non-Contacting Gage

Selection of a caliper gage for this project was based on requirements of extremely high resolution, moderately fast response, compact size, ruggedness, low cost, and compatibility with a wide variety of web materials. Additionally, it may be desirable for the sensor to be non-contacting for production applications on mark sensitive grades. Since many of the commercial caliper measurement systems were bulky, expensive, and did not have a particularly high resolution, alternatives had to be investigated.

Optical methods were first investigated because of their potential accuracy and typically non-contacting nature. Many optical systems, such as the Fotonic sensor by Mechanical Technology Incorporated, require materials with special optical properties, which severely limit the breadth of application. A laser triangulation system with a linear photodetector array, the Chesapeake Laser Systems LTG-2101, was found to be both complex and costly, and had an insufficient resolution of 250 μ inch.

Finally, a non-contacting LVDT caliper gage made by Schaevitz, first noticed in a paper test lab basis weight profiling machine, appeared to have most of the desirable characteristics required for this project. The gage, shown in Figure 76, consists of a double acting air cylinder connected to a LVDT (Linear Variable Differential Transformer), which floats above the work surface on an air film of about 0.003 inches. The float height is carefully controlled with a pneumatic servo-follower which maintains a constant back pressure despite changes in the height of the work piece. The gaging force from the air nozzle of 15-20 grams over a target diameter 0.062" translates to a pressure of about 0.5-0.75 psi. Options include: gaging ranges of ± 0.050 , ± 0.125 and ± 1.00 inches; larger air gap/lighter loading; AC or DC output; breakaway tips; and a special order 5 μ inch repeatability model. Table 13 gives specifications for the Schaevitz gage.

Figure 76
SCHAEVITZ NON-CONTACTING LVDT GAGE

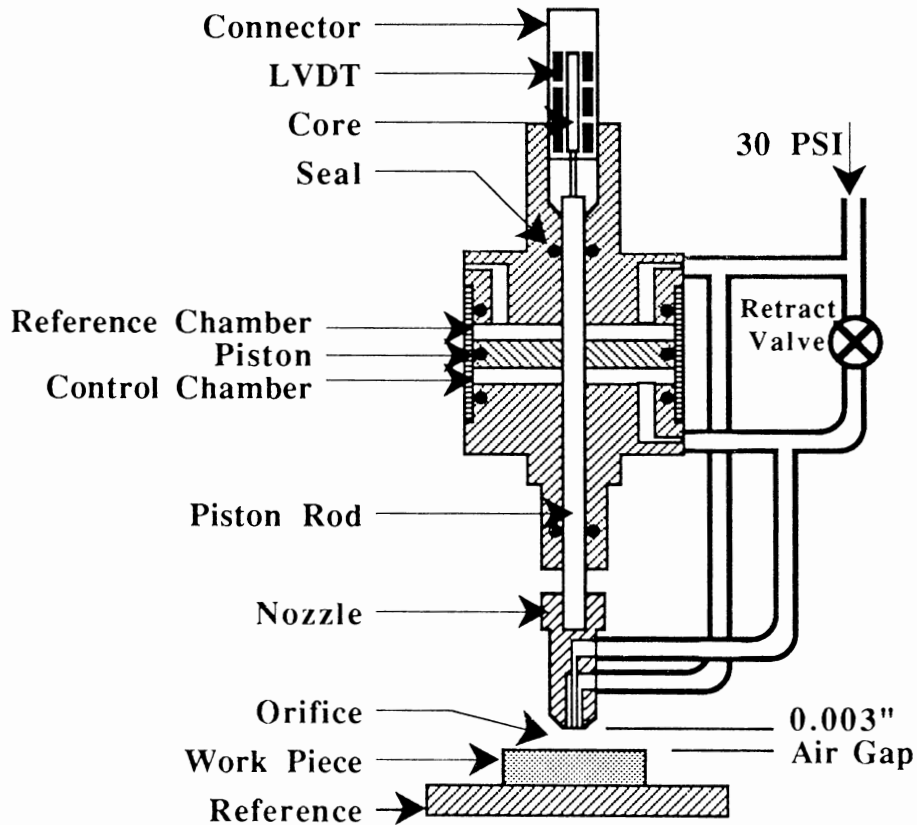


Table 13
SCHAEVITZ NON-CONTACTING GAGE SPECIFICATIONS

Model	PPA-050	Input	120 VAC, 30 psi air
Stroke	± 0.050"	Response	30 Hz for < 0.04"
Repeatability	± 0.0001" *		0.125 in/sec > 0.04"
Output	± 10V DC full scale & 6 digit LED display	Gap	0.003"
		Length	8.5"
Gage Force	15-20 grams	Diameter	1.87" max

*The repeatability of the gage is very conservatively rated.

Testing by the vendor and author indicated a ± 0.000005" repeatability for thin webs.

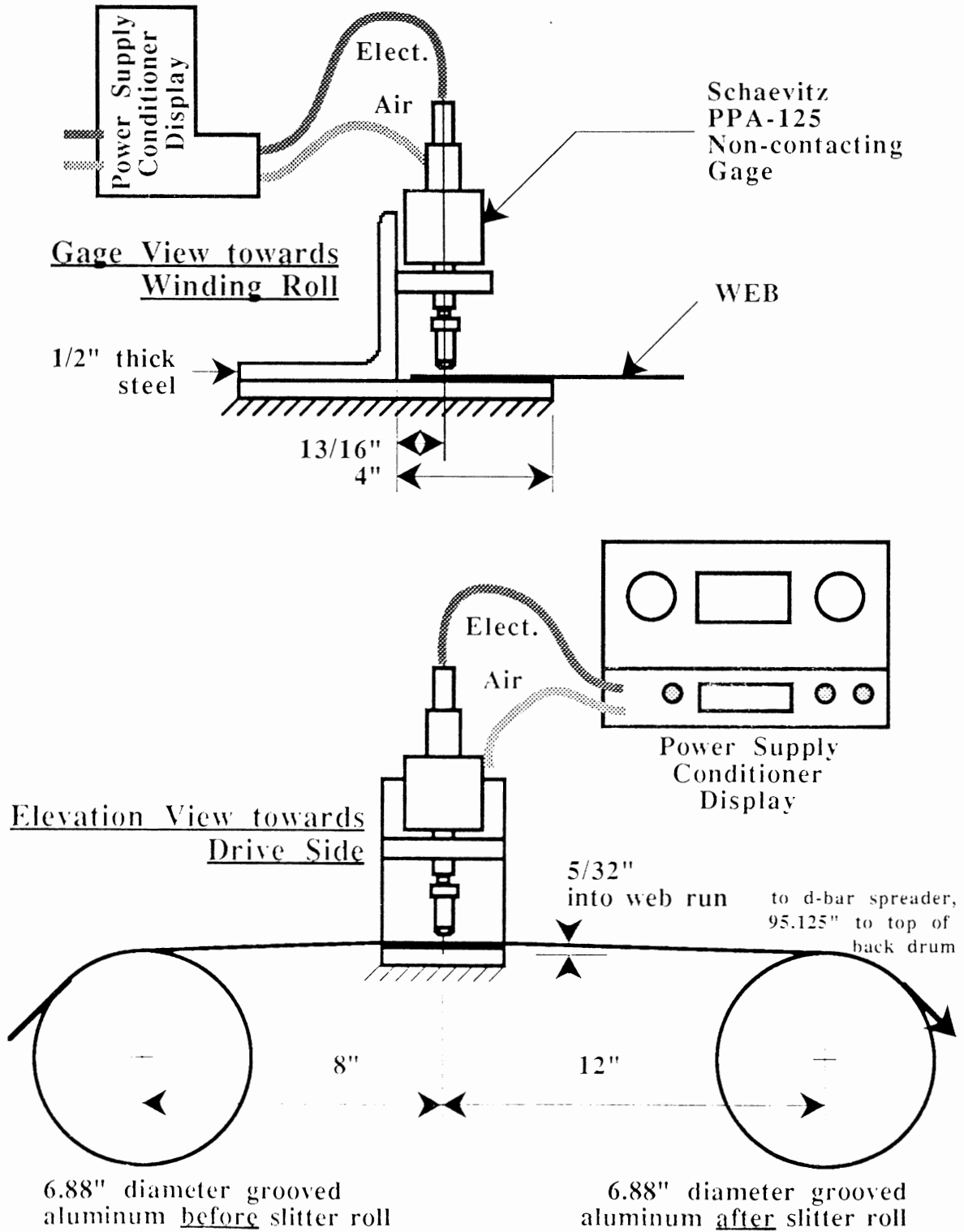
Two concerns were expressed by Schaevitz when the requirement of high speed operation was described to them. First, the maximum frequency response of 30 Hz translates to a minimum resolution of about one foot of web at 6000 FPM. However, this project does not require every peak and valley to be profiled at fractional inch increments, but rather, only to yield the average web thickness over the sample period. Thus, the upper frequency response means that the caliper reading will be some average thickness because the mass of the piston can't follow high frequency variations.

Secondly, Schaevitz was unaware of any application of their sensor at speeds beyond a few feet per minute, much less at the thousands of feet per minute of a high speed winder, and were concerned with the interaction of entrained air affecting the back pressure at the nozzle, and consequently affecting readings. Tests were performed where step changes in winder speed would show step changes in caliper readings, if the readings were effected by speed. However, no steps in the caliper readings were noticeable at speeds to 6000 FPM, although they might have been small enough to be masked by the typically large web caliper variations.

A more thorough testing of the effect of speed on caliper readings would be to sample caliper at the same point on a web running at different speeds. This was not performed due to the time consuming setup required to put timing marks on a web which would serve as triggers to begin caliper sampling. If it turns out there is a measurable effect of speed on caliper readings, this could be easily calibrated out. To simplify the already complex nature of this project, many of the tests were run at a near constant low speed of 500 FPM to reduce any speed effects if they indeed did exist.

The Schaevitz gage was mounted on the back side of the web, and between the slitter rolls as seen in Figure 77. The bottom platen was moved into the sheet run by $5/32$ ", so that web tension would cause the web to be loaded lightly against this reference surface. Desirably, the gage would be located as close as possible to the winding (or unwinding) roll, so that the web passing under the gage during a sample was aligned nearly as possible with the web being wound onto the roll during that same sample. The 95.125" web span between the gage and the 12 o'clock position on the back drum is equivalent to 7.5" rewind roll circumferences at the core, and 0.75" rewind roll circumferences at a diameter of 40 inches. Since a minimum effective wrap count of 10 was displayed, the gage sample and diameter sample overlapped at all times, and substantially for most of the winding cycle. For this reason and others, it was felt that realigning the caliper and diameter data was not necessary, although it could be done without much effort.

Figure 77
CALIPER GAGE LOCATION



Calibrating the Caliper Gage

Calibrating the span of high resolution gages, such as the Schaevitz with a 5 μ inch repeatability, to maximum accuracy is difficult because it is hard to find an independent reference gage with such accuracy. Precision gage blocks or micrometers are commonly available only down to 100 μ inch. Furthermore, even if a target block could be measured to very fine tolerances, it may not contact the platen directly underneath the gage head due to waviness in the surfaces of either the platen or the target block. Though thin flexible materials, such as paper and film with a caliper less than 0.01", will be forced against the platen by the pressure from the nozzle, gage blocks will not likely contact the platen exactly under the measurement point. The dilemma becomes that a thin material does not provide a large distance over which to set the span, and a thick material does not conform exactly to the platen.

Fortunately, the Schaevitz demonstration unit which was used for this project included a means to calibrate the span adjustment over a large range while simultaneously eliminating the platen conformity problem. The demonstration unit included a fixture for holding the gage, as well as a precision 0.0001" micrometer connected to a platen. The gage and the micrometer were both fixtured on the same axis. With this arrangement, span calibration did not require a reference target block, instead the micrometer adjustable platen served as both a platen and a distance reference.

Calibration began by first setting the micrometer near the extended limit of the gage travel and then the unit was zeroed. Then the micrometer was advanced to near the contracted limit of gage travel and then the span was set. These steps were then repeated a couple of times until the zero and span were repeatable. For this PPA-125 gage, the span was adjusted to the 100 μ inch accuracy of the micrometer over a 0.100" range. Thus for example, the accuracy may be expected to be about 3 μ inch for a 0.003" thick web, although this would be extremely difficult to verify. After 10 days of continuous use, the gage span was rechecked to be within the original 100 μ inch micrometer accuracy over the 0.100" range.

Repeatability of the Schaevitz gage was checked in three ways. The first way is to simply retract the gage from the bare platen, lower it to the platen, take a reading, and repeat several times. The results of this test for 10 readings was a range from -20 μ inch to 0 μ inch with a mean of -7.0 μ inch and a standard deviation of 6.7 μ inch. The second way the repeatability was checked was to check the zero after each winding run on the bare platen. The results of this test for 14 runs was a range from -60 μ inch to +130 μ inch with a mean of -0.7 μ inch and a standard deviation of 42.3 μ inch. Thus, even though the product specifications list a 100 μ inch repeatability, the actual performance is considerably better.

Finally, the repeatability of the Schaevitz gage was checked during actual operation by reading nominally the same section of web on every other wind to see if the caliper profiles were repeatable. As seen in Figures 78 and 79 for light weight coated and no-carbon release paper respectively, the profiles are extremely repeatable. There are however, differences in the runs on both a large scale and a small scale. On a large scale, the consecutive runs show a consistent decrease in caliper which is particularly noticeable on the NC paper. This is the result of creep in the paper due to radial loading inside a roll. Secondly, on a smaller scale tiny differences in the profiles are the result of small misalignments of the readings in the CD direction due to slight changes in tracking of the web, misalignment of the readings in the MD direction due to a number of causes, and finally due to uncertainty in readings.

Schaevitz Caliper Readings and Paper Test Lab Standards

The Schaevitz caliper readings were compared with the Tappi standard test procedure 411 as measured by a TMI #449-27 caliper gage. As shown in Figure 80, the Schaevitz gage readings were within the 0.07 mil accuracy of the TMI gage for the majority of the grades. However, there appeared a tendency for the Schaevitz to read consistently smaller despite the lower gaging pressure, especially for the more porous grades. This may be the result of either airflow through the web, or the effective thickness concept discussed earlier. While grades lighter than about 0.010" will be forced against the platen due to the air pressure from the Schaevitz nozzle, heavier grades required a MD tension with a slight protrusion of the platen into the web run to ensure conformity to the platen.

Figure 78
CALIPER REPEATABILITY - LWC

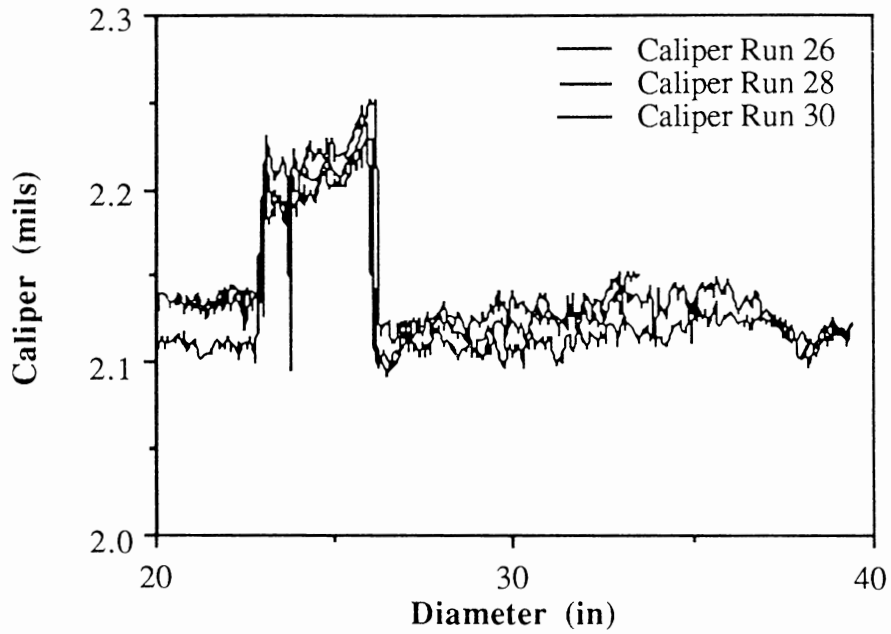


Figure 79
CALIPER REPEATABILITY - NC

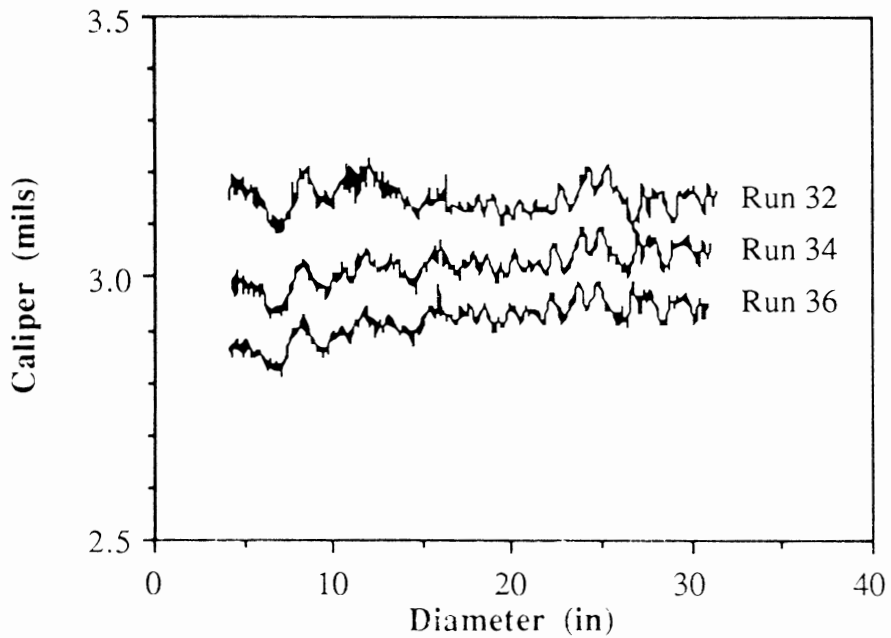
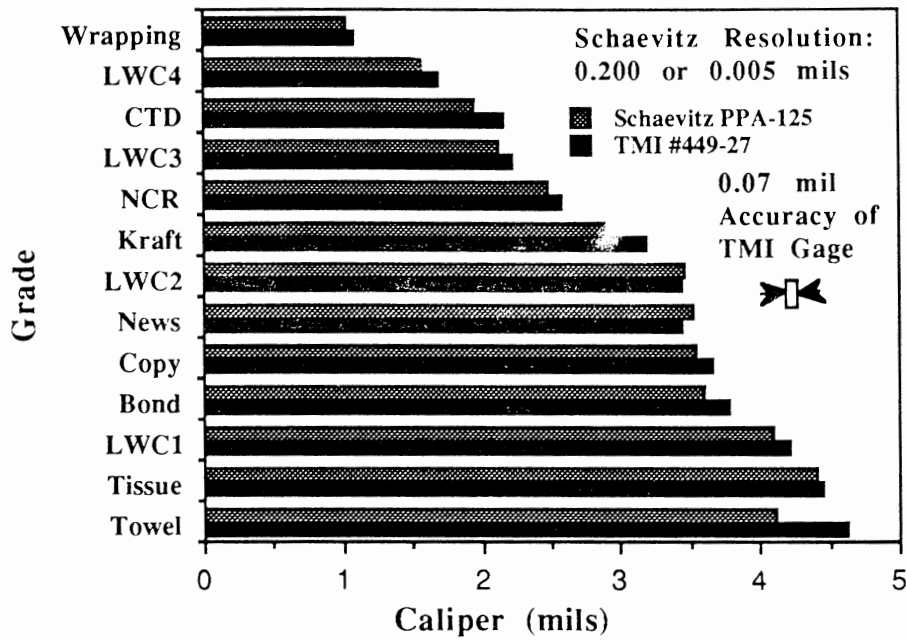


Figure 80

CALIPER MEASUREMENT COMPARISON



Conclusion

The instrumentation required for this project is demanding in precision, occasionally complex, and certainly wide in the scope of complexities. Diameter measurement from encoders is complicated by data acquisition hardware and software considerations detailed in Chapters 6 and 8 respectively, potential slippage or backlash in the system, and the equivalent diameter of noncylindrical rolls based on what is fundamentally a circumference measurement. Caliper measurement is similarly complex in defining what caliper means for rough-surfaced webs, precise calibration to a tiny fraction of the thickness of extremely thin webs, correcting caliper measurements to an unloaded condition, as well as air entrainment and porosity considerations resulting from caliper measurements taken at speed. Also, the Radial Compression or displacement boundary condition is extremely sensitive to small changes in the zero or span of caliper measurement as will be seen in Chapter 10. Consequently, slight adjustments in the span of the theoretical correction to unloaded caliper may be required to give close agreement between WIS predicted by the Chapter 7 model and those independently measured. However, the most serious measurement concern is the extreme accuracy required in the basic measurements required for a moderate accuracy of the resulting calculations for the small differencing ($diameter_{n+1} - diameter_n - caliper$) defined by the model. More will be said about this issue in Chapter 11.

CHAPTER 9

DATA ACQUISITION SOFTWARE

Introduction

In order to implement the new displacement to WIS models given in Chapter 7, the roll diameter and web caliper data must be made available to the computer in digital form as a column array of displacements. Though there may be other ways of obtaining this type of data, this project gathers data using an approach similar to the density analyzer described in Chapter 6 for measuring roll diameter. In addition however, web caliper must also be acquired as an analog value and converted to a digital value in parallel to the roll diameter data.

In order to increase flexibility for this prototype, the software required for measuring and calculating WIS from displacements is broken up into three separate programs. The first is the data acquisition program, DRWIND, which acquires diameter measurements from counters and reads caliper from an analog input board, and stores these values on disk. The second program, DRcompress, reads the output from the first program from disk, smooths the data, and writes radius, density, radial compression, displacement, and caliper to disk. The third program, DisWis, reads a displacement file created by the second program and calculates WIS as well as radial and tangential stresses. The first two programs for data acquisition and data preprocessing are discussed in this chapter, while the third for calculating stresses is discussed in Chapter 7. All program listings are given in Appendix C.

Though the stress model cares not how diameter and caliper measurements are acquired, the choice of hardware and software will effect the data resolution, cost, ease of prototype development, and reduction to practice. Despite the wide variety of computers and industrial controllers that may perform either the data acquisition and/or the model simulation, an IBM PC-AT clone was selected because it is universally available.

However, even within an IBM PC-AT there are a wide variety of hardware and software options for data acquisition, which must read two or more encoder counter channels as well as an analog input channel for web caliper. Since one of the most demanding of the tasks for this project is to acquire and process encoder pulses at high speed and with great integrity, the counter card becomes a rather key element. For this reason, the Metrabyte CTM-05 high speed counter/timer board discussed in Chapter 8 was chosen as an inexpensive but very capable data acquisition option. The Metrabyte Dash16F analog board was then chosen for handling the single caliper channel to maintain system consistency, though many other boards would perform similarly.

Once the boards are chosen, the practical choices of software is limited somewhat due to the desirability of mutual hardware and software support. Since the Metrabyte boards are well established, they are supported by software ranging from custom programming in standard computer languages such as Basic or C, to programming within a data acquisition application such as with Asystant, to menu driven configuration such as with Labtech Notebook. Each of these approaches has advantages and disadvantages that must be considered.

The advantages of using a general purpose data acquisition application include a wider variety of tools and functions, usually a much quicker development time, and the robustness of professionally written software. However, the disadvantages of general purpose data acquisition software include a slower throughput, and a smaller data memory availability due to the overhead of many functions that might not be used for a particular application. Since roll structure resolution will increase with increasing data throughput and memory, it was felt that custom programming was justified for this prototype. Additional justification also includes the potential for interrupt driven multitasking for increased throughput, which is not always available with many general purpose data acquisition applications.

Primarily because of the interrupt capabilities of C, but also because of its slightly faster execution and better portability, it was decided that C would be the best choice of language. In particular, Borland's Turbo C 3.0 was used for this project, though other C implementations would perform similarly. A Metrabyte Drivers Package from Systems Guild was purchased to speed up the development. However, the library contained many more functions than required for this project, did not directly support Turbo C's syntax, and unfortunately caused numerous compilation problems. Consequently, only the library functions minimally required by this project were included, and even they had to be rewritten slightly.

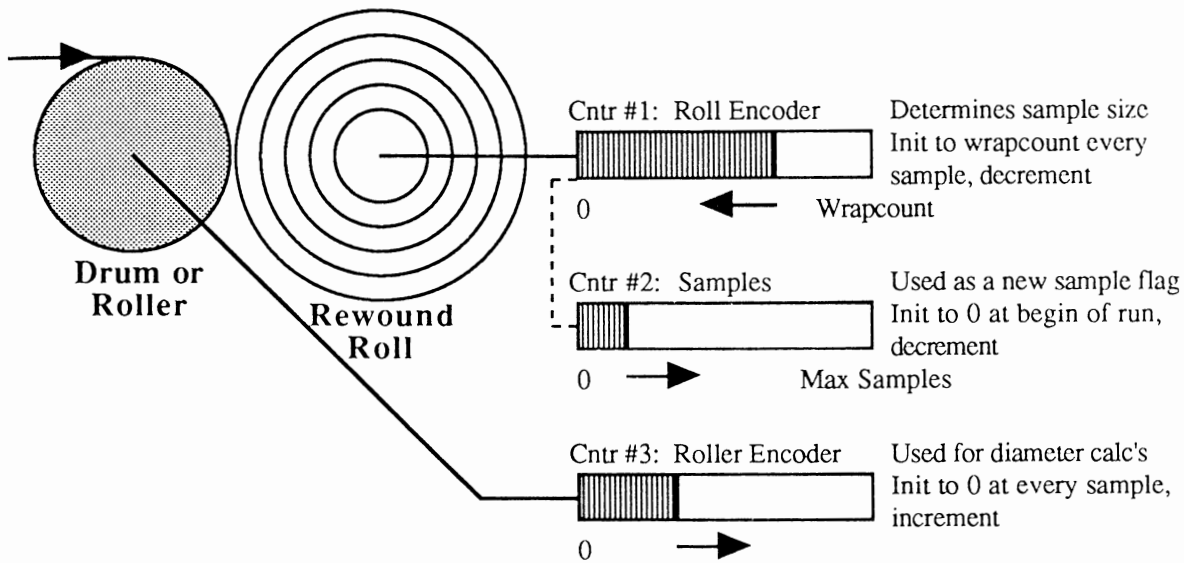
This remainder of this chapter describes the software designed to both acquire and preprocess the data, so that it is suitable to be read as an input file by the new winding model. Included are a discussion of how the data acquisition read can be triggered, the mechanics of how the software controls the data acquisition hardware, and software timing. Though some of this discussion is necessarily dependent on the particular hardware/software implementation of this prototype, many of the principles will hold for other implementations. Finally, a separate program for conditioning the digital data for noise reduction and calculation of density, radial compression, and displacement is described.

Polling and Interrupts

Two encoders are required to calculate roll diameter, one on a fixed diameter drum or roller traveling at web speed and the other connected to the rewind roll as defined by equation (102) and detailed in Chapter 6. However, one is treated as a 'timer' for controlling sample size while the other is actually used for the diameter calculation. Conventionally, the counter on the rewind roll encoder is the 'timer' and is preset prior to a run to a value which determines the number of wraps contained in a sample, and is programmed to decrement to zero. Conversely, the drum roller starts counting from zero up until the sample interval is complete as determined by the roll encoder. A schematic of the arrangement of the encoders and counters in the prototype is shown in Figure 81.

Thus, the data acquisition software structure must handle the incremental roller encoder pulses as they become available as determined by the roll encoder. There are two basic approaches as to how the program interacts with the incoming encoder and caliper samples. While the caliper can be sampled at any time, the encoder samples come in packets that are available on unbuffered boards for only the duration of the time that it takes to wind the next wrapcount of layers. If the roll encoder counter is read too soon, no new data is available. Conversely, if the roll encoder counter is read too late, a sample will be irretrievably missed. Missing even a single sample in what may be thousands taken in the course of winding a roll will severely damage the data and must be avoided. To accommodate this variable timing of the encoder samples without 'missing a beat', the software can either operate in an interrupt driven mode, or in a polling mode.

Figure 81
ENCODER AND COUNTER SCHEMATIC



The simplest approach is the polling mode, where an additional counter (#2 for example) serves as a sample counter which increments by one every time the roll counter (#1 for example) decrements from its initial wrapcount value to zero. In the polling mode, the sample counter is read continuously until an increment is detected, at which time the program reads the roller encoder (#3 for example). Caliper values are read as often as possible during the time it takes to wind a sample and summed, so that an accurate average caliper can be calculated at the end of the sample. Though other schemes are possible, for simplicity the caliper is read every time the sample counter is checked. More caliper readings could be obtained per wrapcount if the sample counter is checked only every n^{th} caliper reading. However, the latency of responding to the new roller encoder samples would be increased such that there is an increased chance of a missed sample at high rewind roll rotational speeds.

A more complex but more computationally efficient approach is by using interrupts generated by countdown of the roll encoder counter to zero, which signals the presence of a new roller encoder sample. In this mode, the program's throughput increases because the sample counter does not have to be checked frequently for the presence of a new sample. Indeed, the sample counter is neither required nor desirable. Similar to the polling mode, the caliper is read as often as possible and summed, so that an accurate average can be computed at the end of the sample.

This type of programming is also known as background/foreground multitasking. The foreground task performs nearly all functions including initialization, reading caliper as often as possible, reducing raw data to engineering quantities, as well as printing, displaying, and saving data. The only functions of the background task are to read the roller counter and set a flag to tell the foreground task that a new sample is available. Though the foreground task is small and simple, it has absolute priority to put the foreground task to sleep temporarily while it processes the new encoder sample. The only communication between the two tasks is a single roller counter value and a data flag status which are both globally accessible by the foreground task.

Since the counter board does all of the necessary low level housekeeping of resetting counters and buffering input and output as explained in Chapter 6, both the polling and interrupt approaches will function identically. However, there are two reasons why the interrupt driven software can have a much higher throughput, which means potentially more encoder and caliper readings, and consequently better roll structure resolution. The first and simplest is that the program does not need to spend time reading a sample counter. However, in practice this overhead is only a small fraction of the total duty of the program, so that it does not in itself justify the additional complexity of interrupts.

The second benefit of multitasking for this project is if the maximum throughput of the program is increased by decreasing the required CPU time for a minimal handling of samples, instead of requiring all data processing and display be performed for every cycle. This can be accomplished by connecting the background data acquisition task and the foreground calculation and display task by a ring memory buffer. In this mode, the background task adds data to the top of the buffer as samples become available which is driven by the roll counter interrupt. The foreground task will read data off the bottom of the buffer as remaining CPU time permits for calculation and display.

Though using a ring buffer will not increase the average throughput, the maximum throughput is increased so that the peak sample frequency, as shown in Figure 54, is more easily accommodated. Additionally, the minimum wrapcount given in equation (116) is reduced because the maximum sample frequency is determined only by the background task execution time rather than the entire execution time of reading data, calculating and displaying a sample. One disadvantage of this approach however, is that when the buffer contains more than one sample, the display is lagging behind the winder so that the computer data acquisition system is no longer operating in real time. This lag was vividly shown on an earlier density analyzer system incorporating multitasking with a ring buffer, which continued to process data from a 10,000 FPM run for a minute after the winder had finished winding the roll.

Since interrupt driven multitasking has some advantage over polling, it was the first approach tried for this project. The first attempt at multitasking was to use relevant core portions of an earlier density analyzer system developed at Beloit which had a background task written in C and a foreground task written in Basic. However, many difficulties emerged when trying to extract the few lines of code from the nearly 10,000 lines in the original program without disabling its operation. Additionally, the original density program was written in a different version of C which used a real-time toolkit, as well as a different version of Basic, so that portability problems were also experienced. The second attempt was to modify a textbook example of keyboard interrupts. However, the program was very prone to shut down the hard disk drive and the problem was not resolved even after consulting an expert in PC programming. Perhaps this was the result of conflict between interrupt vectors or differences between the architecture of the PC-AT clone and an IBM PC-AT upon which the textbook program was based. The final attempt was to use a Basic interrupt toolkit provided with the Metrabyte CTM-05 counter card. Again, language version compatibility problems were unresolved.

Thus, after considerable effort, an interrupt driven structure was abandoned for the prototype in favor of the simpler polling mode. Though data integrity was not compromised in any way because the counter board latches samples, it required slowing the winder so that the wrap count times the rewind roll revolutionary period did not exceed the speed at which the computer could process a sample cycle. It is expected that future applications of this program would incorporate the faster interrupt driven approach.

Data Acquisition Program Structure

The data acquisition program for this project, written entirely in Borland's Turbo C 3.0, is composed of a main program which provides the framework for the application, calculates, displays and saves data. The main program calls two subprograms which initialize and read the counter card and analog/digital card respectively. The subprogram for the counter card is based in part on an earlier density analyzer program, and the subprogram for the analog/digital card is based in part from the Metrabyte Drivers Package from Systems Guild. The main program, counter subprogram and analog/digital subprogram, called DRWIND.C, drctm05.h and drdash16.h respectively, are included in the appendices and will each be discussed in turn. Although the program is set up for polling, only a few modifications would be required to convert the program to interrupt driven execution.

The main program, DRWIND.C, begins by setting up a storage array for roller pulses as an unsigned integer, and caliper as a float. Then execution enters the main loop of the program which first reads the caliper from analog input channel #1, which is later summed to yield an average calculation, and then reads the counter board. There are three possible cases from a poll of the sample counter #2, each of which must be handled differently. These cases are no increment, and increment of one, and an increment of more than one.

If the sample counter #2 shows no increment, the loop of reading the caliper and sample counter is repeated. This means that a new sample is not available. If the sample counter #2 shows an increment of one, the roller counter pulses and average caliper are stored in their respective arrays. This means a new sample is available. Additionally, the sample number, roller counter, caliper value and number of caliper readings during that sample cycle are printed to screen for operator feedback. If the sample counter shows an increment of more than one, a sample has been missed and an error is printed to the screen. If this occurs it will not be possible to 'splice' data across such an event.

After the data acquisition run is terminated either by exceeding the maximum memory storage of about 10,000 sets of samples or on keyboard hit, the sample number, the roller pulses and average caliper arrays are written to disk for later processing into diameter, density, radial compression or stress calculations. An outline of the main program is as follows:

```
initialize program
main
  print startup screen
  initialize Metrabyte CTM-05 counter card
  initialize Metrabyte Dash16 analog/digital card
  enable counters
  while sample # is less than maximum storage and keyboard not hit
    if number of caliper readings less than 32000
      increment caliper reading counter
      read caliper and add to caliper sum
    read counter card
    if new counter sample available
      store roller counter #3 value to array
      compute and store average caliper to array
      print to screen
      zero the caliper reading counter and caliper sum variable
  disable counters
  save data arrays to disk drive
print startup screen subprogram
save data array to disk subprogram
```

The counter subprogram, `drctm05.h` must first configure the operation of the board and each of the five counters from the many possible modes of operation. This includes setting the roll counter #1 in a decrement mode with inputs from channel #1, and the sample counter #2 and the roller counter #3 in an increment mode with inputs from the output of counter #1 and channel #3 respectively. The inputs and outputs for each of the counters may be either physically wired as in the case of the inputs for counters #1 and #2 and outputs from counter #1 to the interrupt, or selected in software such as counter #2's input from the output of counter #1. Additionally, the input triggers must be selected as either rising or level edged. Details of the configuration of this particular counter can be found in the manuals for the Metrabyte CTM-05 board.

During data acquisition operation, the sample counter #2 is read to check for an increment of one. If so, the roller counter #3 and other optional counters are read into a small global data array. Since the counters are 16 bit, while the bus is only 8 bit, the count value must be read as two consecutive 8 bit values from each counter. The total count for each counter is then the low byte plus 256 times the high byte. An outline of the counter program is as follows:

```

initialize program
initialize counter board subprogram
    initialize the master mode register
    for counter #1 to #5
        initialize each counter from a configuration array
    zero all counters
    load counter #1's load register with the wrap count pulse value
read counter board subprogram
    read roll counter #2
    counter flag = sample # - old sample number
    if counter flag = 0
        no new data
    if counter flag = 1
        increment sample #
        read counters #3 to #5
    if counter flag is not equal to 0 or 1
        print error message

```


The analog/digital subprogram is considerably more complex due to the much wider variety of data acquisition and control options of the 16 channel Metrabyte Dash16 board, and will not be discussed in detail. The programming of this board was simplified using portions of the Metrabyte Drivers Package from Systems Guild. It was more expedient to only use relevant portions of the drivers rather than the whole package because there were numerous incompatibilities between the supported list of C compilers and the Turbo C used for this project. The functions used in this subprogram are shown below:

adcD16 - single channel analog to digital conversion
 adcranD16 - sets the conversion channel range for the hardware
 controlD16 - sets up the interrupt, dma and conversion modes
 dacranD16 - sets up digital to analog conversion channel range
 initD16 - initialize IO base address, dma channel etc
 intvID16 - sets timer interval
 lfactor - splits a long into two factors

Though the entire data acquisition program is very plain, it is functional, short and reasonably efficient. More important however, good modular programming practices were used, so that the program is not hardwired to this particular application, but rather is easily expanded to additional capabilities. Changing counter or analog configurations, or adding channels is made relatively easy by numerous define statements and configuration arrays. For example, the counter board can be reconfigured so that an internal clock and/or additional rollers can be read on the unused channels #4 and #5. Similarly, additional analog input channels, perhaps for torque, nip, tension or speed, could be read and stored. For this development prototype however, additional capabilities were not considered because memory and throughput would be reduced for the important parameters of roller counter pulses and analog caliper values.

Program Profiling

Data acquisition throughput is an important parameter that in part determines the maximum rotational speed of the rewind roll and minimum wrapcount. If the computer/software system is too slow, the data acquisition cycle may be overrun and samples will be missed. For this project in particular, the program must be able to read the encoder counters and the caliper gage at least once during the minimum time it takes to wind the layers of web corresponding to the wrapcount setpoint, which usually occurs at the end of the acceleration cycle shown in Figure 54.

One way to measure throughput of a computer program is to use software profilers, which are supplied with some C language development packages. These profilers are small programs that monitor the amount of time spent in user selected portions of the main application. Using these profilers, the software developer can determine quantitatively what portions of the code require the greatest CPU time, so that further development effort can maximize processing speed most effectively. These profilers unfortunately consume some CPU time themselves, so they affect the timing of the software they are trying to measure. Thus profilers may underpredict throughput of software such as data acquisition applications that are free running at high frequency. Additionally, these profilers may not be able to appropriately measure the timing of programs whose execution varies considerably such as during the highly variable winding cycle.

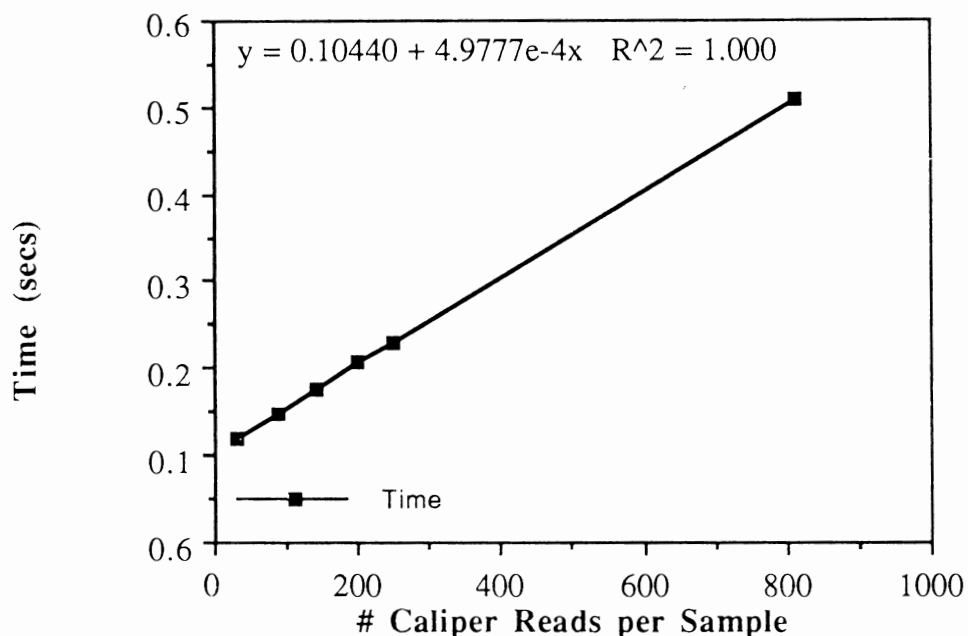
Another alternative to internal timing using software profilers is to use external timing. This approach is commonly used to benchmark programs where the execution time of one or more cycles of a program or subprogram is timed with a stopwatch. Wound roll rotational frequency, determined by surface speed and current diameter, can be used as an external clock to measure throughput of this program. In particular, the number of caliper readings per sample, which must be greater than zero, as a function of the time it takes to wind layers corresponding to the wrapcount value will not only benchmark the program, but will also determine how much time is spent on the data acquisition task versus the calculation and display tasks.

The number of caliper readings per sample, which is printed to the screen and used to calculate average caliper, can be used along with winder speed and diameter to calculate distribution of CPU time as seen in Figure 82. From this data, it takes only 0.5 milliseconds to read and sum the caliper, and read one counter. However, it takes 104 milliseconds to read three counters, compute an average, store data to an array, and print four numbers to the screen. Since the vast majority of CPU time is used to print numbers to the screen, large increases in sample frequency could be achieved by simply reducing the amount of data printed to the screen.

Since the sample number and the number of caliper readings per sample are not very useful for production applications, the throughput would be nearly doubled by eliminating these print statements. Secondly, the data need not be printed every sample, but only every n^{th} sample. The parameter n might be sized to give about 10-100 prints per winding cycle, which is enough for the user to be assured of proper operation, but not enough to create a fine real time picture of roll structure, which would have to await postprocessing. With these project runs for example, only printing two numbers on the screen every 25 acquisitions would yield up to a 50 fold increase in throughput.

Figure 82

DATA ACQUISITION PROGRAM EXECUTION TIME



Another observation that can be made from Figure 82 is that due to the large print overhead, a latency safety factor should be used so that at least one caliper reading, if not many more, should be made with reliability so that missed samples would be rare. If an additional 10% cushion above the required 104 milliseconds is desired, the curvefit indicates that an average of 20 caliper readings per sample would be made. In actual practice, the uncertainty in print latency seriously impaired reliability if the winder speed was above that which produced about 50 caliper readings per sample. Finally, there is no point in reading the caliper gage faster than its response (approximately 30 Hz).

Many of the first runs were made using the normal high acceleration of the lab winder, which caused an overrun of the data acquisition for until the wound roll reached about 18" in diameter. Consequently, for the winder runs numbered 32-41, the winder was accelerated slowly maintaining a minimum of 200 caliper readings until reaching 500 FPM at about a 12 inch rewind roll diameter, at which time the rest of the winding cycle was run at a constant surface speed of 500 FPM. This slow speed is not necessary for production applications, but it might have been helpful for this prototype where the effects of air entrainment on caliper measurements, slippage, and other undesirable behavior were to be reduced while maintaining an extremely low wrapcount.

Data Preprocessing

The design philosophy of the prototype was to both gather data with the best resolution possible, as well as preserve as much flexibility as possible. Attempts to increase data resolution meant using extremely high count encoders. For the latter runs, the encoders used yielded an effective 100,000 pulses per revolution, which was an order of magnitude greater than used on any other density-like instrument. Additionally, extremely low wrapcounts were used so as to increase the number of raw data points which could be used to construct final calculated values. This both slowed the throughput of the prototype and made data set sizes approaching 10,000 samples (200Kb) per run. However, the rationale was that data volume could be reduced after acquisition if need be by simple averaging, but it could not be made finer than originally constructed. Thus, it was hoped that this high data volume would be useful for increasing resolution, allow discrete errors to be more easily detected and corrected (Chauvent's principle or other technique), and giving more berth for applying smoothing and filtering techniques.

The desire for flexibility was achieved by isolating the acquisition task from any consequential calculations which might be difficult to undo. Thus, the acquisition task only stored the raw roller encoder count and caliper value data. However, because the raw data was taken on such fine intervals as described above, it needed preprocessing to average or smooth it sufficiently to be suitable for inputs to density, radial compression or stress calculations. Chapter 6 contains a more detailed discussion of data noise. Thus, a data preprocessing task, DRcompress, was written which reads the data stored on disk from the acquisition task, smooths the raw data, as well as calculate and writes radius, density, radial compression, displacement, and caliper to disk.

Smoothing the encoder and caliper data was the most difficult task, as a variety of techniques were tried with mixed success. However, the following preprocessing combination seemed to yield the best results.

1. smooth roller encoder count and raw caliper
calculate diameter and caliper
2. average diameter and caliper,
(smoothing # = averaging #, corresponding to about 0.05" on radius)
calculate density, deflection, and/or radial compression
3. digital lowpass filter of density, deflection, and/or radial compression
(digital lowpass filter value setpoint approximately 2)

where the strength of the digital lowpass filter can be adjusted by the user prior to the data conditioning run in the algorithm shown below

```
C = VALUE(1)
FOR Q = 3 TO N
    VALUE(Q) = VALUE(Q) + VALUE(Q-1) - C*(1-2*STRENGTH)
    C = VALUE(Q)
NEXT Q
```

A final issue in data preprocessing that the effective wrapcount determined by the value of averaging must be set so that data noise is reasonable. If it is too fine the noise will be excessive, and if too coarse the spatial resolution of the resulting calculated plot of density or other values will be too coarse to detect small duration events such as splices or even speed changes. Though the averaging value effects the plot noise, the statistical resolution as defined in Chapter 10 is relatively unaffected. Thus, the wrapcount multiplied by the averaging is typically set to be aesthetically pleasing.

However as mentioned in Chapters 3 and 7, winding models have an optimum grid size for maximum accuracy, which will not likely be the same size as the effective wrapcount acquired by the instrument. Fortunately, the solution for matching the acquired wrapcount and the required model grid size is straightforward. If the required grid size is coarser than the acquired data, the acquired data is simply averaged. If the required grid size is finer, the acquired data is replicated. In either case, the deflection is proportional to effective wrapcount or grid size as seen in equations (28). Thus for example, if the acquired data is replicated by a factor of 10, then the calculated deflection must be divided by 10.

The result of improvements in density analyzer hardware, the addition of caliper measurements, and improved data conditioning has simultaneously reduced the noise of displayed data points and increased the spatial resolution an order of magnitude better than previous density analyzer setups. Additionally as will be seen in Chapter 10, the sensitivity of the new system to roll structure changes has been statistically determined to be approximately an order of magnitude better than any other roll structure measurement method.

Conclusion

This chapter has described the somewhat dry mechanics of the operation of the data acquisition hardware and software. However, this aspect of the project is important as the serial nature of this displacement to stress approach requires that each component, which includes the data acquisition and preprocessing, maintain data integrity as best possible. Furthermore, any future developments of this approach need be aware of the many issues brought forth here and in other chapters.

Since the software was written strictly for prototype development and use by the author only, there are several improvements that should be considered in future work. First, the high count encoders and very small wrap counts used to attempt to improve resolution simply did not pan out. As mentioned in Chapter 6, the law of diminishing returns applies where improvements resulting from anything above about 10,000 pulses per revolution is masked by other winding equipment sources of noise. Thus, more modest encoders and increased wrap counts are indicated which will greatly speed data throughput and reduce data volume.

Secondly, the data conditioning could be merged with the data acquisition tasks if sufficient experience is gained in a particular operating environment. Thirdly, the program should be converted from polling to interrupt driven to increase throughput. Similarly, the data acquisition screen output can be reduced for increased throughput. This should lead to instruments capable of keeping up with a 10,000 FPM winder, as already demonstrated by similar density-like programs marketed by Beloit. Finally, the plain programming for this prototype has a minimal user interface, which must be expanded for general use. It is anticipated that if this project is implemented by others for either lab studies or production quality control, that an enhanced version of this software will be written which is tailored for a specific application or environment.

CHAPTER 10

SENSITIVITY ANALYSIS

Introduction

This project takes direct measurements of wound roll diameter and web caliper and uses those measurements as inputs to calculate a wide variety of wound roll quantities. These include web length, speed, and density which were previously available by other means. Additionally, this project introduces at least three new measures of roll structure: caliper corrected density discussed in Chapter 6, as well as radial compression and calculated stress profiles which were both discussed in Chapter 7. However, in order to implement these new measures, many developments in wound roll data acquisition were also required as described in Chapter 8. Though the density analyzer does provide the required diameter measurement, it needed to be supplemented by (on-line) web caliper measurements. Furthermore, the precision and resolution of the measurements had to be increased beyond that typical of presently available density analyzers.

The multi-faceted net result of this project can be roughly divided into two areas; experimental developments and analytical modeling developments. Each of these areas must be evaluated in terms of both accuracy and resolution against an independent measure. Thus, this chapter begins with a discussion of accuracy and resolution. Then, the resolution of the radial compression measurement is evaluated by comparing with several popular present methods such as the Rhometer and WIT-WOT winder. This evaluation results from a novel statistical technique developed by the author for comparing sensitivities of instruments which measure in different fundamental quantities or units. Next, wound roll model accuracy is discussed in general. Finally, the displacement-to-stress wound roll model is evaluated for accuracy, numerical stability, and sensitivity to uncertainties in mechanical properties. We will see that while the new measurement method is very sensitive compared with previous methods, the model is demanding in terms of the scope and accuracy of required input parameters.

Accuracy and Resolution Overview

Since the terms accuracy, precision and resolution are often used loosely and synonymously, it is important to bear in mind the distinction used in the discussion of this chapter. Accuracy is the ability for a measurement system to closely reproduce an independent measure, which may be a standard, reference, or alternative measure that is assumed to be more exact and precise. For example, a strain reading on a simple structure under an uniaxial load should give a value close to that calculated by the measured load, cross-sectional area and modulus of elasticity. Crucial to evaluation of accuracy is the existence of an independent measure, with assumed or demonstrated precision. In general, accuracy is often calibrated by a zero and span adjustment against a standard reference.

Resolution is the ability to statistically discern small changes in a relevant and desired measurement parameter; despite sources of noise which increase data uncertainty and undesirable cross-sensitivity to other parameters. For example, a strain gage system measures deformations in a structure, but may have an undesirable sensitivity to changes in temperature. Other strain measurement systems such as brittle coatings may have a greater cross-sensitivity to typical changes in application, temperature, and humidity than they do to the strain parameter which is to be measured. In general, resolution is improved with care in setup, and by properly matching the range of measurement to the application.

However, evaluating roll structure measurement accuracy and resolution is much more difficult than more traditional measurements such as time, length and force for example. One reason for this is that the quantification of roll structure is a relatively new science with only about three decades of development. As a result, few commercial instruments and only one standard exists for roll structure measurement. Another reason, is the practical difficulty of sensor or instrument development that is suitable for the harsh environment of the winder. Furthermore, since only the exterior of a roll is accessible without damaging the web, it is difficult to determine the state of the interior from surface measurements.

Finally, this project is the marriage of both new experimental and analytical techniques which must be separated to analyze their independent contributions to the overall system. This is especially important due to the serial nature of the new system. For example, errors and uncertainties in the initial data acquisition measurements will propagate downstream through to the calculated results. However, good raw measurements processed through calculations which are not numerically stable may result in a similarly appearing results. Thus, the need to separate measurement from calculation.

At this time, it is appropriate to discuss the relative importance of both accuracy and resolution. For both production quality control, as well as lab research studies, resolution is the more important of the two criteria. This is especially true at the time of this writing where there is a near total absence of quantitative first principle roll defect theories based on stress parameters. For quality control, roll structure measurements can and are most useful even if they are not accurate due to the lack of an independent calibration against a known stress or other reference, such as with the Rhometer or density analyzer. Implementation of quality control can be as simple as merely comparing roll structure profiles of a sampled roll against those judged to be acceptable or unacceptable [156]. Indeed, this is the mode of operation of nearly all winders where roll quality is measured. The only real compromise is that the measure of acceptability must be defined for each significantly different grade that might be wound on a winder. As long as a method has good resolution, which many unfortunately do not, and is practically implemented, which unfortunately many are not, the method can be useful without the requirement of accuracy.

The premise that resolution is more important than accuracy, even for research applications, is also easy to demonstrate with the case of the Cameron Gap. Though in principle the gap test should be very accurate because it is based on basic and simple physics of elongation which can be independently verified, the test is almost useless due to extreme data noise. Thus without resolution, accuracy has no application. However, without accuracy, resolution does have lab application. For example, if a study desired to know which of the TNT's caused the more significant roll structure change for a given system, a measurement with resolution only might yield that answer. Thus, resolution without accuracy still allows detection and ranking of many roll structure changes.

However, once a good resolution has been achieved, such as will be demonstrated with this new system, then it is important to turn attention to the accuracy of stress measurement. There are two principal reasons why stress measurement is very important. The first is that a desirable stress profile does not depend as significantly on small differences in web material, as do other measures. Indeed, the typical wound-in-stresses for many grades of film, paper and textiles are similar, allowing some generalizations between materials to be made. Secondly, it is anticipated that quantitative first principle roll defect theories will be developed and validated in the near future. Since these will almost undoubtedly be based on mechanics formulations, practical measurements of stress will be crucial to their ultimate application outside of the laboratory.

Roll Structure Resolution

Comparing the resolution of the various roll structure measurements is difficult because there are no established standards. This is exacerbated by the fact that nearly all of the measurement types have different scales, and there are few first principle or empirical conversions between them. However, this resolution comparison problem was addressed previously by the author in a paper on roll quality measurement [169, 171], and will be discussed in more detail shortly. The technique developed was to wind a roll with a large step change in torque, nip, tension or caliper. Then a series of roll structure measurements of the various methods were made on each side of the step. Finally, statistics were used to determine the number of measurements required for each of the methods to discern a specified step size to a specified statistical confidence. With this method, the resolution of different measurement types could be quantitatively ranked for a grade of web, even if the quantities or scales were different.

Resolution of a roll structure measurement is the sensitivity to changes in the wound roll such as the TNT's of winding, and a limited sensitivity to extraneous parameters that increase data uncertainty and noise. One measure of resolution is repeatability. If for example, we make two nominally identical measurements of tension, we would expect nearly identical values. This would be easy to check for those methods which do not alter the roll in the process of testing. However, if the density analyzer is used to profile a roll, it can't be rewound identically to make another run to check for repeatability. Similarly, the Cameron Gap cannot be checked for repeatability because once a layer is severed to measure the gap, the process cannot be repeated on that same layer, and subsequent layers may be under different tensions. Also, the impact based hardness tests such as the Rhometer and Schmidt Hammer can't be checked for repeatability because the impact compacts the paper at that location making subsequent readings higher, and adjacent positions may be at different levels of hardness.

Factors that affect repeatability are sensitivity to operator technique and measurement noise. Typically, those test methods that are manually operated, and particularly those that are handheld, are very sensitive to operator technique. Though the readings taken by an experienced Rhometer, Schmidt Hammer, or Smith Needle operator may be consistent and repeatable within themselves, they may have a different bias or offset than those taken by a different experienced operator. Those who have less experience operating handheld testers will find considerable scatter in their readings as they alter the exact grip and motions slightly during a series of readings. If a short term study of roll structure requires high quality data, a single experienced operator should perform all of the testing, as was done for this project.

Roll structure measurements are often sensitive to orientation and gravity. If handheld testers are not oriented consistently, noise will be increased. Gravity will always influence measurements because the stresses at the top of the roll are different than at the bottom and sides. Web stresses are the superposition of internal stresses known as roll structure and external stresses due to gravity and support loading as discussed in Chapter 4. One example is a core supported roll, which will have higher readings at the top than the bottom. Similarly, different readings will be obtained if the roll is stored on end, or laying on the floor than when it is supported at the core. Because of this, it is important that the most convenient orientation of instrument and roll be established, and that all tests be performed to that standard for consistency.

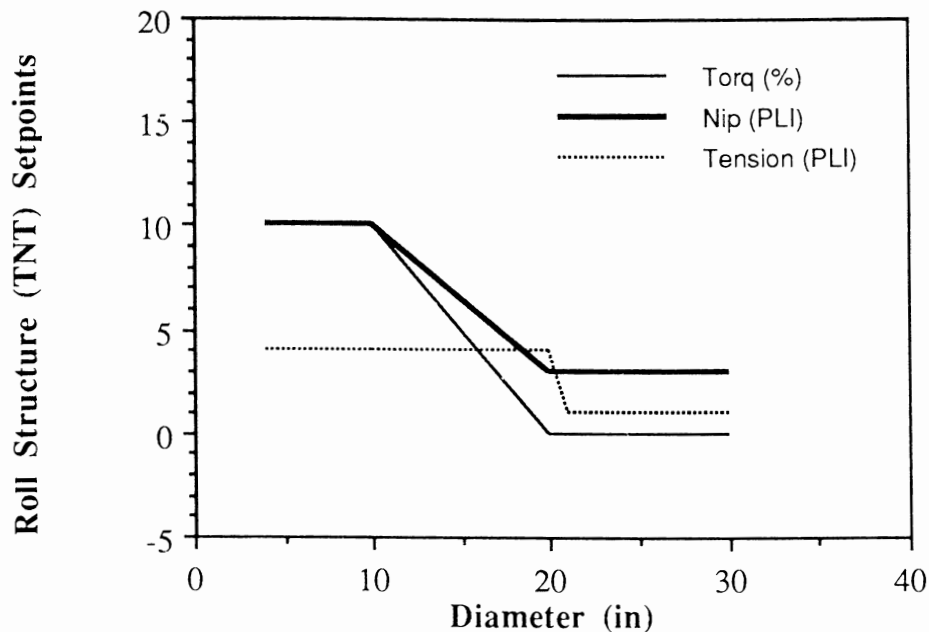
The effect of measurement noise is to decrease the ability to reliably discriminate changes between one roll and the next, or between positions on the same roll. The easiest way to increase the accuracy of roll structure testing is to decrease noise by taking many readings and reporting the average. Though this will increase the cost of testing, in principle any specified level of effective resolution can be obtained simply by taking enough measurements.

To quantify resolution, several observations can be made. First, the measurement must be sensitive to changes in the stresses in a roll, as a function of the TNT's for example. One way to induce a change in roll structure is to wind a roll with a step change in torque, nip, tension and/or caliper. The second observation is that though in principle any specified level of effective resolution can be achieved by simply averaging enough readings, the best measurement methods would detect roll structure changes with the fewest individual readings. The lack of repeatability testing coupled with these observations led the author to develop the only current method of evaluating roll structure testers [169, 171].

To input a known change in roll structuring, a sudden step change in the TNT winding parameters is made at some intermediate diameter. The larger the step, the more accurate will be the evaluation of test methods under consideration. From the core to 20 inches, as much torque, nip and tension is applied as the sheet will reliably tolerate. Then at 20 inches, the torque, nip and/or tension is dropped as much as possible. Figure 83 shows a large step drop from 4 PLI to 1 PLI in tension occurring at a diameter of 20 inches. The object here is not to wind a good roll, but to evaluate the resolution of test methods. If a method can't discriminate gross changes to the roll such as this, which some can't, then it will be of no use whatever to sense smaller and more typical changes seen during winding. Another method to apply a step input would be to splice together two widely different caliper rolls at the unwind, and wind them into a single roll without making a step change to the TNT parameters.

Figure 83

TNT STEP CHANGE TO EVALUATE RESOLUTION



Once this unusual roll has been wound, it must be unwound while carefully making numerous measurements with each of the methods to be evaluated. A minimum of 5 measurements should be made with each of the instruments at diametral increments of 2 inches. Some planning is required in the sequencing of the measurements. The density analyzer must be run on the roll as it is wound. The friction based Core Torque, Pull Tab and Smith Needle should be done prior to unwinding. While most of the other methods would be done on a rewinder's unwind, the Cameron Gap must of course be done last because it destroys the roll for future measurement.

Plots of each of the measurement methods against roll diameter are then made which would desirably show a step decrease in hardness, tension, or whatever roll structure scale is used, at the diameter corresponding to the change in roll structuring input. Though a subjective evaluation of resolution can be made by the visual size of the step in comparison with the noise on the nominally level sections on either side of the step, a quantitative and better evaluation can be made if statistics are applied. In particular, the Z-test for the significance of the difference of means are be applied to data 1-2" on either side of the step.

The Z- test is given as [177]:

$$(145a) \ z = \frac{\mu_1 - \mu_2}{SD} \text{ where}$$

$$(145b) \ SD = \frac{\sigma_1}{n_1^{1/2}} + \frac{\sigma_2}{n_2^{1/2}}$$

and where

z = z test parameter taken from s-normal distribution table

SD = standard error of the estimate

μ_1 = mean 1-2" before the roll structure step

μ_2 = mean 1-2" after the roll structure step

σ_1 = standard deviation before the roll structure step

σ_2 = standard deviation after the roll structure step

n_1 = number of measurements before the roll structure step

n_2 = number of measurements after the roll structure step.

For simplicity, the number of measurements before and after the step, n_1 and n_2 , can be made the same and called n_{measured} . Thus, solving equations (145) for z_{measured} gives

$$(146) \ z_{\text{measured}} = \left[\frac{n_{\text{measured}}^{1/2} (\mu_1 - \mu_2)}{(\sigma_1 + \sigma_2)} \right]$$

where z_{measured} is the value where the normal table is entered to find the corresponding confidence level in per cent. As seen from equation (146), the statistical confidence in detecting the difference in means will increase with the number of measurements made and the difference in means, and decrease with increasing standard deviation or data scatter.

However, it may likely be that the number of initial measurements were too low to give a desired statistical confidence as given by equations (145), or too high to be practical. Thus, equation (146) can be also be written for a desirable confidence level to predict the required number of measurements as

$$(147) \ z_{\text{desired}} = \left[\frac{n_{\text{required}}^{1/2} (\mu_1 - \mu_2)}{(\sigma_1 + \sigma_2)} \right]$$

Solving equations (146) and (147) simultaneously for the required number of measurements to yield a desired confidence level gives

$$(148) \quad n_{\text{required}} = n_{\text{measured}} \left(\frac{z_{\text{desired}}}{z_{\text{measured}}} \right)^2$$

Thus from equation (148), the number of required measurements can be calculated given measurements for each side of a step for which the z_{measured} statistic is calculated, and from a z_{desired} determined from a desired confidence level and the normal table. For this project, the desirable confidence level used was 90%.

The procedure for determining resolution is as follows:

1. Wind a roll with a large step change in torque, nip and/or tension near the midpoint diameter.
2. Take several measurements, at least five and the more the better, at 1-2" on each side of the step.
3. Compute z_{measured} from equations (145).
4. Compute n_{required} from equation (148).
5. This test, though time-consuming, should be done at least once for each grade and measurement method because different grades behave differently; and wound rolls and measurements have uncertainty in themselves, which yields some uncertainty in the resulting evaluation. Additionally, the size of the step used in the test and the number of measurements taken should yield a high z_{measured} to reduce evaluation uncertainty.

There are several issues that result from this work. First, until now the step size was desirably large to increase the resolution of the ranking itself, but unspecified in size. Additionally, a good roll structure measurement method must not only statistically discern the artificially large step produced by this step, but more important, the arbitrarily smaller changes seen in actual winding. However, this same procedure can be used to determine the number of required measurements for any arbitrarily sized step in a similar manner as above only using a smaller difference in means for equation (147). Thus, the number of required measurements are

$$(149) \quad n_{\text{required}} = n_{\text{measured}} \left(\frac{z_{\text{desired}}}{z_{\text{measured}}} \right)^2 \left(\frac{\Delta\mu_{\text{measured}}}{\Delta\mu_{\text{desired}}} \right)^2$$

As seen from equation (149), the number of required measurements increases as one over the square of the size of the desired detectable difference. Thus, it takes four times as many measurements to discriminate changes half the size, and 100 times as many measurements to discriminate to a change 1/10 the size. Clearly, measurement resolution is a very important test design consideration. Additionally as we will see shortly, there is an extremely wide range of resolutions among the various methods.

Another issue that arises is that several methods such as the WIT-WOT, density analyzer and stress calculation does not necessarily have only a discrete number of displayed data points upon which to evaluate resolution. For example, with the same raw data a density analyzer may average 10 sets of raw data to yield a displayed point, or only 5 to display a point on a graph. As the amount of averaging increases, the spatial resolution decreases because there are fewer resulting points. However, each point has been more heavily averaged and consequently has a reduced variance. Thus, these devices can increase the number of displayed points at the expense of increased noise or vice versa.

To accommodate these 'analog' type measurements into the above formulas, one simply interprets n as the number of inches of web added to the diameter of the roll corresponding to any displayed sample size, instead of the number of measured points. It should not be surprising that the statistical measurement resolution of the 'analog' devices are not largely effected by changing the amount of averaging used to produced final data. This is because the resolution is dependent largely on the required amount of material that must be sampled (wound into the roll) before a statistically significant amount is obtained. In other words, many high variance points from low averaging carry a similar significance as do fewer low variance points from high averaging. Thus, the degree of raw data averaging for plots of the WIT-WOT and density-like methods is primarily a matter of taste.

The final issue generated by this type of roll structure measurement evaluation is that conversion formulas between the methods can be generated from the results. Since two values are known for several devices, one for each side of the step, a conversion formula of the form $y = mx + b$ is readily calculated, assuming monotonically continuously increasing measurements, which is true for all the methods, and linearity, which is approximately true for the methods. Thus, it is possible to convert Rhometer readings into wound in-tension for example. However, it must be understood that this empirical conversion will be only valid for a particular web grade wound under very similar circumstances, and that extrapolation to other materials and conditions is likely to be unreliable.

Radial Compression Resolution

In this section, a comparison of the new system with other commonly used roll measurement methods will be given. The desire is that this project has resulted in a measure with an improved sensitivity to changes in roll structure, and an immunity to sources of measurement noise. As given earlier, the net effect of the desirable sensitivity to roll structure and the undesirable sensitivity to noise is statistically quantified by the number of measurements required to obtain a specified confidence for a specified roll structure change.

Though the new project can calculate several different roll structure measures, Radial Compression is selected for comparison for several reasons. First, Radial Compression is a potentially stand-alone product of this new project and may have merit of its own. Secondly, the Radial Compression calculation follows directly from the diameter and caliper measurements so that numerical uncertainty is eliminated, leaving only a measure of the quality of the new instrumentation. Finally, Radial Compression is a nondimensionalization of the displacement boundary condition which drives the new stress model.

The resolution evaluation testing for this project was done on a roll of NCR paper, for runs #38 and #41, which had a step drop in tension from 4 PLI to 1 PLI at a rewind roll diameter of 20". The Rhometer, Schmidt Hammer, Smith Needle, density analyzer, and radial compression data versus roll diameter are plotted in the next several figures. Additionally, results from earlier testing on LWC and newsprint papers are also included [169, 171]. Finally, the results of all testing of this nature is summarized in Table 14. The legend on these graphs include the material, run number, the number of raw data points averaged to produce a display point, and the resolution as defined earlier.

The Rhometer profile, shown in Figure 84, may be visually interpreted as having a step drop. However, despite hundreds of manually obtained readings, the results are disappointing and ambiguous. The Schmidt Hammer, shown in Figure 85, appears to show no sensitivity to the step drop in roll structuring, but rather seem to be composed almost entirely of noise. However, the Smith Needle shown in Figure 86, does reflect a very noticeable step. The Cameron Gap test performed so poorly for Newsprint, shown in Figure 87, LWC which is not graphed, and other non-published work, that it was not even considered for testing on this project. Nearly 400 manually obtained measurements are needed to produce these plots, and each displayed data point in these graphs is the result of averaging 10 raw data readings.

Figure 84
RHOMETER HARDNESS VS DIAMETER

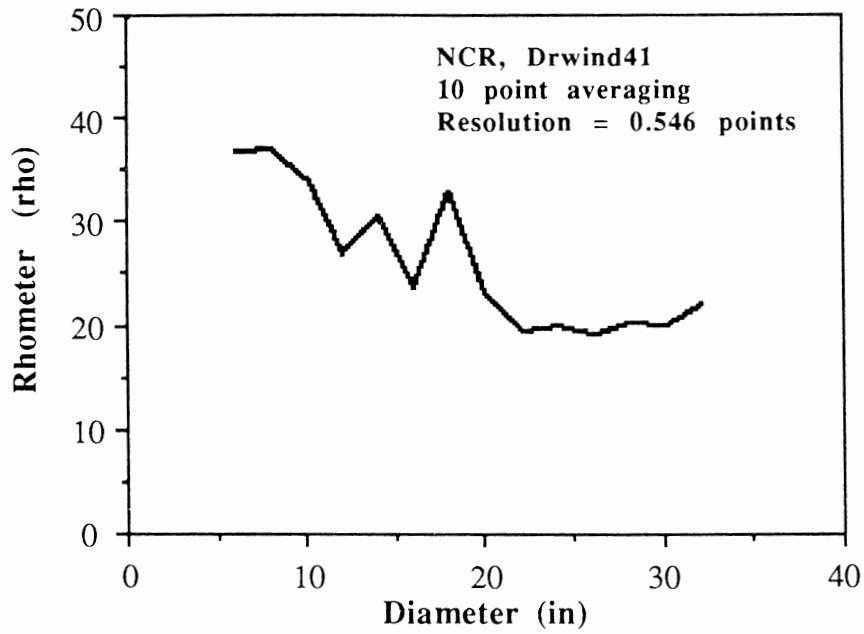


Figure 85
SCHMIDT HARDNESS VS DIAMETER

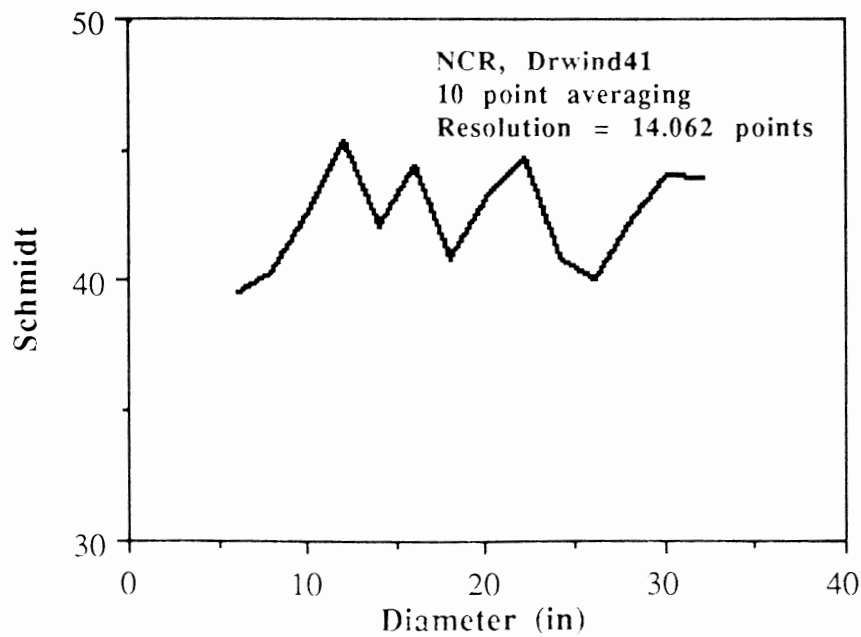


Figure 86
SMITH HARDNESS VS DIAMETER

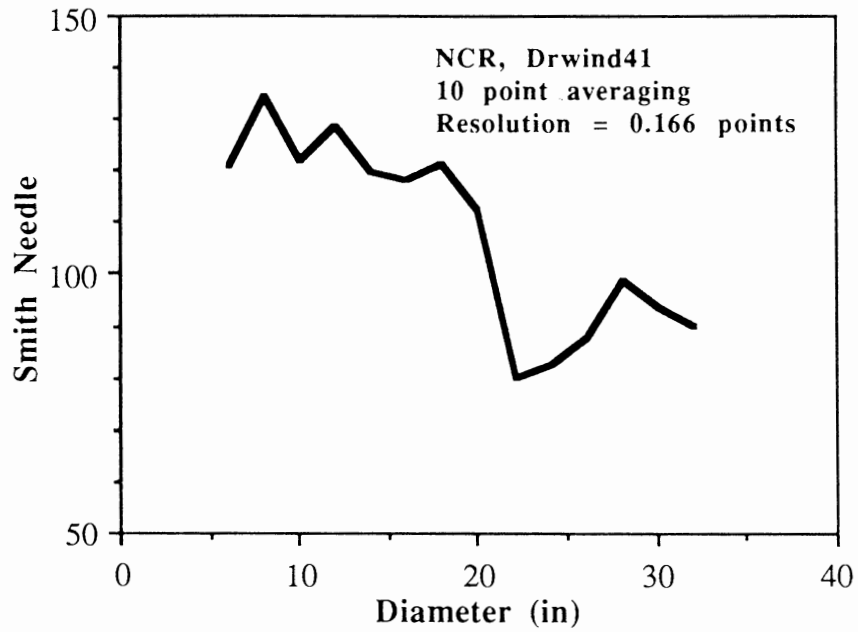
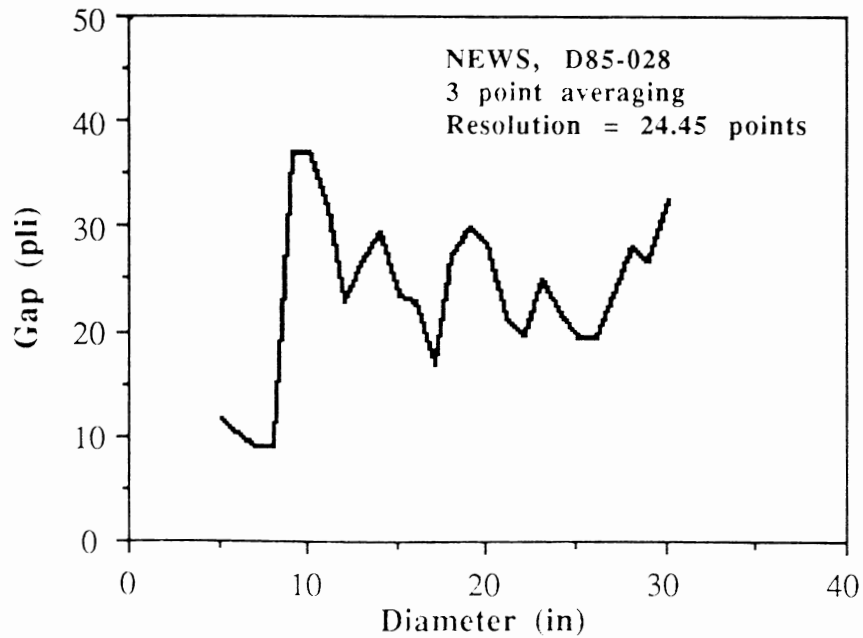


Figure 87
CAMERON GAP VS DIAMETER



The two density analyzer plots, shown in Figures 88 and 89, are apparently sensitive to the step change in roll structure, but contain some amount of noise due primarily to changes in the incoming caliper. Radial Compression, which is a new parameter defined by this project and shown in Figures 90 and 91, gives an unusually fine mesh of data, appears to be relatively sensitive to roll structure changes, and relatively immune to noise. Figure 90 shows more discontinuities that are due to a web break at 9", as well as due to a roll that was getting very beat up by the 10th run. However, Figure 91 for the same roll wound earlier shows a level of roll structure detail and sensitivity that is unprecedented in the thousands of roll structure plots this author has previously witnessed. The trend to note is that the new Radial Compression plot shown in Figure 90 is not only displayed at a finer resolution, it does so with considerably less noise. This is the result of the addition of caliper information as discussed in Chapter 6. The net result is an order of magnitude greater statistical resolution with this new system.

Finally, the WIT-WOT shown in Figure 92, also gives high sensitivity and detail. This is the result of a recent addition of continuous monitoring of the WOT load cells by computerized data acquisition. The WIT-WOT winder is a reference point for the best in roll structure accuracy and sensitivity. The trend to note is that again the new Radial Compression measure has met and exceeded the resolution of the best previously obtainable measure. However, this new system developed here has another distinct and important advantage since it can be applied to most any lab or production winder or unwind, while the WIT-WOT is a specialized instrument that exists in only a few locations in the world.

Table 14 summarizes the resolutions of all methods tested both for this project and previous work [169, 171]. The quantification of resolution agrees with earlier visual observations that there is considerable difference in the performance of the various methods. The Cameron Gap and Schmidt Hammer consistently performed so poorly that little useful data projects above the noise. The Rhometer, density analyzer and Smith Needle, though containing much noise, can discern reasonably small roll structure changes given a sufficient number of measurements. The WIT-WOT and new Radial Compression measures have significantly better resolutions than the other devices.

However, the reader should be aware that both the resolutions and to some extent the ranking of the resolution of these methods can be very application dependent. For example, some devices perform better on soft materials than hard. Therefore conclusions should be based on testing for a specific application instead of applying the results as generalizations.

Figure 88
DENSITY VS DIAMETER

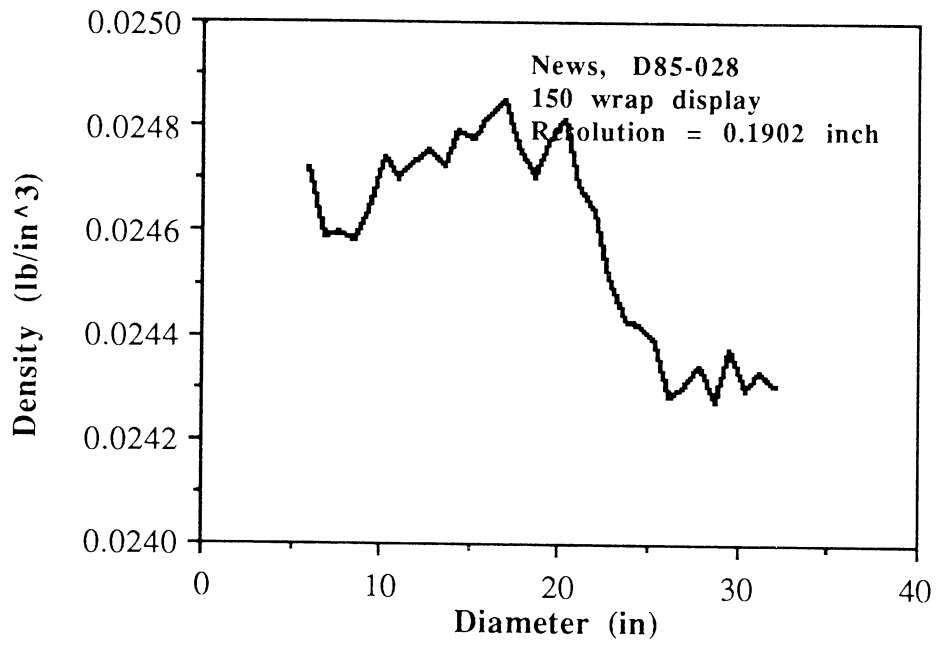


Figure 89
DENSITY VS DIAMETER

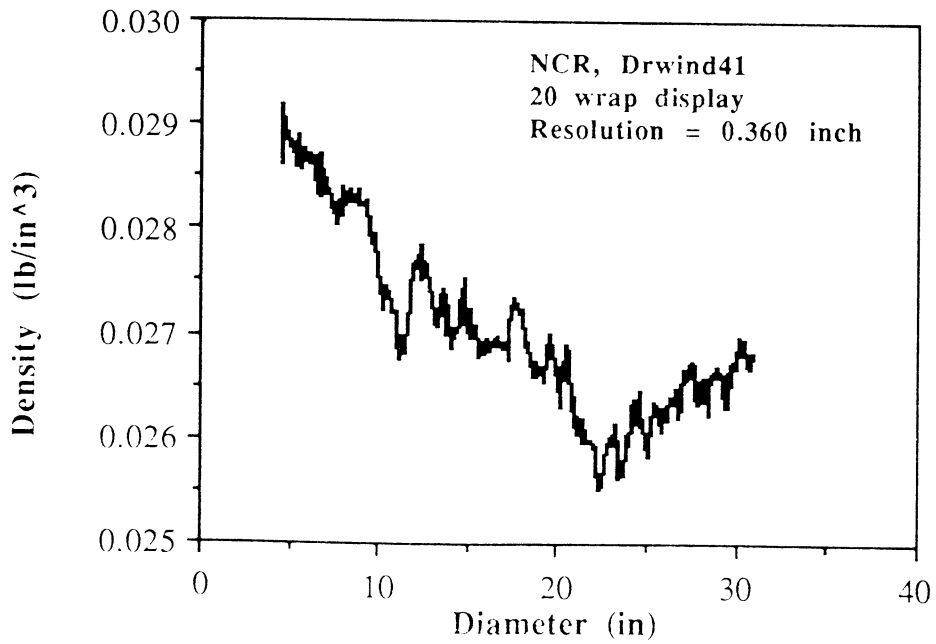


Figure 90
RADIAL COMPRESSION VS DIAMETER

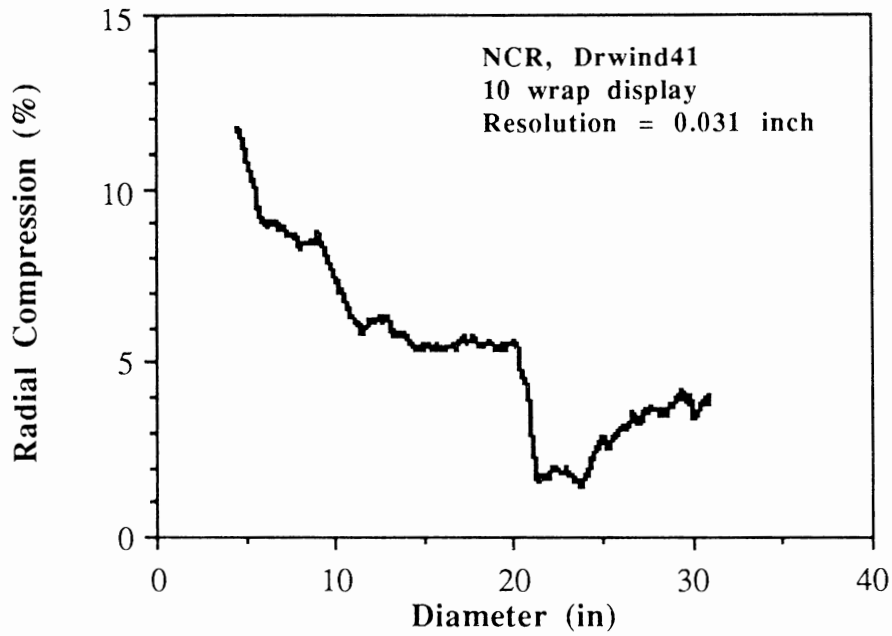


Figure 91
RADIAL COMPRESSION VS DIAMETER

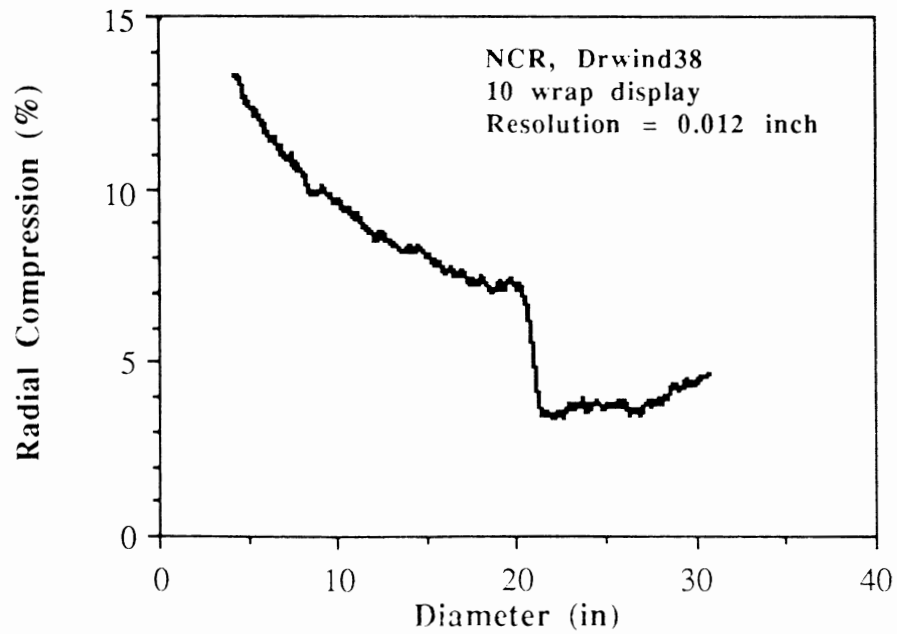
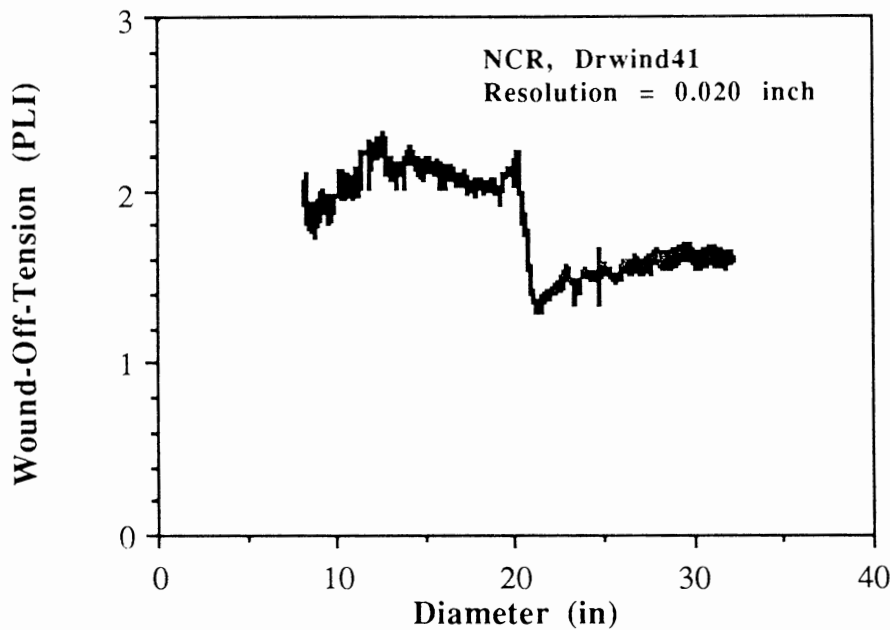


Figure 92
WOUND-OFF-TENSION VS DIAMETER



In conclusion, the new radial compression parameter as well as the computerized WIT-WOT stand out clearly as having resolutions one order of magnitude better than the best alternative, and three orders of magnitude better the Tappi standard Cameron Gap and the Schmidt Hammer made by the leading manufacture of paper test lab instruments. Since the WIT-WOT is not available for general use and is not suitable for production monitoring, the new winder data acquisition system developed for this project appears clearly superior to all other methods currently available due to its extreme resolution and wide application. Consequently, the development efforts for this projects could be justified solely on the basis of the achievement of the new Radial Compression measure.

In the next section, the modeling portion of this project will be evaluated for numerical stability and sensitivity to the various inputs.

Table 14
RESOLUTION OF ROLL STRUCTURE MEASUREMENTS

<u>Material</u>	<u>Run#</u>	<u>Method</u>	<u>Resolution</u>	<u>Units</u>
Newsprint	D85-028	Cameron Gap	24.450	point
		Schmidt Hammer	5.688	point
		Smith Needle	4.631	point
		WIT-WOT	0.650	inch
		Density	0.396	inch
		Rhometer	0.225	point
LWC paper	D86-Hahn	Schmidt Hammer	-	point
		Cameron Gap	2.359	point
		Density	1.276	inch
		WIT-WOT	0.980	inch
		Rhometer	0.840	point
		Smith Needle	0.126	point
NCR paper	Drwind41	Schmidt Hammer	14.062	point
		Rhometer	0.546	point
		Density	0.360	inch
		Smith Needle	0.166	point
		WIT-WOT	0.020	inch
		Radial Compression	0.031	inch
NCR paper	Drwind38	Radial Compression	0.012	inch

NOTE:

These results for Table 14 are for a large programmed step decrease in tension, and at a 90% statistical confidence. Units for discrete measurements are points which are the number of individual readings to be taken. Units for analog measurements which are averageable are for the sample size in inches of radius of the wound roll.

Wound Roll Model Accuracy

Wound roll model accuracy has two elements. First, the mathematical model must adequately describe the behavior of a particular real system despite inevitable approximations. Note that this requirement depends both on the definition of adequate, and the particular system being modeled. Second, the numerical computation of that model must be stable, converge and be insensitive to small changes in non-physical computational parameters such as grid size.

Imbedded within this new system is a winding model. Although in principle, any mechanically consistent model could be used, Hakiel's model was chosen for the prototype as it is one of the most general [132, 133]. Thus, at the very least the new prototype shares any limitations of the model imbedded within. Thus, there are likely to be many applications where complex behavior such as described in Chapter 4 would require an extended or more sophisticated model. However, Hakiel [132, 133] and Willet & Poesch [186] have experimentally verified that the nonlinear anisotropic winding model can well describe at least some winding conditions by using the radial press test described in Chapter 5.

Independent of the Hakiel mathematical model is the numerical accuracy of calculations. Though both the model and numerical calculations must be accurate to result in experimental verification, we can also compare one model against another using the same input parameters. Again, Hakiel's model is well tested against other earlier models. Hakiel [132, 133], Wu [148], and Willet and Poesch [186] have compared the finite difference calculation of the nonlinear model against those of Altmann [127]. Similarly, in this thesis there are numerous comparisons of the Hakiel model against the isotropic, Altmann [127] and Yagoda [149] models which are given in Chapter 3 and tabulated in Appendix A. Until this project however, the independent analytical verification for nonlinear radial moduli was not performed due to the lack of another model. However, with the development of the Displacement Formulation given in Chapter 7, we now have analytic verification for nonlinear radial moduli as well.

The only caveat however, is to be mindful of the undesirable sensitivity to grid size described in Chapter 3 and elsewhere. Thus, the Hakiel finite difference formulation must be checked with varying grid sizes for any particular set of input parameters. Indeed, this is good practice for any wound roll computational model as the system is mathematically ill-conditioned.

Quantitatively evaluating the accuracy of the calculated wound-in-stress for this project has presented some problems. Primarily this is because there are very few methods currently available to measure wound roll stresses. Furthermore, those that do exist are often noisy, not independently verified or impractically difficult. First, the axial press test described earlier is not suitable for the much larger rolls wound for this project. That leaves three other means to independently measure wound-in-stresses, all of which have some uncertainty. The least common method is to strain gage the web prior to winding [160, 168], which is impractically difficult and has not been independently verified. Though the Cameron Gap [174] is a Tappi standard test method and yields a measure that can be converted to wound-in-stress, it has severe limitations. The Cameron Gap has extremely poor resolution, which results in measurement error bands that are so large as to render this method nearly useless [169, 171]. The remaining method that was selected for prototype verification was the WIT-WOT winder [166, 167].

Accuracy of the new Extended Hakiel displacement to stress model, has been already discussed in Chapter 7 where it was developed. As we have seen in Figures 65-67, this model compares favorably with experimental WIT-WOT measurements as well as Pfeiffer's empirical formula [166]. However as we will see later in this chapter on model sensitivity analysis, calculated stress accuracy is very dependent on the accuracy of the many required input parameters.

Data Acquisition Sensitivity Analysis

Before we begin the sensitivity analysis of the new displacement-to-stress model, we will investigate the effect of some of the adjustable parameters on the data acquisition setup as well as data preprocessing. The first parameter of the number of encoder pulses per revolution has already been discussed in Chapter 6. Here it was concluded that as long as the encoder pulse count exceeded some minimum of about 2000-5000 pulses per revolution (for 24" drums), there was little increase in resolution or benefits achieved with higher counts. The point at which the law of diminishing returns takes over depends on a number of application dependent considerations. Tightly coupled systems with little mechanical backlash or web/drum slippage can benefit from slightly higher counts, while sloppier systems will not. While the runs for this project were acquired at incredibly high counts up to 100,000 pulses per revolution, it is now concluded that future systems should use more moderate values which will reduce encoder costs as well as reduce computer memory and disk storage requirements.

The next data acquisition parameter of the wrapcount (the number of revolutions of the rewind roll per sample), was also discussed in Chapter 6. Here it was concluded that the many system design requirements placed a range of acceptable wrapcounts wherein the minimum is determined by considerations such as ensuring that the rewind roll rotational rate does not overrun the computer processing of a sample, and that the maximum does not overflow the maximum number for the storage variable type which is usually single precision integers. However if all other variables are held constant and fall within the range described above, then the actual choice of wrapcount does not significantly change the effective resolution of the acquired data. In other words, the data resulting from a wrapcount of 1 which is averaged by 10 will yield the same results as a wrapcount of 10 with no averaging. Thus, a good choice of wrapcount is somewhat smaller than the anticipated display so there is room for a small but variable amount of averaging.

Figures 93 shows the utility of this approach of gathering data on a somewhat finer scale than will be ultimately used. Here we display the Radial Compression roll structure measure for convenience although the principle applies to the other similar 'analog' measures of density, caliper corrected density, calculated WIS and even WIT-WOT measured stress. In these three figures, all parameters are identical except the amount of averaging used in the final display. The top plot is only lightly averaged by 2 and shows a somewhat noisy display while the bottom plot is more heavily averaged by 8 which begins to limit the spatial resolution for short duration events such as splices or speed changes. As discussed earlier, the amount of averaging for the plots is mostly a matter of taste as the statistical resolution is not appreciably effected by averaging of this type of measure.

However, if this data is to be used as inputs to subsequent numerical calculations such as displacement-to-stress, then there is a potential advantage of heavier averaging to increase numerical stability. Recall from Chapter 7 that the best mesh size for data acquisition and calculation are not necessarily the same. Generally, the acquired data can't be displayed at such a fine mesh as required by winding model calculations without excessive noise. Therefore, the acquired data is usually replicated to give the small mesh required by winding models.

Finally, the effect of varying the strength of the low-pass digital filter is shown in Figures 94. Though the effect appears similar to averaging, there are distinct differences. First, averaging reduces the number of data points while the application of the filter does not. Secondly, if the filter strength is increased too much the data plots will become undesirably rounded as it is unable to follow the short term variations that are seen during winding.

Figure 93
EFFECT OF AVERAGING ON INPUT DATA

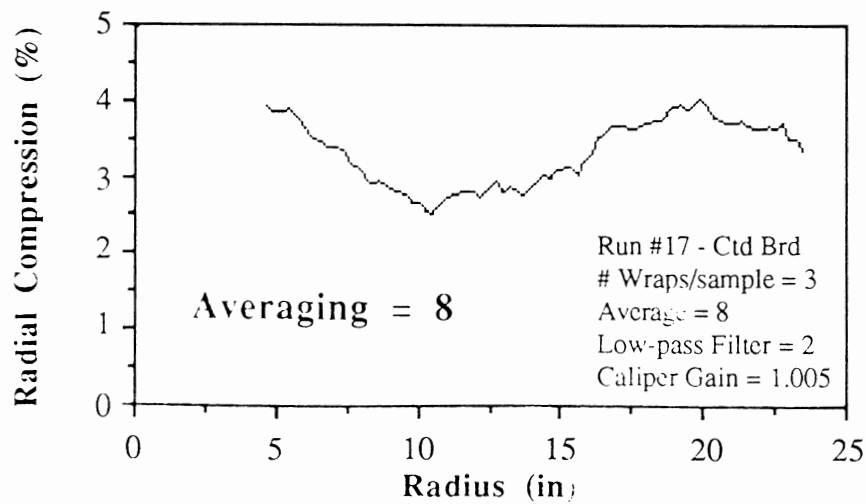
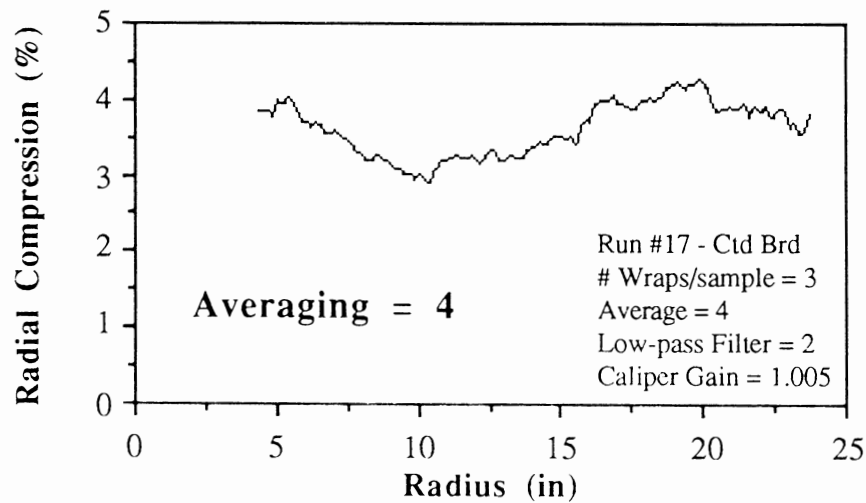
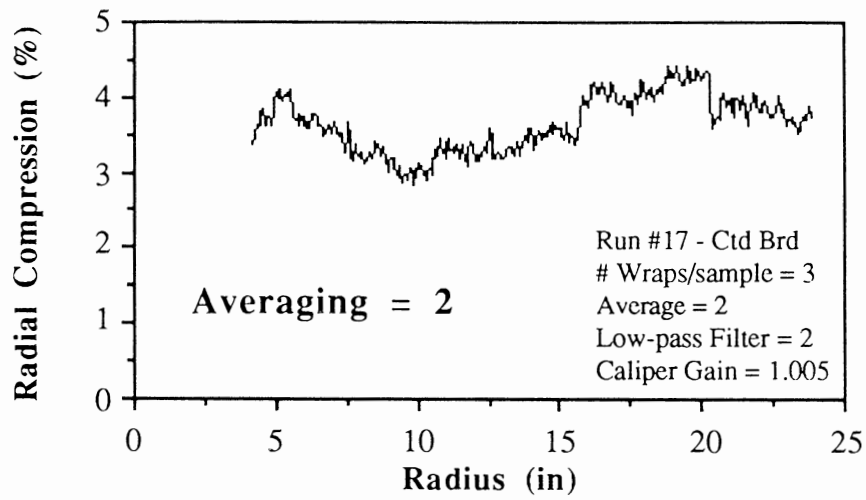
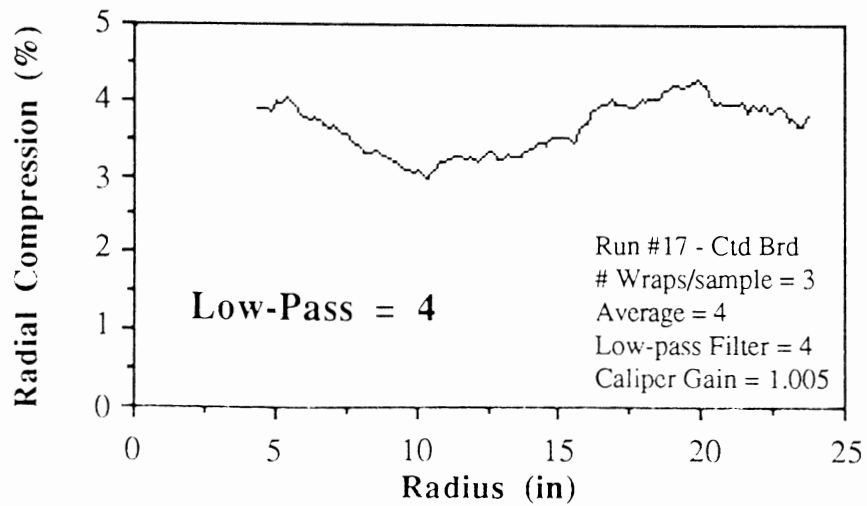
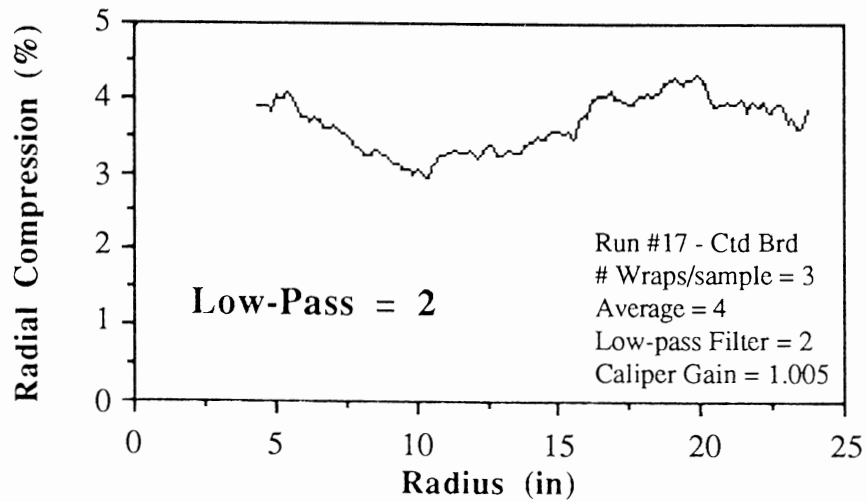
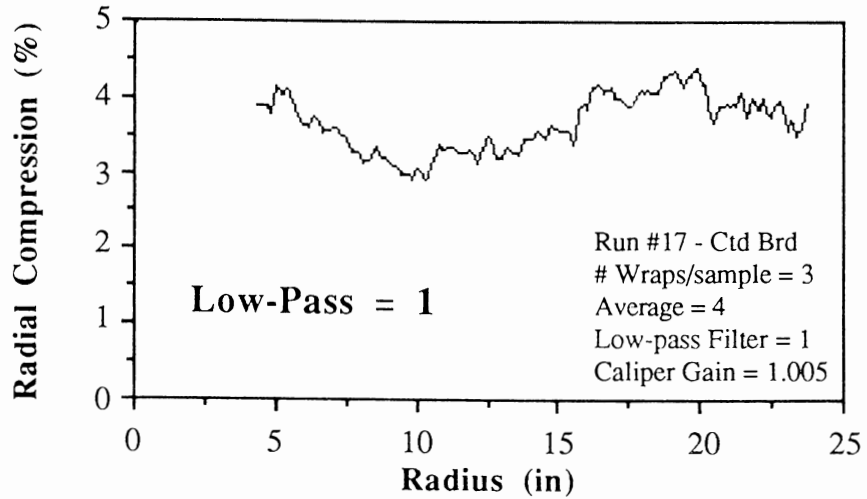


Figure 94

EFFECT OF LOW-PASS FILTER ON INPUT DATA



Model Sensitivity Base Case

The sensitivity analysis in the next sections investigates both numerical stability as well as sensitivity to uncertainties in material parameter inputs. All of these following studies are variations of a single parameter about a base case. Run #17 was chosen for this base for several reasons. First, it is a run that has not been presented earlier. Secondly, the TNT winding conditions were set to that typical of winding for that grade and did not include the step drops that were used for TNT sensitivity and measurement resolutions. In this discussion, we are investigating only the effects of model sensitivity. Finally, the coated and supercalendered food board grade for this run is stiff enough, so that a coarser mesh can be used. This allows the large number of runs required for this analysis to be computed in a reasonable length of time. Most of these runs required about 15 minutes of processing time to complete.

The parameters of the base case and the variations are shown in Table 15, where typically 3 variations are run for each of 9 different model parameters. Additionally, Figure 95 shows the deflection input and the WIS output for the base case run. This figure again reinforces the statements that Radial Compression, displacement and WIS plots are very similar in trends, only the scales are appreciably different. Finally, Figure 96 shows the radial and tangential stresses calculated for the base case. Though sensitivity analysis could be performed on any of the variables calculated by this new model such as radial and tangential stresses and strains, WIS is chosen for several reasons. First, it is the goal of the project. Secondly, if the WIS profile is known, then the other variables can be easily calculated from conventional winding models or extensions of these models. Thirdly, WIS is such a pivotal part of the new model, it is a very representative measure.

Sensitivity analysis for conventional winding models usually investigates the effect of varying material or geometrical properties on the resulting radial and tangential stress distributions. The application of such analysis is to determine what parameters can be effectively controlled to optimize wound roll stresses as described in Chapters 1 and 4. Though many of the parameters have a significant effect on stresses, practical application limits these parameters severely. Typically, an existing winder must process the product given it, and the product's properties have not been determined by any considerations of winding. Therefore, the only parameter that is typically controllable in a practical sense is the WIS profile determined by the TNT's. Though many who have worked with winding models have investigated sensitivity, the only published work of this type was performed by Wu [148].

Figure 95
DEFLECTION INPUT & WIS OUTPUT - BASE CASE

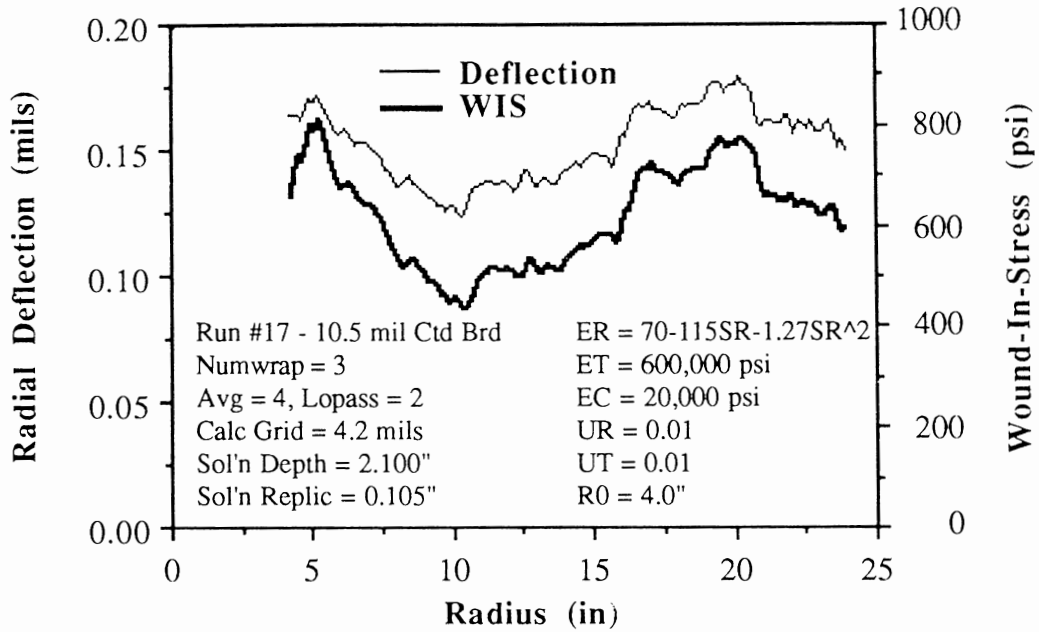


Figure 96
RADIAL AND TANGENTIAL STRESSES - BASE CASE

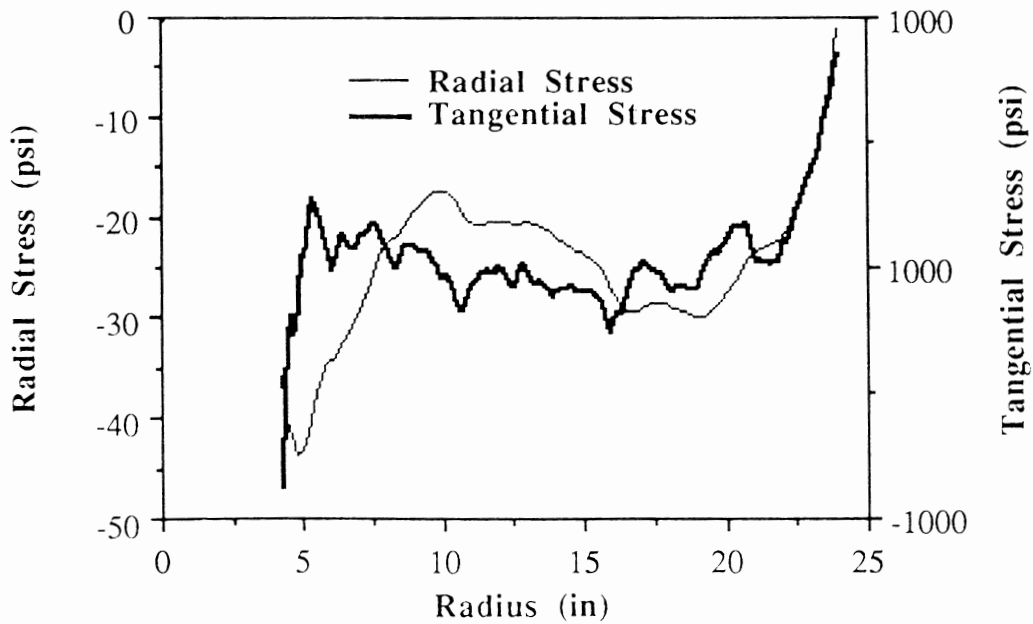


Table 15
SENSITIVITY ANALYSIS PARAMETERS

<u>Parameter</u>	<u>Units</u>	<u>Base</u>	<u>Variations</u>	<u>Figure #</u>
Preprocess				
Average	-	4	2, 4, 8	93
Filter	-	2	1, 2, 4	94
Numerical Stability				
Grid Size	mils	4.2	2.1, 4.2, 8.4, 18.0	97
Calc'n Depth	inch	2.1	1.0, 2.1, 4.2	98
Repl'n Depth	inch	0.21	0.05, 0.10, 0.21	99
Material Properties				
E_R	psi	1x	0.9x, 1.0x, 1.1x	100
E_T	psi	1x	0.9x, 1.0x, 1.1x	101
E_C	psi	20K	20, 20K, 20M	102
μ_R	-	.01	0.9x, 1.0x, 1.1x	103
μ_T	-	.01	0.9x, 1.0x, 1.1x	104
Caliper gain	-	1.005	1.000, 1.005, 1.001	105

Though this new model can also share this interpretation of sensitivity analysis, its primary application is very different. This is because by the time the roll has been wound and the data has been gathered, we can't change parameters such as material properties without changing the acquired deflection data. While we can and have varied properties in the course of this project, its effect on acquired deflection data does not yield many insights.

However, with a different interpretation the sensitivity analysis to be presented in the next sections has great utility. Here we view sensitivity as investigating how uncertainties in the input parameters effect the resulting WIS calculation. This is important because we can't measure any property precisely, and many are not presently practical to sample continuously over the entire web. An example of error in measurement is the critical calibration of the web caliper gauge. An example of sampling error is how deviations of the moduli of the web wound into the roll from the sample measured in the lab effect the WIS profile calculation. Thus, we can simulate uncertainties in the model parameters using the same input data to see its effect on calculated WIS.

Model Numerical Stability

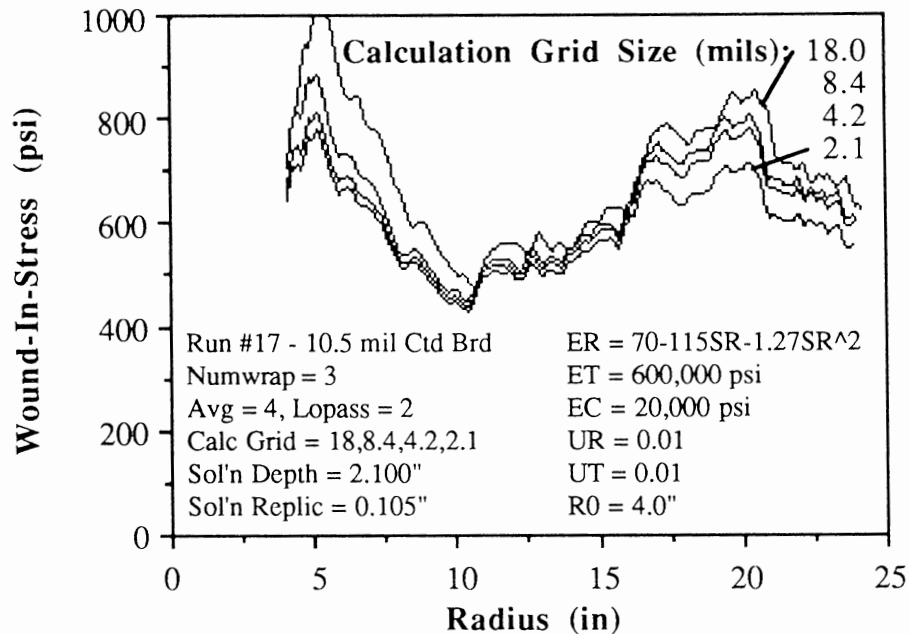
Before we investigate sensitivity to material properties, we must ensure that the model is numerically stable for the base case to be investigated. An example of this type of analysis has been performed in Chapter 3 and elsewhere, where we showed how the Hakiel finite difference solution should be run for several different grid sizes to ensure that the grid was neither too coarse to follow the extreme stress gradients, nor too fine as to cause solution instability. However, though Hakiel's model is embedded in this new displacement-to-stress model, using his model for determining optimum grid size such as given in Figures 18 and 19 would only be a starting point. This is because the Extended Hakiel Formulation contains more calculations which has their own numerical implications. Additionally, the real data used here contains more noise than does the typically smooth WIS profiles used as inputs for conventional winding models.

Therefore, in Figure 97 the grid size is varied by almost one order of magnitude to see whether the solution is effected appreciably. As seen here, the WIS profiles are close in magnitude except at the two extremes of 18.0 mils where the grid size is becoming significantly coarse as seen at the lower radii, and at 2.1 mils where the grid size is becoming too fine and is beginning to deviate at high radii. This is consistent with earlier observations that the optimum grid size is finer near the core than at the roll outside. However, the 4.2 mil base case seems to be an optimum and stable compromise for the large finish/core diameter ratio range of this wound roll.

If this was a conventional solution, we would need proceed no further for model stability checks. However, as described in Chapter 7 we are using solution acceleration techniques which also must be investigated separately. The first acceleration technique is the depth limited solution which capitalizes on the fact that only the outer portion of the roll is appreciably affected by the addition of wraps. As seen in Figure 98, the solution depth for the base case of 2.1" is conservative as doubling the depth has no significant effect on the resulting WIS profile. However, care must be used because reducing the depth even slightly below the base case will have an undesirable effect on accuracy as seen for the 1.0" depth. Recall that stiffer materials require a greater solution depth.

Similarly, we investigate the replication solution acceleration technique as shown in Figure 99. Here we see that the replication depth of 0.10" used on the base case is perhaps even too conservative and that further solution speedup is possible without compromising accuracy. The net effect of depth limited and replication acceleration will speed up this and any other model by 10-1000 times with a 84 times improvement seen for this base case.

Figure 97
SENSITIVITY TO CALCULATION GRID SIZE



Sensitivity to Material Parameters

As mentioned earlier, there are measurement and sampling uncertainties in the inputs to this or any other winding model. Thus, we will investigate how these uncertainties effect the calculated WIS profiles. The variations of the material properties about the base case given in this section are estimates as to how close we can be sure of these properties for typical measurements and sampling practices found in labs or mills (for paper grades). In other words, we attempt to bound our uncertainty by varying each property above and below its measured value.

Figure 100 shows the effect of a 10% greater and smaller radial modulus. Here we see that a high radial modulus input will increase calculated WIS profiles approximately proportionally and vice versa. Similarly, Figure 101 shows the effect of a 10% variation upon tangential modulus. However, in this case an overestimate of tangential modulus will underpredict WIS profiles, but will do so to a lesser degree than the proportionality of radial modulus.

Figure 98
SENSITIVITY TO CALCULATION DEPTH

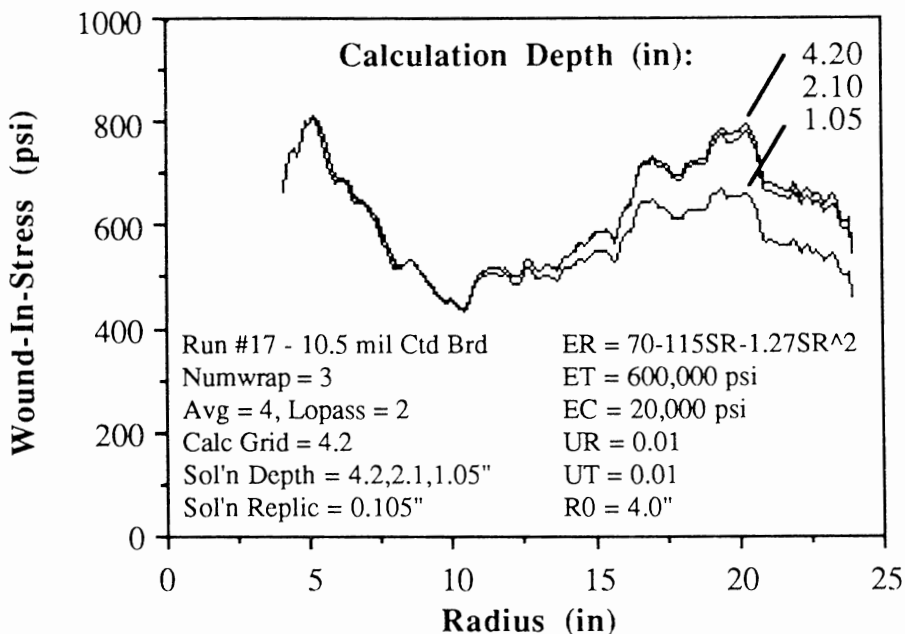


Figure 99
SENSITIVITY TO CALCULATION REPLICATION

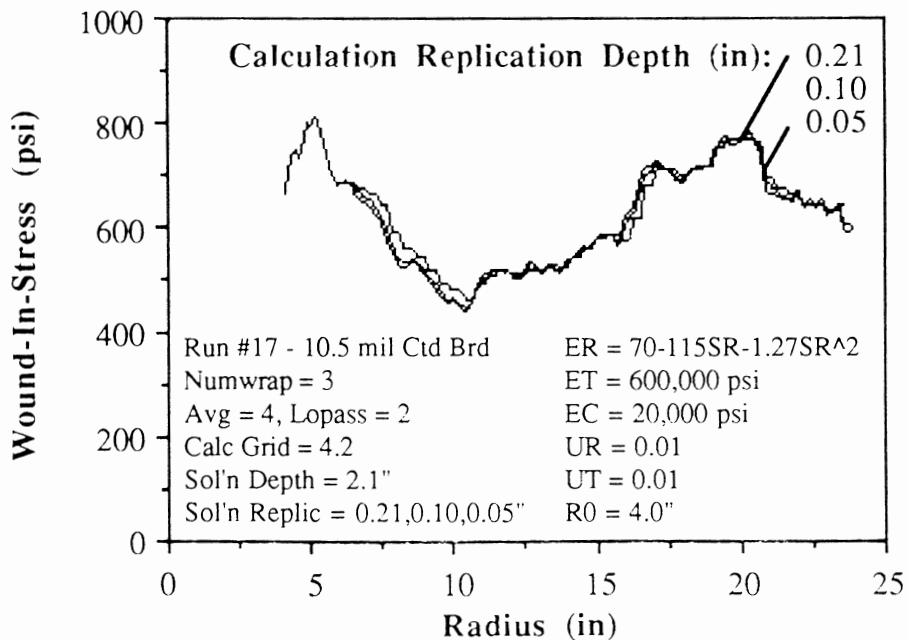


Figure 100
SENSITIVITY TO RADIAL MODULUS

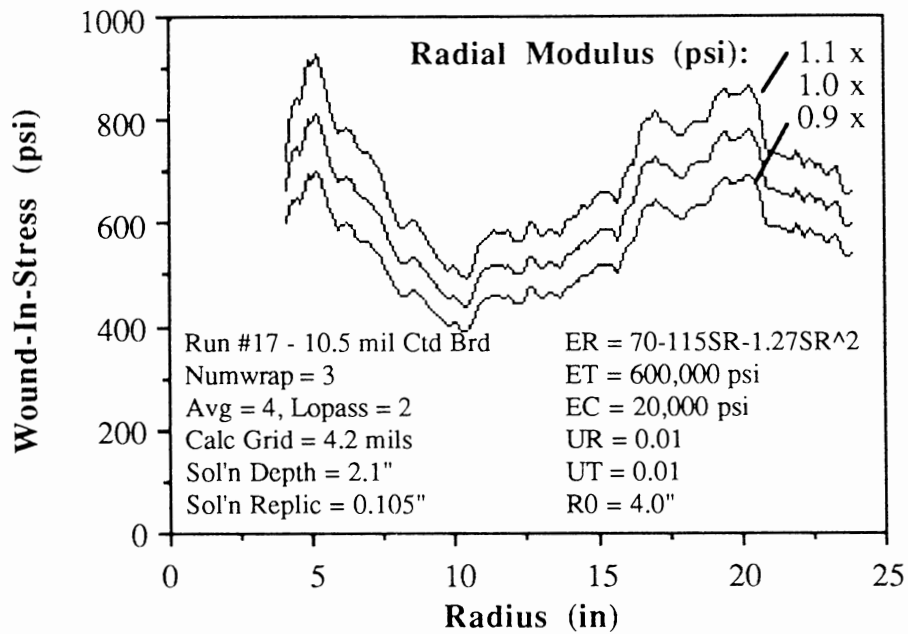


Figure 101
SENSITIVITY TO TANGENTIAL MODULUS

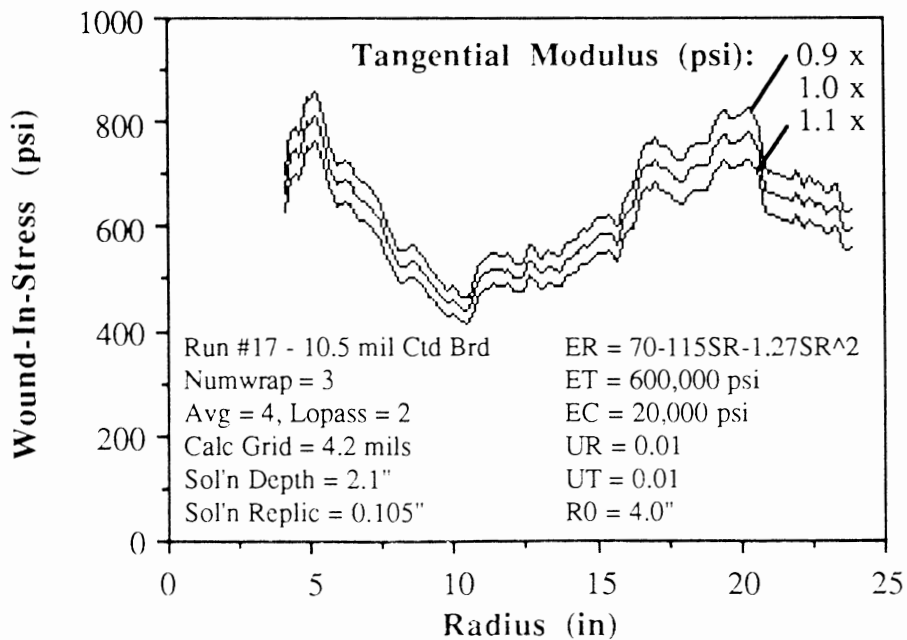


Figure 102
SENSITIVITY TO CORE MODULUS

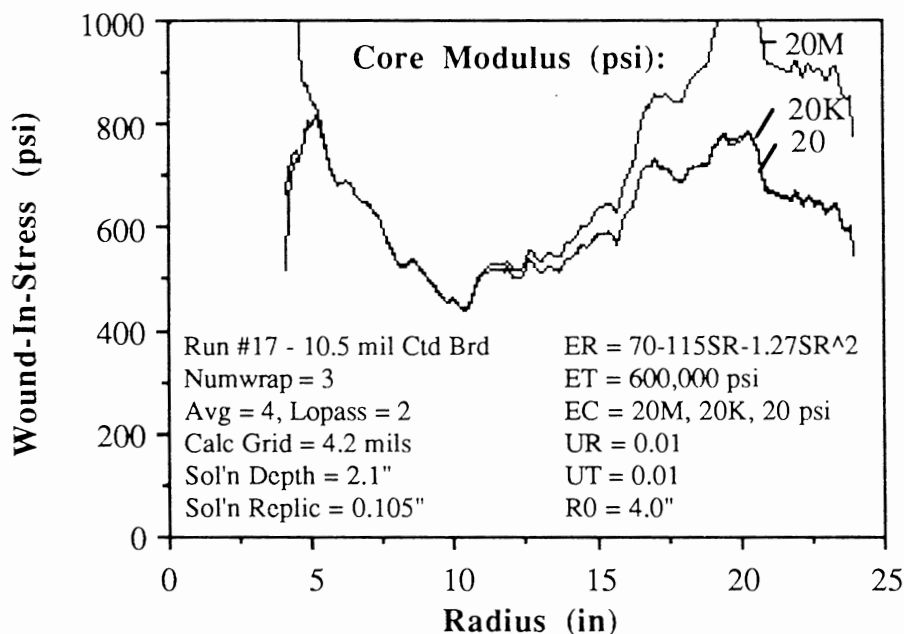


Figure 102 for the sensitivity to core modulus has many interesting curiosities, but first a review of material given earlier is in order. All consistent winding model implementations have a core boundary condition which yields large gradients in both radial and tangential stresses, but are localized to very near the core as was seen in Figure 13. However, though all models predict this behavior, it has not been experimentally verified. Also, most finite difference implementations do not rigorously begin immediately at the core, but rather after a couple of 'wraps' where the minimal matrix can be filled. The core stresses are extrapolated from the rigorous portion of the calculated stresses. Finally, the optimum grid size for the core is considerable finer than the remainder of the roll.

Similarly, data acquisition hardware complications abound at the core. As mentioned in Chapter 6, for a variety of reasons density-like hardware is not presently able to gather data beginning immediately from the core. The amount of material wound onto the core before the first good diameter difference sample can be calculated may be as few as a hundred wraps to many inches if the system is sized such that rewind roll rotation overruns the sample processing. Also, if the winder is stopped in the middle of a run for any reason such as a web break, the data gathered before and after the stop can't be aligned, interpolated or spliced together. Thus, analysis would have to take both halves separately, where the second half would require an effective core stiffness input for a radius at which the second half began.

Returning to the sensitivity of core modulus on WIS profiles given in Figure 102, we see that varying the core modulus from 20 psi to 20,000 psi has essentially no effect on the calculated WIS profile. It is only until the modulus has been increased far beyond these values that the stress near the core is effected. However, no published work has verified experimentally whether the stress gradients predicted near the core by conventional models well represents real behavior. Indeed, the stresses predicted immediately above the core for some real winding cases is beyond web material limits. The situation for the displacement-to-stress model is even more complicated by data acquisition considerations. Thus, a conservative approach to interpreting stress data near the core would indicate caution.

The next interesting observation is how the 20M core stiffness case suddenly begins to deviate from the others at a radius of 13". What makes this so intriguing is that the effect of core stiffness for this case should be physically and numerically significant only for about an inch or so, yet the deviation begins far above that. Furthermore, the solution given here implements the depth limited acceleration, so that the 20M core stiffness is no longer even used in the calculations above a radius of 6". Anything above that uses an effective core stiffness determined by the radial modulus at the interlayer pressure at the calculation depth below the current surface. Though the details of why this numerical instability occurred would be difficult to determine, the basic cause can be summarized as too many measurement and numerical derivatives in the displacement-to-stress system. This topic will be discussed in more detail in the next chapter.

Generally, Poisson ratio has only a minimal effect on most mechanics applications and solutions. While this can also be true for winding models, there is an exception as seen in Figures 103 and 104. If the Radial Poisson ratio exceeds 0.010, it begins to have a tremendous effect on the calculations. Thus, if the strain-energy (Maxwell's) relation is used (which is not always in experimental agreement [186]), then the solution will also be effected if the Radial Poisson ratio becomes large. While Wu [148] comes to similar conclusions, the issue of Poisson Ratios in winding mechanics is far from settled.

Finally, the effect of caliper is shown in Figure 105. As seen here, caliper uncertainties as small as 0.5% have a large effect on WIS calculations. This means that for a 1 mil material, a caliper gauge calibration and repeatability of and incredibly tight 5 μ inch would be required. However, softer materials such as the NC paper were not quite as sensitive in that a 1 or 2% caliper uncertainty would lead to a similar change in the WIS profile. While the Schaevitz gauge used in this prototype has a specified 5 μ inch repeatability, calibrating and maintaining that level accuracy is very difficult. As discussed in Chapter 8, this requires either precision gage blocks or micrometers to be used to set the span, as well as many other considerations such as platen deflection and instrument drift.

Figure 103
SENSITIVITY TO RADIAL POISSON RATIO

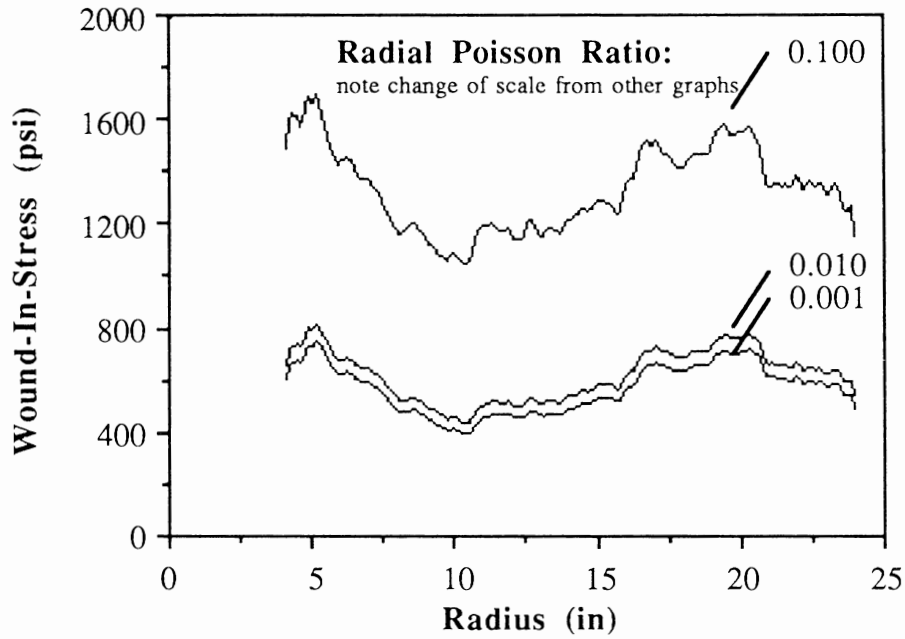


Figure 104
SENSITIVITY TO TANGENTIAL POISSON RATIO

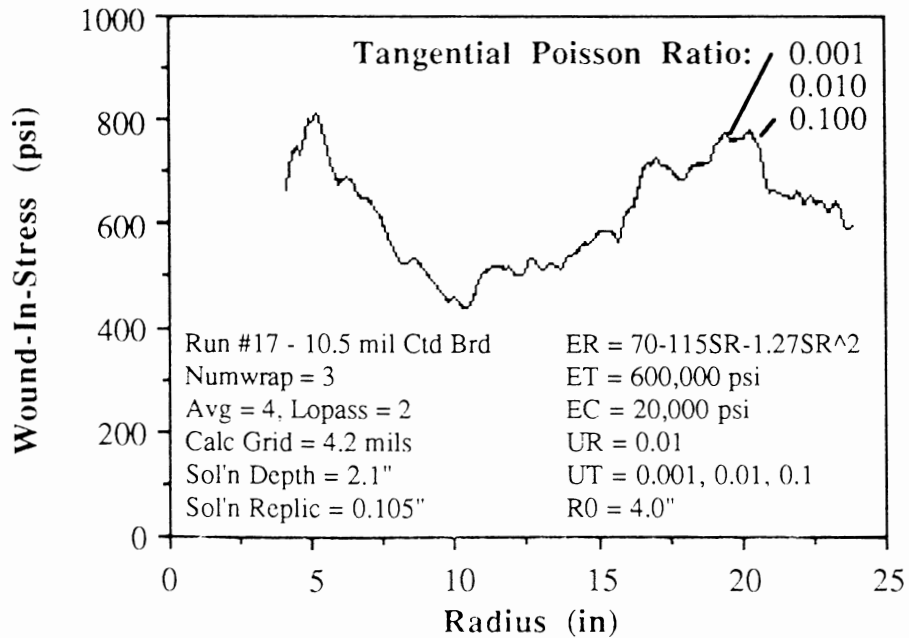
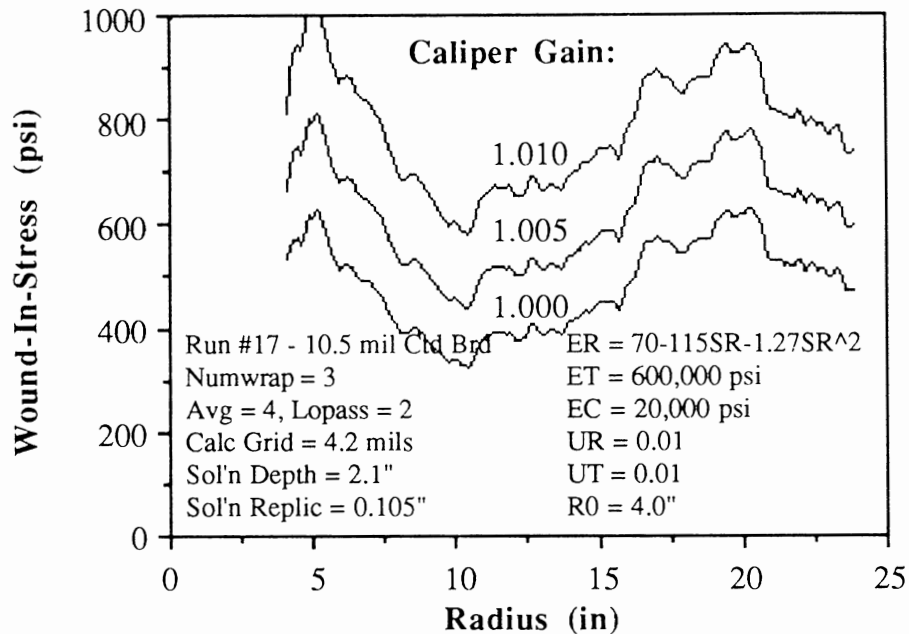


Figure 105
SENSITIVITY TO CALIPER GAIN



Conclusion

In this chapter, we have investigated accuracy and resolution from many viewpoints. From this study, we have found that the data acquisition hardware and Radial Compression calculation development has led to a roll structure measure which meets and exceeds the resolution of any presently available. Thus because of its ease of use in a wide variety of applications, this development may be a significant contribution to winding.

However, the case of the displacement-to-stress model is mixed. Though the only difference between the Radial Compression and WIS profiles are one of scale, the displacement-to-stress model yields a far richer array of information. However, this additional information comes at a high price. First, the calculations can be quite computer intensive, so that the system may not run in real-time as can Radial Compression. Secondly, though we have demonstrated some level of accuracy for the stress calculations, good results will only be achieved if the material and geometric properties are known very closely. In particular, the caliper measurement and the radial moduli have the greatest effect and are also among the most difficult to measure. In the next chapter, the achievements and shortcoming of this project will be reviewed, with suggestions given for future improvements beyond that implemented on this prototype.

CHAPTER 11

CONCLUSIONS AND RECOMMENDATIONS

Project Summary

This project began from several simple insights. First, the best current description of wound roll structure is given by winding models using consistent mechanics descriptions of displacements, strains and stresses. However, current models were limited since a Wound-In-Stress profile was needed as an input, and this was difficult to obtain except for the isolated case of pure centerwinding equipped with tension and web caliper measurement. Secondly, prior to this time most roll structure measurements were unsatisfactory in terms of resolution, wide application, ease of use or other important criteria. Though the density analyzer possessed most of the desirable characteristics, it had a limitation. The density value is not consistent with mechanics formulations. Thus, the most important analytical and experimental winding tools available would not work well together.

Thus, the need was defined to measure the fundamental quantities of stresses during winding in a manner that was similarly convenient as the density analyzer which can be installed on most any machine and operate in a fully automatic manner. The inspiration that modeling and measurement could be married came with the insight that the rate of roll growth was what the density analyzer actually measured, and that the rate of roll growth might somehow be related to the strains and consequently stresses in a roll. Furthermore, winding models were determined systems, so that the roll could only grow at a unique rate for a unique set of parameters.

This project was then proposed for a thesis topic. Its impetus was merely those insights strengthened by the boundless optimism of youth. Though several reviewers initially stated that the project could not be done, work was begun with idealistic conviction that not only would the project succeed, but that it would revolutionize quality control and machine control of winders.

Looking back after the project prototype has been completed however, the truth lies between the impossible and the probable. The insights were transformed into a mechanically consistent and simple boundary condition of roll deflection, but only after many sketches were drawn to postulate behavior. Next, a system had to be developed to measure the deflection data based on roll diameter and caliper. Though roll diameter was not particularly difficult, the measurement of caliper to the tolerances required was not off-the-shelf affordable technology. Then, a winding model had to be rederived from basic constitutive equations to describe wound roll physics from an entirely new perspective. Once a working model was achieved however, it was scrapped in order to develop yet another that calculated with more practical speed.

Only after the entire system was assembled and experimentally verified did the tremendous scope and complexity of the project become apparent. The project's goal was to integrate modeling and measurement, which was ground-breaking in itself. However in order to do so, both modeling and measurement also had to be pioneered. Furthermore, because of the breadth of the project, a careful building block approach was required. Thus, wound roll models were rederived and checked numerically where they were previously assumed correct. In this process, many missing pieces were filled in such as defining core stiffness, and measuring creep inside a roll by changing caliper. Additionally, many problems were uncovered such as Pfeiffer's model which was found to be inconsistent, and finite difference sensitivity to grid size.

Thus, one thing led to another, and the project grew far beyond its original intentions. This was not without compensation however. First, old winding models were scrutinized closer than ever before for mechanical consistency and numerical accuracy. Secondly, several new models or extension to existing models were developed. Thirdly, a several new roll structure measures were developed including caliper corrected density, radial compression and WIS which can all utilize the same raw data. Most promising of which was the radial compression which was statistically evaluated at a resolution exceeding previous measurement methods. Fourthly, it collected and integrated historical and new developments in the science of wound roll modeling and measurement into a single source.

Finally, it did achieve to some degree the original objective of measuring stresses during roll winding. Unfortunately, this measure is somewhat more complicated and less robust than originally anticipated. In the remainder of this chapter, the products and shortcomings of this project will be reviewed with a vision toward present application and future research

Contributions

Due to the scope of this project which encompasses both modeling and measurement, this project has resulted in many contributions. Some of these are revolutionary such as new winding models and measures. However, there are also many incremental or evolutionary facets such as the development of the core stiffness formula and the design criteria for sizing encoders. This section will review only those insights and developments which are new to the public domain and resulted from this project.

Chapter 1 clarifies the relationship between control, wound roll physics and measurement as given in Figure 4. In particular, it redefines what it is a controllable parameter in practice. For example, while it is trivial to change the value of E_T in a wound roll model, in practice this would rarely be done for the purpose of optimizing the winding process. It concludes that the primary application of roll structure modeling and measurement is to control the TNT's of winding such that the propensity to application dependent defects are minimized.

Chapter 2 gives an unusually detailed development of the constitutive equations of wound roll physics and their assembly into a differential equation. Additionally, boundary conditions are either more fully developed, or alternatives give. For example, equation (23) and others for calculating the core stiffness used in winding models based on geometry and material properties was developed. Furthermore, alternatives to the outer boundary condition are given such as equations (28b) and (28c) for tangential stress and displacement winding differential equation formulations. Finally, equation (29) is given to estimate the calculation time for winding models based on the number of wraps.

Chapter 3 reviews the Isotropic, Altmann and Hakiel models, as well as portions of the Yagoda model, to check for mathematical integrity. In all of these models except the Isotropic, several minor problems were uncovered. For example, the Hakiel model omitted high order derivative terms, which may be negligible for most cases, and assumed the strain-energy relation between moduli and Poisson Ratios, which is at odds with experimental evidence. Additionally, Yagoda makes some approximations in his model whose impact is not easy to determine. Finally, the Pfeiffer model which was becoming popular was found to be flawed and mechanically inconsistent with all the other models. Though we would have expected mathematical checks to have been performed on preceding models, it seems to have escaped publication.

It is difficult to determine the effect of minor mathematical inconsistencies and assumptions. Additionally, it may be possible for the mathematics to be correct but the calculation either difficult or improperly executed. Consequently, another method of checking model consistency needed to be defined and performed. Chapter 3 insists that all winding models yield the same calculated stress outputs for the same inputs within the application range of the particular models. Here, the Isotropic, Altmann, Yagoda and Hakiel models have been verified to calculate consistently to within engineering accuracy with only a few exceptions. These exceptions are unusual inputs to the Yagoda model, and numerical problems if the Altmann integration grid is not fine enough or the Hakiel model is not within a range of grid sizes determined indirectly by the input parameters used. From this comparison, we have discovered that care must be used with many winding models to ensure numerical accuracy. Additionally, the Yagoda model was found to be both orders of magnitude faster and more accurate than all other models within its application range. Finally, Chapter 3 describes the measurement of nonlinear moduli in more detail than given by Pfeiffer.

Chapter 4 describes a wide range of complex wound roll behavior that is either inadequately modeled or not modeled at all. These include loading effects such as gravity, nips and handling; complex material behavior such as creep; and complex wound roll behavior such as air entrainment. These areas are deficiencies of the present state-of-the-art and serve as a list of potential future research work.

However, two new behavior descriptions were included here which was done by the author, but outside of this thesis project. The first is the modeling of the hygrothermal response of a wound roll. Here we found that simple models can describe the changing moisture or temperature of a roll as it heads toward equilibrium with its environment. The importance of this behavior is that changing moisture or temperature effects both stresses and strains in a roll. Second, a simple model of interlayer slippage is given which is based on the single assumption that slippage is a function of depth. The importance of interlayer slippage is that it also effects web stresses and strains in a wound roll. This model is integrated with and verified by and extension to the J-line experimental technique.

Chapter 5 contains a description and classification of roll structure measurement. In addition to principles of operation, application limitations are described based on experiences of the author and other colleagues working in the area. While there is not much new material here, its completeness and collection into a single source is unique.

Chapter 6 describes not only the theory and operation of the density analyzer which has been done previously, but the design criteria for sizing samples, sampling rates, encoders, counters and memory storage which has not been published. This will be useful for developers of similar instrumentation. Additionally, an investigation of data noise reduction techniques using averaging, smoothing, digital filters, Chauvenet's criterion and FFT analysis can be used to improve data quality. Finally and most importantly, caliper corrected density and radial compression was developed to mitigate the most glaring deficit of current density analyzers, which is noise due to caliper variations.

Chapter 7 which is the analytical essence of this project introduces three new roll structure models or measures. First is radial compression which is easily implemented, extremely fast to calculate, and contains the displacement boundary condition which drives the solution of stresses in a winding roll. Secondly, the Displacement Formulation was derived which calculates all stresses and strains in a wound roll given the measured outer boundary displacement. Unfortunately, this straightforward displacement-to-stress solution does not calculate quickly enough to be practical. Thus, the Extended Hakiel Formulation was derived which solves the same problem using an extension to an embedded model. This model which is the culmination of the project was experimentally verified using a WIT-WOT winder and Pfeiffer's empirical equations to predict WIS within engineering accuracies.

Chapter 8 describes in detail the winder, sensors, and instrumentation used for the development of this prototype. Though much of this equipment is not new, there are incremental improvements in both operation and understanding resulting from this project. However, an innovation developed was the adaptation of a noncontacting gauge for inexpensive and accurate online caliper measurement. This sensor was verified to read caliper within the tolerances of standard test lab instruments. Although MD creep has already been measured and reported by others, the caliper gauge was used to conclusively demonstrate ZD creep as caliper changes on consecutive winds of the same material.

Chapter 9 on software does not introduce any innovations that were not previously implemented. However, Chapter 10 develops a statistical procedure to quantify and rank roll structure measurement resolution for devices using different principles and units. From this method, the Radial Compression measure was found to meet and exceed the resolution of any currently available method. Finally, while the Appendices do not contain any truly unique material, it contains the most extensive winding bibliography as well as wound roll computer program listing and output yet published.

Complications

While this project has introduced many evolutionary and revolutionary developments, it has uncovered many areas that would benefit from additional research. However to introduce this, it would be appropriate to reiterate and summarize the scope and complexity of this stress measurement prototype. From Table 16 which summarizes the minimal inputs for this system, we can see that not only are there numerous parameters that must be selected or measured, but that many are currently very difficult to obtain. Furthermore, these are only the immediate inputs to the computer programs which in many cases require some amount of calculation just to obtain. For example, Chapter 6 gives a lengthy design procedure just to obtain encoder counts and sample sizes. Additionally, the radial modulus results from curve-fitting a derivative of a calculation upon load-deflection data.

The data acquisition inputs of diameter and caliper, while not necessarily new technology, required far greater precision in this application than that of typical quality control practice. Indeed as we have seen, the calculated stress output is extremely sensitive to caliper as the wound roll deformations are quite small. Thus, we are faced with not only measurement accuracy, but also with resolution to reduce data noise. Ideally, we would like the (averaged and filtered) diameter and caliper measurements to be made to accuracies better than about 10 μ inch, which is approximately an order of magnitude higher than the prototype can achieve consistently. This presents not only many technical and practical difficulties, but also one of definition. What is the effective stack thickness of materials whose surface roughness or void volume is no longer a small portion of its thickness? Similar difficulties arise in measuring and defining the nonlinear radial modulus for materials which are typically hysteretic.

The model also presents complications which can be more fully explored. First, as winding models have become more general, they have become less robust and more lengthy to calculate. Thus, new solution techniques are required so that we can solve the current models faster and without checking sensitivity for every new case. This will become even more acute if any of the many complications described in Chapter 4 are also included. Indeed, any of these complications would be a good research topic in itself. However, the relative importance of those currently unmodeled behaviors such as creep, slippage, or air entrainment varies widely with application. Thus while the behavior currently modeled is embedded and relevant in all real systems, much of the unmodeled behavior has a narrower scope of application and may not be significant in all cases. Thus the law of diminishing returns holds were modeling new behavior requires more effort than more basic behavior, and yields a diminishing range of interest and application.

Table 16
MINIMAL INPUTS FOR THE
DISPLACEMENT-TO-STRESS MEASUREMENT SYSTEM

Measurement

- Roller encoder pulses per revolution
- Rewound roll encoder pulses per revolution
- Drum Diameter
- Wrap count sample size
- Caliper gage gain

Data Preprocessing

- Averaging value
- Smoothing value
- Digital low-pass filter strength

Model Numerical Parameters

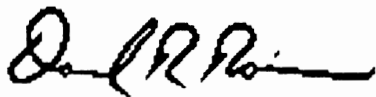
- Winding model (eg Altmann, Hakiel etc)
- Grid size
- Solution depth (for accelerated technique)
- Solution replication depth (for accelerated technique)

Model Physical Parameters

- Core and finish diameters (measured by hardware)
- $E_R = f(\sigma_R)$
- $E_T = f(\sigma_T)$
- E_C
- μ_R
- μ_T

Further opportunities exist for the improvement of the robustness of the displacement-to-stress model solution technique arise by recognizing that better solutions would result if the number of derivatives were reduced. The input to the winding model is expressed as the difference of consecutive diameters and caliper, which typical of displacements is a very small number compared to the diameter. This small differencing, though inherently noisy, may be unavoidable because it is the essence of the displacement-to-stress model. Additionally, the winding differential equation is currently solved as a finite difference approximation. Thus, the solution is composed of almost innumerable small differences for every wrap of the roll and for every wrap added. Though finite difference is ideally suited for many models, the winding model is iterative and has large stress gradients spanning tens of orders of magnitudes and may be too ill-conditioned for this solution technique. Alternatives may exist however. For example, Altmann posed the winding differential equation as an integration, and Yagoda posed it as an infinite series, both of which are very stable. Perhaps other technologies such as nondimensional approximations or Boundary Element Methods may be applied for better and faster solutions.

In summary, though this project has contributed to wound roll modeling and measurement, there remains considerable opportunities for improving the implementation pioneered by this prototype as well as researching new capabilities of this approach. Fortunately, this displacement-to-stress model is extensible and can grow to accommodate new wound roll models or diameter/caliper measurement techniques. Thus, this project is more than a model and measurement technique, it is a methodology for solving wound roll structure problems in a new way.



2/23/90

BIBLIOGRAPHY

Selected

- Altmann, H. C. "Formulas for Computing the Stresses in Center-Wound Rolls." Tappi Journal, vol. 51, no. 4, pp. 176-179, April 1968.
- Blaedel, K. L. "A Design Approach to Winding a Roll of Paper." Ph.D Thesis, Dept. of Mechanical Engineering, University of Wisconsin, Madison, 1974.
- Eriksson, L. G. and Lydig, C. and Viglund, J. K. and Komulainen, P. "Measurement of Paper Roll Density During Winding." Tappi Journal, vol. 66, no. 1, pp. 63-66, January 1983.
- Hadlock, A. H. "The Principles of Winding." Pima, pp. 13-16, February 1979.
- Hakiel, Z. "Nonlinear Model for Wound Roll Stress." Tappi Journal, vol. 70, no. 5, pp. 113-117, May 1987.
- Hussain, S. M. and Farrell, W. R. and Gunning, J. R. "Most Paper in the Roll is in Unstable Condition." Canadian Pulp and Paper Industry, pp. 52-54, August 1968.
- McDonald, J. D. and Farrell, W. R. "Winder Optimization using an On-line Microcomputer." Pulp & Paper Canada, vol. 86, no. 9, September 1985.
- Pfeiffer, J. D. "Wound-off Tension Measurement in Paper Rolls." Tappi Journal, vol. 64, no. 4, pp. 106-108, March 1977.
- Pfeiffer, J. D. "Measurement of the K2 Factor for Paper." Tappi Journal, vol. 64, no. 4, pp. 105-106, April 1981.
- Rand, T. and Eriksson, L. G. "Physical Properties of Newsprint Rolls During Winding." Tappi Journal, 56, no. 6, pp. 153-156, June 1973.
- Roisum, D. R. "Paper Stresses During Winding." Advances and Trends in Winding Technology, Proceedings of the First Winding Technology Conference, Stockholm Sweden, pp. 7-23, March 16, 1987.
- Roisum, D. R. "How to Measure Roll Quality." Tappi Journal, vol. 71, no. 10, October 1988.
- Tramposch, H. "Anisotropic Relaxation of Internal Forces in a Wound Reel of Magnetic Tape." Journal of Applied Mechanics, Transactions of the ASME, vol. 34, no. 4, no. 89, pp. 888-894, 1967.
- Yagoda, H.P. "Resolution of a Core Problem in Wound Rolls." Journal of Applied Mechanics, vol. 47, pp. 847-854, 1980.

Cores

1. Anonamous. "Drying of Wound Tubes." Algemeine Papier-Rundschau, no. 24/25, pp. 758, 560.
2. Anonamous. "Report on the Use of Cores in the Paper and Board Industry." Paper Technology Industry, vol. 23, no. 8, pp. 233-235.
3. Boqvist, I. "Paper Cores Cut and Handles Setwise for Streamlined Operation to the Winder." Tappi Paper Finishing and Converting Conference (Minneapolis) Proceedings, pp. 39-45, October 1983.
4. Cartwright, D. "Air Shafts give Converters a Grip on Roll Mounting." Converter, vol. 23, no. 7, pp. 8-12, July 1986.
5. Corbitt, M. R. "The Fiber Paper Mill Core." Tappi Paper Finishing and Converting Conference Proceedings, pp. 125-126, October 1982.
6. Crooks, J. "Rolling Friction Lets Core Chucks Do a Better Job." Paperboard Packaging, vol. 72, no. 4, pp. 58-60, 62, April 1987.
7. Diltz, J. L. "Straight Talk on Spin-out Solutions." Paper Film and Foil Converter, vol. 58, no. 4, pp. 74, 76, April 1984.
8. Diltz, J. L. "How to Avoid Core Spin-out." PIMA, vol. 67, no. 2, pp. 44-45, February 1985.
9. Johnson, D. "Taking Core Manufacture out of the Dark Ages." Tappi Calendering and Winding Technology Conference, TAPPI Press, pp. 111-112, January 1985.
10. Nygaard, D. C. "Iron Core Processing." Tappi Paper Finishing and Converting Conference Proceedings (Wausau), pp. 29-33, October 1978.
11. Roisum, D. R. "Cores I - VI", Beloit Research internal Reports, D87-003, 4, 6, 10, 13, 27, January - June 1987.
12. Secor, A. "Centering in on Core Chucks." Paper Age, vol. 101, no. 3, pp. 46-47, March 1985.
13. Timell, H. "State of the Art in Core Manufacture, Handling and Preparations." Tappi Paper Finishing and Converting Conference Proceedings (Albany), pp. 157-159, October 1985.

Density

14. Anon. "The ASEA HYLTE System for Roll Hardness Control." ASEA unpublished sales brochure, 1986.
15. Anon. "Rewinding Technology." ATIPCA, vol. 23, no. 4, pp. 14, 16-18, 20-22, October/November 1984 (Spanish).
16. Anon. "Roll Density Control for Winders." Voith unpublished sales brochure, 1987.
17. Baum, S. A. "Multi-Station Density Proposal." Beloit Research internal memo, August 12, 1987.
18. Baum, S. A. "Effect of Sheet Caliper and Hardware Resolution on Determination of Wound Roll Density." Beloit Research internal report, #D89-001, January 27, 1989.
19. Eriksson, L. G. and Lydig, C. and Viglund, J. K. and Komulainen, P. "Measurement of Paper Roll Density Distribution." Report to the Swedish Newsprint Center (TFL), Djursholm Sweden.
20. Eriksson, L. G. and Lydig, C. and Viglund, J. K. and Komulainen, P. "Measurement of Paper Roll Density During Winding." Tappi Journal, vol. 66, no. 1, pp. 63-66, January 1983.
21. Eriksson, L. G. and Lydig, C. and Viglund, J. and Komulainen, P. "Computerized Control of Reel Winding Improves Quality." Svensk Papperstidning, no. 4, pp. 86, April 1983.
22. Granlund, B. "Computerized On-line Fault Detection in Paper Reels." Advances and Trends in Winding Technology, Proceedings of the First Winding Technology Conference, Stockholm Sweden, pp. 167-176, March 16, 1987.
23. Hewinson, V. K. and Barlow, R. and Fogarty, E. "Method and Apparatus for Forming a Fibrous Cylindrical Element." United States. patent 4,146,188, issued March 27, 1979, 34 claims, 10 p.
24. Holmer, H. and Larsson, P. and Svahn, T. and Westman, L. and Warner, M. "Changes in Reel-Density Curves Induced by Different Winding Parameters." Advances and Trends in Winding Technology, Proceedings of the First Winding Technology Conference, Stockholm Sweden, pp. 153-164, March 16, 1987.
25. Komulainen, P. "Roll Quality Measurement and Control." TAPPI Paper Finishing and Converting Conference (Portland) Proceedings, pp. 87-92, ABIPC 54, abstr. 159, October 17, 1982.

26. Komulainen, P. and Tulkki, M. "Winding Quality - Computer Measurement and Control During Winding." ATIP Review, vol. 37, no. 8 pp. 434, 513-520, October 1983 (French).
27. Lane, G. C. "Automatic Roll Quality Control on the Two-Drum Winder." TAPPI Paper Finishing and Converting Conference (Hershey) Proceedings, pp. 133-138, October 6, 1980.
28. Larsson, P. and Svahn, T. and Westman, L. and Warner, M. "Comparison Between Different Methods for the Evaluation of Reel Density." Advances and Trends in Winding Technology, Proceedings of the First Winding Technology Conference, Stockholm Sweden, pp. 181-191, March 16, 1987.
29. Lucas, R. G. "Roll Density Computation." Beloit Research internal memo, February 6, 1984.
30. McDonald, J. D. and Farrell, W. R. "Winder Optimization using an On-line Microcomputer." Pulp & Paper Canada, vol. 86, no. 9, September 1985.
31. Murdoch, J. and Cavan, C. and Klassen, J., Assignee: Canadian General Electric Company "Apparatus for Determining Finished Roll Density in a Mill." United States Patent #4,594,880, June 17, 1986.
32. Odell, M. H. and Symons, R. E. and Brown, G. S. "Control of the Winding Process by Roll Density Measurement." Appita, vol. 38, no. 5, pp. 359-369, September 1985.
33. Popova, N. B. and Rokhman, M. G. "Control of the Wound Density of Roll Materials." Bumazh. Prom., no. 1, pp. 30, January 1983 (Russian).
34. Roisum, D. R. "Mechanics of Roll Winding V" Beloit Research internal report #D85-029, October 2, 1985.
35. Roisum, D. R. "Density I - Effect of Caliper" Beloit Research internal report #D87-028, July 7, 1987.
36. Shvetsov, Y. N. "Importance of Winding Density of Paper Rolls." Bumazh. Prom., no. 6, pp. 21-22, June 1970, (Russian).
37. Ul'yanov, V. I. "Tensometric Apparatus for the Control of Web Winding." USSR Patent #249,929, November 30, 1967 (Russian).
38. Westlund, K. B. "Roll Structure Analysis for KNP Lanaken Belgium.", Beloit Research internal report, #D85-004, January 4, 1985.

Web Handling

39. Adams, R. J. and Westlund, K. B. "Off-line Testing for Newsprint Runnability."
40. Brink, R. "Instrumentation for Roller Nip Studies." TAGA Proceedings, pp. 103-117, 1963.
41. Daly, D. A. "Factors Controlling Traction Between Webs and their Carrying Rolls." Tappi Journal, vol. 48, no. 9, pp. 88A-90A, September 1965.
42. Deshpande, N. V. "Calculation of Nip Width, Penetration, and Pressure for Contact Between Cylinders with Elastomeric Covering." Tappi Journal, vol. 61, no. 10, pp. 115-118, October 1978.
43. Ducotey, K.S. "Dynamic Coefficient of Friction Including the Effects of Air Entrainment Between a Roller and Web." MS Thesis, Web Handling Research Center at Oklahoma State University, December 1987.
44. Hallberg, B. "Statistical Models for Break Frequencies of Newsprint." Thesis, Institute of Mathematics and Statistics, University of Umeaa, 1976.
45. Haller, H. S. and MacDonald, J. "Comment on the Analysis of Web Break Statistics." Tappi Journal, vol. 71, no. 5, August 1988.
46. Knox, K. L, Sweeny, "Fluid Effects Associated with Web Handling." Ind. Engr. Chem. Proc., vol. 10, pp. 201-205, October 1971.
47. Page, D. H. and Seth, R. S. "The Problem of Pressroom Runnability." Tappi Journal, vol. 65, no. 8, pp. 92-95, August 1982.
48. Pfeiffer, J. D. "Web Guidance Concepts and Applications." Dept. of Mechanical Engineering of McGill University internal report, Montreal Quebec.
49. Pramila, A. "Sheet Flutter and the Interaction Sheet and Air." Tappi Journal, vol. 69, no. 7, pp. 70-74, July 1986.
50. Riddiford, A. W. "Airflow Between a Paper Web and a Dryer Surface." Tappi Journal, vol. 52, no. 5, pp. 939-942, May 1969.
51. Shelton, J. J. "Lateral Dynamics of a Moving Web." Ph.D Thesis, Web Handling Research Center at Oklahoma State University, July 1968.
52. Shelton, J. J. "Dynamics of Web Tension Control with Velocity or Torque Control." Proceedings of the American Control Conference. Seattle WA, June 1986.
53. Tajuddin, B. "Mathematical Modelling of Air Entrainment in Web Handling Applications." MS Thesis Web Handling Research Center at Oklahoma State University, December 1987.

Web Property Measurement

54. Andersson, O. et al, "Tensile Studies of Paper at Different Rates of Elongation." Svensk Papperstidning, vol. 56, no. 16, pp. 615, August 1953.
55. Baum, G. A. and Bornhoeft, L. R. "Estimating Poisson Ratios in Paper Using Ultrasonic Techniques." Tappi Journal, vol. 62, no. 5, pp. 87-90, May 1979.
56. Baum, G. A. and Habeger, C. C. "On-line Measurement of Paper Mechanical Properties." Tappi Journal, vol. 63, no. 7, pp. 63-66, July 1980.
57. Baum, G. A. and Brennan, D. C. and Habeger, C. C. "Orthotropic Elastic Constants of Paper." Tappi Journal, vol. 64, no. 8, pp. 97-101, August 1981.
58. Brezinski, J. P. "The Creep Properties of Paper." Tappi Journal, vol. 39, no. 2, pp. 116-128, February 1956.
59. Brezinski, J. P. and Hardacker, K. W. "Poisson Ratio Values." Tappi Journal, vol. 65, no. 8, pp. 114-117, August 1982.
60. Byrd, V. L. et al, "Method for Measuring the Interlaminar Shear Properties of Paper." Tappi Journal, vol. 58, no. 5, pp. 132-134, May 1968.
61. Castagnede, B. and Seo, Y. B. "Optimized Determination of In-plane Poisson Ratios and Shear Modulus for Machine-made Papers." Tappi Journal, vol. 70, no. 9, pp. 113-117, September 1987.
62. Craven, B. D. "An Analysis of the Stress/Strain Curve for Paper." Appita, vol. 15, no. 2, pp. 59, September 1961.
63. Craven, B. D. "Stress Relaxation and Work Hardening in Paper." Appita, vol. 16, no. 2, pp. 57-70, September 1962.
64. Craver, J., K. and Taylor, D. L. "Nondestructive Sonic Measurement of Paper Elasticity." Tappi Journal, vol. 48, no. 3, pp. 142-147, March 1965.
65. Elias, T. C. "An Investigation of the Compression Response ... " Tappi 21st Engineering Conference, November 3, 1966.
66. George, H. O. and Arnoult, J. E. "The IBM Paper Friction Tester." Tappi Journal, vol. 40, no. 12, pp. 972-974, December 1957.
67. Gess, J. M. and Segre, G. "Cross-machine Direction Profile Measurements and their use by the Papermaker." Tappi Journal, vol. 60, no. 8, pp. 117-118, August 1977.
68. Habeger, C. C. and Baum, G. A. "On-line Measurement of Paper Mechanical Properties." Tappi Journal, vol. 69, no. 6, pp. 106-111, June 1986.
69. Hansen, A. "A Portable Instrument for Web-tension Control and Cross-profile Recording." Tappi Journal, vol. 69, no. 12, pp. 48-51, December 1986.

70. Jones, A. R. "An Experimental Investigation of the In-Plane Elastic Moduli of Paper." Tappi Journal, vol. 51, no. 5, pp. 203-209, May 1968.
71. Linna, H. and Moilanen, P. "Comparison of Methods for Measuring Web Tension." Tappi Journal, vol. 71, no. 10, pp. 134-138.
72. Mann, R. W. and Baum, G. A. and Habeger, C. C. "Determination of all Nine Orthotropic Elastic Constants for Machine-Made Paper" Tappi Journal, vol. 63, no. 2, pp 163-166, February 1980.
73. Merricks, J. A. and Masey, W. M. "Utilization of Dynamic Measurement of Caliper on a Paper Machine." Tappi Journal, vol. 56, no. 2, pp. 83-86, February 1973.
74. Miller, L. A. and Springer, G. "A New On-line Caliper Gage." Tappi Journal, vol. 56, no. 2, pp. 45-47, February 1973.
75. Page, D. H. et. al. "The Elastic Modulus of Paper: The Controlling Mechanisms." Tappi Journal, vol. 62, no. 9, September 1979.
76. Papadakis, E. P. "Ultrasonic Methods for Modulus Measurement in Paper." Tappi Journal, vol. 56, no. 2, pp. 74-77, February 1973.
77. Parker, H. V. "What's Happening in Off-line and On-line Test Equipment." Tappi Journal, vol. 65, no. 7, pp. 27-31, July 1982.
78. Pecht, M. and Johnson, M. W. and Rowlands, R. E. "Constitutive Equations for the Creep of Paper." Tappi Journal, vol. 67, no. 5, pp. 106-108, May 1984.
79. Pfeiffer, J. D. "Measurement of the K2 Factor for Paper." Tappi Journal, vol. 64, no. 4, pp. 105-106, April 1981.
80. Rye, T. W. "Using Tenscan to Measure the Tension Profile." Tappi Paper Finishing and Converting Conference Proceedings, October 1982.
81. Rutledge, W. "Sensors for Pulp & Paper: Advances, Trends, Needs." Intech, pp. 25-34, June 1987.
82. Savoie, K. A. "Engineering Properties of Paper." Beloit Research internal report, D85-032, October 18, 1985.
83. Schulgasser, K. "On the In-Plane Elastic Constants of Paper." Fibre Science and Technology, vol. 15, pp. 257-270, 1981.
84. Schulgasser, K. "The In-Plane Poisson Ratio of Paper." Fibre Science and Technology, vol. 19, pp. 297-309, 1983.
85. Senko, E. and Thorpe, J. "On-line Ultrasonic Measurement of Sheet Modulus." Tappi Journal, vol. 68, no. 2, pp. 95-99, February 1985.
86. Uesaka, T. and Murakami, K. and Imamura, R. "Biaxial Tensile Behavior of Paper." Tappi Journal, vol. 62, no. 8, pp. 111-114, August 1979.

87. Uesaka, T. and Murakami, K. and Imamura, R. "On the Poisson Ratio of Paper and its Experimental Determination." Tappi Journal, vol. 65, no. 8, pp. 115-116, August 1982.
88. Van Liew, G. P. "The Z-direction Deformation of Paper." Tappi Journal, vol. 57, no. 11, pp. 121-124, November 1974.
89. Wink, W. A. and Baum, G. A. "A Rubber Platen Caliper Gauge - A New Concept in Measuring Paper Thickness." Tappi Journal, vol. 66 no. 9, pp. 131-133, September, 1983.

Winding

90. Adams, R. J. "The Evolution of Winder Control." Tappi Journal, vol. 67, no. 10, pp. 72-75, October 1984.
91. Bagnato, L. J. "Have Computer, Will Travel: Beloit's Electronic Winder Spreadsheet." Pima, vol. 66, no. 10, pp. 46-48.
92. Bagnato, L. J. "Winder Automation Past Present and Future." Southern Pulp & Paper Mfr, vol. 42, no. 11, pp. 15-19.
93. Bergeron, J. A. "Analyzing Winders: a Quantitative Method." Tappi Journal, vol. 67, no. 10, pp. 66-70, October 1984.
94. Bhooshanan, S. "Development of a Prototype Expert System for Winding Defects." Preliminary Exam, Web Handling Research Center at Oklahoma State University, May 1988.
95. Daly, D. A. "Study of Defects in Wound Rolls Leads to Better Winding Control." Paper Trade Journal, pp 46-48, December 4, 1967.
96. Frye, K. G. "Winding Variables and Their Effect on Roll Hardness and Roll Quality." Tappi Journal, vol. 50, no. 7, pp. 81-6A, July 1967.
97. Frye, K. G. "Today's Flexible Winding Equipment Delivers more Quality, Fewer Defects." Pulp & Paper, pp. 102-106, February 1985.
98. Frye, K. G. "New Winding Methods and Basic Winding Parameters." Tappi Journal, vol. 68, no. 5, pp. 66-72., May 1985.
99. Gilmore, W. G. "Report on Roll Defect Terminology - Tappi CA 1228." Tappi Paper Finishing and Converting Conference Proceedings, October 1973.
100. Girgash, M. E. "Programmable Digital Winder Drives." Tappi Paper Finishing and Converting Conference Proceedings, pp. 39-45, October 1988.
101. Hadlock, A. H. "Unwind Brake Systems." Tappi Paper Finishing and Converting Conference Proceedings, October 1982.
102. Hadlock, A. H. "The Principles of Winding." Pima, pp. 13-16, February 1979.
103. Hari, Y. "Analysis of Lay-on Roll for a Film Winder." Mechanical Engineering and Engineering Science Dept., University of North Carolina, Charlotte NC, unpublished paper.
104. Klikunov, S. D. "Control System for S5P-201 Slitter Stations." Bumazh. Prom. no. 4, pp. 30-31, April 1987 (Russian).
105. Kolesnikov, V. I. et. al. "Structural Diagrams of the Electric Drive of the S5-303 Slitter." Bumazh. Prom., no. 2, pp. 18-19, February, 1987 (Russian).

106. Lucas, R. G. "Internal Gearing in a Roll of Paper." Tappi Paper Finishing and Converting Conference Proceedings, October 1974.
107. Lucas, R. G. "Better Spreading of Web in the Winder - How to Achieve it." Pulp & Paper, vol. 51, no. 4, pp. 154-157.
108. Lucas, R. G. "Dishing in Winding Rolls of Paper." Tappi Journal, vol. 60, no. 7, pp. 121-125, July 1977.
109. Lucas, R. G. "Winder Crepe Wrinkles - Their Causes and Cures." Tappi Paper Finishing and Converting Conference Proceedings, pp. 91-98, October 1981.
110. Pfeiffer, J. D. "Mechanics of a Rolling Nip on Paper Webs." Tappi Journal, vol. 51., no. 8, pp. 77A-85A, August 1968.
111. Pfeiffer, J. D. "Effect of Rewinder Variables on Paper Smoothness." Pulp & Paper Canada, vol. 82, no. 11, November 1981.
112. Pfeiffer, J. D. "Relative Motion Between Web and Winder Drum at the Nip and the Effect of Additional Torque." Advances and Trends in Winding Technology, Proceedings of the First Winding Technology Conference, Stockholm Sweden, pp. 39-53, March 16, 1987.
113. Roisum, D. R. "The Winder Vibration Book." Beloit Research internal publication, February 1985.
114. Roisum, D. R. "Mechanics of Roll Winding VII: Hygroscopic Diffusion in a Paper Roll." Beloit Research internal report, D85-035, December 11, 1985.
115. Roisum, D. R. "The Mechanics of Roll Winding." Beloit Research internal publication, February 1986.
116. Roisum, D. R. "A History of Paper Stresses During Winding." Tappi Paper Finishing and Converting Conference (Mobile) Proceedings, October 1986.
117. Roisum, D. R. "A History of Paper Stresses Before, During and After Winding." Paper Age, October 1986.
118. Roisum, D. R. "Hygroscopic Diffusion in a Paper Roll - Revisited." Beloit Research internal report, D87-016, March 2, 1987.
119. Roisum, D. R. "Paper Stresses During Winding." Advances and Trends in Winding Technology, Proceedings of the First Winding Technology Conference, Stockholm Sweden, pp. 7-23, March 16, 1987.
120. Roisum, D. R. "Winder Vibration." Tappi Paper Finishing and Converting Conference Proceedings, October 1987.
121. Roisum, D. R. "The J-Line Revisited" Beloit Research internal report, D88-003, January 4, 1988.
122. Roisum, D. R. "Winder Vibration." Tappi Journal, vol. 71, no. 1, January 1988.

123. Seidel, K. L. "Practical Approach to Winding Principles." Tappi Paper Finishing and Converting Conference, pp. 23-39, October 1982.
124. Smith, R. D. "Converting to Shaftless Winding Boosts Efficiency at Slitter-Winder." Pulp and Paper, vol. 51, no. 10, pp. 74-76, September 1977.
125. Ward, E. J. "Roll Quality Control in Mill Type Winders." Pulp & Paper Magazine of Canada, vol. 71, no. 18, pp. 85-90, September 1970.
126. Wong, G. H. "High-Production Winding Systems for Today's High-Speed Paper Machines." Pulp & Paper, pp. 180-184, October 1979.

Winding Models

127. Altmann, H. C. "Formulas for Computing the Stresses in Center-Wound Rolls." Tappi Journal, vol. 51, no. 4, pp. 176-179, April 1968.
128. Blaedel, K. L. "A Design Approach to Winding a Roll of Paper." Ph.D Thesis, Dept. of Mechanical Engineering, University of Wisconsin, Madison, 1974.
129. Catlow, M. G. and Walls, G. W. "A Study of Stress Distribution in Pirns." Journal of Textile Institute Part 3, pp. T410-429, 1962.
130. Chang, C. I. "A Closed-Form Solution for an Orthotropic Rotating Disk." Transactions of the ASME, vol. 4, no. 2, December 1974.
131. Gutterman, R. P. "Theoretical and Practical Studies of Magnetic Tape Winding Tensions and of Environmental Roll Stability." US Contract No. DA-18-119-SC-42, 1959.
132. Hakiel, Z. "Nonlinear Model for Wound Roll Stress.", Tappi Paper Finishing and Converting Conference (Mobile) Proceedings, pp. 9-15, October 1986.
133. Hakiel, Z. "Nonlinear Model for Wound Roll Stress.", Tappi Journal, vol. 70, no. 5, pp. 113-117, May 1987.
134. Harland, W. G. "Stress Distribution and Winding Faults in Reels of Plastic Film." Polymer Engineering & Science, January 1967.
135. Harland, W. G. "Theoretical Aspects of Winding Reels." Plastic & Polymers, pp. 162-165, August 1974.
136. Harvey, D. M. "Operating Variables in Spiral Winding: Theoretical Interrelationships and Significance." Tappi Journal, vol. 53, no. 8, pp. 1521-1524, August, 1970.
137. Lekhnitskii, S. G. Theory of Elasticity of Anisotropic Elastic Body, translated by P. Fern, Holden-Day, Inc., 1963.
138. Monk, D. W. and Lautner, W. K. and McMullen, J. F. "Internal Stresses Within Rolls of Cellophane." Tappi Journal, vol. 58, no. 8, August 1975.
139. Penner, A. "Roll Structure Theory." Tappi Journal, vol. 72, no. 10, pp. 207-210 October 1989.
140. Pfeiffer, J. D. "Prediction of Roll Defects From Roll Structure Formulas." Tappi Journal, vol. 62, no. 10, pp. 83-85, October 1979.
141. Pfeiffer, J. D. "An Update of Pfeiffer's Roll-Winding Model." Tappi Journal, vol. 70, no. 10, pp. 130-131, October 1987.
142. Spitz, D. A. "The Effect of Cross Direction Caliper Variations in Winding." Tappi Journal, vol. 52, no. 6, pp. 1168-1170, June 1969.
143. Struik, L. C. "The Winding of Webs into Rolls." TNO Rubber and Plastics Institute Report, Delft, Netherlands,

144. Tramposch, H. "Relaxation of Internal Forces in a Wound Reel of Magnetic Tape." Journal of Applied Mechanics, vol. 32, no. 4, Transactions of the ASME, no. 87, pp 865-873, December 1965.
145. Tramposch, H. "Anisotropic Relaxation of Internal Forces in a Wound Reel of Magnetic Tape." Journal of Applied Mechanics, Transactions of the ASME, vol. 34, no. 4, no. 89, pp. 888-894, 1967.
146. Wolferman, W. "Gunstige Kennlinien der Balmzug-Kraft beim Wickeln von Elasticity." Papier and Kunststoff-Verarbeiten, August 1978.
147. Wolferman, W. and Schroder D. "Web Forces and Internal Tensions for the Winding of an Elastic Web." Advances and Trends in Winding Technology, Proceedings of the First Winding Technology Conference, Stockholm Sweden, pp. 25-37, March 16, 1987.
148. Wu, Z. "A Treatise of Wound Roll Models: The Current Art." Web Handling Research Center at Oklahoma State University preliminary exam, July 1987.
149. Yagoda, H. P. "Integral Formulas for Wound Rolls." Mechanics Research Communications vol. 7, no. 2, pp. 103-112, 1980.
150. Yagoda, H. P. "Centrifugally Induced Stresses Within Center Wound Rolls - Part I." Mechanics Research Communications vol. 7, no. 3, pp. 181-193, Part I, 1980.
151. Yagoda, H. P. "Centrifugally Induced Stresses Within Center Wound Rolls - Part II." Mechanics Research Communications, vol. 7, no. 4, pp. 233-240, 1980.
152. Yagoda, H.P. "Resolution of a Core Problem in Wound Rolls." Journal of Applied Mechanics, vol. 47, pp. 847-854, 1980.
153. Yagoda, H. P. "Generalized Formulas for Stresses in Wound Rolls." Tappi Journal, vol. 64, no. 2, pp. 91-93, February 1981.
154. Zsombor-Murray, P.J. "Tangential and Radial Stress in a Roll of Wound Paper." Technical Notes, pp. 65-4, McGill University, June 28, 1965.

Wound Roll Structure Measurement

155. Bonazza, L. "Automatic Reel Hardness Control with the Backtenders Friend." Pulp and Paper Canada, vol. 80, no. 7, pp. T208-T210, July 1979.
156. Burns, J. W. "The Rho Hardness Meter." Tappi Journal, vol. 61, no. 1, p. 91, January, 1978.
157. Eriksson, L. G. "Deformations in Paper Rolls." Advances and Trends in Winding Technology, Proceedings of the First Winding Technology Conference, Stockholm Sweden, pp. 55-76, March 16, 1987.
158. Eriksson, L. G. "What Happens to a Paper Roll in the Printing Plant." Advances and Trends in Winding Technology, Proceedings of the First Winding Technology Conference, Stockholm Sweden, pp. 195-212, March 16, 1987.
159. Hurst, F. "Hardness of Paper Rolls using Schmidt Concrete Test Hammer." Tappi Journal, vol. 54, no. 7, pp. 1177, July 1971.
160. Hussain, S. M. and Farrell, W. R. and Gunning, J. R. "Most Paper in the Roll is in Unstable Condition." Canadian Pulp and Paper Industry, pp. 52-54, August 1968.
161. Hussain, S. M. and Farrell, W. R. "Roll Winding - Causes, Effects and Cures of Loose Cores in Newsprint." Tappi Journal, vol. 60, no. 5, pp. 112-114, May 1977.
162. Quint, R. J. "Measurement and Control of Paper Roll Condition." Tappi Journal, vol. 51, no. 9, pp. 373-378, September 1968.
163. Lin, C. "An Evaluation of Force Sensing Resistors to Measure Interlayer Pressure." MS Thesis, Web Handling Research Center at Oklahoma State University.
164. Miyanishi, T. and Iida, K. and Sotobayashi, H. "Computerized Tomography of a Paper Roll." Tappi Journal, vol. 71, no. 10, October 1988.
165. Pfeiffer, J. D. "Internal Pressures in a Wound Roll of Paper." Tappi Journal, vol. 49, no. 8, pp. 342-347, August 1968.
166. Pfeiffer, J. D. "Nip Forces and Their Effect on Wound-in Tension." Tappi Journal, vol. 60, no. 2, pp. 115-117, February 1977.
167. Pfeiffer, J. D. "Wound-off Tension Measurement in Paper Rolls." Tappi Journal, vol. 64, no. 4, pp. 106-108, March 1977.
168. Rand, T. and Eriksson, L. G. "Physical Properties of Newsprint Rolls During Winding." Tappi Journal, 56, no. 6, pp. 153-156, June 1973.
169. Roisum, D. R. "Roll Quality Measurement." Tappi Paper Finishing and Converting Conference Proceedings, Richmond VA, October 1988.

170. Roisum, D. R. "The Measurement of Web Stresses During Roll Winding." Web Handling Research Center at Oklahoma State University preliminary exam, February 1988.
171. Roisum, D. R. "How to Measure Roll Quality." Tappi Journal, vol. 71, no. 10, October 1988.
172. Ryti, N. et. al. "Method to Measure the Structure of Newsprint." Tappi Paper Finishing and Converting Conference Proceedings, October 1972.
173. Swedish Newsprint Research Centre (TFL) "Paper Roll Unroundness Meter", Swedish Newsprint Research Centre Advertisement, Djursholm Sweden, March 1986.
174. TAPPI "Routine Control Method RC317." (Cameron Test for Determining residual Strain in Paper), Tappi Journal, vol. 46, no. 12, pp. 123A, December 1963.

Late Additions

175. Tappi. "Tappi Test Methods, vol's 1&2." Tappi Press, Atlanta Ga, 1989.
176. Roark, R. J., and Young, W. C. Formulas for Stress and Strain. Fifth Edition, McGraw-Hill, 1975.
177. O'Connor, P. D. Practical Reliability Engineering. Second Edition, John Wiley & Sons, 1985.
178. Roisum, D. R. "Runnability of Paper." Tappi Paper Finishing and Converting Conference Proceedings, Kansas City KS, October 1989.
179. Hari, Y. "Tension Pattern for Film Winding." Unpublished Report of the Dept. of Mechanical Engineering of the University of N. Carolina at Charlotte.
180. Parker, H. V. Quality Progress, vol. 14, no. 3, pp. 18, 1981.
181. Pfeifer, R. J. Pulp & Paper, vol. 55, no. 2, pp. 68, February 1981.
182. Hazelwood, E. Paper Trade J., vol. 157, no. 29, pp. 30, 1973.
183. Setterholm, V. C. Tappi Journal, vol. 53, no. 3, pp. 164, March 1974.
184. Rosenthal, M. R. "Effective Thickness of Paper: Appraisal and Further Development." USDA Forest Service Research, Paper FPL 287, 1977.
185. American Paper Institute "Measurement of Thickness." American Paper Institute, Instrumentation Program Report, no. 60, December 1975.
186. Willett, M. S. and Poesch, W. L. "Determining the Stress Distributions in Wound Reels of Magnetic Tape Using a Nonlinear Finite Difference Approach." J. of Applied Mechanics, vol. 55, pp. 365-371, June 1988.
187. Bertram, N. and Eshel A. "Recording Media Archival Attributes." RADC-TR80-123, Griffis Air Force Base, New York 1980.
188. Connolly, D. and Winarski, J. "Stress Analysis of Wound Magnetic Tape." Tribology & Mechanics of Magnetic Storage Media Special Publication 16, Am. Soc. of Lubrication Engineers, 1984.
189. Eshel, A. and Baker, S. "Mechanical Aspects of Archival Storage of Magnetic Tape." Tribology & Mechanics of Magnetic Storage Media Special Publication 16, Am. Soc. of Lubrication Engineers, 1984.
190. Thorpe, J. "Analysis of Dimensional Stability - Roll Cockle." Nordic Pulp & Paper Research Journal, pp 51-54, January 1985.
191. Roisum, D. R. "Runnability of Paper - Part I Web Break Statistics." Tappi Journal, vol. 73, no. 1, January 1990.
192. Roisum, D. R. "Runnability of Paper - Part II Diagnosing Web Breaks." Tappi Journal, vol. 73, no. 2, February 1990.
193. Hall, K. M and McLemore. "Mill Experience in Improving Mechanical Reel Condition." Tappi Paper Finishing and Converting Conference Proceedings, Kansas City Mo., October 1989.
194. Anon. "Skiing Over Cockles" Paper, October 10, 1989.

195. Anon. "Slitting and Rewinding Fundamentals for Converters." Converting Equipment Manufacturing Association Seminar Notes, 2nd Edition, Wilmington DE, November 8, 1987.
196. Boresi, A. P. et. al. Advanced Mechanics of Materials. John Wiley and Sons, New York, Third Edition, 1978.
197. Knox, K. L. and Sweeney, T. L. "Fluid Effects Associated with Web Handling." Ind. Eng. Chem. Process, no. 10, pp. 201-205, 1971.
198. Block, H. and Van Rossum, J. J. "The Foil Bearing - a New Departure." Lub. Eng., no. 9, pp 316-320, 1953.
199. Langlois, W. E. "The Lightly Loaded Foil Bearing at Zero Angle of Wrap." IBM J. of Res. & Dev., no. 7, pp 112-116, 1963.
201. Eshel, A. and Elrod, H. G. "The Theory of Infinitely Wide, Perfectly Flexible, Self-Acting Foil Bearing." J. of Basic. Tech., 87, pp 831-836, 1965.
202. Barlow, E. J. "Derivation of Governing Equations for Self-Acting Foil Bearing." J. of Lub. Tech, 89, pp 334-340, 1967.
204. Basheer, M. S. "An Experimental Study of Air Entrainment in Web Handling Applications." MS Thesis, Oklahoma State University, July 1988.
205. Ozisik, M. N. Heat Conduction. John Wiley and Sons, New York, 1980.
206. Lin, J. Y. and Westmann, R. A. "Viscoelastic Winding Mechanics." J. of Applied Mechanics, vol 56, no. 12, pp. 821-827, December 1989.

APPENDIX A

WINDING MODEL COMPUTER PROGRAM LISTINGS

Linear Isotropic Model - Roisum

'WindLiso

'Stresses During Roll Winding

'Linear Isotropic, Variable Wound in Stress

'Roisum Model, 'Mechanics of Roll Winding Vol. 1; Chapt 1-3,4,C-1-3,4

'Written in Microsoft Quickbasic Basic 1.0 for Macintosh and 4.0 for PC

'David R Roisum 4/24/89

DEFDBL A-Z :'your Basic Language may not support double precision

**** DEFINE INPUT VARIABLES HERE ****

 'Wound-In-Stress as a Function of Radius

 WIS0 = 750

 WIS1 = 0

 WIS2 = 0

 DEF FNWIS(R) = WIS0 + WIS1*R + WIS2*R^2

 RIR = 2 :'Radius Inner Roll

 ROR = 20 :'Radius Outer Roll

 IR = .01 :'Increment in Radius (set to give 100-1000 steps)

 PIR = 1 :'Print Increment in Radius (set >= IR)

 ER = 10000 :'Modulus, Roll

 EC = 100000! :'Modulus, Core

 UR = .01 :'Poisson Ratio, Roll

 COMMENTS\$ = "Linear Isotropic Winding Model"

**** DEFINE INPUT VARIABLES HERE ****

STARTRUN:

GOSUB USERIN

'Getting Started

 NUMPTS% = (ROR-RIR)/PIR + 1:'Number of total solution points

 DIM SR(NUMPTS%) :'Radial Stress Array

 DIM ST(NUMPTS%) :'Tangential Stress Array

 FOR Q% = 1 TO NUMPTS% :'Initialize Wound-In-Stresses (tang'l stress)

 RPR = RIR + (Q%-1)*PIR

 ST(Q%) = FNWIS(RPR)

```

NEXT Q%

'Echo Input
LPRINT
LPRINT "ROISUM LINEAR ISOTROPIC WINDING MODEL"
LPRINT
LPRINT "WEB HANDLING RESEARCH CENTER"
LPRINT "OKLAHOMA STATE UNIVERSITY"
LPRINT
LPRINT COMMENTS$
LPRINT TIME$, DATE$: 'your Basic may not support this statement
LPRINT
'Calculate and print wound-in-stress at core, middle and outside of roll
LPRINT "WOUND IN STRESS = "; WIS0; " + "; WIS1; "*"R + "; WIS2; "*"R^2"
LPRINT "MODULUS, WEB = "; TAB(20); ER
LPRINT "MODULUS, CORE = "; TAB(20); EC
LPRINT "POISSON, WEB = "; TAB(20); UR
LPRINT "INCREM RADIUS = "; TAB(20); IR
LPRINT
LPRINT TAB(5); "RADIUS"; TAB(19); "RADIAL STRESS";
LPRINT TAB(33); "TANG STRESS"; TAB(58); WIS
LPRINT
CLS
LOCATE 2,1
PRINT "CALCULATING CURRENT FINISH RADIUS = "

**** MAIN LOOP - Compute Winding Stress at various Diameters ****
'Add layers of thickness IR from core radius RIR to roll finish radius ROR
'Roll Present Radius is RPR

FOR RPR = (RIR+IR) TO ROR STEP IR

    LOCATE 2,35
    PRINT RPR           : 'Screen feedback
    WIS = FNWIS(RPR)    : 'Wound-In-Stress
    'Pres under Outer wrap PO, Pres under Inner Wrap PI, due to add of 1 wrap
    PO = WIS * IR / RPR
    PI = 2*RPR^2*EC*PO / ((RPR^2-RIR^2)*(ER+UR*EC) + (RPR^2+RIR^2)*EC)
    'Q% is a pointer for stress array, C1 and C2 are intermediate calcs
    Q% = 0
    C2 = (PI*RIR^2-PO*RPR^2)/(RPR^2-RIR^2)

    'Calculate (print) increment in stresses on all layers
    'beneath the outer wrap and sum assuming superposition
    FOR RRR = RIR TO RPR STEP PIR
        Q% = Q% + 1
        C1 = RPR^2*RIR^2*(PO-PI)/(RPR^2-RIR^2)/RRR^2
        SR(Q%) = SR(Q%) + C1 + C2
        ST(Q%) = ST(Q%) - C1 + C2
    NEXT RRR

NEXT RPR

```

```
**** END MAIN LOOP ****
```

```
'Print loop for calculated stresses
```

```
FOR Q% = 1 TO NUMPTS%
```

```
RPR = RIR + (Q%-1)*PIR
```

```
LPRINT USING "#####.#####"; RPR, SR(Q%), ST(Q%), FNWIS(RPR)
```

```
NEXT Q%
```

```
INPUT "DO YOU WANT ANOTHER RUN ??", RESPONSE$
```

```
IF RESPONSE$ = ("Y" OR "y") GOTO STARTRUN
```

```
IPRINT "THANK YOU, HAVE A NICE DAY !!"
```

```
END
```

```
'*****
```

```
**** EDITING SUBROUTINES ****
```

```
'*****
```

```
USERIN:
```

```
PRINT "Calculation for the Wound Roll Stress Distribution for the"
```

```
PRINT "LINEAR ISOTROPIC WINDING MODEL with a 2nd order Wound-In-Stress Profile"
```

```
PRINT "Copyright 1989, David Roisum, Web Handling Research Center"
```

```
PRINT
```

```
PRINT "During input, default values may be selected with a <CR> or"
```

```
PRINT "may be changed by typing in a new value."
```

```
PRINT "Errors before <CR> may be corrected by backspacing."
```

```
PRINT "As stresses are calculated, they are printed to screen and LPT1"
```

```
PRINT "The variable wound in stress profile is given as
```

```
PRINT "WIS(R) = WIS0 + WIS1*R + WIS2*R^2 where R is the radius in inches"
```

```
PRINT :PRINT
```

```
CALL EDNUM("WIS0 (PSI)", CDBL(-10000), WIS0, CDBL(+10000))
```

```
CALL EDNUM("WIS1 (PSI)", CDBL(-1000), WIS1, CDBL(+1000))
```

```
CALL EDNUM("WIS2 (PSI)", CDBL(-100), WIS2, CDBL(+100))
```

```
PRINT
```

```
CALL EDNUM("Radius Inner Roll (in)", CDBL(0), RIR, CDBL(100))
```

```
CALL EDNUM("Radius Outer Roll (in)", CDBL(RIR), ROR, CDBL(200))
```

```
PRINT
```

```
PRINT "Radial calculation increment should be set to give"
```

```
PRINT "100-1000 steps between inner and outer roll radius"
```

```
CALL EDNUM("Calculation increment (in)", CDBL(.001), IR, CDBL(1))
```

```
PRINT
```

```
PRINT "Radial print increment should be set to give"
```

```
PRINT "10-100 steps between inner and outer roll radius"
```

```
CALL EDNUM("Print increment (in)", CDBL(.01), PIR, CDBL(10))
```

```
PRINT
```

```
CALL EDNUM("Modulus. Roll (psi)", CDBL(10), ER, CDBL(10000000&))
```

```
CALL EDNUM("Modulus. Core (psi)", CDBL(0), EC, CDBL(10000000&))
```

```
CALL EDNUM("Poisson Ratio", CDBL(0), UR, CDBL(1))
```

```
CALL EDALPHA("Comments?", COMMENT$)
```

```
RETURN
```

```
SUB CHKLM(LOWLIM, NEWNUM, UPLIM, YNFLAG%) STATIC
```

```
IF NEWNUM < LOWLIM THEN YNFLAG% = 0
```

```
IF NEWNUM > UPLIM THEN YNFLAG% = 0
```

```
END SUB
```

```
SUB EDALPHA(TEXT$, ALPHA$) STATIC
  PRINT TEXT$; TAB(20); ALPHA$; TAB(40);
  INPUT RESPONSE$
  IF RESPONSE$ <> "" THEN ALPHA$ = RESPONSE$
END SUB
```

```
SUB EDNUM(TEXT$, LOWLIM, DEFNUM, UPLIM) STATIC
  YNFLAG% = 0
  WHILE YNFLAG% <> 1
    PRINT TEXT$; TAB(30);
    PRINT USING "#####.###"; DEFNUM;
    INPUT NEWNUM$
    IF NEWNUM$ <> "" THEN
      CALL ISANUM(NEWNUM$, YNFLAG%)
      NEWNUM = VAL(NEWNUM$)
      CALL CHKLM(LOWLIM, NEWNUM, UPLIM, YNFLAG%)
      IF YNFLAG% <> 1 THEN
        BEEP
        PRINT "***ERROR** NOT A NUMBER BETWEEN "; LOWLIM;" AND ";UPLIM
      END IF
    ELSE
      YNFLAG% = 1
      NEWNUM = DEFNUM
    END IF
  WEND
  DEFNUM = NEWNUM
END SUB
```

```
SUB ISANUM(NEWNUM$, YNFLAG%) STATIC
  YNFLAG% = 1
  LENGTH% = LEN(NEWNUM$)
  FOR Q% = 1 TO LENGTH%
    ASCII% = ASC(MID$(NEWNUM$,Q%,1))
    IF(ASCII%<48 ORASCII%57)ANDASCII%<>46ANDASCII%<>45THEN YNFLAG% = 0
  NEXT Q%
END SUB
END
```

Linear Anisotropic Model - Altmann

'WindAltm

'Stresses During Roll Winding

'Linear Anisotropic, Variable Wound in Stress

'Altmann Model, Tappi Vol 51, No. 4

'Written in Microsoft Quickbasic 1.0 for Macintosh and 4.0 for PC

'David R Roisum 4/24/89

DEFDBL A-Z :your Basic may not support this statement

* * * * DEFINE INPUT VARIABLES HERE * * *

'Wound-In-Stress as a Function of Radius

WIS0 = 750

WIS1 = 0

WIS2 = 0

DEF FNWIS(R) = WIS0 + WIS1*R + WIS2*R^2

RIR = 2 :Radius Inner Roll

ROR = 20! :Radius Outer Roll

PIR = 1 :Print Increment in Radius

ER = 1000 :Modulus, Radial

ET = 750000! :Modulus, Tangential

EC = 100000! :Modulus, Core

UR = .01 :Poissons Ratio, Radial

UT = .01 :Poissons Ration, Tangential

PANEL% = 200 :Number of Panels for Integration (Even Integer,100-1000)

COMMENT\$ = "Lin Ani Std"

**** DEFINE INPUT VARIABLES HERE ***

STARTRUN:

GOSUB USERIN

'Getting Started

NUMPTS% = (ROR-RIR)/PIR + 1

DIM SR(NUMPTS%) :Radial Stress Array

DIM ST(NUMPTS%) :Tangential Stress Array

DEF FNINTEG(S,V, J)=WIS*S^(B-1)/(1+A*S^GAM2) :WINDING INTEGRAL

'Echo Input

LPRINT

LPRINT "ALTMANN LINEAR ANISOTROPIC WINDING MODEL"

LPRINT

LPRINT "WEB HANDLING RESEARCH CENTER"

LPRINT "OKLAHOMA STATE UNIVERSITY"

LPRINT

LPRINT COMMENT\$

LPRINT TIME\$, DATE\$:your Basic may not support this statement

LPRINT

'Calculate and print wound-in-stress at core, middle and outside of roll

LPRINT "WOUND IN STRESS = "; WIS0; " + "; WIS1; "*"R + "; WIS2; "*"R^2"

```

LPRINT "MODULUS, RADIAL = "; TAB(20); ER
LPRINT "MODULUS, TANGEN = "; TAB(20); ET
LPRINT "MODULUS, CORE = "; TAB(20); EC
LPRINT "POISSON, RADIAL = "; TAB(20); UR
LPRINT "POISSON, TANGEN = "; TAB(20); UT
LPRINT "# OF PANELS = "; TAB(20); PANEL%
LPRINT
LPRINT TAB(5); "RADIUS"; TAB(18); "RADIAL STRESS";
LPRINT TAB(35); "TANG STRESS"; TAB(58); "WIS"
LPRINT

```

```
'Calculate Intermediate Parameters
```

```

ERD = ET/ER      :'Dimensionless Radial Modulus
ECD = ET/EC      :'Dimensionless Core Modulus
V=(UT+ERD*UR)/2
DEL=(UT-ERD*UR)/2
GAM=(DEL^2+ERD)^.5
GAM2 = 2*GAM
ALP=GAM-DEL
BET=GAM+DEL
A=(GAM-V-ECD)/(GAM+V+ECD)
B=1-ALP
RORD = ROR/RIR      :'Dimensionless Outer Radius
Q% = 0               :'Q is a pointer for stress arrays

```

```
**** MAIN LOOP - Compute Winding Stress at various Diameters ***
```

```
FOR RPR = RIR TO ROR STEP PIR
```

```

Q% = Q% + 1
RPRD = RPR/RIR      :'Dimensionless Present outer Radius

```

```

'Compute Winding Integral (WI) with 2 decades
WI=0 : LOLIM = RPRD : UPLIM = RPRD+.1*(RORD-RPRD)
GOSUB INTEG
WI = SUM : LOLIM = UPLIM : UPLIM = RORD
GOSUB INTEG
WI = WI + SUM

```

```

'Compute Stresses and Print
CONST = WI / (RPRD^B)
SR(Q%) = -(1+A*RPRD^-GAM2) * CONST
ST(Q%)=FNWIS(RPR) - (ALP-(A*BET*RPRD^-GAM2)) * CONST
LPRINT USING "#####.#####"; RPR, SR(Q%), ST(Q%), FNWIS(RPR)

```

```
NEXT RPR
```

```
**** END MAIN LOOP****
```

```

INPUT "DO YOU WANT ANOTHER RUN ??", RESPONSE$
IF RESPONSE$ = ("Y" OR "y") GOTO STARTRUN
PRINT "THANK YOU, HAVE A NICE DAY !!"

```

```
END
```

INTEG:

'Integration by Simpson's 1/3 Rule, FNINTEG is function to integrate

DX = (UPLIM-LOLIM) / PANEL% :'PANEL WIDTH

WIS = FNWIS(LOLIM*RIR)

ES = FNINTEG(LOLIM,WIS) :'END SUM

WIS = FNWIS(UPLIM*RIR)

ES = ES + FNINTEG(UPLIM,WIS)

EVS = 0 : ODS = 0 :'EVEN AND ODD SUM

FOR QQ% = 1 TO (PANEL%/2)

S = LOLIM + DX*(2*QQ%-1)

WIS = FNWIS(S*2)

ODS = ODS + FNINTEG(S,WIS)

WIS = FNWIS(S*2)

S = LOLIM + DX*(2*QQ%)

EVS = EVS + FNINTEG(S,WIS)

NEXT QQ%

S = LOLIM + PANEL%*DX

EVS = EVS - FNINTEG(S,WIS)

SUM = (ES+4*ODS+2*EVS) *DX/3

RETURN

END

NOTE:

Input Editing Subroutines similar to Roisum Linear Isotropic program are not repeated here

Linear Anisotropic Model - Yagoda

'WindYago

'Stresses During Roll Winding

'Linear Anisotropic, Variable WIS

'Yagoda's Model, ASME 80-WA/APM-23

'Written in Microsoft Quickbasic 1.0 for Macintosh and 4.0 for PC

'David R Roisum 4/24/89

DEFDBL A-Z

*** DEFINE INPUT VARIABLES HERE ***

WIS0 = 750 :Wound in Stress constant
WIS1 = 0 :Wound in Stress constant, radius multiplier
WIS2 = 0 :Wound in Stress constant, radius squared mult'r
RIR = 2 :Radius Inner Roll
ROR = 20 :Radius Outer Roll
PIR = 1 :Print Increment in Radius
ER = 1000 :Modulus, Radial
ET = 750000! :Modulus, Tangential
EC = 100000! :Modulus, Core
UR = .01 :Poissons Ratio, Radial
UT = .01 :Poissons Ratio, Tangential
SMALL = 1D-30 :Error Tolerance (set tiny, but avoid overflow)
COMMENT\$ = "Lin Ani Std"

*** DEFINE INPUT VARIABLES HERE ***

STARTRUN:

GOSUB USERIN

'GETTING STARTED

NUMPTS% = (ROR-RIR)/PIR + 1
DIM SR(NUMPTS%) :Radial Stress Array
DIM ST(NUMPTS%) :Tangential Stress Array
DIM WIS#(3)
WIS#(0) = WIS0
WIS#(1) = WIS1*RIR
WIS#(2) = WIS2*RIR^2

'ECHO INPUT

LPRINT
LPRINT "YAGODA LINEAR ANISOTROPIC WINDING MODEL"
LPRINT
LPRINT "WEB HANDLING RESEARCH CENTER"
LPRINT "OKLAHOMA STATE UNIVERSITY"
LPRINT
LPRINT COMMENT\$
LPRINT TIMES\$, DATE\$:your Basic may not support this statement
LPRINT
'Calculate and print wound-in-stress at core, middle and outside of roll


```

LPRINT "WOUND IN STRESS = "; WIS0; " + "; WIS1; "*"R + "; WIS2; "*"R^2"
LPRINT "MODULUS, RADIAL = "; TAB(20); ER
LPRINT "MODULUS, TANGEN = "; TAB(20); ET
LPRINT "MODULUS, CORE = "; TAB(20); EC
LPRINT "POISSON, RADIAL = "; TAB(20); UR
LPRINT "POISSON, TANGEN = "; TAB(20); UT
'LPRINT "SMALL = "; TAB(20); SMALL
LPRINT
LPRINT TAB(5); "RADIUS"; TAB(18); "RADIAL STRESS";
LPRINT TAB(35); "TANG STRESS"; TAB(58); "WIS"
LPRINT

```

'Calculate Intermediate Parameters

```

ERD = ET/ER      :'Dimensionless Radial Modulus
ERC = ET/EC      :'Dimensionless Core Modulus
V = (UT+ERD*UR)/2
DEL = (UT-ERD*UR)/2
GAM = (DEL^2+ERD)^.5
ALP = GAM-DEL
BET = GAM+DEL
A = (GAM-V-ERC)/(GAM+V+ERC)
B = 1-ALP
GAM2 = 2*GAM
RORD = ROR/RIR      :'Dimensionless Outer Radius
Q% = 0:'Q is a pointer for stress arrays

```

*** MAIN LOOP - Compute Winding Stress at various Diameters ***

FOR RPR = RIR TO ROR STEP PIR

```

Q% = Q% + 1
RPRD = RPR/RIR      :'Dimensionless Present outer Radius

'Compute Winding Series Double Summation and Print
OUTSERIES = 0
FOR PHI% = 0 TO 2      :'WIS polynomial loop
  IF ABS(WIS#(PHI%)) < SMALL THEN GOTO SKIP1
  'Don't calc small or 0 WIS terms
  D1 = 1 + (B+PHI%)/GAM2
  D2 = (RORD^GAM2/A)*(RPRD/RORD)^GAM2
  SERIES = 0
  FOR N% = 2 TO 100      :'Winding integral series
    DENOM = (N%-D1)*D2^N%
    IF ABS(DENOM) < SMALL THEN GOTO SKIP2
    '1st term of iso'c case = 0
    IF ABS(DENOM) > 1/SMALL THEN GOTO SKIP3
    'exit when terms small
    TERM = (-1)^N%/DENOM
    SERIES = SERIES + TERM
  SKIP2:
  NEXT N%
SKIP3:
'if-isotropic, else anisotropic

```

```

      IF ABS(B+PHI%) < SMALL THEN
      SERFUNC = -LOG(RPRD/RORD) - RPRD^GAM2*SERIES/(GAM2*A)
      ELSE
      SERFUNC = -(1-(RPRD/RORD)^(-B-PHI%))/(B+PHI%) -
RPRD^GAM2*SERIES/(GAM2*A)
      END IF
      OUTSERIES = OUTSERIES + SERFUNC*WIS#(PHI%)*RPRD^PHI%
      SKIP1:
      NEXT PHI%

SR(Q%) = -(1+A*RPRD^-GAM2)*OUTSERIES
ST(Q%) = WIS#(0) + WIS#(1)*RPRD + WIS#(2)*RPRD^2 - (ALP-A*BET*RPRD^-
GAM2)*OUTSERIES
LPRINT USING "#####.#####"; RPR, SR(Q%), ST(Q%),
WIS0+WIS1*RPR+WIS2*RPR^2

NEXT RPR

' * * *   END MAIN LOOP * * *

INPUT "DO YOU WANT ANOTHER RUN ??", RESPONSE$
IF RESPONSE$ = ("Y" OR "y") GOTO STARTRUN
PRINT "THANK YOU, HAVE A NICE DAY !!"

END

```

NOTE:

Input Editing Subroutines, similar to Roisum Linear Isotropic program, are not repeated here

NonLinear Anisotropic Model - Hakiel

'WindHaki

'Stresses During Roll Winding

'Nonlinear Anisotropic, Variable WIS

'Hakiels Model, Tappi Journal, vol 70 no 5, May 1987

'Written in Microsoft Quick Basic 1.0 for the Macintosh

'David R Roisum 6/16/89

DEFDBL A-Z

CLEAR, 500000&

*** DEFINE INPUT VARIABLES HERE ***

'Wound-In-Stress as a Function of Radius

WIS0 = 750 :'Wound in Stress constant

WIS1 = 0 :'Wound in Stress constant, radius multiplier

WIS2 = 0 :'Wound in Stress constant, radius squared multiplier

DEF FNWIS(R) = WIS0 + WIS1*R + WIS2*R^2

RIR = 2 :'Radius Inner Roll

ROR = 20 :'Radius Outer Finished Roll

IR = .05 :'Radial Thickness of Calculation Interval ie gridsize

PIR = .5 :'LPRINT Increment in Radius

'Radial Modulus as a Function of Radial Stress

ER0 = 750 :'Radial Modulus constant

ER1 = 0 :'Radial Modulus constant, radius multiplier

ER2 = 0 :'Radial Modulus constant, radius squared multiplier

DEF FNER(SR) = ER0 + ER*R + ER*R^2

ET = 750000& :'Modulus, Tangential

EC = 100000& :'Modulus, Core

UR = .01 :'Poissons Ratio, Radial

UT = .01 :'Poissons Ratio, Tangential

COMMENT\$ = "Lin Ani Std Input"

OUTFILE\$ = "HD 40:Athesis:DispWIS:Nonlinout"

*** DEFINE INPUT VARIABLES HERE ***

'Getting Started

NUMPTS% = (ROR-RIR)/IR :'Number of total solution points

DIM SR(NUMPTS%+5) :'Radial Stress Array

DIM ST(NUMPTS%+5) :'Tangential Stress Array

DIM DSR(NUMPTS%+5) :'Differential Radial Stress Array

DIM DST(NUMPTS%+5) :'Differential Tangential Stress Array

DIM AA(NUMPTS%+5,3) :'Square Matrix of Diff Eq Terms

DIM B(NUMPTS%+5) :'Forcing Function Array

'Echo Input

LPRINT

LPRINT "Hakiel/Roisum Nonlinear Anisotropic Winding Model"

LPRINT

LPRINT "WEB HANDLING RESEARCH CENTER"

LPRINT "OKLAHOMA STATE UNIVERSITY"

```

LPRINT
LPRINT COMMENT$
LPRINT TIME$ , DATE$ : 'your Basic might not support this
LPRINT
LPRINT "WOUND IN STRESS = "; WIS0; " + "; WIS1; "**R + "; WIS2; "**R^2"
LPRINT "MODULUS, RADIAL = "; ER0; " + "; ER1; "**R + "; ER2; "**R^2"
LPRINT "MODULUS, TANGEN = "; TAB(20); ET
LPRINT "MODULUS, CORE = "; TAB(20); EC
LPRINT "POISSON, RADIAL = "; TAB(20); UR
LPRINT "POISSON, TANGEN = "; TAB(20); UT
LPRINT "RADIAL INCREMENT = "; TAB (20); IR
LPRINT
LPRINT TAB(5); "RADIUS"; TAB(18); "RADIAL STRESS";
LPRINT TAB(35); "TANG STRESS"; TAB(58); "WIS"
LPRINT

```

*** MAIN LOOP - Compute Winding Stress at Various Diameters ***

```

STARTRUN:
GOSUB USERIN

```

```

GOSUB FIRSTLAYERS

```

```

FOR Q% = 2 TO (NUMPTS%-2)
  PRINT Q%
  GOSUB FILLMAT
  NN% = Q%
  GOSUB TRIDIAG
  GOSUB SUMSTR
NEXT Q%

```

```

GOSUB CALCTANG

```

```

' * * * END MAIN LOOP * * *

```

'Final LPRINT and Save Loop

```

OPEN OUTFILES$ FOR OUTPUT AS #1
FOR Q% = 0 TO NUMPTS% STEP (PIR/IR)
  LPRINT USING "#####.#####"; (RIR+Q%*IR), SR(Q%), ST(Q%),
  FNWIS(RIR+Q%*IR)
  PRINT #1, (RIR+Q%*IR), CHR$(9), SR(Q%), CHR$(9), ST(Q%)
NEXT Q%
CLOSE #1

```

```

END

```

```

.....
' * * * SUBROUTINES AND STUFF * * *
.....

```

```

FIRSTLAYERS:

```

```

'Approximation assuming small IR
DDSR = -FNWIS(RIR)*IR/(RIR)

```

```

FOR QQ% = 0 TO 3
    SR(QQ%) = (3-QQ%)*DDSR
NEXT QQ%
RETURN

```

FILLMAT:

```

'Zero Square Matrix
FOR ZZ% = 1 TO Q%
    FOR ZZZ% = 1 TO 3
        AA(ZZ%,ZZZ%) = 0
    NEXT ZZZ%
NEXT ZZ%

```

```

'Initialize First Layer
ERHERE = FNER(SR(0))
CORCONSTH = EC*ERHERE*RIR/(2*EC*ERHERE*IR-2*ERHERE*ET*IR-
    3*EC*ERHERE*RIR-2*EC*ET*IR*UR)
RPR = RIR + IR
ERHERE = FNER(SR(1))
ADIFF = 3 + UT - UR*ET/ERHERE
BDIFF = 1-ET/ERHERE*(1+UR)+UT
AA(1,2) = (BDIFF*IR^2 + 2*ADIFF*CORCONSTH*IR*RPR - 2*RPR^2 -
    4*CORCONSTH*RPR^2)/IR^2
AA(1,3) = (ADIFF*IR*RPR - ADIFF*CORCONSTH*IR*RPR + 2*RPR^2 +
    2*CORCONSTH*RPR^2)/(2*IR^2)
B(1) = 0

```

```

*** INTERMEDIATE LAYERS ***
FOR QQ% = 2 TO (Q%-1)
    ERHERE = FNER(SR(QQ%))
    RPR = RIR + QQ%*IR
    ADIFF = 3 + UT - UR*ET/ERHERE
    BDIFF = 1-ET/ERHERE*(1+UR)+UT
    AA(QQ%,1) = RPR*(-ADIFF*IR + 2*RPR)/(2*IR^2)
    AA(QQ%,2) = BDIFF - (2*RPR^2)/IR^2
    AA(QQ%,3) = RPR*(ADIFF*IR + 2*RPR)/(2*IR^2)
    B(QQ%) = 0
NEXT QQ%

```

```

'Initialize Under Second Layer
ERHERE = FNER(SR(Q%))
RPR = RIR + Q%*IR
ADIFF = 3 + UT - UR*ET/ERHERE
BDIFF = 1-ET/ERHERE*(1+UR)+UT
AA(Q%,1) = RPR*(-ADIFF*IR + 2*RPR)/(2*IR^2)
AA(Q%,2) = BDIFF - (2*RPR^2)/IR^2
B(Q%) = (FNWIS(RPR+2*IR)*IR/(RPR+2*IR))*RPR*(ADIFF*IR + 2*RPR)/(2*IR^2)
RETURN

```

SUMSTR:

```

DSR(0) = CORCONSTH * (-4*DSR(1) + DSR(2))
DSR(Q%+1) = -FNWIS(RIR + (Q%+2)*IR)*IR/(RIR + (Q%+2)*IR)

```

```

DSR(Q%+2) = 0
'Total Accumulated Stresses
FOR QQQ% = 0 TO Q%+2
    SR(QQQ%) = SR(QQQ%) + DSR(QQQ%)
NEXT QQQ%
RETURN

```

CALCTANG:

```

FOR QQ% = 1 TO (NUMPTS%-1)
    RPR = RIR + QQ%*IR
    DSR = (-SR(QQ%-1) + SR(QQ%+1))/(2*IR)
    ST(QQ%) = RPR*DSR + SR(QQ%)
NEXT QQ%
RPR = RIR + NUMPTS%*IR
ST(NUMPTS%) = FNWIS(RPR)
ST(0) = 2*ST(1) - ST(2)
RETURN

```

TRIDIAG:

```

'Forward
FOR I% = 2 TO NN%
    AA(I%,2) = AA(I%,2) - AA(I%,1)* AA(I%-1,3)/AA(I%-1,2)
NEXT I%
DSR(NN%) = B(NN%)/AA(NN%,2)
'Back Substitution
FOR I% = NN% - 1 TO 1 STEP -1
    DSR(I%) = (B(I%) - AA(I%,3)*DSR(I%+1))/AA(I%,2)
NEXT I%
RETURN

```

END

NOTE:

Input Editing Subroutines, similar to Roisum Linear Isotropic program, are not repeated here

APPENDIX B

WINDING MODEL COMPUTER OUTPUT

Standard Sets of Input Parameters

<u>TestName</u>	<u>LinIsoStd</u>	<u>LinIsoTst</u>	<u>LinAniStd</u>	<u>LinAniTst</u>	<u>NonLinStd</u>	<u>NonLinTst</u>
WIS	750	900-60R+3R ²	750	900-60R+3R ²	1000-20R	900-60R+3R ²
Eradial	10,000	1,000	1,000	1,000	50+100P	1000+P
Etangen	-	-	750,000	2,000	750,000	2,000
Ecore	100,000	3,000	100,000	3,000	100,000	3,000
μradial	0.01	.3	0.01	0.1	0.01	0.1
μtangen	-	-	0.01	0.2	0.01	0.2

The roll inner and outer diameters are 4" and 40" respectively.

Gridsizes are listed on output and are approximately optimized for each input set.

Test Input Parameters Solvable by Various Winding Models

<u>TestName</u>	<u>LinIsoStd</u>	<u>LinIsoTst</u>	<u>LinAniStd</u>	<u>LinAniTst</u>	<u>NonLinStd</u>	<u>NonLinTst</u>
LinIso	YES	YES	no	no	no	no
Altmann	YES	YES	YES	YES	no	no
Yagoda	YES	YES	YES	YES	no	no
Hakiel	YES	YES	YES	YES	YES	YES

Output listings were calculated using the programs given in Appendix A on an Apple Macintosh II engineering workstation with a 68881 math coprocessor running compiled Microsoft QuickBasic 2.0.

Roisum Linear Isotropic - Linear Isotropic Standard Input

Double Precision, 0.01" grid spacing

<u>RADIUS</u>	<u>RADIAL STRESS</u>	<u>TANG STRESS</u>
2	-2716.089139648347	451.230195245774
3	-1776.913316531786	-93.214215577751
4	-1368.961016622711	-161.784541855927
5	-1124.334302714681	-118.656875741218
6	-950.988223462363	-45.403753015089
7	-816.087111214338	34.181055037843
8	-704.999209561983	112.287578296520
9	-610.122189840559	186.353363744073
10	-527.040454773716	255.715551158843
11	-452.966445333454	320.426033756962
12	-386.024596155377	380.796059449537
13	-324.888737438378	437.212794403569
14	-268.583543474473	490.064768891615
15	-216.368632120621	539.713025379619
16	-167.667228040589	586.481912318726
17	-122.020260203774	630.658279192062
18	-79.055693418783	672.494076783292
19	-38.467369450627	712.210117552146
20	0	750

Roisum Linear Isotropic - Linear Isotropic Test Input

Double Precision, 0.01" grid spacing

<u>RADIUS</u>	<u>RADIAL STRESS</u>	<u>TANG STRESS</u>
2	-1848.919804040042	-378.982564599534
3	-1363.746898511339	-369.304171243662
4	-1104.677183896124	-279.271883753002
5	-930.988545185037	-191.428270300997
6	-801.397805381332	-114.391719023837
7	-698.468316023048	-46.329171071259
8	-613.138429876936	15.828922233406
9	-540.045966930974	74.796555675239
10	-475.728746191923	132.738917241148
11	-417.808446176886	191.347110797941
12	-364.574218966494	251.944447230655
13	-314.750773101348	315.576322026107
14	-267.360179098793	383.078429403311
15	-221.635009714122	455.127017576642
16	-176.961339806047	532.275758802559
17	-132.839987412588	614.982956510562
18	-88.859361306901	703.631821072781
19	-44.675951192975	798.545753174523
20	0	900

Altmann Linear Anisotropic - Linear Isotropic Standard Input

Double Precision, 500 integration panels

<u>RADIUS</u>	<u>RADIAL STRESS</u>	<u>TANG STRESS</u>
2	-2719.168287720908	450.891488958481
3	-1778.907507957044	-94.160536674405
4	-1370.388470577621	-162.735285109017
5	-1125.413863173908	-119.490940497067
6	-951.832554369637	-46.109948902550
7	-816.761794367702	33.589266518715
8	-705.545763521336	111.793188736527
9	-610.568556757327	185.940998458297
10	-527.406336797364	255.372409009581
11	-453.266254064694	320.141708003654
12	-386.269190986620	380.562122606048
13	-325.086504199421	437.022394105196
14	-268.741092584622	489.912292817215
15	-216.491266683294	539.593837811090
16	-167.759267220252	586.392150766477
17	-122.085268444883	630.594697985566
18	-79.096646593645	672.453926434986
19	-38.486777674079	712.191051146170
20	0	750

Altmann Linear Anisotropic - Linear Isotropic Test Input

Double Precision, 500 integration panels

<u>RADIUS</u>	<u>RADIAL STRESS</u>	<u>TANG STRESS</u>
2	-1852.384515179313	-381.176881695709
3	-1365.702047218821	-370.904571332521
4	-1105.880824749988	-280.347601429153
5	-931.753381955097	-192.140068747041
6	-801.884657171346	-114.854874488709
7	-698.771196311386	-46.621150147191
8	-613.316998690568	15.655294946497
9	-540.140226606387	74.704362994868
10	-475.766537620731	132.701798475285
11	-417.809624251420	191.345950079936
12	-364.553141673888	251.965263283587
13	-314.717867758662	315.608879540561
14	-267.322972337603	383.115296799364
15	-221.598830139093	455.162909519322
16	-176.929812455930	532.307065751763
17	-132.815391083203	615.007400465651
18	-88.842892783967	703.648198563683
19	-44.667924620176	798.553739915461
20	0	900

Altmann Linear Anisotropic - Linear Anisotropic Standard Input

Double Precision, 500 integration panels

<u>RADIUS</u>	<u>RADIAL STRESS</u>	<u>TANG STRESS</u>
2	-30.8741467309446	286.887804211512
3	-24.6824177314037	-24.682424759321
4	-24.6824175581176	-24.682419426456
5	-24.6824175294366	-24.682418526276
6	-24.6824175357524	-24.682418724501
7	-24.6824175497266	-24.682419163095
8	-24.6824175591793	-24.682419459780
9	-24.6824175591991	-24.682419460399
10	-24.6824175352383	-24.682418708366
11	-24.6824172227737	-24.682408901352
12	-24.6824130484000	-24.682277884448
13	-24.6823665169296	-24.680817447600
14	-24.6819327377797	-24.667202854115
15	-24.6784729392648	-24.558613609243
16	-24.6543838395132	-23.802553063980
17	-24.5055243563802	-19.130448952763
18	-23.6778006169784	6.848490409501
19	-19.4884753435726	138.334663954891
20	0	750

Altmann Linear Anisotropic - Linear Anisotropic Test Input

Double Precision, 500 integration panels

<u>RADIUS</u>	<u>RADIAL STRESS</u>	<u>TANG STRESS</u>
2	-1222.218749964698	-267.2562536119005
3	-934.355059111110	-387.1369809187124
4	-792.486401136330	-339.4661065370583
5	-695.292736856860	-273.5589436236932
6	-619.607257123521	-209.6429664804782
7	-556.697294050866	-149.4340633627709
8	-502.151925123341	-91.4240975395550
9	-453.321945041163	-33.7366355072319
10	-408.438684471206	25.2972758076904
11	-366.237844013558	87.0600763540708
12	-325.772224219263	152.6790243471283
13	-286.307544379941	223.0747693807944
14	-247.259561387981	299.0049763868126
15	-208.153720674793	381.0991751543895
16	-168.598015685745	469.8856278274778
17	-128.264039057171	565.8118678968592
18	-86.873347898423	669.2604393670998
19	-44.187404944633	780.5610437435063
20	0	900

Yagoda Linear Anisotropic - Linear Isotropic Standard Input
 Double Precision

<u>RADIUS</u>	<u>RADIAL STRESS</u>	<u>TANG STRESS</u>
2	-2713.7723117286	451.4850463164265
3	-1774.8455371134	-92.2329741272212
4	-1366.7934015479	-160.3408207463474
5	-1122.0349029861	-116.8803672957441
6	-948.5709866395	-43.3819832461357
7	-813.5710105869	36.3880161229551
8	-702.4009212461	114.6378798454161
9	-607.4552118269	188.8171869115788
0	-524.3155217324	258.2711273280686
11	-450.1921085522	323.0570958744581
12	-383.2077240358	383.4901890384831
13	-322.0349041508	439.9603274398612
14	-265.6973216209	492.8580552367575
15	-213.4538118258	542.5459163368045
16	-164.7269816328	589.3493985622766
17	-119.0572670220	633.5562299459363
18	-76.0722353424	675.4190485669375
19	-35.4654047849	715.1592116401897
20	3.0187787848	752.9707545982819

Yagoda Linear Anisotropic - Linear Isotropic Test Input
 Double Precision

<u>RADIUS</u>	<u>RADIAL STRESS</u>	<u>TANG STRESS</u>
2	-1861.984655260331	-387.256970528129
3	-1373.214886776563	-377.054256545626
4	-1112.330738890395	-286.112017474197
5	-937.487380947160	-197.476438194652
6	-807.069010593882	-119.786892134994
7	-703.502921358998	-51.182571805065
8	-617.660234267182	11.432249532064
9	-544.141144896211	70.791179765009
10	-479.460479415376	129.073606451090
11	-421.224915012706	187.980976675944
12	-367.713309884723	248.844263353252
13	-317.643020371932	312.714647458195
14	-270.030692313218	380.432274102813
15	-224.104786851638	452.676875490123
16	-179.248191210749	530.004894283433
17	-134.959204079437	612.876868394174
18	-90.824209747287	701.677833603243
19	-46.498047433688	796.732699084761
20	-1.689597323547	898.317971631785

Yagoda Linear Anisotropic - Linear Anisotropic Standard Input

Double Precision

<u>RADIUS</u>	<u>RADIAL STRESS</u>	<u>TANG STRESS</u>
2	-30.8741485220513	286.8877773449125
3	-24.6824174985462	-24.6824174508583
4	-24.6824174966308	-24.6824174966307
5	-24.6824174966308	-24.6824174966307
6	-24.6824174966308	-24.6824174966307
7	-24.6824174966304	-24.6824174966200
8	-24.6824174966108	-24.6824174960037
9	-24.6824174959148	-24.6824174741590
10	-24.6824174790398	-24.6824169445210
11	-24.6824171781760	-24.6824075016094
12	-24.6824130164965	-24.6822768831249
13	-24.6823664963603	-24.6808168020134
14	-24.6819327259460	-24.6672024827024
15	-24.6784729333297	-24.5586134229635
16	-24.6543838370349	-23.8025529861975
17	-24.5055243555966	-19.1304489281714
18	-23.6778006168298	6.8484904141685
19	-19.4884753435651	138.3346639551283
20	0	750

Yagoda Linear Anisotropic - Linear Anisotropic Test Input

Double Precision

<u>RADIUS</u>	<u>RADIAL STRESS</u>	<u>TANG STRESS</u>
2	-1221.988316905104	-267.0565449595658
3	-934.205640788028	-386.9556142699403
4	-792.378403290726	-339.3233607654115
5	-695.208174623984	-273.4435788887624
6	-619.533857873585	-209.5413692997986
7	-556.625863789909	-149.3344385067588
8	-502.075484500010	-91.3170180407181
9	-453.235266704417	-33.6148869946906
10	-408.337978752548	25.4389760262427
11	-366.120524159736	87.2253514544250
12	-325.636723768542	152.8700725538183
13	-286.153171938466	223.2925593945338
14	-247.086383379183	299.2494088485162
15	-207.962465503616	381.3692162201099
16	-168.389994560671	470.1794202508006
17	-128.041079936435	566.1268240366979
18	-86.637739892529	669.5933196327355
19	-43.941851134566	780.9080232419544
20	0.252422907315	900.3567255612833

Hakiel NonLinear Anisotropic - Linear Isotropic Standard Input

Double Precision, 0.05" grid spacing

<u>RADIUS</u>	<u>RADIAL STRESS</u>	<u>TANG STRESS</u>
2	-2722.6282124230	404.6215611544
3	-1783.2370382505	-100.5110124930
4	-1375.1743940724	-168.0070181216
5	-1130.1369687597	-122.8713164331
6	-956.2458358644	-48.2694193663
7	-820.8013279135	32.2919633590
8	-709.2099937433	111.1226720859
9	-613.7913772823	187.1403737604
10	-530.1208500148	257.8299992484
11	-455.4718825617	323.4012885740
12	-387.9993296893	384.2626257039
13	-326.3921200147	440.8646017269
14	-269.6820269910	493.6393326467
15	-217.1314694468	542.9791696380
16	-168.1641276827	589.2318303999
17	-122.2988614159	633.2785706920
18	-79.1662110963	674.3948101958
19	-38.4807037619	712.8839890342
20	0	750

Hakiel NonLinear Anisotropic - Linear Isotropic Test Input

Double Precision, 0.05" grid spacing

<u>RADIUS</u>	<u>RADIAL STRESS</u>	<u>TANG STRESS</u>
2	-1853.5184285449	-402.5804090006
3	-1368.0755764382	-379.1286715968
4	-1109.6423963395	-287.3862202508
5	-936.0276507209	-197.3456585154
6	-806.2293055923	-118.7641672231
7	-702.9922295757	-49.5209878887
8	-617.3233754971	13.5769829196
9	-543.8124977281	74.5600120999
10	-478.9998140736	133.9973866259
11	-420.5672409642	193.7083757542
12	-366.8363444183	255.0886878442
13	-316.5502531128	319.2250478267
14	-268.7421212590	386.5760002960
15	-222.6516563941	459.0290052960
16	-177.6699209789	535.9408688305
17	-133.2786888770	618.7967768121
18	-890.7282441544	706.9190068387
19	-447.3623328983	800.6621797210
20	0	900

Hakiel NonLinear Anisotropic - Linear Anisotropic Standard Input

Double Precision, 0.01" grid spacing

<u>RADIUS</u>	<u>RADIAL STRESS</u>	<u>TANG STRESS</u>
2	-33.5326106256	411.0095214159
3	-25.8785184941	-24.6686179947
4	-25.5774100982	-24.7252041672
5	-25.3990529480	-24.6891359960
6	-25.2804318503	-24.6940539513
7	-25.1963730280	-24.7009541574
8	-25.1394961546	-24.8875996675
9	-25.0957409353	-24.7185655959
10	-25.0583635383	-24.7229046151
11	-25.0281801760	-24.7273102410
12	-25.0033801280	-24.7315243552
13	-24.9827043926	-24.7354274874
14	-24.9652170238	-24.7377369117
15	-24.9499464797	-24.7285419513
16	-24.9335262275	-24.5773409454
17	-24.7849857052	-19.1454885618
18	-23.9334529540	7.3008613135
19	-19.6755443890	140.3023768920
20	0	750

Hakiel NonLinear Anisotropic - Linear Anisotropic Test Input

Double Precision, 0.05" grid spacing

<u>RADIUS</u>	<u>RADIAL STRESS</u>	<u>TANG STRESS</u>
2	-1222.6849293757	-275.0327539291
3	-934.8807941796	-392.2738390796
4	-794.1913762711	-344.3370238078
5	-697.5878534286	-277.6279542071
6	-622.1736790714	-213.1423311926
7	-559.3736045302	-152.4383811438
8	-504.8442068329	-93.9694729972
9	-455.9079269859	-34.8230595858
10	-410.8063649337	25.3535960457
11	-368.3306859685	88.0292248093
12	-327.5657801674	154.3697767992
13	-287.7976791014	225.3108813167
14	-248.4561253012	301.6124500785
15	-209.0769738050	383.8989285474
16	-169.2765250568	472.6886144921
17	-128.7115927026	569.0166601885
18	-87.1127887758	672.2522475833
19	-44.2702372215	782.7479116315
20	0	900

Hakiel NonLinear Anisotropic - NonLinear Anisotropic Standard Input

Double Precision, 0.01" grid spacing

<u>RADIUS</u>	<u>RADIAL STRESS</u>	<u>TANG STRESS</u>
2	-77.6815414186	359.9498760896
3	-62.0306167993	-48.1836314597
4	-57.9193130083	-43.1579601670
5	-54.4150998069	-37.8519497723
6	-51.2500446622	-33.0707361052
7	-48.3305288084	-28.6544947909
8	-45.6292088090	-25.0099039336
9	-43.0573492005	-20.2682211276
10	-40.5818386604	-16.3884475694
11	-38.2163706463	-12.7695385457
12	-35.9522310366	-9.3517385462
13	-33.7794191490	-6.0720344780
14	-31.6832929687	-2.7644736124
15	-29.6338513182	1.0324849453
16	-27.5575993522	6.6694088665
17	-25.1595421234	21.3030853285
18	-21.7924138092	54.9238357992
19	-15.6998537278	150.7385355474
20	0	600

Hakiel NonLinear Anisotropic - NonLinear Anisotropic Test Input

Double Precision, 0.05" grid spacing

<u>RADIUS</u>	<u>RADIAL STRESS</u>	<u>TANG STRESS</u>
2	-1606.7501990180	-478.6888308415
3	-1216.1136272759	-388.7629958997
4	-996.0858068427	-286.1492850801
5	-845.3995618266	-201.9904082711
6	-732.2470343837	-132.7670858519
7	-642.2377386288	-72.5707511778
8	-567.5369524182	-17.0887416340
9	-503.3154449438	37.8828893583
10	-446.4474240906	93.0602323483
11	-394.8254219853	150.1885144313
12	-346.9183532130	210.5777956981
13	-301.5775291716	275.2421265309
14	-257.9178743242	344.9872754532
15	-215.2418899377	420.4685061278
16	-172.9891330679	502.2298064073
17	-130.6792803717	591.3454001875
18	-87.9852061243	687.1921818585
19	-44.4608925984	790.1639541074
20	0	900

APPENDIX C

STRESS MEASUREMENT COMPUTER PROGRAMS

Data Acquisition Program - Main

```
/ *   DRWIND.c - interface routine for
 *   gathering Wound-in-Stress data using
 *   Metrabyte data acquisition cards
 *   CTM-05 counter/timer
 *   Dash16 analog cards
 *   Written in Borland Turbo C 3.0
 *   Copyright (C) 1988 Beloit & WHRC
 *   (all rights reserved)
 *
 *   v10 12/17/88 link with DRDASH.h for reading analog card
 *   v11 12/18/88 link with DRCTM05.h for reading counter card
 */
```

```
#define TRUE 1
#define FALSE 0
```

```
#include "stdio.h"           /* our std header files */
#include "dos.h"
#include "c:\tc\drcount\drdash16.h" /* Dash16 functions */
#include "c:\tc\drcount\drctm05.h" /* CTM05 functions */
```

```
/* ***** /
/* Program constants */
/* ***** /
```

```
#define MAXSAMPLE 10000 /* maximum samples */
#define WRAPCOUNT 12500 /* wrap count */
#define FILENAME "c:drwind.dat"
FILE *out;
```

```
/*
 *
 * .....
 * External functions from stdlib and dos
 * .....
 */
```

```
extern int kbhit();
extern int inport();
extern void outport();
```



```

/ *
.....
External functions from drdash16
.....
* /
extern int initD16();
extern int adcranD16();
extern int adcD16();

/ *
.....
External functions from drctm05
.....
extern int initctm();
extern int readctm();
* /

/ *
.....
Internal function declarations
.....
* /
void prt_hdr();           /* print header during signon */
void saveit();           /* save data array */

/ *
.....
Global Data Items
.....
* /
unsigned int sample = 0;
unsigned int oldsample = 0;
unsigned int cflag = 1;
unsigned int count[6];
unsigned int cnt3data[MAXSAMPLE];
float ain1data[MAXSAMPLE];

/* main:
 * This function reads analog input 1 channel as fast as possible
 * until a new data flag from the counter 2 is detected.
 * Then the average caliper and counter 3 data is stored in array.
 * Exits either on Maxsample or Kbit and data is written to disk.
 */
main ()
{
    int ain1sample = 0;
    double ain1sum = 0;

    prt_hdr();
    initD16(0x310, 1);           /* initialize Dash16 */
    adcranD16(0,0);           /* sets channels for Dash16 */
    initctm(WRAPCOUNT);       /* initialize CTM05 */
    ENABLE;

```

```

while(sample < MAXSAMPLE && !kbhit())
{
    if(ain1sample < 32000)
    {
        ain1sample = ain1sample + 1;
        ain1sum = ain1sum + adcD16();
    }
    readctm();
    if(cflag)
    {
        cnt3data[sample] = count[3];
        ain1data[sample] = ain1sum/ain1sample;
        printf("\n%8u %8u %f %8d", count[2], cnt3data[sample],
ain1data[sample], ain1sample);
        ain1sample = 0;
        ain1sum = 0;
    }
}

DISABLE;
getchar();
getchar();
saveit();

} /* main */

/* prt_hdr()
prints informative header message
*/
void prt_hdr()
{
    printf ("\nDRwind\n");
    printf ("\nOn countdown of counter 1,");
    printf ("\ncounter 3 is read and counters reset");
    printf ("\nelse analog in 1 is read as often as possible.\n\n");
} /* prt_hdr */

/* saveit:
*saves data array to disk
*/
void saveit()
{
    int i;
    printf("Saving data to disk drive\n");
    out = fopen(FILENAME, "w");
    for(i=1 ; i<sample ; i++)
    {
        fprintf(out, "%u \t%f \n", cnt3data[i], ain1data[i]);
        /*
        printf("\n %6d %6d %6d", i, cnt3data[i], ain1data[i]);
        */
    }
}

```

```
    }  
    fclose(out);  
    printf("\n\nThank you for using DRwind\n");  
} /* saveit */
```

```
/* end of file DRWIND.c */
```

Data Acquisition Program - Counter

```
/* DRCTM05.h
 * read Metrabyte CTM-05 counter/timer card
 * on interrupt from countdown of counter #1
 * Written in Borland Turbo C 3.0
 * by David Roisum 11/11/88
 *
 * * v17 12/18/88 give up on interrupts, use counter 2 as dataflag
 * v18 12/18/88 full implementation of polling 2 for dataflag
 * v19 12/18/88 success cal drctm05.h from drwind10.c
 */

/ *
 * .....
Interrupt and addresses
 * .....
 * /
#define CINT_NO      0x0A      /* IRQ2 -- level of the CTM-05 */
#define CPORT       0x301     /* address of command port = base + 1 */
#define DPORT       0x300     /* address of data port = base */
#define DPTR        0x17      /* Data ptr select code */

/ *
 * .....
Command codes for the Metrabyte CTM-05 card
 * .....
 * /
#define DISARM      0xdf      /* cmd: disarm or stop counting */
#define LATCH       0xbf      /* cmd: save current value to hold reg */
#define ARM         0x7f      /* cmd: load from load reg and arm cntr */
#define MREAD       0x10      /* modifier for reading */
#define MLOAD       0x08      /* modifier for load regs */
#define ENABLE      outputb(CPORT,ARM) /* these cmds affect all 5 cntrs */
#define DISABLE     outputb(CPORT,DISARM)

/ *
 * .....
External functions from stdlib and dos
 * .....
 * /
extern void outputb(int portid, unsigned char value);
extern unsigned char inputb(int portid);

/ *
 * .....
internal function declarations
 * .....
 * /
void initctm(unsigned int wrapcount); /* initialize CTM-05 card */
void zeroctm(); /* load all counter regs with zero */
void readctm(); /* read ctm board */
/ *
 * .....
```

Counter Configuration Arrays

```
*****
* /
static unsigned int cconfigl[6] = {0xF0, 0xA5, 0xe8, 0xA8, 0xA8, 0xA8};
static unsigned int cconfigh[6] = {0xCA, 0x01, 0xc0, 0xC3, 0xC4, 0xC5};

/ *
*****

Global Data Items
*****
* /
unsigned int cintnum = CINT_NO;          /* default interrupt number */
extern unsigned int sample;
extern unsigned int oldsample;
extern unsigned int cflag;
extern unsigned int count[6];

/* initctm()
   do the one-time only initialization of the CTM-05 card
   this configures each channel's counting features.
   also sets up the wrap count for channel #1.
* /
void initctm(unsigned int wrapcount)
{
    unsigned int i;
    unsigned int lobyte;
    printf("\nInitializing Metrabyte CTM-05 counter timer board");

    outportb (CPORT, DPTR);      /* set the data pointer */
    outportb (DPORT, cconfig[0]); /* init Master Mode Reg */
    outportb (DPORT, cconfigh[0]);

    /* Configure all counters from array */

    for (i=1; i<=5; i++)
        {
            outportb (CPORT, i);
            outportb (DPORT, cconfig[i]);
            outportb (DPORT, cconfigh[i]);
        }

    zeroctm();                  /* set all load regs with 0 */

    lobyte = wrapcount & 0xFF;
    outportb (CPORT, (MLOAD+1)); /* load ONE's load reg with our wrap count */
    outportb (DPORT, lobyte);    /* low bits first */
    outportb (DPORT, wrapcount >> 8); /* hi bits */
}
```

```

} /* initctm */

/* readctm()
   Reads current value from hold register. Normally, the last interrupt
   will have saved the values and all we have to do is read them,
   without disturbing the counting process.
*/
void readctm()
{
    unsigned int i;
    /*outportb (CPORT, LATCH);*/      /* uncomment to read values in for debug */

    /* Read sample counter 2 and check for new data */
    outport (CPORT, (MREAD + 2));
    sample = inportb (DPORT) + 256*inportb (DPORT);
    cflag = sample - oldsample;

    if (cflag == 0)                    /* no new data */
        ;
    if (cflag == 1)                    /* new data */
    {
        count[2] = sample;
        oldsample = sample;
        for (i=3; i<=5; i++)
        {
            outport (CPORT, (MREAD+i));
            count[i] = inportb (DPORT) + 256*inportb (DPORT);
        }
    }
    if (cflag != 0 && cflag != 1)
    {
        printf("\nCount Data ERROR");
        oldsample = sample;
    }
} /* readctm */

/* zeroctm()
   sets all ctm05 load registers to zero
*/
void zeroctm()
{
    unsigned int i;
    DISABLE;                          /* stop counting */

    for (i=1; i<=5; i++)
    {

```

```
        outportb (CPORT, (MLOAD+i));
        outportb (DPORT, 0);
        outportb (DPORT, 0);
    }
} /* zero */
```

```
/* end of file DRCTM05.c */
```

Data Acquisition Program - Analog Input

```
/*
 *   DRDASH16.h
 *   read Metrabyte Dash16 analog card
 *   by David Roisum 12/16/88
 *   Written in Borland's Turbo C 3.0
 *   v1 12/16  standalone source
 *   v2 12/17  2048 offset subtracted
 *   v3 12/17  success call drdash16.h from drwind10.c
 */

#define BASEADDR iobaseD16          /* Dash16 registers */
#define ADLOW (BASEADDR)
#define ADHIGH (BASEADDR + 1)
#define ADMUX (BASEADDR + 2)
#define DAC0LOW (BASEADDR + 4)
#define DAC1LOW (BASEADDR + 6)
#define STATUS (BASEADDR + 8)
#define CONTROL (BASEADDR + 9)
#define CNTENB (BASEADDR + 10)
#define CNT1 (BASEADDR + 13)
#define CNT2 (BASEADDR + 14)
#define CNTCTL (BASEADDR + 15)

#define SINGLEEND 0x20              /* Ready/busy bits in status reg */

#define INTENB 0x80                 /* Command bits in control reg */
#define USEDMA 0x04

#define LOBYTE(x) (x & 0xff)       /* Device control macros */
#define HIBYTE(x) ((x) >> 8)
#define SETMUX(a, b) csoutp(ADMUX, (b << 4) | (a & 0xf))
#define STARTADC csoutp(ADLOW, 0)
#define GETADC ((int) csinp(ADLOW) | (int) (csinp(ADHIGH) << 8))
#define ISSINGLE (csinp(STATUS) & SINGLEEND)
#define CLEARINT {csoutp(STATUS, 0);}
#define TIMEROFF {csoutp(CNTENB,0);}

#define DACMASK 1                   /* Masks for useless bits */
#define ADCMASK (ISSINGLE? 0xF : 0x7)

#define csoutp(a,b) outportb(a,b)   /* Compiler syntax for Turbo C */
#define csinp(a) inportb(a)

/* Runtime variables */
static int iobaseD16 = 0x310;       /* Base address */
static int intD16 = 0;              /* Programmable interrupt vector */
static int dmachanD16 = 0;          /* DMA channel */
static int adclowc, adchighc;       /* ADC channel range */
static int dacchan = 0, scanning = 0; /* DAC channel and scan flag */
static int dacports[2];            /* DAC port lookup table */
```



```

/ *
    * *****
    * Metrabyte Dash16 functions for
    * initializing card, setting channel range
    * and reading in unlocked mode
    * *****
* /

/* adcD16
    Single channel ADC conversion.
    Note: this will do auto-scanning if adclowc != adchighc.
* /
int adcD16()
{
    int val;
    STARTADC;
    val = GETADC;
    val = (val >> 4) & 0xFFF;
    if(!ISSINGLE)
        val = val - 2048;
    return (val);
}

/* adcranD16()
    Sets conversion range for hardware
* /
int adcranD16(lc, hc)
int lc, hc;
{
    adclowc = lc & ADCMASK;
    adchighc = hc & ADCMASK;
    SETMUX(adclowc, adchighc);
}

/* controlD16()
    Set up interrupt, dma, and conversin modes.
    If intlev > 1, interrupts will occur at this level.
    If usedma != 0, ADC converter will make DMA requests.
    If mode = 0, conversions are software triggered.
        mode = 2, conversion start with rising trigger 0.
        mode = 3, conversions are triggered by clock.
* /
int controlD16(intenb, intlev, usedma, mode)
int intenb, intlev, usedma, mode;
{
    char val;
    val = 0;
    if (intenb)
        val |= INTENB;
    val |= ((intlev & 7) << 4);
}

```

```

        if (usedma)
            val |= USEDMA;
        val |= (mode & 3);
        csoutp(CONTROL, val);
    }

/* dacranD16()
   set dac channels
* /
int dacranD16(lowc, highc)
int lowc, highc;
{
    dacchan = lowc & DACMASK;
    if (lowc != highc)
        scanning = 1;
    else scanning = 0;
}

/* initD16()
   Initialize Dash16 software and hardware.
   Sets IO base address, DMA channel,
   adrng to 0,0 and dacrange to 0,0,
   and timer interval to 1 msec
* /
int initD16(iobase, dmachan)
int iobase;
int dmachan;
{
    if (iobase)
        iobaseD16 = iobase;
    if (dmachan)
        dmachanD16 = dmachan;
    TIMEROFF;
    CLEARINT;
    controlD16(0, intD16, 0, 0);
    adcranD16(0,0);
    dacports[0] = DAC0LOW;
    dacports[1] = DAC1LOW;
    dacranD16(0, 0);
    intvID16(1000L);
}

/* intvID16()
   Sets timer intvl in microseconds
* /
int intvID16(intvl)
long intvl;
{
    int fact1, fact2;
    int error;
    if (intvl < 30L)

```

```

        intvl = 30L;
        error = lfactor(intvl, &fact2, &fact2);
        csoutp(CNTCTL, 0x74);
        csoutp(CNT1, LOBYTE(fact1));
        csoutp(CNT1, HIBYTE(fact1));
        csoutp(CNTCTL, 0xB4);
        csoutp(CNT2, LOBYTE(fact2));
        csoutp(CNT2, HIBYTE(fact2));
        return (error);
    }

```

```

/* lfactor()
   Splits a long into two factors 2 <= x <= 32767.
*/

```

```

static int lfactor(rate, pf1, pf2)
long rate;
int *pf1, *pf2;
{
    long x, y;
    int div;
    x = 1;
    y = rate;
    while (x < 2 || y > 32767L)
    {
        for (div = 2; div < y; div++)
        {
            if (y % div == 0)
            {
                x *= div;
                y /= div;
                break;
            }
        }
        if (div == y)
        {
            x *= 2;
            y /= 2;
        }
    }
    *pf1 = x;
    *pf2 = y;
    return ((int) (rate - (x * y)));
}

```

```

/* end of file DRDASH16.h */

```

Data Reduction - Diameter, Caliper, Density, Radial Compression, and Deflection (for Stress Model)

'Reads in sequence of raw Pulses (long integer)
'and analog Caliper (single float) values
'in two tab separated columns from disk.

'Calculates and Prints to LPT1
'Rewound Roll Diameter, Caliper,
'Density and Caliper Corrected Density,
'and Radial Compression
'Deflection is written to disk

'Note that this program is written to clearly illustrate the calculations
'A more efficient program can be made (which the author uses)
'by elimination of calculations of parameters of no interest
'and nesting the remaining like calculations in the same loop

'Written in Microsoft Quickbasic Basic 1.0 for the Mac and 4.0 for PC
'David R Roisum 4/24/89

```
DEFDBL A-Z
MATSIZE = 1000
DIM PULSE$(MATSIZE), CALIPER(MATSIZE)
DIM DIAM(MATSIZE), CALIP(MATSIZE)
DIM DENSO(MATSIZE), DENSC(MATSIZE), RADCOMP(MATSIZE), DEFL(MATSIZE)
```

DEFINE INPUT VARIABLES HERE

```
INFILE$ = "HD 40:DRwind38.DAT"
LOPASS = .5
NUMAVG% = 2
ROLLERDIA = 24
ROLLERPPR = 100000&
NUMWRAP = 20
BASISWT = 7.2082999999999999D-05
CALIPERGAIN = 69.7
REPLIC% = 10 : 'see note near bot of program list
COMMENT$ = "Density & Compression Run 38"
DEFLFILE$ = "DeflOut"
'Note that caliper is acquired in inches but displayed in mils
'all other variables are in a consistent in-lb-sec system
```

DEFINE INPUT VARIABLES HERE

```
STARTRUN:
GOSUB USERIN
```

'Getting Started

```
DIAGAIN# = ROLLERDIA/ROLLERPPR/NUMWRAP/NUMAVG%
DENSCONST# = 2*BASISWT*(NUMWRAP*NUMAVG%)^2*ROLLERPPR/ROLLERDIA
```

```

PRINT "READING RAW DATA FOR INPUT"
OPEN INFILE$ FOR INPUT AS #1
Q% = 1
WHILE NOT EOF(1)
    INPUT #1, PULSE&(Q%), CALIPER(Q%)
    Q% = Q% + 1
WEND
NUMSAMPLE% = Q%-1
CLOSE #1

'Echo Input
LPRINT
LPRINT "ROISUM DENSITY AND COMPRESSION"
LPRINT
LPRINT "WEB HANDLING RESEARCH CENTER"
LPRINT "OKLAHOMA STATE UNIVERSITY"
LPRINT
LPRINT "Input Data File is "; INFILE$
LPRINT COMMENT$
LPRINT TIME$ , DATE$:your Basic may not support this statement
LPRINT
LPRINT "Lowpass Filter Setting = ";          TAB(30);          LOPASS
LPRINT "Averaging Number = ";              TAB(30);          NUMAVG%
LPRINT "Original Wrap Count = ";           TAB(30);          NUMWRAP
LPRINT "Effective Wrap Count = ";          TAB(30);          NUMWRAP*NUMAVG%
LPRINT "Number of Raw Samples = ";         TAB(30);          NUMSAMPLE%
LPRINT
LPRINT "Drum Roller Diameter = ";          TAB(30);          ROLLERDIA; " inch"
LPRINT "Drum Roller Pulses per Rev = ";    TAB(30);          ROLLERPPR
LPRINT "Analog Caliper Gain = ";           TAB(30);          CALIPERGAIN
LPRINT "Nominal Basis Weight = ";          TAB(30);          BASISWT
LPRINT "Replication for Grid Matching = "; TAB(30);          REPLIC%
LPRINT
LPRINT
LPRINT "Diameter"; TAB(15); "Caliper"; TAB(30); "Raw Density";
LPRINT TAB(45); "Cal. Density"; TAB(60); "Rad. Comp."
LPRINT

*** MAIN LOOPS - Compute Densities and Radial Compression ***

'Note that effective means after averaging the raw acquired data
EFFSAMPLE% = INT((NUMSAMPLE%-NUMAVG%)/NUMAVG%)
EFFWRAP% = NUMWRAP*NUMAVG%

PRINT "CALCULATING DIAMETERS"
FOR Q% = 0 TO EFFSAMPLE%
    PULSESUM& = 0
    FOR QQ% = 1 TO NUMAVG%
        PULSESUM& = PULSESUM& + PULSE&(NUMAVG%*Q%+QQ%)
    NEXT QQ%
    DIAM(Q%) = PULSESUM&*DIAGAIN#
NEXT Q%

```

```

PRINT "CALCULATING CALIPER AVG"
CALIPAVG# = 0
FOR Q% = 0 TO EFFSAMPLE%
    CALIPERSUM = 0
    FOR QQ% = 1 TO NUMAVG%
        CALIPERSUM = CALIPERSUM + CALIPER(NUMAVG%*Q%+QQ%)
    NEXT QQ%
    CALIP(Q%) = CALIPERSUM / NUMAVG%/CALIPERGAIN
    CALIPAVG# = CALIPAVG# + CALIP(Q%)
NEXT Q%
CALIPAVG# = CALIPAVG#/(EFFSAMPLE%+1)

PRINT "CALCULATING DENSITIES"
PULSESUM1& = 0
FOR Q% = 1 TO NUMAVG%
    PULSESUM1& = PULSESUM1& + PULSE&(Q%)
NEXT Q%
FOR Q% = 1 TO EFFSAMPLE%
    PULSESUM2& = 0
    FOR QQ% = 1 TO NUMAVG%
        PULSESUM2& = PULSESUM2& + PULSE&(NUMAVG%*Q%+QQ%)
    NEXT QQ%
    DENSO(Q%) = DENSCONST# / (PULSESUM2& - PULSESUM1&)
    DENSC(Q%) = DENSO(Q%) * CALIP(Q%)/CALIPAVG#
    PULSESUM1& = PULSESUM2&
NEXT Q%

PRINT "CALCULATING RADIAL COMPRESSION"
FOR Q% = 1 TO EFFSAMPLE%
    TEMPVAR1 = 2*EFFWRAP%*CALIP(Q%)/1000
    RADCOMP(Q%) = -100*(DIAM(Q%)-DIAM(Q%-1)-TEMPVAR1)/TEMPVAR1
    'note positive is defined as compression
NEXT Q%

PRINT "CALCULATING OUTER BOUNDARY DEFLECTION"
FOR Q% = 1 TO EFFSAMPLE%
    TEMPVAR1 = EFFWRAP%*CALIP(Q%)/1000
    DEFL(Q%) = (DIAM(Q%)-DIAM(Q%-1))/2-TEMPVAR1
    'note positive is defined outward
NEXT Q%

PRINT "LOW PASS DIGITAL FILTER FOR DENSITY, COMPRESSION and DEFLECTION"
TEMP1 = DENSO(1)
TEMP2 = DENSC(1)
TEMP3 = RADCOMP(1)
TEMP4 = DEFL(1)
FOR Q% = 2 TO EFFSAMPLE%
    TEMP1 = (DENSO(Q%)+DENSO(Q%-1)-TEMP1*(1-2*LOPASS))/(1+2*LOPASS)
    DENSO(Q%) = TEMP1
    TEMP2 = (DENSC(Q%)+DENSC(Q%-1)-TEMP2*(1-2*LOPASS))/(1+2*LOPASS)
    DENSC(Q%) = TEMP2
    TEMP3 = (RADCOMP(Q%)+RADCOMP(Q%-1)-TEMP3*(1-2*LOPASS))/(1+2*LOPASS)
    RADCOMP(Q%) = TEMP3

```

```

        TEMP4 = (DEFL(Q%)+ DEFL(Q%-1)-TEMP4*(1-2*LOPASS))/(1+2*LOPASS)
        DEFL(Q%) = TEMP4
NEXT Q%

PRINT "PRINTING RESULTS TO LPT1"
FOR Q% = 2 TO EFFSAMPLE%
    LPRINT CSNG(DIAM(Q%)); TAB(15); CSNG(CALIP(Q%)); TAB(30); CSNG(DENSO(Q%));
    LPRINT TAB(45); CSNG(DENSC(Q%)); TAB(60); CSNG(RADCOMP(Q%))
NEXT Q%

PRINT "SAVING DEFLECTION FILE TO DISK"
'For input to deflection-to-stress programs
'Note first you must select averaging to obtain
'the required smoothness of displayed data
'displaygridsize = EFFWRAP%*averagecaliper
'Then you must select the optimumgridsize
'for the stress calculation by using sensitivity
'analysis such as given in Chapters 3 and 10
'Then the replicationfactor is the
'integer of (displaygridsize/optimumgridsize)
'Finally the incremental radius used in the
'deflection-to-stress program is given as
'IR = displaygridsize/replicationfactor
'Note that this somewhat involved description
'is nothing more than independently selecting
'the gridsize for a good smoothing of the raw data and
'the gridsize for the deflection-to-stress models
'and then being able to convert data from one spacing
'to another
OPEN DEFLEFILE$ FOR OUTPUT AS #1
FOR Q% = 3 TO (EFFSAMPLE%-1)
    FOR QQ% = 1 TO REPLIC%
        PRINT #1, DEFL(Q%)/REPLIC%
    NEXT QQ%
NEXT Q%
CLOSE #1

****END MAIN LOOPS****

INPUT "DO YOU WANT ANOTHER RUN ??", RESPONSE$
IF RESPONSE$ = "Y" GOTO STARTRUN
IF RESPONSE$ = "y" GOTO STARTRUN

PRINT "THANK YOU, HAVE A NICE DAY !!!"
END

.....
**** EDITING SUBROUTINES ****
.....

USERIN:
PRINT

```

```

PRINT "Calculation for the Wound Roll Structure Distribution"
PRINT "including; Diameter, Caliper,"
PRINT "Density, Caliper Corrected Density and Radial Compression."
PRINT "Copyright 1989, David Roisum, Web Handling Research Center"
PRINT
PRINT "Input is read from the disk drive upon which has been stored"
PRINT "two tab separated columns of"
PRINT "drum roller pulse count (long integer) and caliper (single float)."
```

PRINT "This post processing routine uses values that have previously"

PRINT "been acquired from a data acquisition routine."

```

PRINT
PRINT "Two user selectable noise reduction techniques are incorporated."
PRINT "The averaging number will reduce noise greatly, but also reduce"
PRINT "the number of data points. The Lowpass Filter will reduce noise"
PRINT "without reducing the number of data points displayed."
PRINT "Replication is used for displacement-to-stress model and"
PRINT "is described in more detail in the program listing"
PRINT
PRINT "During input, default values may be selected with a <CR> or"
PRINT "may be changed by typing in a new value."
PRINT "Errors before <CR> may be corrected by backspacing."
PRINT "After all values are calculated, they are printed to LPT1."
PRINT
PRINT
CALL EDALPHA("Input file name",INFILE$)
NUMAVGFLT = NUMAVG%
CALL EDNUM("Averaging Number", CDBL(2), NUMAVGFLT, CDBL(100))
NUMAVG% = NUMAVGFLT
CALL EDNUM("Lowpass Filter Setting", CDBL(0), LOPASS, CDBL(2))
PRINT
CALL EDNUM("Drum Roller Diam (inches)", CDBL(0), ROLLERDIA, CDBL(100))
CALL EDNUM("Drum Pulses/Rev", CDBL(1000), ROLLERPPR, CDBL(1000000&))
CALL EDNUM("Number of Wraps/Sample", CDBL(.1), NUMWRAP, CDBL(1000))
PRINT
CALL EDNUM("Nominal Basis Weight (lb/in2)", CDBL(0), BASISWT, CDBL(1))
CALL EDNUM("Gain on Caliper (Reading/mils)",CDBL(0), ROLLERPPR, CDBL(1000))
REPLICFLT = REPLIC%
CALL EDNUM("Replication for Defl-to-Stress Models",CDBL(1), REPLICFLT, CDBL(100))
REPLIC% = REPLICFLT
CALL EDALPHA("Comment?",COMMENT$)

RETURN
```



```

SUB CHKLIM(LOWLIM, NEWNUM, UPLIM, YNFLAG%) STATIC
  IF NEWNUM < LOWLIM THEN YNFLAG% = 0
  IF NEWNUM > UPLIM THEN YNFLAG% = 0
END SUB

SUB EDALPHA(TEXT$, ALPHA$) STATIC
  PRINT TEXT$; " "; ALPHA$; TAB(30);
  INPUT RESPONSE$
  IF RESPONSE$ <> "" THEN ALPHA$ = RESPONSE$
END SUB

SUB EDNUM(TEXT$, LOWLIM, DEFNUM, UPLIM) STATIC
  YNFLAG% = 0
  WHILE YNFLAG% <> 1
    PRINT TEXT$; TAB(30);
    PRINT USING "#####.####"; DEFNUM;
    INPUT NEWNUM$
    IF NEWNUM$ <> "" THEN
      CALL ISANUM(NEWNUM$, YNFLAG%)
      NEWNUM = VAL(NEWNUM$)
      CALL CHKLIM(LOWLIM, NEWNUM, UPLIM, YNFLAG%)
      IF YNFLAG% <> 1 THEN
        BEEP
        PRINT "***ERROR** NOT A NUMBER BETWEEN ";
        PRINT LOWLIM;" AND ";UPLIM
      END IF
    ELSE
      YNFLAG% = 1
      NEWNUM = DEFNUM
    END IF
  WEND
  DEFNUM = NEWNUM
END SUB

SUB ISANUM(NEWNUM$, YNFLAG%) STATIC
  YNFLAG% = 1
  LENGTH% = LEN(NEWNUM$)
  FOR Q% = 1 TO LENGTH%
    ASCII% = ASC(MID$(NEWNUM$,Q%,1))
    IF (ASCII%<48 OR ASCII%>57) AND ASCII%<>46 AND ASCII%<>45 THEN YNFLAG%=0
  NEXT Q%
END SUB

END

```

Extended Hakiel Formulation - Deflection-to-Stress Model

'DisWis7

'Wound-in-Stresses During Roll Winding

'Extended Hakiel Formulation

'Takes a single column of outer roll deflections

'as an input from disk

'Outputs Radius, Radial Stress, Tangential Stress,

'Deflection, and Wound-In-Stress

'Uses Depth Limited and Replication Acceleration Techniques

'Written in Microsoft Basic 3.0 for the Macintosh

'David R Roisum 1/18/90

DEFDBL A-Z

CLEAR, 2000000&

* * * * DEFINE INPUT VARIABLES HERE * * *

FILENAME\$ = "HD 40:DRcomp"

OUTFILE\$ = "HD 40:WIS38"

COMMENT\$ = "From Drwind38, avg 20, lopass 2, /40 for 0.25 wrap"

'Wound-In-Stress as a Function of Radius

'which may be curvefitted from independently obtained data

WIS0 = 900

WIS1 = -60

WIS2 = 3

DEF FNWISIN(R) = WIS0 + WIS1*R + WIS2*R^2

'Radial Modulus as a Function of Radial Stress

ER0 = 20

ER1 = -3.5

ER2 = 0

DEF FNER(SR) = ER0 + ER1*SR + ER2*SR^2

RIR = 2 :Radius Inner Roll

MAXPTS% = 20000 :Number of sets of data, Maximum

IR = .0027/4 :Thickness of sample, Nominal

DEPTH% = 2000 :Depth of complete solution, points

DUPLIC% = 40 :Number of times solution is replicated

PIR = .1 :LPRINT Increment Radius

ET = 600000& :Modulus, Tangential

EC = 100000& :Modulus, Core

UR = .01 :Poissons Ratio, Radial

UT = .01 :Poissons Ratio, Tangential

* * * * DEFINE INPUT VARIABLES HERE * * *

'ECHO INPUT

LPRINT

LPRINT "DisWis7"

LPRINT "Displacements >> WIS, with Real Data"

LPRINT "Modified Hakiel Formulation"

LPRINT "Nonlinear ER, 3 pt deriv"

LPRINT

LPRINT "WEB HANDLING RESEARCH CENTER"

```

LPRINT "OKLAHOMA STATE UNIVERSITY"
LPRINT
LPRINT COMMENT$
LPRINT FILENAME$
LPRINT TIMES$ , DATE$           :your Basic might not support this
LPRINT
LPRINT "WOUND IN STRESS = ";           WIS0; " + "; WIS1; "**R + "; WIS2;
**R^2"
LPRINT "MODULUS, RADIAL = ";           ER0; " + "; ER1; "**SR + "; ER2; "**SR^2"
LPRINT "MODULUS, TANGEN = ";           TAB(20);           ET
LPRINT "MODULUS, CORE = ";           TAB(20);           EC
LPRINT "POISSON, RADIAL = ";           TAB(20);           UR
LPRINT "POISSON, TANGEN = ";           TAB(20);
UT
LPRINT "RADIAL INCREMENT = ";           TAB (20);           IR
LPRINT "SOLUTION DEPTH = ";           TAB (20);           DEPTH%
LPRINT "REPLICATION = ";           TAB (20);           DUPLIC%
LPRINT
LPRINT TAB(5); "RADIUS"; TAB(14); "RAD STR"; TAB(24); "TAN STR";
LPRINT TAB(34); "DEF-MIL"; TAB(43); "WIS-CALC"; TAB(54); "WIS-ACT"; TAB(67);
"ERR%"
LPRINT

'DIMENSION DATA ARRAY
DIM D(MAXPTS%)           :Deflection Data

'RETRIEVE FROM DISK
'Data is a single column of double precision floats of deflection
OPEN "I", #1, FILENAME$
Q% = 1
WHILE NOT EOF(1)
    INPUT #1, D#
    D(Q%) = D#
    Q% = Q% + 1
WEND
CLOSE #1
PIRD% = PIR/IR
NUMPTS% = PIRD%*INT((Q%-1)/PIRD%)           :Rounds to nearest LPRINT increment

'DIMENSION ARRAYS
DIM WIS(NUMPTS%)           :Wound-In-Stress at current outer radius
DIM SR(NUMPTS%)           :Radial Stresses
DIM ST(NUMPTS%)           :Tangential Stresses
DIM DSR(DEPTH%)           :Differential Radial Stresses
DIM DST(DEPTH%)           :Differential Tangential Stresses
DIM SRX(DEPTH%)           :Differential Radial Stresses, temporary
DIM W(DEPTH%)           :Displacement field
DIM DW(DEPTH%)           :Differential Displacement field
DIM AA(DEPTH%+4,3)           :Square matrix (coefficients for displacement)
DIM B(DEPTH%)           :Known forcing function displacement vector

'CALCULATE CONSTANTS FOR SPEED OF EXECUTION
IRSQ = IR^2

```

```

IRSQ2 = 2*IR^2
'ADIFF = 3 + UT - UR*ET/ERHERE = CONST1 - URET/ERHERE
'BDIFF = 1-ET/ERHERE*(1+UR)+UT = CONST3 - CONST2/ERHERE
URET = UR*ET
CONST1 = UT + 3
CONST2 = ET*(1+UR)
CONST3 = UT + 1

```

```

* * * * MAIN LOOP - Calculate Stresses from Displacements * * * *

```

```

'For Nonlinear ER or for internal stresses, it is required that
'gosub firstlayers and main loop steps from 4 to numpts step 1
'Tangential stresses are calculated at all times however a more
'accurate final tangential stress is computed from final radial
'stresses using calctang

```

```

GOSUB FIRSTLAYERS
RIRE = RIR
ECE = EC

```

```

'Calculate explicitly at every solution point until
'solution depth is reached

```

```

FOR QA% = 5 TO DEPTH%
  Q% = QA%
  QB% = 0
  WIS(QA%) = WIS(QA%-1)
  GOSUB FILLMAT
  GOSUB TRIDIAG
  GOSUB CALCDTANG
  GOSUB SUMDIS
  GOSUB CORSTR
  GOSUB SUMSTR
  RPR = RIRE + Q%*IR
  WISIN = FNWISIN(RPR)
  RELERR = 100*(WIS(QA%)-WISIN)/WISIN
  PRINT USING "#####.#####": RPR, WIS(QA%), FNWISIN(RPR), RELERR
NEXT QA%

```

```

'Only calculate to a significant depth deep for remainder of wrap addition

```

```

FOR QA% = (DEPTH%+1) TO (NUMPTS%-DUPLIC%+1) STEP DUPLIC%
  Q% = DEPTH%
  QB% = QA% - DEPTH%
  WIS(QA%) = WIS(QA%-1)
  RIRE = RIR + QB%*IR
  ECE = FNER(SR(QB%))
  GOSUB FILLMAT
  GOSUB TRIDIAG
  GOSUB CALCDTANG
  GOSUB SUMDIS
  GOSUB CORSTR
  GOSUB DUPSTR
  RPR = RIRE + Q%*IR

```

```

WISIN = FNWISIN(RPR)
RELERR = 100*(WIS(QA%)-WISIN)/WISIN
PRINT USING "#####.####"; RPR, WIS(QA%), FNWISIN(RPR), RELERR
NEXT QA%

```

```

GOSUB CALCTANG

```

```

OPEN "O", #1, OUTFILES$

```

```

'Final Write to Disk Loop

```

```

FOR Q% = 0 TO NUMPTS%
  RPR = RIR + Q%*IR
  WISIN = FNWISIN(RPR)
  RELERR = 100*(WIS(Q%) - WISIN)/WISIN
  WRITE #1, RPR, SR(Q%), ST(Q%), D(Q%)*1000, WIS(Q%)

```

```

NEXT Q%

```

```

CLOSE #1

```

```

'Final LPRINT Loop

```

```

FOR Q% = 0 TO NUMPTS% STEP PIRD%
  RPR = RIR + Q%*IR
  WISIN = FNWISIN(RPR)
  RELERR = 100*(WIS(Q%) - WISIN)/WISIN
  LPRINT USING "#####.##"; RPR, SR(Q%), ST(Q%), D(Q%)*1000, WIS(Q%),

```

```

WISIN, RELERR

```

```

NEXT Q%

```

```

LPRINT

```

```

LPRINT TIMES$

```

```

* * * End Main Loop * * *

```

```

END

```

```

.....
* * * SUBROUTINES AND STUFF * * *
.....

```

```

CALCDTANG:

```

```

'Calculates differential tangential stresses from SR and equilibrium

```

```

'Note that at the end the accumulated tangential stresses are recalculated

```

```

DSR(0) = CORCONSTH * (-4*DSR(1) + DSR(2))

```

```

RPR = RIRE + Q%*IR

```

```

DSR(Q%-1) = -WIS(QA%)*IR/(RPR)

```

```

DSR(Q%) = 0

```

```

RPR = RIRE

```

```

DDSR = (-3*DSR(0) + 4*DSR(1) - DSR(2))/(2*IR)

```

```

DST(0) = RPR*DDSR + DSR(0)

```

```

FOR QQ% = 1 TO (Q%-2)

```

```

  RPR = RIRE + QQ%*IR

```

```

  DDSR = (-DSR(QQ%-1) + DSR(QQ%+1))/(2*IR)

```

```

        DST(QQ%) = RPR*DDSR + DSR(QQ%)
NEXT QQ%
RPR = RIRE + (Q%-1)*IR
DDSR = (DSR(QQ%-3) - 4*DSR(QQ%-2) + 3*DSR(QQ%-1))/(2*IR)
DST(Q%-1) = RPR*DDSR + DSR(Q%-1)
DST(Q%) = WIS(QA%)
RETURN

```

CALCTANG:

```

'Note this recalculates over previously calculated
'incrementally added tangential stresses
FOR QQ% = 1 TO (NUMPTS%-1)
    RPR = RIRE + QQ%*IR
    DSR = (-SR(QQ%-1) + SR(QQ%+1))/(2*IR)
    ST(QQ%) = RPR*DSR + SR(QQ%)
NEXT QQ%
RPR = RIRE + NUMPTS%*IR
ST(0) = 2*ST(1) - ST(2)
ST(NUMPTS%) = WIS(NUMPTS%)
RETURN

```

CORSTR:

```

'Linear correction of differential stresses resulting from comparing
'calculated versus measured outer roll deflections
FOR QQ% = 0 TO Q%
    DSR(QQ%) = (D(QB%+Q%)/W(Q%))*DSR(QQ%)
    DST(QQ%) = (D(QB%+Q%)/W(Q%))*DST(QQ%)
NEXT QQ%
RETURN

```

DUPSTR:

```

'Replication acceleration technique
'Duplicates the incremental stress solution several times by moving
'it outward to follow the outer surface during wrap addition
WIS(QA%) = (D(QB%+Q%)/W(Q%))*WIS(QA%)
FOR QQ% = 1 TO (DUPLIC%-1)
    WIS(QA%+QQ%) = WIS(QA%)
NEXT QQ%
FOR QQ% = 0 TO (DUPLIC%-1)
    FOR QQQ% = 0 TO Q%
        SR(QB%+QQ%+QQQ%) = SR(QB%+QQ%+QQQ%) + DSR(QQQ%)
        ST(QB%+QQ%+QQQ%) = ST(QB%+QQ%+QQQ%) + DST(QQQ%)
    NEXT QQQ%
NEXT QQ%
RETURN

```

FILLMAT:

```

'Fill matrices with terms of differential equation written in terms of dsr
'Zero Square Matrix
FOR ZZ% = 1 TO DEPTH%

```

```

        FOR ZZZ% = 1 TO 3
            AA(ZZ%,ZZZ%) = 0
        NEXT ZZZ%
NEXT ZZ%
'Initialize First Layer
ERHERE = FNER(SR(QB))
CORCONSTH = ECE*ERHERE*RIRE/(2*ECE*ERHERE*IR-2*ERHERE*ET*IR-
        3*ECE*ERHERE*RIRE-2*ECE*ET*IR*UR)
RPR = RIRE + IR
ERHERE = FNER(SR(QB+1))
ADIFFIR = (CONST1 - URET/ERHERE)*IR
BDIFF = CONST3 - CONST2/ERHERE
AA(1,2) = (BDIFF*IRSQ + 2*ADIFFIR*CORCONSTH*RPR - 2*RPR^2 -
        4*CORCONSTH*RPR^2)/IRSQ
AA(1,3) = (ADIFFIR*RPR - ADIFFIR*CORCONSTH*RPR + 2*RPR^2 +
        2*CORCONSTH*RPR^2)/IRSQ2
B(1) = 0
*** INTERMEDIATE LAYERS ***
FOR QQ% = 2 TO (Q%-3)
    ERHERE = FNER(SR(QB%+QQ%))
    RPR = RIRE + QQ%*IR
    ADIFFIR = (CONST1 - URET/ERHERE)*IR
    BDIFF = CONST3 - CONST2/ERHERE
    AA(QQ%,1) = RPR*(-ADIFFIR + 2*RPR)/IRSQ2
    AA(QQ%,2) = BDIFF - (2*RPR^2)/IRSQ
    AA(QQ%,3) = RPR*(ADIFFIR + 2*RPR)/IRSQ2
    B(QQ%) = 0
NEXT QQ%
'Initialize Under Second Layer
ERHERE = FNER(SR(QB%+Q%-2))
RPR = RIRE + (Q%-2)*IR
ADIFFIR = (CONST1 - URET/ERHERE)*IR
BDIFF = CONST3 - CONST2/ERHERE
AA(Q%-2,1) = RPR*(-ADIFFIR + 2*RPR)/IRSQ2
AA(Q%-2,2) = BDIFF - (2*RPR^2)/IRSQ
B(Q%-2) = (WIS(QA%)*IR/(RPR+2*IR))*RPR*(ADIFFIR + 2*RPR)/IRSQ2
RETURN

```

FIRSTLAYERS:

```

'Approximation for first couple of wraps until minimal matrix can be filled
STARTWIS = 1000
DDSR = -STARTWIS*IR/(RIR)
FOR QQ% = 0 TO 5
    WIS(QQ%) = STARTWIS
    SR(QQ%) = (5-QQ%)*DDSR
    ST(QQ%) = STARTWIS - (5-QQ%)*DDSR
NEXT QQ%
RETURN

```

SUMDIS:

```

'Sum displacement of each layer to yield outer boundary deflection
FOR QQ% = 0 TO Q%

```

```

        SRX(QQ%) = SR(QB%+QQ%) + DSR(QQ%)
    NEXT QQ%
    DW(0) = DSR(0) * RIRE / ECE
    FOR QQ% = 1 TO (Q%-1)
        DW(QQ%) = (DSR(QQ%)/FNER(SRX(QQ%))-UT*DST(QQ%)/ET)*IR
    NEXT QQ%
    RPR = RIRE + Q%*IR
    DW(Q%) = (.5*DSR(Q%-1)/FNER(SRX(Q%-1))-UT*(WIS(QA%)+.5*DST(Q%-1))/ET)*IR
    W(0) = DW(0)
    FOR QQ% = 1 TO Q%
        W(QQ%) = W(QQ%-1) + DW(QQ%)
    NEXT QQ%
RETURN

```

SUMSTR:

'Calculate accumulated stresses = old stress + incremental stress

WIS(QA%) = (D(QB%+Q%)/W(Q%))*WIS(QA%)

FOR QQ% = 0 TO Q%

SR(QB%+QQ%) = SR(QB%+QQ%) + DSR(QQ%)

ST(QB%+QQ%) = ST(QB%+QQ%) + DST(QQ%)

NEXT QQ%

RETURN

TRIDIAG:

'Tridiagonal matrix solution method

'Forward

FOR I% = 2 TO Q%-2

AA(I%,2) = AA(I%,2) - AA(I%,1)* AA(I%-1,3)/AA(I%-1,2)

NEXT I%

DSR(Q%-2) = B(Q%-2)/AA(Q%-2,2)

'Back Substitution

FOR I% = Q%-2 - 1 TO 1 STEP -1

DSR(I%) = (B(I%) - AA(I%,3)*DSR(I%+1))/AA(I%,2)

NEXT I%

RETURN

END

APPENDIX D

EXPERIMENTAL RUN DETAILS

Web Material Properties

CtdBrd

Coated Board
similarly to milk or food carton stock paper
Runs numbered 15-25

LWC

Lightweight Coated and Supercalendered
glossy magazine paper
Runs numbered 26-31

NC

No Carbon
similar to writing or bond paper
Runs numbered 32-41

<u>Property</u>	<u>Units</u>	<u>CtdBrd</u>	<u>LWC</u>	<u>NC</u>
Basis Weight	g/m ²	219.57	60.19	51.23
Caliper	μm	260.6	55.1	80.8
Density	g/cm ³	0.843	1.092	0.634
MD Tensile Strength	N-m/g	71.34	44.42	67.22
CD Tensile Strength	N-m/g	30.16	23.48	17.84
MD TEA	J/Kg	827.9	377.1	520.5
CD TEA	J/Kg	1206	826.3	586.3
MD Modulus	MN-m/Kg	8.887	7.669	9.502
CD Modulus	MN-m/Kg	3.344	4.309	2.615
Air Perm Bendtsen	ml/min	41	17	64
Rough Bendtsen	ml/min	96/13	25/21	412/454
Rough Sheffield	Shef	99/19	42/30	242/242
Air Resist, Gurley	s/100ml	-	-	406.5

Winder and Data Acquisition Setup

For selected runs given in thesis

Run #17

Material	Ctd Brd
Core Chuck PPR	100
Back Drum PPR	5000
Wraps/Sample	4
TNT Program	Plain
Torque	+10% to 10", linear taper to 0% @ 20", 0%
Nip	10 PLI to 10", linear taper to 3 PLI @ 20", 3 PLI
Tension	5 PLI

Run #24

Material	Ctd Brd
Core Chuck PPR	100x4
Back Drum PPR	5000x4
Wraps/Sample	0.75
TNT Program	Tension Drop
Torque	+10% to 10", linear taper to 0% @ 20", 0%
Nip	10 PLI to 10", linear taper to 3 PLI @ 20", 3 PLI
Tension	8 PLI to 27", linear taper to 3 PLI @ 28", 3 PLI

Run #31

Material	LWC
Core Chuck PPR	100x4
Back Drum PPR	5000x4
Wraps/Sample	0.75
TNT Program	Nip Drop
Torque	+10% to 10", linear taper to 0% @ 20", 0%
Nip	12 PLI to 25", linear taper to 3 PLI @ 26", 3 PLI
Tension	2 PLI

Run #38

Material	NC
Core Chuck PPR	2500x10
Back Drum PPR	2500x10x4
Wraps/Sample	0.50
TNT Program	Tension Drop
Torque	+10% to 10", linear taper to 0% @ 20", 0%
Nip	10 PLI to 10", linear taper to 3 PLI @ 20", 3 PLI
Tension	4 PLI to 20", linear taper to 1 PLI @ 21", 1 PLI

VITA

David Robert Roisum

Candidate for the Degree of

Doctor of Philosophy

Thesis: THE MEASUREMENT OF WEB STRESSES DURING ROLL WINDING

Major Field: Mechanical Engineering

Biographical:

Personal Data: Born in Madison, Wisconsin, May 20, 1955, the son of Robert R. Roisum and Audrey J. Roisum. Married to Jane Marie Halpin on December 15, 1979.

Education: Graduated from Pardeeville High School, Pardeeville, Wisconsin in May 1973; received Bachelor of Science Degree in Mechanical Engineering from University of Wisconsin Center, Baraboo, Wisconsin in May 1979; completed requirements for the Master of Science Degree in Engineering Mechanics at University of Wisconsin, Madison, Wisconsin in December 1984.

Professional Experience: Engineer, Beloit Corporation Winding Department, Beloit, Wisconsin, 1979 to 1983; Teaching Assistant, Engineering Mechanics Department, University of Wisconsin, 1983 to 1984; Manager of Winding Research, Beloit Corporation R&D, Rockton, Illinois, 1984 to 1987; Winder Consultant, Beloit Corporation R&D, Rockton, Illinois, 1987 to 1989; Senior Research Engineer, Web Handling Research Center, Oklahoma State University, Stillwater, Oklahoma, 1987 to 1989; Senior Research Scientist, Kimberly-Clark, Neenah, Wisconsin, 1989 to present.